Joseph Costello

Flow and transfer processes at abrupt expansions

Ph. D
Thesis

UNIVERSITY OF ASTON IN BIRMINGHAM

December 1969

Acknowledgement

The author wishes to express his gratitude

to The Gas Council, Midlands Research Station for the provision of a grant in support of the Research Project,

to Dr. B. Gay, for his guidance,

to Prof. G. V. Jeffreys, for the use of Chemical Engineering Department facilities and the staff of the Chemical Engineering Department and the library for their assistance.

Summary

Variations in wall static pressure immediately downstream of abrupt expansions were determined for a range of expansion ratios ($D_2/D_1 < 7/1$) in order to ascertain the rate of development of enclosed jets.

Theoretical expressions for the recovery of static head from velocity head and the loss of pressure energy due to eddy turbulence were examined initially. Experimental data showed only slight deviations from predicted values. This discrepancy was not attributable to non-flat velocity profiles, but was shown to arise from the inherent approximations in the theory.

At a given expansion ratio the static pressure distribution pattern could be represented by a single curve independent of velocity. The separate curves for each expansion ratio would not, however, reduce to a universal curve.

The parameters of principal interest were the locations of the eye of the recirculating eddy and the point of reattachment of the jet. The position of each of these features was deduced from the changes in gradient of the pressure distribution curve.

Local mass transfer coefficients downstream of abrupt expansions were determined by electrolysis of acidified copper sulphate solution under diffusion-controlled conditions. Results were presented in the form of the dimensionless transfer factor j_D, thus giving heat transfer factors by analogy.

Peak local values were correlated in terms of the fully developed value

$$(j_D)\,max/(j_H)f.d. = 15.25\,(D_2/D_1)^{0.8}\,Re_2^{-0.18}$$

Recorded data were 10 - 25 per cent higher than values obtained by other researchers, and occurred closer to the plane of enlargement.

Comparison of the results of each series of experiments suggested that peak transfer coefficients correspond to the eye of the recirculation eddy.

TABLE OF CONTENTS

I. 1. Introduction.

In conventional furnaces radiant heat transfer is almost exclusively responsible for raising the temperature of the stock. Increasing demand for more rapid heating techniques in the processing industries has led to improved burner design and the development of small-scale furnaces which, by making use of the momentum of the combustion gases, increase the rate of heat transfer to the stock by convection. Such furnaces differ essentially from the conventional type in that the combustion process is eliminated from furnace design considerations, being confined to a small tunnel set into the furnace wall. A cylindrical furnace, fired tangentially with air-blast tunnel burners, for heating metal billets to their hot-working temperatures has been described by Lawrence and Spittle (1). The results of cold model studies of convective heat transfer in rapid billet heaters of this design have recently been published by Francis and others (2).

The success of the tunnel burner depends upon obtaining a high velocity stream of hot combustion products using reasonable air and gas supply pressures (3). The short hot flames required for this purpose are produced by premixing the fuel gas with the requisite amount of air. In this respect the tunnel burner is unlike the vast majority of combustion systems in which mixing and combustion occur simultaneously, giving generally longer flames with a more even temperature. A corollary of premixing is that combustion space and hence duct/nozzle area ratio may be reduced. The other notable difference between the situation existing in the tunnel and normal furnace conditions arises from the increased velocity imparted to the jet, which results in appreciably higher rates of heat transfer to the tunnel wall by convection.

The tunnel burner is thus another example of a practical situation requiring a critical appreciation of jetting and transport phenomena at abrupt expansions in pipes and ducts. Model studies of tunnel burners using confined fluid jets would provide information on flow and heat transfer distribution patterns required for their more efficient operation. Such studies would also serve to form a link between recent independent investigations of furnace flame behaviour (in systems with high chamber/nozzle ratios) and convective heat transfer in the separation and reattachment regions downstream of abrupt changes of section (low expansion ratios). Since the essential problem in the design of any flame heated system is the evaluation of heat transfer and temperature distribution in relation to flow and combustion patterns the forging of such a link could have a direct bearing on the analysis of furnace performance generally.

I. 2. Flow and heat transfer distribution patterns in industrial furnaces.

The accurate prediction of temperature and heat transfer distribution within the combustion chambers of industrial furnaces is one of the most intricate problems of heat transmission. In conventional furnaces the main heat transfer process is by radiation from the flame and gases to the refractory surface, and then back through the flame to the stock, which also receives some heat by direct radiation from the flame.

Theoretical considerations normally relate to a somewhat simplified system in which convective heat transfer from the flame to the refractory surface is equated to the external losses from the walls of the chamber. The theory of radiant heat transfer in a gas-filled enclosure has been fully developed by Hottel et al (4) (5), but detailed theoretical analysis of practical systems in which mixing, combustion and heat transfer occur simultaneously remains seldom possible or reliable.

Empirical approaches have provided only partial solutions to the general problem since the singular nature of each of the systems examined means that information obtained from experimental measurements is not universally applicable.

Most furnace calculations are therefore based on simpliflying assumptions and semi-empirical correlations appropriate to a particular class of furnace.

Furnaces may be broadly classified according to the type of fuel burned, with further subdivisions according to function, manner of firing, and other operating variables.

The characteristic feature of all gas, pulverised-coal or oil-fired systems is a jet of flame spreading from an orifice in the chamber wall. Although these fuels lend themselves to great flexibility in burner arrangement and furnace design, the combustion chamber of such a furnace may be considered, in its simplest form, as a horizontal cylinder with the jet firing along the axis. Flames are most commonly of the turbulent diffusion type, i.e., combustion air is supplied via an annulus surrounding the fuel nozzle and turbulent mixing of air and fuel takes place within the combustion chamber. The expansion of the fuel jet is limited by the walls of the chamber, and under normal operating conditions the excessive entrainment capacity of the enclosed jet induces recirculation of partially or totally reacted combustion products. It is this complex mixing process which largely determines the combustion pattern of the flame.

Systematic studies of flow patterns in combustion chambers and models and their relation to mixing, temperature distribution and refractory wear were begun more than twenty years ago with the work of Chesters on open-hearth furnaces (6). Subsequent investigations of a variety of flame-heated systems produced a substantial volume of literature relating to the aerodynamics of furnace flames (7), and the fundamental processes associated with the propagation of turbulent diffusion flames (8). The effects of recirculation on such parameters as luminosity, stability and length of flame, rates of combustion and heat release, combustion noise, and heat transfer within the furnace have become increasingly apparent from turbulent diffusion flame studies (9).

Because of the difficulty of achieving complete combustion when diffusion flames are used the amount of air supplied is generally much in excess of the stoichiometric quantity and greater combustion space is accordingly necessary. In order to accelerate mixing - thus shortening the flame and increasing combustion intensity - means of promoting internal recirculation have been sought (10). Recent investigations of swirling air jets, double-concentric jets and bluff body recirculation have been reported in (11) to (14).

In the limit, complete premixing of air and fuel results in almost instantaneous combustion at the burner mouth and the greatest rate of heat release per unit combustion volume. The short, fierce flame thus produced is generally referred to as the 'premix' flame. Recirculation in the annulus surrounding the spreading flame jet is, clearly, an integral feature of the single, premix flame fired into an expanded chamber or tunnel.

The commonest use of premixing burners, however, is to produce a well distributed supply of heat, steady heating conditions and a very uniform furnace atmosphere. This is readily achieved by distributing the combustible mixture to a number of different points throughout the furnace (15).

The type of flame considered by Spalding (16) (17) is that which spreads from the wake of a flame holder mounted in a steady stream of premixed combustible material flowing at high speed through a duct of constant area with plane walls. Theoretical predictions have been made of flame shape and velocity distribution in the flame on the hypothesis that the gas burns as soon as it is entrained into the region of turbulent shear flow in the central region of the duct. The rate of flame spread is thus governed by the rate of entrainment of cold gas by hot which may be predicted from data on the mixing of parallel fluid streams under non-recirculating conditions.

I. 3. The Tunnel Burner.

The air-blast tunnel burner essentially comprises an injector, mixing zone, combustion chamber and exit nozzle. Gas at approximately atmospheric conditions is entrained by air under slight pressure and the resulting air/gas mixture burns as a jet in the expanded tunnel. Operation is normally under stoichiometric conditions and, since thorough mixing is readily achieved, combustion of the supply gas is virtually instantaneous and almost complete. The products of combustion, at a temperature approaching the theoretical or adiabatic flame temperature, issue from the exit nozzle at high velocity into the furnace proper. Different designs of tunnel burners do not produce appreciable variations in exit gas temperature or heat release for a given gas input. At the air pressures employed design procedures treat the air/gas mixture as incompressible. Full design details are given by Francis in references (3) and (18).

Since both fuel gas and combustion air enter via one central nozzle the nozzle/chamber diameter ratio is higher ($\simeq 1/7$) than is normally used with diffusion flames, and the velocity reduction at the abrupt expansion is correspondingly less. The increased velocity imparted to the jet results in appreciably higher rates of heat transfer to the tunnel wall by convection.

Experimental investigations of tunnel burners may be modelled on abrupt expansions, corresponding to the simplest combination of nozzle and tunnel geometry. Since buoyancy forces may be neglected cold models using water or other liquids may conveniently be employed.

I. 4. Objectives of Research Work.

The objectives of the present study were twofold.

(a) It was initially proposed to investigate the expansion of jets at abrupt enlargements in pipes of circular section by recording the variation in static pressure (at the boundary) in the downstream section. The aim of these preliminary experiments was to establish a correlation for predicting the jet length (the distance required by the jet to expand and fill the downstream section) and the location of the eye of the recirculation eddy in terms of the expansion ratio.

Detailed measurements of the static pressure change would also allow a fresh examination of the validity and accuracy of the generally accepted simple theoretical expressions for the loss of head due to eddy turbulence and the net rise in pressure at abrupt expansions. The possibility of developing a universal pressure rise curve, perhaps incorporating a similitude parameter such as that of Thring and Newby (21) or Craya and Curtet (23) was also to be investigated.

A review of the literature relating to jetting flows at abrupt enlargements together with details and results of these initial experiments is given in Section A.

(b) In the subsequent series of experiments it was planned to determine local values of the mass transfer coefficient - throughout the region defined by the results of the earlier trials - by means of an electrolytic technique and from this data deduce heat transfer coefficients by applying the Chilton-Colburn analogy. The advantages of this method of investigation over straightforward measurement of the heat transfer coefficients are elaborated in the introduction to the second section (Section B).

The results of previous studies of convective

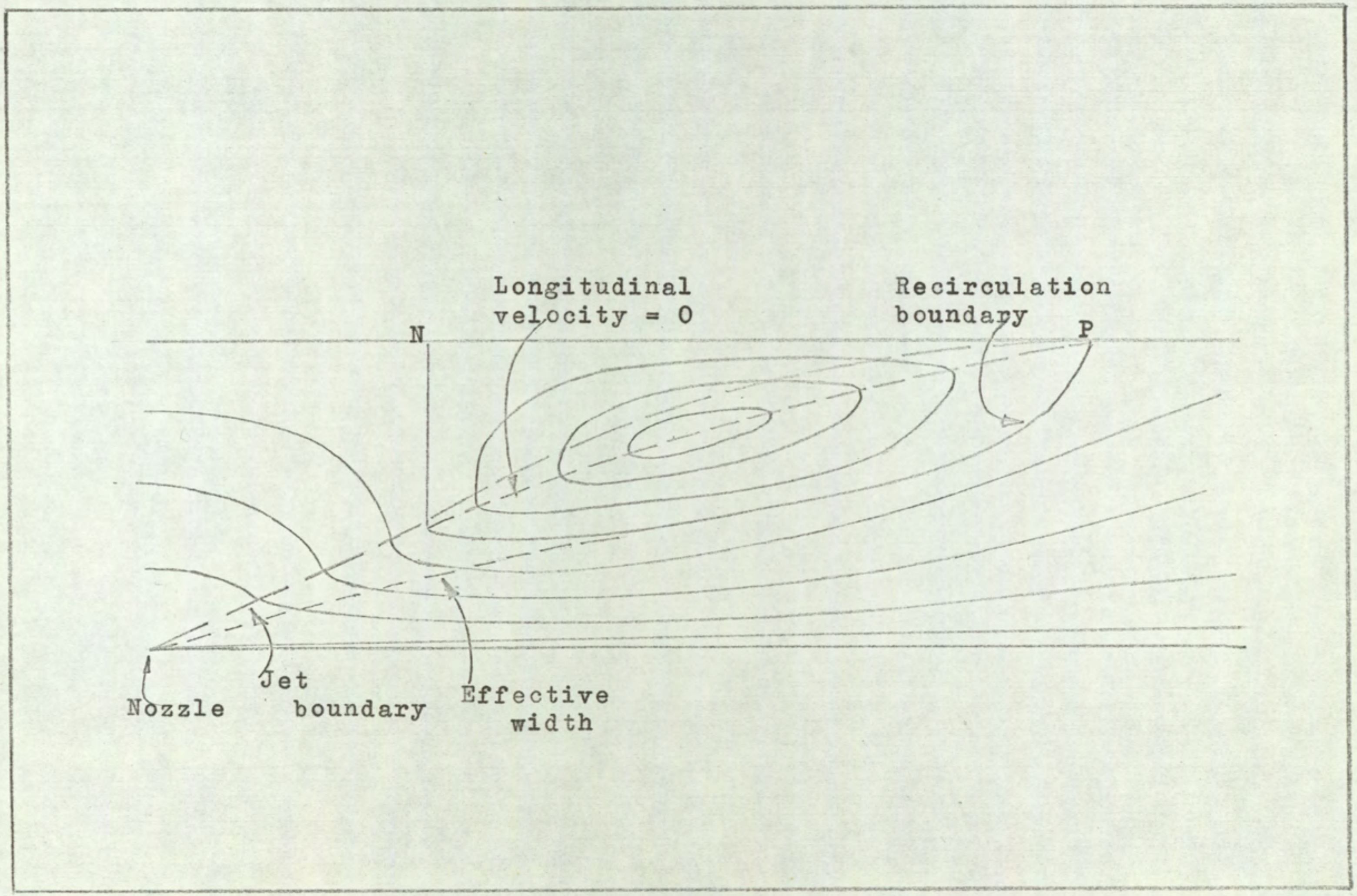
Longitudinal velocity = 0
Recirculation boundary
N
P
Nozzle
Jet boundary
Effective width

Fig. 1

heat transfer at abrupt changes in section are reviewed in section B.

The final section is devoted to a comparison of the results of the two series of experiments in order to relate the variation in transfer coefficients to the flow pattern.

SECTION A

2. 1. Studies of confined jets with recirculation.

In recent years increasing attention has been devoted to the fundamental aspects of recirculation arising from the spreading of a jet issuing from a nozzle.

The instability of the surface of separation gives rise to small vortices which bring about the transfer of momentum, heat and mass in a transverse direction (19). This turbulent mixing of the jet and surrounding fluid leads to an increase in the cross-section of the jet and dissipation of the constant velocity core. In the absence of confining walls the jet subsequently becomes similar in appearance to a flow of fluid from an infinitesimally small source.

When the jet is confined in a duct the amount of entrainable fluid is limited and recirculation eddies will develop if the entraining power of the jet exceeds the feed rate of the secondary stream.

Riviere's suggestion that differences in static pressure downstream of the jet are responsible for setting up a recirculation force at the walls of the duct was examined by Sunavala (20), who concluded that recirculation is a function of jet entrainment only, provided the duct length is greater than seven times the width or diameter.

If the secondary stream is wholly entrained before the jet has expanded to fill the downstream section the entrainment capacity of the jet must be satisfied with recirculated fluid. Some of the mean streamlines then take the form of a closed loop (figure 1). A recirculation flow rate can be defined by the integral of the negative velocities across a cross-section. This has a maximum value around the centre or eye of the eddy and falls to zero at the two zero-velocity points corresponding to the upstream and downstream limits of the eddy. The concept of an expanding jet becomes somewhat arbitrary, particularly with regard to the definition of the jet boundary, and considerable confusion has arisen concerning the point of reattachment of the jet. The essential features of recirculatory flows have best been described by Barchillon and Curtet (26).

The earliest significant theoretical approach to the problem of natural recirculation in combustion chambers was proposed by Thring and Newby (21). The theory of free jets, which had already been applied to the problem of ducted jet mixing under non-recirculating conditions, was further extended by Thring and Newby (21), who assumed that the confined jet obeyed the same entrainment law as the free jet until it approached the wall.

The mass of fluid entrained over a distance x is given by the equation:

$$m_x = m_o \left[0.2 \frac{x}{r_1} - 1.0 \right]$$

where m_o is the mass flow rate of nozzle fluid.

Hence, the total mass of ambient fluid is entrained over a distance x_a defined as,

$$\frac{x_a}{r_1} = 5.0 \left(\frac{m_o + m_a}{m_o} \right)$$

This is considered as a first characteristic mixing length in the model or furnace. A second characteristic length is given as x_L, the distance at which a free jet would touch the chamber wall.

$$x_L = 4.5 \; (r_2)$$

At this distance the mass of fluid entrained would be m_L. Thring and Newby propose as a first approximation that the mass of recirculated material (m_r) equals the difference between the mass of material entrained over the distance x_L and the mass of the surroundings,

$$\text{i.e.}\quad m_r = m_L - m_a = m_o\left[\frac{0.2x_L}{r_1} - 1.0\right] - m_a$$

whence,

$$\frac{m_r}{m_o + m_a} = 0.2\left[\frac{m_o}{m_o + m_a}\right]\left[\frac{4.5r_2}{r_1}\right] - 1.0$$

$$= \frac{0.9}{\theta} - 1.0 \qquad \text{......}\ 2.1.$$

where,

$$\theta = \left[\frac{m_o + m_a}{m_o}\right] \times \left[\frac{r_1}{r_2}\right] \qquad \text{......}\ 2.2.$$

Experimental evidence obtained when the nozzle/chamber diameter was very low and the velocity ratio of the secondary/primary streams was also very low showed that mixing in an actual furnace could be reasonably well predicted by the use of cold models and the application of the similarity theory developed.

A more rigorous analysis of ducted jet flow was made by Curtet (22) (23), developing an approximate theory established previously by Craya and Curtet (24). Model studies of two-dimensional jets were conducted to illustrate the general characteristics of jets and check the accuracy of theoretical predictions. The theory was then used to forecast the basic laws governing three-dimensional recirculating flow.

Craya and Curtet considered the mixing of two co-axial streams with different initial velocities within a cylindrical chamber. Examination of the velocity profile in a cross-section of a confined jet before it joins the boundary layer at the chamber wall has shown the existence of two distinct zones: the mixing zone or jet in which the primary and secondary (or ambient) fluids mix, and a surrounding zone in which the longitudinal velocity u_a is practically constant at a given abscissa (x). If u is the longitudinal velocity at any point (x,y) within the jet, the excess velocity w is defined by

$$w = u - u_a$$

On the jet axis $u = u_o$ and $w = w_o$.

The similarity of the excess velocity profiles is expressed by a relationship of the form $w/w_o = f(y/l)$ where f is a function of (y/l) only and l is a reference width related to the spreading of the jet. This width is defined by,

$$\pi w_o l^2 = q = \int_0^{\lambda} 2\pi y w dy$$

where q is the excess flow rate, i.e., the volume of revolution bounded by the excess velocity profile, and λ is the jet boundary radius.

The three variables w_o, u_a and l are unknown functions of x.

A differential system of equations is developed.

(i) The continuity equation gives the total volumetric flow rate in a chamber of radius r_2 (neglecting boundary layer thickness).

$$Q = \pi w_o l^2 + \pi u_a r_2^2$$

(ii) The momentum equation provides a second relationship between the three variables. The form used incorporates a shape factor k for the excess velocity profile f.

$$k = \int_o^{\lambda/l} f^2 . \eta \, d\eta \qquad \text{with } \eta = y/l$$

(iii) A weighted mean of Reynolds' first equation across a cross-section is introduced in the form of a moment of momentum equation.

This system of equations can be integrated in the particular case of a chamber of constant radius, leading to an expression for a similarity criterion, m:

$$m = -\frac{3R_r^2}{2} + R_r + \frac{kR_r^2}{L_r^2} \qquad .....2.3$$

where, $R_r = q/Q$ and $L_r = l/r_2$

This equation applies both in an established regime (k constant) and in the potential core of the jet (k varying with x). The value of m can therefore be deduced by substituting the values of R, L and k at the nozzle mouth section.

When r_1/r_2 is small in comparison with θ it is further shown that,

$$m = \frac{1}{\theta^2} \qquad \text{.....2.4}$$

The recirculation flow rate (q_r) can be related to the variables R_r and L_r by a simple calculation.

$$\frac{q_r}{Q} = (R_r - 1) \left\{ L_r^2 \left[1 - \log(L_r^2 (R_r - 1)/R_r) \right] - 1.0 \right\} \text{.... 2.5}$$

The theoretical curves for the variation of the recirculation rate with distance show that, for a constant value of m the rate of recirculation increases from a certain abscissa onwards and tends towards a critical value at which the tangent to the curves is vertical. On comparing this value with the results of systematic tests by the Sogreah team to determine the maximum recirculation rate for various values of θ (25) it was concluded that the recirculation rate can be predicted with a satisfactory degree of accuracy provided that the duct is cylindrical and the nozzle diameter is small in comparison with the chamber diameter.

In a preliminary trial ($\theta = 0.264$) it was found that the recirculation rate was a maximum at a distance of 2 chamber diameters from the burner and that its value between 1.5 and 2.5 diameters was of the same order as the flow rate of the secondary stream. The theoretical and experimental curves for the development of the recirculation eddy were not exactly the same, however, particularly near the eye of the eddy. Furthermore the region beyond the eye of the eddy could not be approached theoretically.

The theories of Craya and Curtet and Thring and Newby were compared with regard to the location of the eye of the recirculation eddy. Thring and Newby were able in their analysis to determine the zero velocity points upstream and downstream of the eddy. Curtet assumed that the eye of the eddy was midway between these points and noted good agreement with the position predicted by the Craya-Curtet theory.

Barchillon and Curtet (26) subsequently examined in greater detail the structure of the recirculation eddy using a water rig to visualize and measure the mean velocities and an air rig to measure velocity fluctuations. When the Craya-Curtet parameter was varied by reducing the flow rate of the secondary stream (with the nozzle/chamber diameter ratio fixed at for instance, 1/15) the recirculation eddy extended in size untilfinally it occupied the complete chamber when the secondary discharge was zero. The streamlines showing the time-average structure of the flow were deduced from the velocity measurements. The flow networks (with a time scale representing 1 minute) clearly showed the position of both zero-velocity points associated with the recirculation eddy as well as the eye of the eddy which was approximately mid way between these two. A series of 20 photographs confirmed the location of the upstream stagnation point. The experimental data showed reasonable agreement with the predicted position in this case.

With a smaller time scale quite a different flow pattern emerged and a photograph taken with an exposure of 1/20 second showed the jet spreading at a very shallow angle then wrinkling and breaking up as it came into contact with recirculated fluid. The jet did not in fact appear to reach the wall of the chamber and instead of a single large recirculation eddy a number of small vortices were formed. Near the wall could be seen a recirculated fluid stream. The whole phenomenon of course varied considerably with time.

These instantaneous flow patterns and measurements of the velocity fluctuations indicated unusually high turbulence levels in the jet and back flow and clearly showed the need for improved analytical techniques since turbulence characteristics play such a dominant role in recirculation (26).

Measurements of the static pressure variation at the boundary downstream of the change of section showed the existence of two distinct zones which were most easily distinguished at low values of $Ct(= m^{-\frac{1}{2}})$. The static pressure varied little in the first zone, thereafter increasing rapidly towards the value predicted by the momentum equation. Comparison with the results obtained from velocity measurements showed that the junction of the two zones corresponded to the eye of the recirculation eddy. In the case of zero ambient flow ($C_t = 0.075$) the static pressure fell by not more than 1 cm. of water in the first zone and the approximate position of the eye of the eddy was marked by the change in gradient of the pressure versus distance curve.

The same graph further indicated that the recovery of static pressure from velocity head was not quite complete when the jet reattached to the wall, the point of reattachment being defined as the downstream stagnation point P, figure (1). The remaining pressure increase was provided by the dissipation of lateral gradients in the mean velocity as the transition from full-bore to fully-developed flow took place.

The principle features of the recirculation eddy according to Curtet's definitions are shown in figure (1). The eye of the eddy lies within the jet whose boundary is defined by λ . Furthermore, the definition of the jet boundary (λ) does not correspond to the condition that the longitudinal component of the velocity equals zero, except at the point of reattachment of the jet (P). The "effective" jet values correspond more closely to the common conception of the radius of a jet with an attendant recirculation eddy (cf. fig. (2)) but only as far downstream as the eye of the eddy. The "effective" jet radius does not expand beyond this section to the radius of the duct. Other figures given in ref.(26) show that the effective radius differs only slightly from the velocity half-radius

The effect of the Craya-Curtet parameter on turbulent mixing patterns was also investigated by Becker and others (27). A fixed nozzle/chamber diameter ratio was used (1/31) and the positions of the stagnation points and the eye of the recirculation eddy were hence given as unique functions of the parameter Ct $(= m^{-1/2})$

The approximate position of the downstream limit of the eddy, estimated as the point where the velocity half-radius of the jet equalled half the duct radius was indicated graphically as a function of Ct . This definition led to physically unacceptable results: for values of Ct = 0.55 the eye of the recirculation eddy lay downstream of the predicted downstream limit of the eddy. Barchillon's paper (26), which was published later, shows that the velocity half radius varies little with distances between the eye of the eddy and the downstream limit and is therefore an unsuitable criterion for defining the downstream limit.

Becker also examined the axial variation of the mean static pressure (measured at the wall), expecting a change in the law of static pressure variation between the jet mixing zone and the succeeding zone. The intersection of the two laws was identified as the point at which entrainment ceases and the secondary stream vanishes i.e. the point at which the jet reattaches to the wall. This again gave a physically impossible situation and in a subsequent paper (28) Becker added that, in the event of recirculation, this section also corresponds to the eye of the eddy. The downstream limit of the eddy was redefined as the downstream limit of the recirculatory zone of negative mean velocities.

A further rigorous analysis of ducted jet flow has been proposed by Hill (29). In the absence of recirculation a reasonable prediction can be made of the behaviour of turbulent confined jets but the simplifications involved in the calculations allow only a qualitative discussion of recirculatory flows.

Defining,

$$\lambda = \text{jet radius}$$

and

$$\xi = \frac{u_a}{u_o - u_a}$$

where u_a = velocity of secondary stream

u_o = jet maximum velocity.

The assumption that velocity profiles are self-preserving leads to the conclusion that the variables λ/D_2 and ξ are dependent on x/D_2 and a parameter $(m_o + m_a)/(M\rho)^{\frac{1}{2}}$ only.

$(m_o + m_a)$ = total mass flow per unit area through duct

$\frac{1}{2}M$ = average sum of momentum and pressure forces per unit area = constant in a uniform duct if wall shear stresses are neglected.

With a finite secondary flow rate a value of the parameter $(m_o + m_a)/(M\rho)^{\frac{1}{2}}$ of unity corresponds to free jet flow, whilst a value of zero signifies no net flow in the duct, i.e., a jet issuing into a duct whose downstream end is closed. Recirculation occurs at values of the parameter less than 0.45. With zero secondary flow the form of the parameter reduces to

$$\frac{m_o}{(M\rho)^{\frac{1}{2}}} = \frac{1}{\sqrt{2}}\left[\frac{D_1}{D_2}\right] \qquad \text{........ 2.6}$$

In this case a value of zero corresponds to free jet flow and simple pipe flow is represented by the value $1/\sqrt{2} = 0.707$.

If the theoretical curves presented by Hill are interpreted in the light of Barchillon's definitions, the eye of the recirculation eddy - indicated by maximum reverse flow at the duct wall - lies in the region

$$1.75 < \frac{x}{D_2} < 2.5 \qquad \text{..........} \; 2.7$$

and moves towards the nozzle mouth as $(M\rho)^{-\frac{1}{2}}(m_o + m_a)$ is reduced to zero (finite secondary stream). A plot of the pressure variation with distance confirms this result.

Hubbard (25) prepared a resume of the essential findings of the complete course of experiments carried out at Grenoble, in which a critical examination of the effect of the fundamental variables on the recirculation pattern was undertaken. Both the flow rate of the secondary stream and the nozzle/chamber diameter ratio were varied beyond the range normally found in industrial furnaces.

Hubbard concluded that the mass flow rate of recirculated material can be related to a mixing parameter $(m_o + m_a)/m_o$ and a dynamic parameter r_1/r_2. In many industrial applications it is the product of these two that is important and the characteristics of the recirculation eddy can be expressed in terms of a single parameter, such as that of Craya and Curtet (m) or Thring and Newby (θ).

$$\theta = \left[\frac{m_o + m_a}{m_o}\right]\left[\frac{r_1}{r_2}\right] \qquad \text{....... 2.2}$$

$$\theta \doteq Ct = m^{-\frac{1}{2}} \qquad \text{....... 2.4}$$

if r_1/r_2 is small compared with θ.
In most injector type flames the value of θ is of the order 0.2 to 0.3 and that of the mixing parameter 10 to 20.

Outside this range it is necessary to consider the values of $(m_o + m_a)/m_o$ and r_1/r_2 independently. Experimental results obtained using greater nozzle/chamber diameter ratios and zero secondary flow are especially interesting in the context of the present work. The main parameters of interest are the downstream limit of the jet and the location of the section at which the flux of recirculated material is a maximum (corresponding to the eye of the recirculation eddy).

The effect of increasing the relative size of the nozzle was investigated and values of the maximum recirculated flow plotted versus $^1/\theta$. The general trials in which m_a was also varied are reviewed first.

(i) For nozzle/chamber diameter ratios less than 1/50 the maximum flux of recirculated material can be predicted by the empirical equation

$$\left[\frac{m_r}{m_o + m_a}\right]_{max.} = 0.44 \left[\frac{m_o}{m_o + m_a}\right]\left[\frac{r_2}{r_1}\right] - 0.88 \quad .... \; 2.8$$

Values agree with the Craya-Curtet theory.

(ii) As r_1/r_2 is increased up to 0.15 the maximum recirculation rate progressively exceeds the predicted value. The experimental data advanced by Curtet in support of the Craya-Curtet theory in fact fall into the lower region of this group: values of θ ranged from 1/12 to 1/3 , with $0.027 < r_1/r_2 < 0.09$.

(iii) Above the value 0.15 the ratio r_1/r_2 has little further effect and a single correlation can be used for the maximum recirculated flux, which is 34 - 40 per cent higher than the Craya-Curtet theory predicts.

$$\left[\frac{m_r}{m_o + m_a}\right]_{max.} = 0.62 \left[\frac{m_o}{m_o + m_a}\right]\left[\frac{r_2}{r_1}\right] - 0.90 \quad .... \; 2.9$$

The case of specific interest, in which secondary flow is zero is reviewed next.

(i) No experimental data were obtained for expansion ratios r_2/r_1 greater than 50:1. A jet confined in such a large duct must clearly resemble a free jet.

(ii) Two contradictory statements are made concerning data relating to expansion ratios in the range $0.027 < r_1/r_2 < 0.09$.

(a) Hubbard reproduces Curtet's original graph adding several points obtained when m_a equals zero. These extra points clearly show that the recirculation rate increases as r_2/r_1 is increased from approximately 20:1 to 40:1 and lead to the conclusion that "when both 'fuel' and 'combustion air' enter via a central nozzle the maximum flux of recirculated material asymptotically approaches some constant value as θ (i.e. r_1/r_2) tends to zero." (25) As the expansion ratio is increasingly enlarged the situation will resemble more and more closely the case of a free jet. The stated effect of confining a free jet in a large duct is thus to reduce the recirculated flux.

This point is confirmed by Cohen de Lara et al (30). Equation 2.8 is first rewritten in the form:

$$\frac{m_r + m_o + m_a}{m_o} = 0.44 \left[\frac{2r_2}{z}\right]\left[\frac{z}{2r_1}\right] + 0.12 \left[\frac{m_o + m_a}{m_o}\right]$$

where $(m_r + m_o + m_a)$ = maximum flux in jet and

z = location of the eye of the recirculation eddy relative to the plane of enlargement.

For $m_a = o$ and low values of θ reference (30) gives

$$\frac{z}{2r_2} = 1.88 \qquad \text{....... 2.10}$$

Thus, $$\frac{\text{maximum flux in jet}}{\text{flux leaving nozzle}} = 0.28 \frac{z}{2r_1} + 0.12 \qquad \text{.... 2.11}$$

Ricou and Spalding (31) have shown that for a jet in free space

$$\frac{\text{flux in jet}}{\text{flux leaving nozzle}} = 0.32 \frac{z}{2r_1} \qquad \text{.... 2.12}$$

Thus the maximum flux in a confined jet is approx. 35 per cent lower than that which the same jet would have had at the same section without limiting walls.

(b) In contrast, measurements of the rate of decay of axial velocity as the expansion ratio r_1/r_2 is increased through the range 0.027, 0.047, 0.062, 0.089 are interpreted as showing that the recirculation rate increases. The error of this inference may readily be appreciated by considering two expansion ratios (a) and (b) in which $(r_1)_a > (r_1)_b$ and $(r_2)_a = (r_2)_b$. For a given mean velocity in the post jet-mixing zone,

$$(v_2 av)a = (v_2 av)b$$

Since $$A_1 v_1 = A_2 v_2$$

$$(v_1)a < (v_1)b$$

Results show $$\frac{(v_1)a}{(v_2\ max)a} > \frac{(v_2)b}{(v_2\ max)b}$$

$$\therefore \quad (v_2\ max)a >> (v_2\ max)b$$

In the immediate vicinity of the enlargement, therefore, the velocity profile is flatter in case (b) - the larger of the two expansion ratios $\left[(r_2/r_1)b > (r_2/r_1)a\right]$. Recirculation thus is less at the larger expansion ratio.

This error is undoubtedly bound up with a misleading statement in (30). The recirculated flux is expressed,

$$\frac{m_r}{m_o + m_a} = A(\sqrt{m} - B)$$

in which A and B are empirical functions of (r_1/r_2). At $r_1/r_2 = 0.15$ the value of A reaches a maximum and it is wrongly concluded that the expression $A(\sqrt{m} - B)$ therefore has a maximum value also.

(iii) In this final series of experiments r_1/r_2 was increased over the range 0.158, 0.231, 0.354, 0.590. Experimental data are given in detail in reference (30). Predictably, the recirculation rate falls as conditions approach simple pipe flow. Cohen de Lara et al suggest that this is the result of recirculation developing in the transition zone of the jet.

The section at which maximum recirculation occurs is shown as a function of θ for fixed values of r_1/r_2 (25). The eye of the eddy was found to move towards the nozzle mouth as $(m_o + m_a)/m_o$ was reduced at a fixed nozzle/chamber ratio, and also as the ratio r_1/r_2 was increased.

The Craya-Curtet theory, in contrast, shows the position of the eye of the eddy as a unique function of the similitude parameter (m).

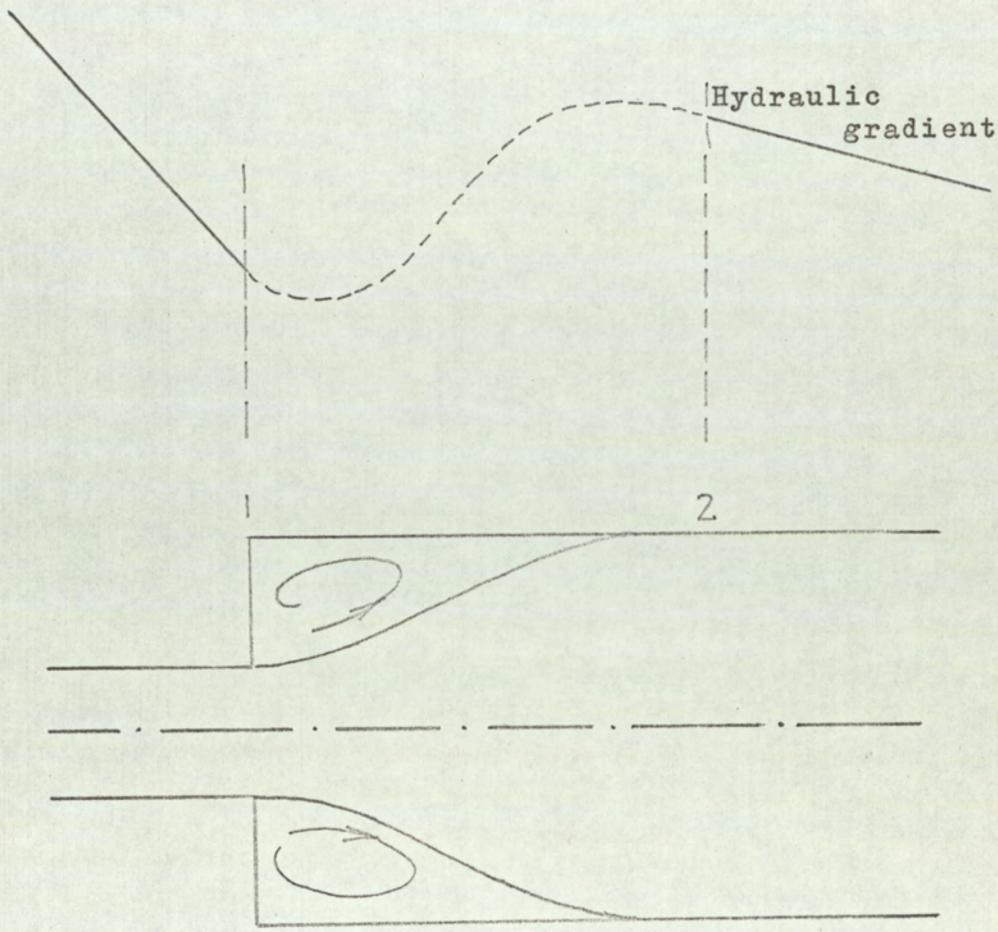

Fig. 2

3. Static pressure variations at abrupt enlargements.

3. 1. Introduction.

For steady incompressible flow through a horizontal pipeline the decrease in kinetic energy caused by the sudden deceleration at an abrupt expansion in the cross-section of the pipe results in an increase in static pressure. As the fluid leaves the boundary at the enlargement turbulent eddies are developed in the annulus surrounding the expanding jet. The energy dissipated by these eddies constitutes a partial loss of head, the so-called expansion loss. The net effect of the expansion, however, is to produce an initial increase in static pressure. With the onset of full bore flow lesser changes in static pressure occur due to the dissipation of lateral gradients in the mean velocity and the growth of the boundary layer. Once fully developed flow is established in the downstream section the static pressure decreases at a constant rate in accordance with the friction gradient. A graph of the static pressure variation with distance will hence show a maximum in the reattachment region of the jet. The system is depicted in figure (2).

Previous investigations of the pressure changes occuring at sudden expansions have been exclusively concerned with the frictional loss due to eddy turbulence and the accuracy of the Borda-Carnot equation for predicting this loss.

$$H_L = \frac{V_1^2}{2g}\left[1 - \frac{A_1}{A_2}\right]^2$$

This expression for the loss of head at the expansion is derived from momentum and energy balances conducted between the plane of enlargement and a section downstream marking the onset of full-bore flow. In the course of the derivation certain simplifications are assumed with regard to the complex situation existing at the expansion. The Borda-Carnot equation has been found satisfactory for the majority of practical cases. Results obtained under turbulent flow conditions have generally confirmed the predicted value of H_L within a few percent. In the case of laminar flow, although relatively large discrepancies may be recorded, the low velocities result in losses which normally prove negligibly small in comparison with the total loss around a specific flow network. Streeter (32) concludes that the steady flow picture of figure (2) is a useful approximation to a truer but much more unsteady flow pattern and that the expansion loss may be considered to occur in a much more localised zone than is implied by figure (2).

In view of such observations little attention has hitherto been paid to the pressure recovery in the region of the expanding jet. Dougherty (33) records that the wall static pressure in this zone is less than the static pressure within the jet and presents in evidence a single line diagram drawn to scale. Salient details such as the scale of the diagram and operating conditions are unfortunately omitted.

Before proceeding to a detailed examination of the static pressure variations in this zone it is expedient to reconsider the simple theoretical analysis based upon general principles of hydrodynamics. A review of previous experimental work will then serve to indicate the limitations of the simplifying assumptions and the degree of accuracy of the Borda-Carnot equation. Expansion losses are determined as the difference between the ideal or loss- less pressure rise (i.e. 100 per cent conversion of kinetic energy lost) and the maximum value of the observed rise. Inaccuracies in the value of H_L will, hence, reflect discrepancies between the theoretical rise predicted by a momentum balance and the maximum observed rise (observed values generally not being recorded). It is, of course, the observed rise which is of primary importance in the present context since the variation in static pressure is related to the development of the jet and the maximum rise serves to define the downstream limit of the zone subsequently to be investigated in the mass transfer experiments.

3. 2. Pressure changes at abrupt expansions (simple theory)

An expression for the theoretical pressure rise at an abrupt enlargement may be obtained from momentum considerations. The simplifications generally assumed are that the velocity is uniform over the flow cross-sections and that the small shear force on the pipe wall between sections (1) and (2) of figure (2) may be neglected. It is further assumed that the pressure on the washer-shaped area of the plane of enlargement is equal to the pressure in the smaller tube immediately before the enlargement.

The component of the momentum balance in the direction of flow is

$$F = m_1V_1 - m_2V_2 + p_1A_1 - p_2A_2$$

Substituting for F, noting that for incompressible fluids

$$m_1 = m_2 = A_1V_1$$

$$F = - p_1(A_2 - A_1) = V_1A_1(V_1 - V_2) + p_1A_1 - p_2A_2$$

Solving for the pressure change

$$p_2 - p_1 = \frac{V_1A_1(V_1 - V_2)}{A_2}$$

$$= V_1^2B(1 - B)$$

where $B = A_1/A_2 = V_2/V_1$ 3.2

Thus $\Delta h = \dfrac{p_2 - p_1}{\rho g} = \dfrac{V_1^2}{g}\left[B(1 - B)\right]$ 3.3

Δh so defined will be positive at the enlargement.

If there were no loss of head due to eddy turbulence the (ideal) pressure rise would equal the kinetic energy change

$$(\Delta h)\ \text{ideal} = V_1^2(1 - B^2)/2g \quad .... \ 3.4$$

An energy balance between sections (1) and (2) gives

$$\frac{V_1^2}{2g} + \frac{p_1}{\rho g} = \frac{V_2^2}{2g} + \frac{p_2}{\rho g} + H_L \quad ...... \ 3.5$$

where H_L is the friction loss due due to eddy turbulence.

Hence $H_L = \dfrac{V_1^2 - V_2^2}{2g} - \dfrac{p_2 - p_1}{\rho g}$

Substituting from (3.3) and rearranging gives,

$$H_L = \frac{V_1^{\,2}(1 - B^2)}{2g} - \frac{V_1^{\,2}(B - B^2)}{g}$$

$$= \frac{V_1^{\,2}(1 - B)^2}{2g} \qquad \text{.....3.1}$$

which is generally referred to as the Borda-Carnot equation.

The relative magnitude of the pressure terms may usefully be recorded at this stage.

(a) Comparing equations (3.1.) and (3.4.)

$$\frac{H_L}{\text{K.E. change}} = \frac{(1 - B)^2}{1 - B^2} = \frac{1 - B}{1 + B} \qquad 1.0$$

Hence the head loss should never exceed the pressure recovered and an abrupt expansion will always produce an increase in static pressure.

(b) Comparing equations (3.3.) and (3.1.)

$$\frac{\text{Rise } \Delta h}{\text{Loss } H_L} = \frac{2B}{1 - B}$$

$B = \frac{1}{2}$; net rise $= 2H_L$

$B = \frac{1}{3}$; net rise $= H_L$

$B < \frac{1}{3}$; net rise $< H_L$

(c) Differentiation of equation (3.3) gives

$$\frac{d(\Delta h)}{dB} = \frac{V_1^{\,2}}{2g}\left(1 - 2B\right)$$

When $d(\Delta h)/dB = 0$, $B = \frac{1}{2}$

Also $d^2(\Delta h)/dB^2$ is negative.

Hence, for a given upstream velocity maximum pressure recovery (maximum maximorum) will be obtained at $B = \frac{1}{2}$.

3. 3. Discussion of assumptions.

The accuracy of the Borda-Carnot expression for most practical cases is generally taken as sufficient proof of the validity of the simplifications assumed, any deviations which are registered being attributed to the assumption of a uniform velocity distribution - which is approached only with turbulent flow. A more rigorous solution can be obtained by modifying the simple theory to take account of the velocity distribution within the tubes. (This is developed in Section (3.5.)).

Nusselt (34) investigated the distribution of pressure over the wall face in the plane of the enlargement using high velocity air flow and concluded that the pressure p_1 in the upstream tube immediately before the expansion acts over the entire cross-sectional area A_2 at Section (1).

Whilst it is customary in developing theoretical equations to neglect the loss of head caused by skin friction between sections (1) and (2), figure (2), in practice experimental data do take account of such loss. This follows from the way in which the local head loss is defined. Flow disturbances introduced by the change of section will take some time to die away even after full bore flow has become established. Boundary layer growth will occur simultaneously and eventually flow in the larger section will become fully-developed. The individual contributions of these phenomena are not distinguishable in quantitative terms and the head loss caused by the abrupt change of section is defined as that loss over and above normal frictional loss incurred with full bore/fully developed flow. The following empirical rule is commonly adopted.

Friction gradients upstream and downstream of the change of section are extrapolated to the plane of enlargement and the step change in pressure at this point taken as the observed rise. The required head loss is given by the difference between the maximum pressure rise theoretically possible from the kinetic energy change and this measured rise.

Alternatively, recorded data may be corrected for frictional loss according to empirical correlations or predetermined data which, strictly speaking, apply only to full bore/fully developed flow. If plots are then prepared of boundary pressure vs. distance, the applied corrections have the effect of producing curves which become horizontal once the full regain of pressure head from velocity head has been realised. This maximum constant value of the pressure rise should exactly correspond to the value obtained by the previous method.

3. 4. Literature Survey.

On the assumption that full bore flow was established within 2 pipe diameters of the expansion, Baer (35) failed to record the full regain of pressure energy from kinetic energy and experimentally determined head losses were consequently in excess of the theoretical values.

Brightmore (36) studied the loss of head at abrupt expansions using 3" or 4" diameter upstream pipes and a 6" downstream section. Preliminary experiments were conducted to determine friction factors required in the main series of experiments. Results obtained under fully turbulent flow conditions were presented graphically in the form of plots of experimental vs. theoretical values. Good agreement was claimed in only one case and even here some discrepancy may be noted. Recorded losses were found to be less than the predicted values, the deviation decreasing with increasing expansion ratio (A_2/A_1).

Gibson (37) (38) followed the same procedure in a comprehensive series of experiments using pipes of different cross sections with diverging boundaries inclined at various angles. Little information is available on the head loss at abrupt enlargements in circular pipes, though a greater range of expansion ratios was employed than by Brightmore. Experimental values were expressed as a percentage of the theoretical loss. This percentage was not found to vary in any definite manner with velocity but could be correlated by the formula,

$$H_L = \frac{102.5 + 0.25(A_2/A_1) - 2.0(D_1)}{100} \times \left[\frac{(V_1 - V_2)^2}{2g} \right]$$

Velocities used were ambiguously reported as "averaging" between 1.83 and 21.0 ft./sec.

The summary of Gibson's data reproduced below shows that experimental losses were generally somewhat higher than the theoretical values, (simple theory).

TABLE (1)

pipe size (ins.)			percentage loss:	
D_1	D_2	A_2/A_1	experimental	by formula
0.65	2.15	10.96	103.5	103.9
0.50	1.50	9.00	102.8	103.7
1.00	3.00	9.00	102.1.	102.8
1.50	3.00	4.00	101.7	100.5
2.00	3.00	2.25	99.2	99.1
Brightmore's findings compare as follows:				
3.00	6.00	4.00	97.5	97.5
4.00	6.00	2.25	92.0 (approx.)	95.0

Archer (40) produced a highly detailed paper dealing specifically with head losses incurred at abrupt expansions using pipes of circular section. An extensive range of area ratios was investigated for fully turbulent flow. Allowance for friction loss was made according to such empirical correlations as were available at the time. The maximum pressure recovery and subsequent decrease in static pressure due to frictional loss were clearly recorded in all trials. Tappings were unfortunately rather widespread around the point of reattachment of the jet and measured data were in some cases much in excess of the theoretical rise. Archer's results may be summarised:-

$$H_L = 1.098\, V_1^{1.919}\, (1 - B)^{1.919} / 2g$$

$$L = 17.4(D_2 - D_1)^{0.4}$$

Where L = distance of peak (observed) rise from plane of enlargement (ins.)

and D_2, D_1 are expressed in inches.

A thorough examination of Archer's work is reported in a later section (A.II) following an account of the author's own experiments.

The apparatus of Schutt (39) was so designed as to obviate the need for friction loss corrections. The abrupt expansion was affected by inserting a nozzle into a length of straight pipe of uniform bore, the nozzle being specially shaped to avoid any "vena contracta" at the enlargement. Photographs illustrating the flow pattern in a similarly constructed expansion are given by Rouse (41). The friction gradients upstream and downstream of the nozzle were consequently equal and the observed pressure rise was defined by the vertical distance between the two parallel gradients. (This is simply a variation on the basic technique described above for determining the experimental rise.)

In conjunction with a 6" nominal bore tube four nozzle sizes were used giving a range of expansions from $B = 0.111$ to $B = 0.353$. Pressure tappings extended some 25 pipe diameters upstream and 40 pipe diameters downstream of the change of section. Fully turbulent flow conditions prevailed throughout the complete set of experiments, the Reynolds number in the pipe being not less than 20,000 in any instance. Average deviations were less than 1.5% of the value predicted by the Borda-Carnot equation, the occasional negative result implying that even this was to some extent caused by experimental error.

These early studies (all completed before 1930) whilst not entirely in agreement with one another clearly indicate that discrepancies between theory and practice are only slight when flow is fully turbulent in both sections.

With the exception of Archer's paper no information is given about the location of the section at which full-bore flow may be considered to begin nor are static pressure measurements quoted for the intervening zone.

More recent studies have been concerned with more complex flow conditions e.g. laminar flow, compressible fluid flow, incompressible flows at elevated temperatures and pressures, flow of visco-elastic fluids, and two-phase flows. Such studies have necessitated various modifications of the simple theory. These may conveniently be set out in full at this stage.

3. 5. Pressure changes at abrupt expansions (modified theory)

The simple theoretical equations quoted earlier are repeated below for easy reference.

Bernoulli equation
$$\left[\frac{p_2 - p_1}{\rho g}\right]_s = \frac{V_1^2}{2g}(1 - B^2) - (H_L)_s \quad \ldots\ldots 3.5$$

theoretical rise
$$\left[\frac{p_2 - p_1}{\rho g}\right]_s = \frac{V_1^2}{g}(B - B^2) \quad \ldots\ldots 3.3$$

head loss, by difference
$$(H_L)_s = \frac{V_1^2}{2g}(1 - B)^2 \quad \ldots\ldots 3.1$$

Where V_1 is the average value over the cross-sectional area A_1 of the time-smoothed velocity.

i.e. V_1 = total flow rate/total area.

The suffixes M and S will be used from hereon to denote theoretical values according to the modified or simple theory.

(a) In order to take the effect of velocity distribution into account Kays (42) introduced momentum correction factors defined as

$$\alpha = \frac{1}{AV^2}\int_0^A u^2\, dA$$

where u is the time-smoothed velocity at any point in the stream,

and **V** is the average velocity as before.

From the basic equation $F = \alpha_1 m_1 V_1 - \alpha_2 m_2 V_2 + p_1 A_1 - p_2 A_2$

the pressure rise is now obtained as

$$\Delta h_M = \left[\frac{p_2 - p_1}{\rho g}\right]_M = \frac{V_1^{\,2}}{g}\left(\alpha_1 B - \alpha_2 B^2\right) \quad \ldots\ldots 3.6$$

α_1, α_2 referring to the upstream and downstream section respectively.

If the Bernoulli equation is written

$$\left[\frac{p_2 - p_1}{\rho g}\right]_M = \frac{V_1^{\,2}}{2g}\left(1 - B^2\right) - H_L^{*}$$

Substituting from (3.6.) leads to

$$H_L^{*} = \frac{V_1^{\,2}}{2g}\left[1 - 2B\alpha_1 + B^2(2\alpha_2 - 1)\right] \quad \ldots\ldots 3.7$$

which clearly reduces to

$$H_L^* = \frac{V_1^2}{2g}(1 - B)^2 = (H_L)_s$$

if $\alpha_1 = \alpha_2 = 1.0$

(b) Mendler (43) suggested that the Bernoulli equation, too, should be rewritten, incorporating kinetic energy correction factors to account for the velocity profiles.

Defining $$\gamma = \frac{1}{AV^3}\int_0^A u^3 dA$$

the Bernoulli equation in its modified form reads

$$\left[\frac{p_2 - p_1}{\rho g}\right]_M = \gamma_1 \frac{V_1^2}{2g} - \frac{\gamma_2 V_2^2}{2g} - (H_L)_M$$

$$= \frac{V_1^2}{2g}(\gamma_1 - \gamma_2 B^2) - (H_L)_M$$

Substituting for $\left[\frac{p_2 - p_1}{\rho g}\right]_M$ leads to

$$(H_L)_M = \frac{V_1^2}{2g}\left[\gamma_1 - 2B\alpha_1 + B^2(2\alpha_2 - \gamma_2)\right] \quad \ldots 3.8$$

Where $(H_L)_M$ is the true head loss predicted by the modified theory.

In appendix I a method of evaluating α and γ (plotted as a function of Reynolds number in Fig 46)

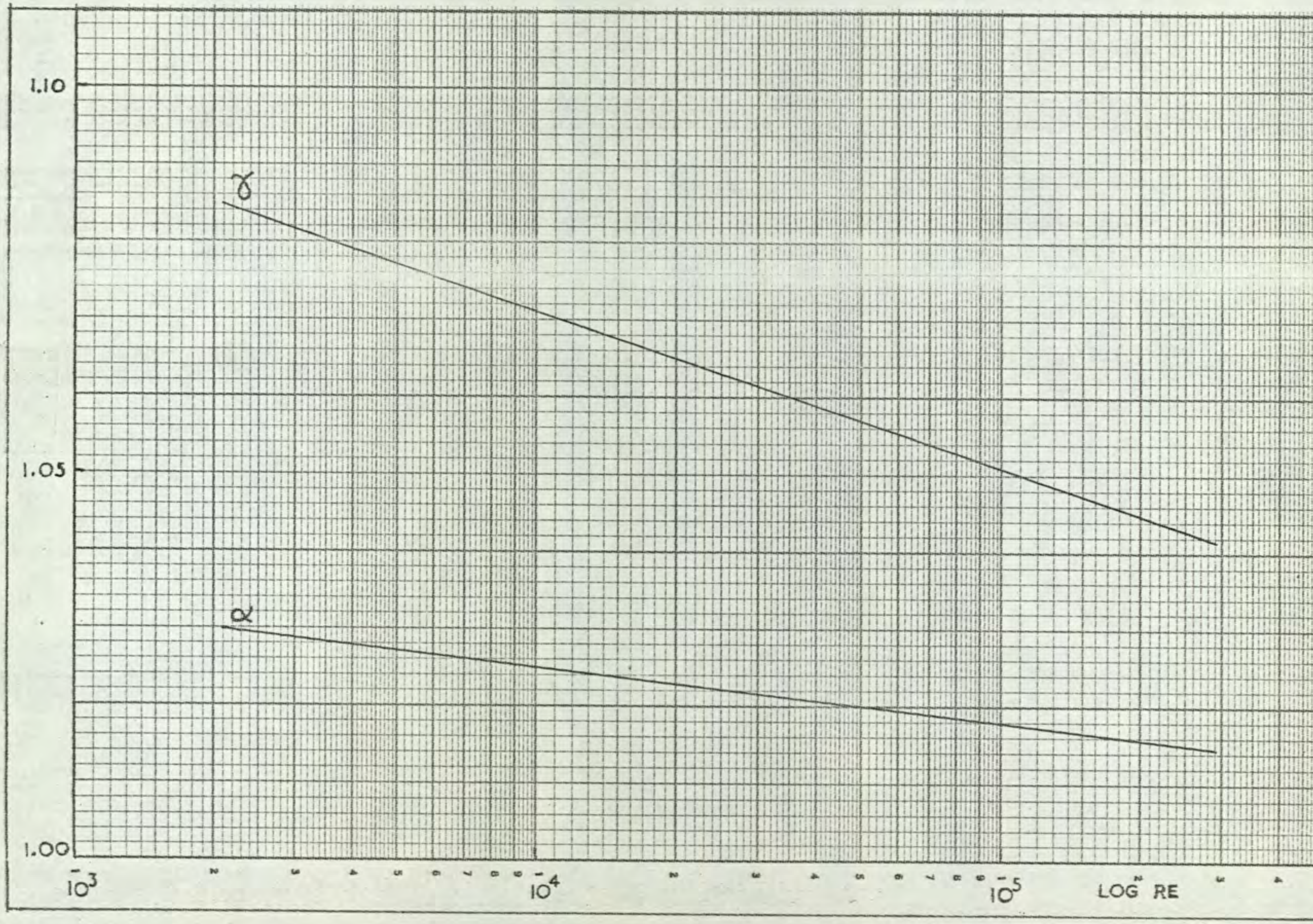

FIG 46

is developed. It is sufficient for the moment to observe that γ is greater than α and that both α and γ tend to unity with increasing Reynolds number (i.e. as the velocity profiles become flatter). According to this analysis the values under turbulent flow conditions range from

$$\alpha = 1.03, \qquad \gamma = 1.085 \quad \text{at} \quad Re = 2100, \text{ to}$$

$$\alpha = 1.018, \qquad \gamma = 1.051 \quad \text{at} \quad Re = 10^5$$

Writing $\alpha = 1 + \Delta$ the corresponding value of γ is given by $\gamma \simeq 1 + 2.8\Delta$

The general effect of modifying the simple theory may usefully be recorded at this stage. Only the case in which turbulent flow conditions exist in both sections is examined here.

Consider first the modified form of the momentum equation:

$$\left[\frac{p_2 - p_1}{\rho g}\right]_M = \Delta h_M = \frac{V_1^{\,2}}{g}\left[\alpha_1 B - \alpha_2 B^2\right] \qquad \ldots\ldots \; 3.6$$

(i) At small expansion ratios

$$\alpha_2 \simeq \alpha_1$$

and the above equation simplifies to

$$\Delta h_M \simeq \frac{V_1^{\,2}}{g}\,(B - B^2)\alpha_1$$

i.e. $\quad \Delta h_M \simeq \alpha_1 \Delta h_s \qquad \ldots\ldots \; 3.9$

by comparison with equation (3.3.).

Thus the modified theory predicts a greater pressure rise than the simple theory.

(ii) Large expansion ratios (B small).

In the extreme,

$\alpha_1 = 1.00$ and $\alpha_2 = 1.03$

Hence, $\Delta h_M = \Delta h_s \left[\dfrac{1 - 1.03B}{1 - B} \right]$

showing that it is theoretically possible for Δh_M to be less than Δh_s.

The value of B required to affect such a change in α would, however, be so excessively low that

$(1 - 1.03B)/(1 - B)$ approaches 1.0

Hence $\Delta h_M \simeq \Delta h_s$

Head losses are predicted by the modified theory according to the equation

$$(H_L)_M = \frac{V_1^{\,2}}{2g} \left[\gamma_1 - 2B\alpha_1 + B^2(2\alpha_2 - \gamma_2) \right] \qquad \ldots.\ 3.8$$

By comparison with the simple theoretical equation,

$$(H_L)_s = \frac{V_1^{\,2}}{2g} \left[1 - 2B + B^2 \right] \qquad \ldots.\ 3.1$$

noting that $\alpha = 1 + \Delta$, $\gamma \simeq 1 + 2.8\Delta$

and hence $B^2(2\alpha_2 - \gamma_2) \simeq B^2$

$(H_L)_M > (H_L)_S$

Thus the general effect of modifying the simple theory is to predict greater pressure recoveries and also slightly higher eddy losses.

3. 6. Literature Survey (continued).

Experimental data obtained by Bissiri (44) were incorporated in a paper by Kays (42) primarily concerned with abrupt contraction and expansion losses in multiple-tube systems, such as compact heat exchanges. Using a single tube system Bissiri determined expansion losses for two expansion ratios with water as the fluid medium. The maximum Reynolds number in the upstream section was of the order of 7000. In order to obtain measurable pressure changes under conditions of low Reynolds number, pipe diameters were extremely small: an upstream section 0.18 ins. I.D. was coupled with downstream sections 0.34 ins. I.D. ($B = 0.280$) or 0.555 ins. I.D. ($B = 0.105$). Sufficient pressure tappings (in the form of piezometer rings) were provided upstream and downstream to enable the static pressure to be determined as a function of distance. The experimental rise was then ascertained by extrapolation to the plane of enlargement. To take into account the velocity distribution within the pipes - a significant factor at low Reynolds numbers - the basic theory was modified by introducing momentum correction factors

$$\alpha = \frac{1}{AV^2}\int_0^A u^2 dA$$

By substituting into this expression for α the modified Karman-Prandtl relationship.

$$u = V\left[\sqrt{4\psi}\,(2.15 \log {}^{y}/r + 1.43) + 1.0\right]$$

the following expression was obtained

$$\alpha = 1.09068(4\psi) + 0.05884(4\psi)^{\frac{1}{2}} + 1.0$$

in which ψ is a friction factor defined by

$$\psi = \frac{\tau}{v^2/2g}$$

Values of ψ were calculated from the correlation

$$\psi = 0.049\mathrm{Re}^{-0.2}$$

Graphs of α as a function of Reynolds number are given by Kays for various tube geometries. For the case of single tubes of circular cross-section the computed values of α ranged from 1.058 at Re = 2100 to 1.039 at Re = 20,000. These values are seen to be rather higher than those calculated by the author (1.03 to 1.023) and also show a greater variation with increasing Reynolds number.

Calculated values of ψ do not differ significantly from values of 2ϕ calculated from the Blasius equation

$$\phi = 0.0396\,Re^{-0.25}$$

The factor 2.0 arises from the definition of ϕ as

$$\phi = \frac{\tau}{V^2/g}$$

Re = 2100	$\psi = 0.01061$	$2\phi = 0.01170$
Re = 20000	$\psi = 0.00676$	$2\phi = 0.00666$

Bissiri's results are presented in the form of loss coefficients defined according to the equation:

$$H_L^* = \frac{V_1^2}{2g}(K) \quad \ldots\ldots 3.7$$

where $K = 1 - 2\alpha_1 B + B^2(2\alpha_2 - 1)$

Since this expression for K neglects the greater kinetic energy correction factors a sounder and more straightforward check on the modified theory may be made by comparing the measured rise with the predicted rise according to equation (3.6).

$$\Delta h_M = \frac{V_1^2}{g}(B\alpha_1 - B^2\alpha_2) \quad \ldots\ldots 3.6$$

Since the transition from laminar to turbulent flow takes place at different mass flow rates in each section three distinct flow situations are possible:

flow in both tubes turbulent; upstream flow turbulent downstream flow laminar; and laminar flow in both tubes.

(i) The case of turbulent/turbulent flow has already been considered but requires a brief re-examination in the light of Kays' higher values for α

The general relationship is obtained from equations 3.6 and 3.3

$$\Delta h_M = \Delta h_s \left[\frac{\alpha_1 - \alpha_2 B}{1 - B} \right] \qquad \ldots\ldots\ 3.10$$

for values of $\alpha_2 \simeq \alpha_1$ this simplifies to

$$\Delta h_M = \Delta h_s \ (\alpha_1) \qquad \ldots\ldots\ 3.9$$

When α_2 is significantly greater than α_1

Δh_M will exceed Δh_s

if the term in square brackets [eqn. (3.10)] is greater than 1.0,

i.e. if $\dfrac{\alpha_1 - \alpha_2 B}{1 - B} > 1.0$

In the extreme $\alpha_2 = 1.070$ corresponding to $Re_2 = 2100$.

Thus the required condition is that

$$\alpha_1 - 1.0 > 0.07B$$

Substituting the minimum value of B employed - 0.105 the required condition is: $\alpha_1 > 1.0 + .00735$.

In fact, since Re_1 max $\simeq 7000$, $\alpha_1 \not< 1.05$ (Kay's Value).

(ii) The laminar/laminar case is the simplest to analyse since $\alpha_1 = \alpha_2 = 4/3$ (app.I)

$$\therefore \Delta h_M = \Delta h_s (4/3)$$

(iii) The interdependence of α_1, α_2 and B makes it difficult to formulate a perfectly general expression for the turbulent/laminar case.

From equation (3.10)

Δh_M will be greater than Δh_s

if $$\frac{\alpha_1 - \alpha_2 B}{1 - B} > 1.0$$

i.e. if $\alpha_1 - \frac{4B}{3} > 1 - B$ in the present case.

Simplifying: $\Delta h_M > \Delta h_S$ if $B < 3(\alpha_1 - 1)$ (3.11)

The two expansion ratios investigated by Bissiri will now be examined separately.

(a) $B = 0.28$

Max. Re_2 for laminar flow conditions $= 2,100$:

$\alpha_2 = 4/3$

Max. $Re_1 = 3970$ - corresponding min

$\alpha_1 = 1.057$

Min. $Re_1 = 2100$ - corresponding max

$\alpha_1 = 1.070$

Substitution of these values into equation (3.11) reveals that the required condition is not fulfilled in this case. The modified theory predicts

$$\Delta h_M = \Delta h_S (0.966)$$

or

$$\Delta h_M = \Delta h_S (0.951)$$

for the particular values of α_1 quoted above.

(b) $B = 0.105$ max.$Re_2 = 2100$ $\alpha_2 = 4/3$

max. $Re_1 = 6480$ $\therefore \alpha_1 = 1.053$

min. $Re_1 = 2100$ $\therefore \alpha_1 = 1.070$

For this expansion ration $B < 3(\alpha_1 - 1)$ and

$$\Delta h_M = 1.04 (\Delta h_S)$$

or

$$\Delta h_M = 1.02 (\Delta h_S)$$ respectively.

In contrast, the author's data for α predict smaller rises according to the modified theory for both expansion ratios, the actual factors being of the order of 0.91 (when $B = 0.28$) and 0.99 (when $B = .105$).

Figures (3) and (4) show the measured rise in static pressure (as a fraction of the value predicted by the simple theory) plotted against log Re. The

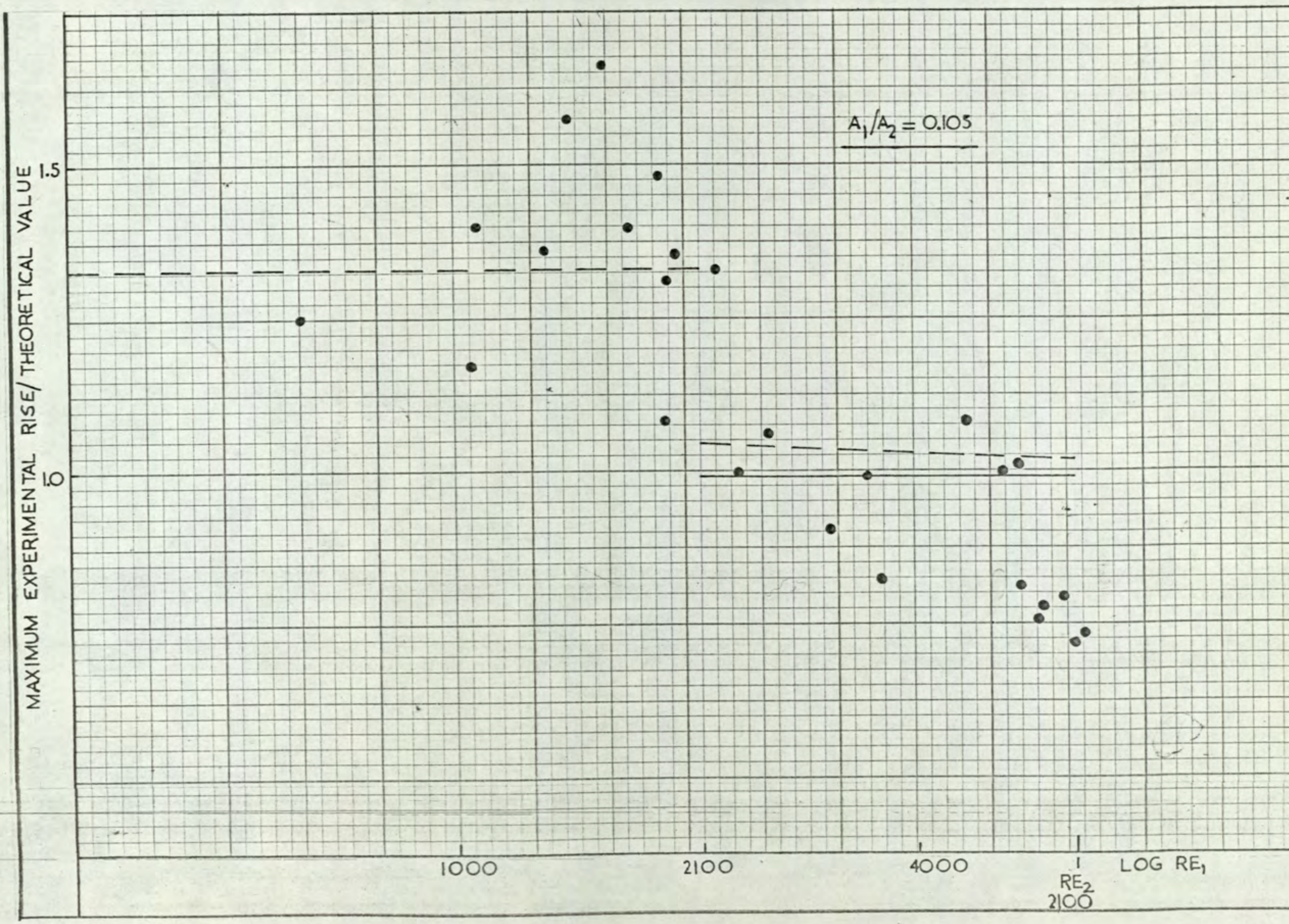

$A_1/A_2 = 0.105$
1.5
1.0
MAXIMUM EXPERIMENTAL RISE/ THEORETICAL VALUE
1000
2100
4000
1
RE_2
2100
LOG RE_1

fig. 3

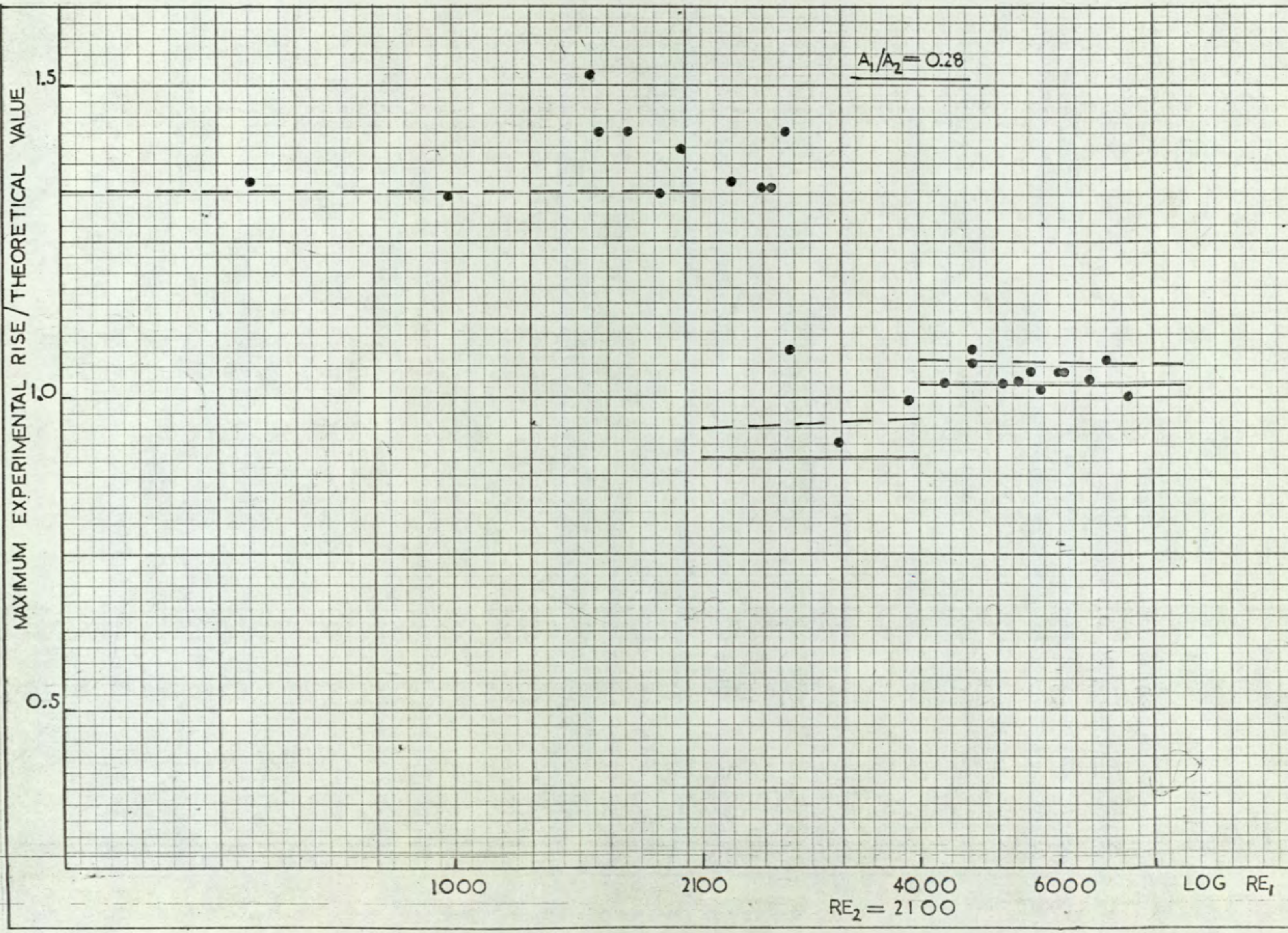
A1/A2 = 0.28
MAXIMUM EXPERIMENTAL RISE / THEORETICAL VALUE
1.5
1.0
0.5
1000
2100
4000
6000
LOG RE1
RE2 = 2100

Fig. 4

dashed lines indicate values according to the modified theory. (Using Bissiri's values of α above $Re_1 = 2100$.)

Considerable scattering of the data is to be observed in the case when $B = 0.105$, at which expansion ratio downstream Reynolds numbers never exceed 2,200.

When $B = 0.28$ laminar flow conditions appear to persist in the upstream section up to $Re = 2600$. The onset of turbulent flow in the downstream section occurs when $Re_1 = 4000$. The dashed and full lines shown above $Re_1 = 2100$ represent theoretically predicted values using Bissiri's data and the author's data for α respectively. The average increase predicted by modifying the basic theory is only 3.2% in this zone. On the basis of these results Bissiri's values of α appear to over-correct for the velocity distribution.

In conclusion it may be stated that the modified theory (i) is a marked improvement on the simple theory for laminar/laminar flow: (ii) offers no advantage over the simple theory for turbulent/laminar flow, and (iii) is of advantage in the case of turbulent/turbulent flow only when circumstances demand a very precise value and extreme care has been

fig. 5

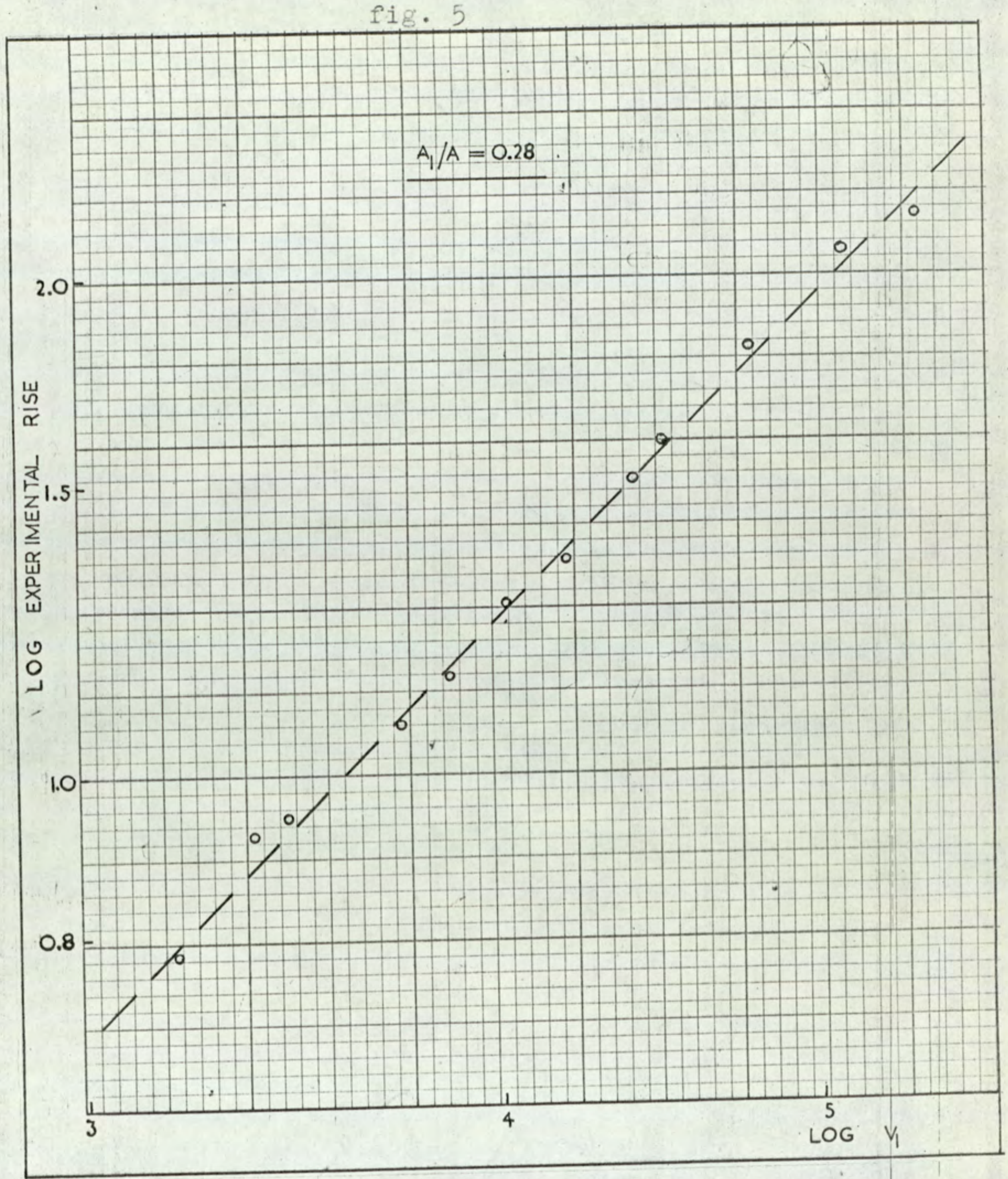

taken in setting up the pipeline.

In anticipation of the author's own findings a plot of log (observed rise) vs. log (V_1) for the turbulent/turbulent case is presented here (fig. 5.). The dashed line on fig (5) is drawn with a slope of 2.0 and indicates that there is no discrepancy in this respect between theory and practice.

A recent thesis by Mendler (43) reporting the results of two-phase flow studies at abrupt expansions includes a brief account of preliminary single phase experiments, using water at 500 psia and approximately 410°F. A range of expansion ratios was obtained by joining various diameter upstream sections to a single downstream section (1 ins. I.D. nominal bore). Pressure tappings in the expanded section were located not less than 9 pipe diameters from the plane of enlargement and the point of reattachment of the jet cannot therefore be ascertained in Mendler's experiments. Hydraulic gradients upstream and downstream were extrapolated to the plane of enlargement and the step change at this point taken as the experimental rise. Results were expressed in the form of loss coefficients, experimental head losses being considerably less than the values predicted by the simple Borda-Carnot equation. This discrepancy exceeded any error that could result from failing to take account of the velocity profile even at the lowest flow rates (minimum Reynold's number).

Mendler suggested that the Bernoulli equation could be rewritten incorporating kinetic energy correction factors. No means of evaluating γ was, however, formulated. In any case, discrepancies in the value of H_L are the result of differences between the measured pressure rise and the theoretical rise (for which the modified theory had already been developed). It has further been shown (section 3.5.) that the introduction of momentum and kinetic energy correction factors leads to correlations which predict increased values of both the pressure rise and the loss due to eddy turbulence.

Figure (6) compares the experimental rise with the predicted rise according to simple theory. A slight dependence upon expansion ratio may be observed, experimental values approaching the theoretical (dashed) curve as B increases.

In figure (7) the experimental rise is plotted as a function of mass flow rate, $G/10^6$ (ρ being constant within $\pm\frac{1}{2}\%$). The dashed lines express

fig. 6

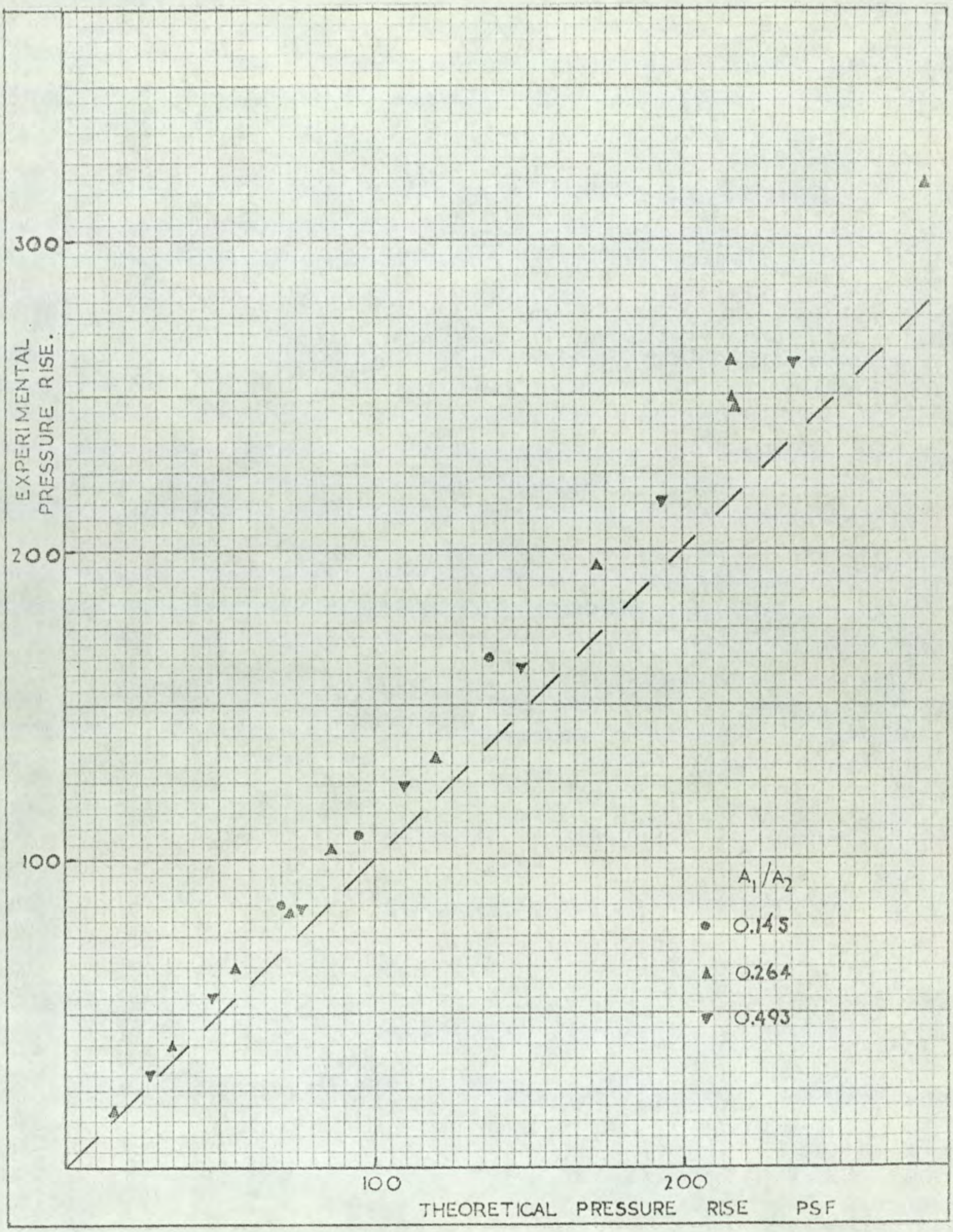
300
200
100
EXPERIMENTAL PRESSURE RISE.
100
200
THEORETICAL PRESSURE RISE PSF
A_1/A_2
0.145
0.264
0.493

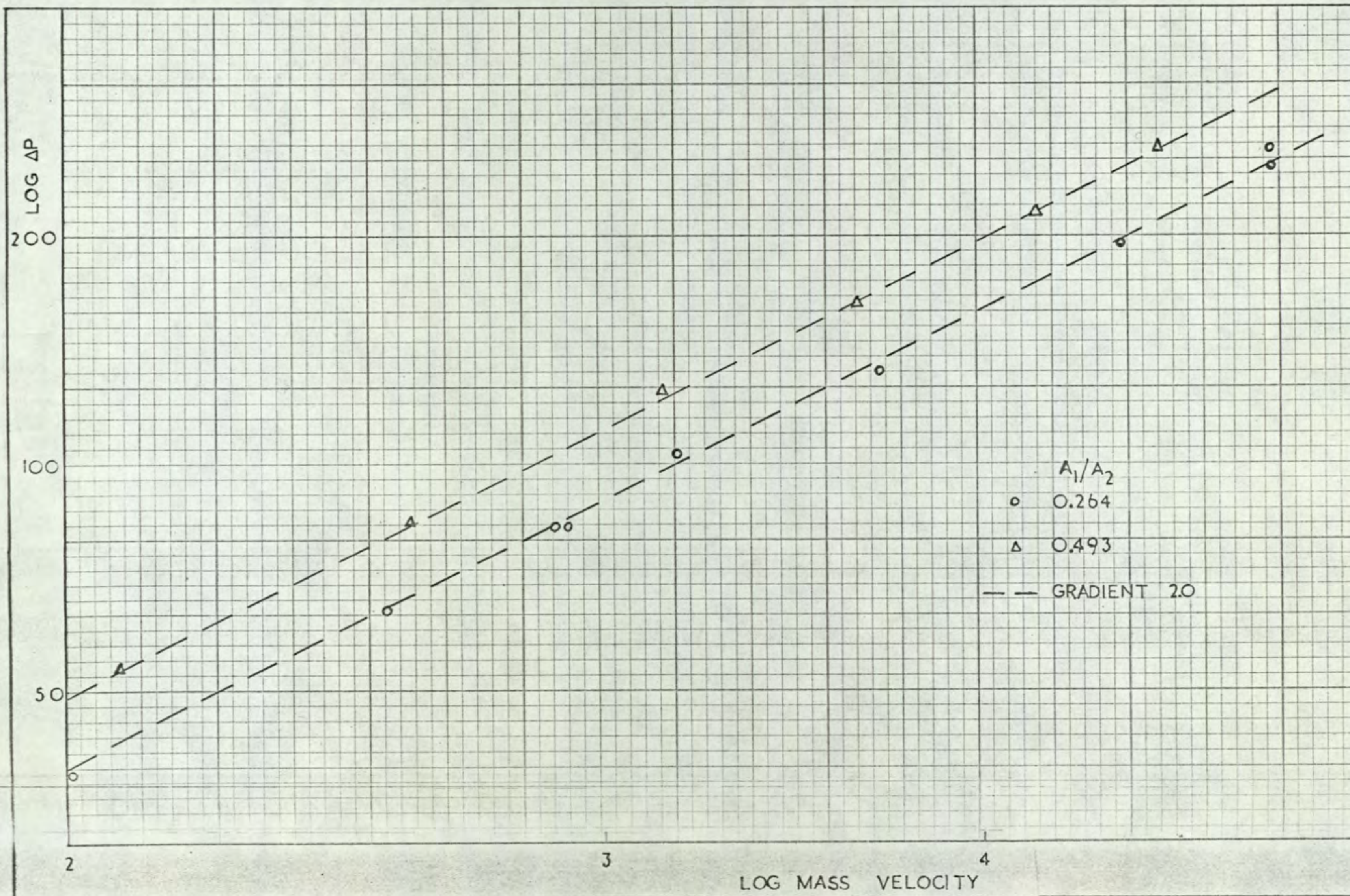
LOG ΔP
200
100
50
2
3
4
LOG MASS VELOCITY
A1/A2
0.264
0.493
GRADIENT 2.0

fig.7

the theoretical relationship between pressure rise and the square of the fluid velocity.

Astarita and Nicodemo (45) have investigated the flow of visco-elastic fluids through abrupt expansions using dilute aqueous solutions of a vinyl polymer.

The modified forms of the equations for predicting the pressure rise and expansion loss, presented here in section 3.5, were developed since correction factors for momentum and kinetic energy are more significant in the case of visco-elastic fluids. The momentum correction factor is introduced as,

$$\alpha' = \alpha \phi_M$$

where α takes into account the non-flat velocity profile and ϕ_M accounts for departure from Newtonian flow. The kinetic energy factor is similarly defined:

$$\gamma' = \gamma \phi_E$$

Premature substitution for the momentum terms ($mV = \rho A V^2$) inadvertently led to additional corrections for kinetic energy in the momentum equation (45).

Since velocity profiles in steady turbulent flow of visco-elastic liquids are steeper than for

Newtonian fluids values of α cannot be determined as in appendix I. The velocity profile is defined as

$$\frac{u}{V} = \frac{u\ max}{V}\left[1 - \frac{r}{R}\right]^{q}$$

where u,V are the point and average velocities,

$$\frac{u\ max}{q} = \frac{q+2}{q} \quad \text{and} \quad q > 1.0$$

When $q = 2$ this expression corresponds to laminar flow of Newtonian fluids.

Correlations for α and γ may be derived as in appendix I.

$$\alpha = (q + 2)/(q + 1)$$

$$\gamma = 3(q + 2)^2/(q + 1)(3q + 2)$$

Setting $q = 1.0$ gives a triangular velocity profile and the extreme values of α and γ

$$\alpha = 1.5, \qquad \gamma = 2.7$$

A single expansion was used (diameter ratio = 9.6/20) and results are only of a qualitative nature. Increased pressure rises and higher losses due to eddy turbulence were recorded in accordance with the predictions of the modified theory. Values of ϕ_M ϕ_E and q were not, however, capable of being determined from the results obtained.

If the rate of energy dissipation in a turbulent flow field is lower in viscoelastic liquid than in a purely viscous liquid increased jet lengths would be expected (jet length being defined as the distance from the plane of enlargement to the peak pressure rise). Comparative tests with water confirmed this theory. Further increases in jet length were obtained when the concentration of the solution was increased or the velocity was increased at a fixed concentration.

The experiments performed with water were not described in detail. Measured pressure rises essentially agreed with values predicted by the simple theory though a slight increase with increasing velocity could be detected. Jet lengths were unvarying with velocity. When observed static pressure changes were expressed in the dimensionless form,

$$\frac{p_2 - p}{g} \times \frac{1}{\Delta h_s} \quad \text{i.e.} \quad \frac{p_2 - p}{V_1^2(B - B^2)}$$

where p is the measured pressure at any station between sections 1 and 2 of figure (2)., the pressure distribution was found to be constant in the downstream section, irrespective of velocity. Expressed in velocity heads the static pressure falls from unity at the plane of enlargement ($p = p_1$) to zero in the reattachment region of the jet (where $p = p_2$).

Benedict, Carlucii and Swetz (46) claim to have "essentially confirmed" the loss coefficients predicted by the Borda-Carnot expression, using water as the test fluid. Very slight evidence was however presented in support of this claim, the bulk of the published data relating to head losses sustained when compressible fluids (air) flow through abrupt enlargements. Compressible loss coefficients differed significantly from those predicted for constant density fluids, particularly at high flow rates. The use of a total pressure parameter was advocated as having greater significance and utility than the loss coefficient parameter. The total pressure loss (expressed as the ratio T.P.R.) across a given abrupt enlargement essentially is conserved in the sense of being the same for all fluids.

$$\left[\frac{1}{\text{T.P.R.}}\right]_{\text{Inc}} = \frac{P_2}{P_1} = 1 - (1 - R)K$$

where

$$P = \rho V^2/2g + p \quad \text{(at stations 1 or 2)}$$

$$p = \text{absolute pressure}$$

$$R = p_1/P_1$$

$$K = \text{loss coefficient} = (1 - B)^2$$

A plot of $^1/$T.P.R. vs R may be prepared by substituting specimen values of R (0.95, 0.9, 0.85 etc.) into the above expression, for each expansion ratio.

For adiabatic flows the compressible total pressure ratio is given by

$$\left[\frac{1}{\text{T.P.R.}}\right]_{comp} = \frac{P_2}{P_1} = \frac{\Gamma_1}{\Gamma_2} \times \frac{A_1}{A_2}$$

in which Γ is a generalised compressible flow function defined in (46).

When experimental total pressure losses for compressible flows were evaluated from the above expression and compared with the predicted values for constant density fluids striking agreement was noted, maximum deviations being less than 0.4%.

4. Experimental Study: Static Pressure Variations at Abrupt Expansions.

4. 1. Apparatus.

Using water as the fluid medium, variations in the static pressure downstream of an abrupt enlargement were determined experimentally for a range of expansion ratios.

The basic flow loop, which was subsequently to be employed in the mass transfer experiments, was conveniently of an all-glass construction. The complete circuit for the present series of experiments is shown diagramatically in figure (8) and also presented in plates (1), (2).

The reservoirs each had a capacity of 20 litres and connecting pipework was $1\frac{1}{2}$ ins. I.D. Water was circulated by a centrifugal pump with a glass impeller, heat developed by the pump being removed with the aid of a cooling coil in order to maintain a constant fluid density. A sensitive mercury thermometer graduated in $^1/_5$°C indicated the temperature of the test fluid. The rate of flow was accurately measured with specially calibrated rotameters. After flowing through the test-section the water was returned to the reservoirs via a dip pipe extending well below the surface level. In order to facilitate starting up a by-pass was provided across the cooling coil and also a return line from the pump outlet to flow loop.

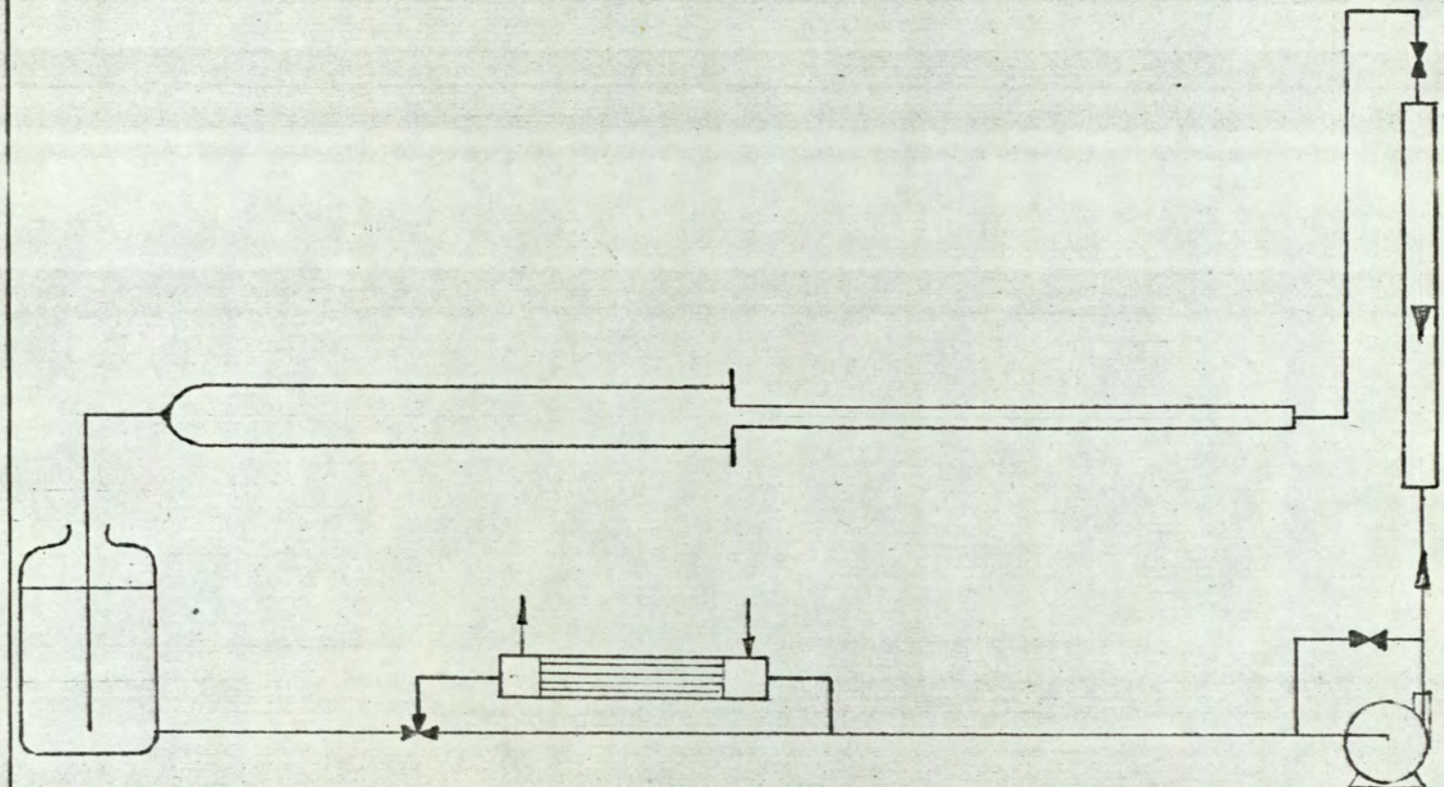

fig. 8

inlet side.

The test sections were fabricated from clear perspex tubing, cast tubes being used in preference to extruded tubes because of the closer tolerances on the bore. A range of expansion ratios was obtained by joining downstream sections of various diameters to a single upstream pipe, (0.74 ins ID).

Flanges were cut from ½" perspex sheeting and glued into the tubes using a cement made by dissolving perspex shavings in chloroform. Care was taken that the tubes should be normal to the flanges. Gaskets were cut from soft natural rubber and mild-steel backing flanges used to ensure a leak-proof joint without distortion of the flanges. The rigidity of the flanges effectively guarranteed that the tubes were co-axial when supported horizontally by means of 'U' bolts.

Pressure tappings were made by drilling 1/16" diameter holes in the tube wall taking care to leave no burrs on the inside surface. 1 ins. pieces of 1/8" I.D. tubing were glued into position over these holes. Clear polythene tubing connected these to the manometers or manifold.

The upstream section was 72" long (approx. 100 pipe diameters) to ensure that flow was fully-developed at the expansion. Two pressure tappings were provided in this section $\frac{3}{4}$" from the plane of enlargement, at opposite ends of the horizontal diameter. Each of these was joined to one limb of a pair of manometers.

Downstream sections were 3 ft. long for tubes up to 3" I.D. and 6 ft. long for larger diameters. 10 to 12 pressure tappings were provided in the downstream sections. These were largely concentrated in the region where the peak rise was to be expected in the light of Archer's work (40). The precise positions of the tappings in each case are clearly shown in Tables 4

With regard to the problem of determining true average static pressures Perry (47) notes that this is generally impractical except in the case where flow is in straight lines parallel to the confining walls. For streams of this class the sum of the static head and gravitational potential head is the same at all points of a cross-section taken perpendicular to the direction of flow. An average static pressure measurement can therefore be obtained by making a piezometer opening in the duct wall at any convenient point on the circumference. The belief that a piezometer ring automatically averages the possibly slightly differing pressures on the various openings is dismissed. Should there be any real difference between the time-averages of the pressures on the separate openings it is prima facie evidence that the flow is not wholly parallel to the walls. Under such conditions, even supposing that the reading on a gauge connected to a piezometer ring is actually the mean of the readings that would be obtained by attaching several gauges to the separate holes, the reading has no definite relation to the true average static pressure (47).

For the present series of experiments pressure tappings were located along the base of the downstream section. All the pressure tappings in the downstream section were connected to a common manifold.

The manifold itself was made from two 3 ft. lengths of 1" I.D. copper ~~water pipe~~ blanked off at one end and joined by a short length of hose. The two sections of the manifold were arranged in line for 6 ft. tubes or side by side for 3 ft. downstream sections. The manifold was fitted with a total of 18 taps. The most appropriate of these were connected to the piezometer openings in the downstream section by short lengths of clear polythene tubing and another to the second limb of the manometer. Great care was taken that no air pockets should remain in the manifold during test-runs.

4. 2. Manometry.

When measuring large changes in static pressure a simple inverted manometer was used (air/water). A bleeder cock fitted at the U bend allowed air to be expelled when setting up the manometer. Taps were also provided at the foot of each limb of the manometer.

In order to measure accurately small pressure differences a manometer fluid was required with a density close to that of water. Such a system would have a magnifying power, compared to an air/water manometer, equal to the reciprocal of the difference in densities: thus the more nearly equal the densities, the greater the magnification factor. Fluctuations in static pressure due to the unsteady nature of the flow in the annulus surrounding the expanding jet would of course be magnified by the same factor and a judicious balance had to be chosen between increased magnification and excessive sensitivity.

Of the organic liquids commonly used with water benzyl alcohol ($\rho = 1.048$) was considered unsuitable because of its limited range, while carbon tetrachloride ($\rho = 1.594$) would not have provided the necessary magnification without resorting to the use of inclined manometers.

Paraffin ($\rho = 0.787$) was used in a number of trials but the vast majority of low values were measured with o-xylene ($\rho = 0.881$).

Densities of manometer fluids relative to water were determined at ambient temperature, which differed by no more than 2 or 3 degrees from the temperature of the test fluid. Densities were determined by weighing a glass sinker in air, water, and the manometer fluid. By Archimedes' principle :

$$\text{Relative density} = \frac{\text{wt. of sinker in air} - \text{wt. in fluid}}{\text{wt. of sinker in air} - \text{wt. in water}}$$

Precautions against inaccurate weighings due to wall and surface tension effects were carefully observed.

The density of pure o-xylene determined in this manner was 0.877 which compares well with the data given by Timmermans (48). However after preliminary trials a slight increase was noted in the density of the reclaimed fluid due to the pure liquid becoming saturated with water. The relative density of the saturated o-xylene was determined as 0.881. No significant change was recorded in the density of water after prolonged contact with o-xylene.

The magnification factor is evaluated as follows:

$$\text{Pressure difference} = \frac{\Delta \mathring{h} \rho_w - \Delta \mathring{h} \rho_f}{30.48} \text{ ft. of water}$$

where, $\Delta \mathring{h}$ is the observed pressure difference measured in cms., and, ρ_w and ρ_f are the densities of water and saturated fluid at the working temperature (relative to water at $4^{\circ}C$).

$$\therefore \text{Pressure change} = \frac{\Delta \mathring{h} \rho_w (1 - S.G.)}{30.48} \text{ ft. of water}$$

For o-xylene, S.G. = 0.881

$\therefore$ Pressure difference $= \Delta \mathring{h}(0.998)(0.119)/30.48$

$= \Delta \mathring{h}/256.65$

For paraffin, S.G. = 0.787

$\therefore$ Pressure difference $= \Delta \mathring{h}(0.998)(0.213)/30.48$

$= \Delta \mathring{h}/143.38$

The similarity of the densities meant that alternate slugs of water and o-xylene, once formed in the narrow bore of the manometer ($\frac{1}{4}$") would not settle out, and it was therefore imperative to avoid violent movement within the manometer. As a precaution against film wetting of the manometer surface, manometers were regularly cleaned by washing with a little alcohol and soaking overnight in decon solution, all traces of which were thoroughly rinsed away before the manometers were recharged.

Manometers were charged in the following manner. The manometer was first completely filled with water and a funnel fitted to the bleeder cock with a short length of tubing was filled with the manometer fluid. With this tap open water was slowly allowed to drain from each limb in turn thus drawing in the fluid. When the meniscus reached the mid-position in each limb (the zero of the scale) the tap at the base of the limb was closed. The short length of tube below the tap remained filled with water due to surface tension effects, allowing the connecting tube - also filled to avoid trapping air - to be gently pushed on.

4. 3. Calibration of Rotameters.

To calibrate the rotameter the fiducial velocity (F_T) is first calculated from the equation,

$$F_T = K_2 \left[\frac{w(\sigma - \rho)}{\sigma \times \rho} \right]^{\frac{1}{2}}$$

where K_2 is a constant for the particular rotameter = 5.81

w is the weight of the float = 416.0 gms.

and σ is the density of the float material = 2.53 gms/cc

At the working temperature (21°C) ρ = 0.998 gms/cc.

$\therefore$ F_T = 92.32

The actual flow rate is given by

$$F' = f' \times F_T$$

the factor f' depending upon the rotameter reading.

fig. 9

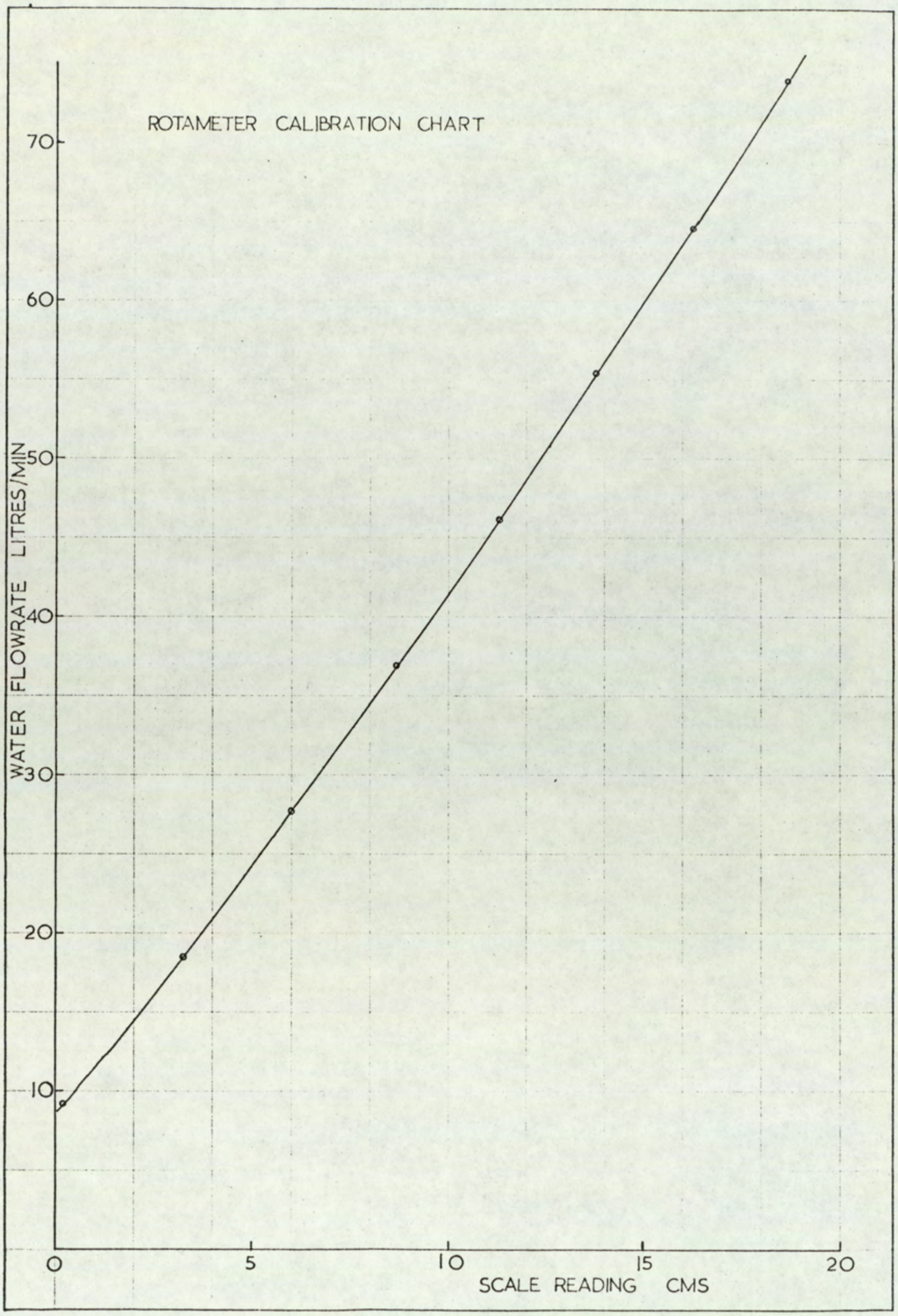
ROTAMETER CALIBRATION CHART
WATER FLOWRATE LITRES/MIN
10
20
30
40
50
60
70
0
5
10
15
20
SCALE READING CMS

Charts of scale reading (cms) as a function of flow impedance I', with f' as a parameter, enable the actual flow rate to be determined in relation to the scale reading. The flow impedance is constant for an incompressible fluid at constant temperature and is given by,

$$I' = \log_{10}\left\{ K_1 \times \frac{\mu}{\rho} \times 10^4 \times \left[\frac{\sigma \times \rho}{w(\sigma - \rho)}\right]^{\frac{1}{2}} \right\}$$

where $K_1 = 3.44$ and $\mu = .0098$ poises at $21^{\circ}C$

$\therefore \quad I' = 1.33$

Table 2.

f'	0.1	0.2	0.3	0.4	0.5	0.6	0.7	0.8
scale	0.2	3.27	6.0	8.67	11.3	13.8	16.27	18.67
F'	9.23	18.46	27.70	36.93	46.16	55.39	64.62	73.86

The calibration curve of flow rate vs scale reading is plotted in figure (9).

The accuracy of this calibration procedure has been confirmed by Akers (49).

4. 4. Corrections for Friction loss between Pressure Tappings.

Measured values of the pressure change include a friction loss upstream and downstream of the enlargement. The question of correcting measured data for friction losses downstream of the enlargement was raised in section 3.3

and will be discussed in section 5 - (analysis of results).

Friction losses for the upstream and downstream sections were computed from full bore/fully developed flow correlations. Friction factors were calculated by means of the Blasius equation which applies for smooth tubes with Reynolds numbers less than 10^5:

$$\phi = 0.0396\ Re^{-0.25}$$

Friction losses were obtained from the equation:

$$h_f = 4\phi \left[\frac{l}{d}\right]\left[\frac{u^2}{g}\right] \quad \frac{\text{ft. head}}{\text{ft. length}}$$

Friction data are appended in Table (3).

4. 5. Start-up Procedure.

The lower section of the circuit, comprising reservoirs, supply line and pump, was filled with water and the three-way tap arranged so that the water supply by-passed the cooling coil. A stopcock was initially included in the circuit between the pump and rotameter to allow the pump to be started against a back pressure at this stage. Considerable difficulty was, however, experienced in maintaining a leak-proof valve in this position and the valve had therefore to be removed and the following procedure adopted. The valve at the head of the rotameter was firmly shut off and the return line from the pump outlet to inlet side cracked open. This reduced the risk of damaging the

the lower floatstop in the rotameter due to compression of the air and surging of the float when the pump was switched on. This return line was subsequently kept closed. As the rotameter and test section gradually filled up, water pumped from the reservoirs was replenished until eventually the system was completely filled. The level in the reservoirs was maintained as high as possible to avoid vortex formation and the consequent entrainment of air. In order to sweep all air from the rotameter and test section the flow rate had to be increased to the point where the float rested against the upper stop. The by-pass across the cooling coil was provided solely to avoid damaging the coil during this step. In the case of the $4\frac{1}{2}$ ins. diameter test section a bleeder valve was required on the top of the pipe near to the enlargement to allow air trapped in the recirculation zone to be expelled.

The rapid expansion of the fluid at the enlargement and also immediately following the valve resulted in dissolved air being expelled from solution. Deaeration of the test fluid was further aided by recirculating the water without cooling - the solubility of gases decreasing with increasing temperature. The main objective in de-aerating the water was to avoid the development of large air bubbles which could persist indefinitely in the recirculation zone at low flow rates, and which would perhaps seriously affect the shape of the jet as they oscillated to and fro. The use of a diaphragm valve at the head of the rotameter was found to produce serious fluctuations in flowrate and the original valve was therefore replaced by a needle valve.

4. 6. Experimental Procedure.

Preparatory to each test run the temperature of the water was raised to 21°C by continuous recirculation without cooling. The three-way tap was then arranged so that the fluid passed through the heat exchanger section and, with the rotameter set at the required position, the cooling water rate was adjusted to maintain a constant temperature of $21 \pm \frac{1}{2}$°C. The static pressure difference between the upstream and downstream tappings was observed by opening, in turn, each connection to the manifold. Screw clips on the connectors to the manometers served to damp out fluctuations in pressure and also ensured a slow change in meniscus level as each successive tap was opened. The height of the meniscus in each limb was read to the nearest $\frac{1}{2}$ mm., the meniscus itself oscillating between concave and convex with fluctuating pressure. At the end of each trial the meniscus was allowed to return to the zero position. With the rotameter set to provide a greater velocity the cooling water rate was readjusted before beginning the next run. Experimental runs were in general conducted at the same rotameter settings for each expansion ratio. Considerable difficulty was however experienced in maintaining a rotameter setting of 4.0 cms and in later trials a setting of 4.5 cms. was used.

5. Experimental Results

5.1 Mean Measured Pressure Change

Recorded data, converted to feet of flowing fluid, are appended in Table (4), which clearly shows the manometer fluid used in each case. The reproducibility of the data is demonstrated in figure (10)*: for a single expansion ratio (D_2 = 1 ins.) all measured pressure changes are plotted as a function of distance, with velocity - designated by the rotameter scale reading - as a parameter. In view of the minimal scattering of the data the observed rise was evaluated as the mean of recorded values.

Seemingly poor results were obtained with D_2 = 0.865 ins. (see figure 11). The fact that such results were reproducible suggests possible misalignment of the tubes or a marked difference in jet behaviour in this instance.

The results of Archer (40) reveal that it is not inconceivable that complete sets of measured pressure changes at a particular velocity should be in error. Such an event would suggest error in velocity measurement rather than static pressure measurement. In the experiments conducted by the author the difficulty experienced in maintaining a steady rotameter setting of 4.0 cms. scale reading could possibly be a source of such error. As a final check on the accuracy of the raw data graphs were

*INSIDE BACK COVER.

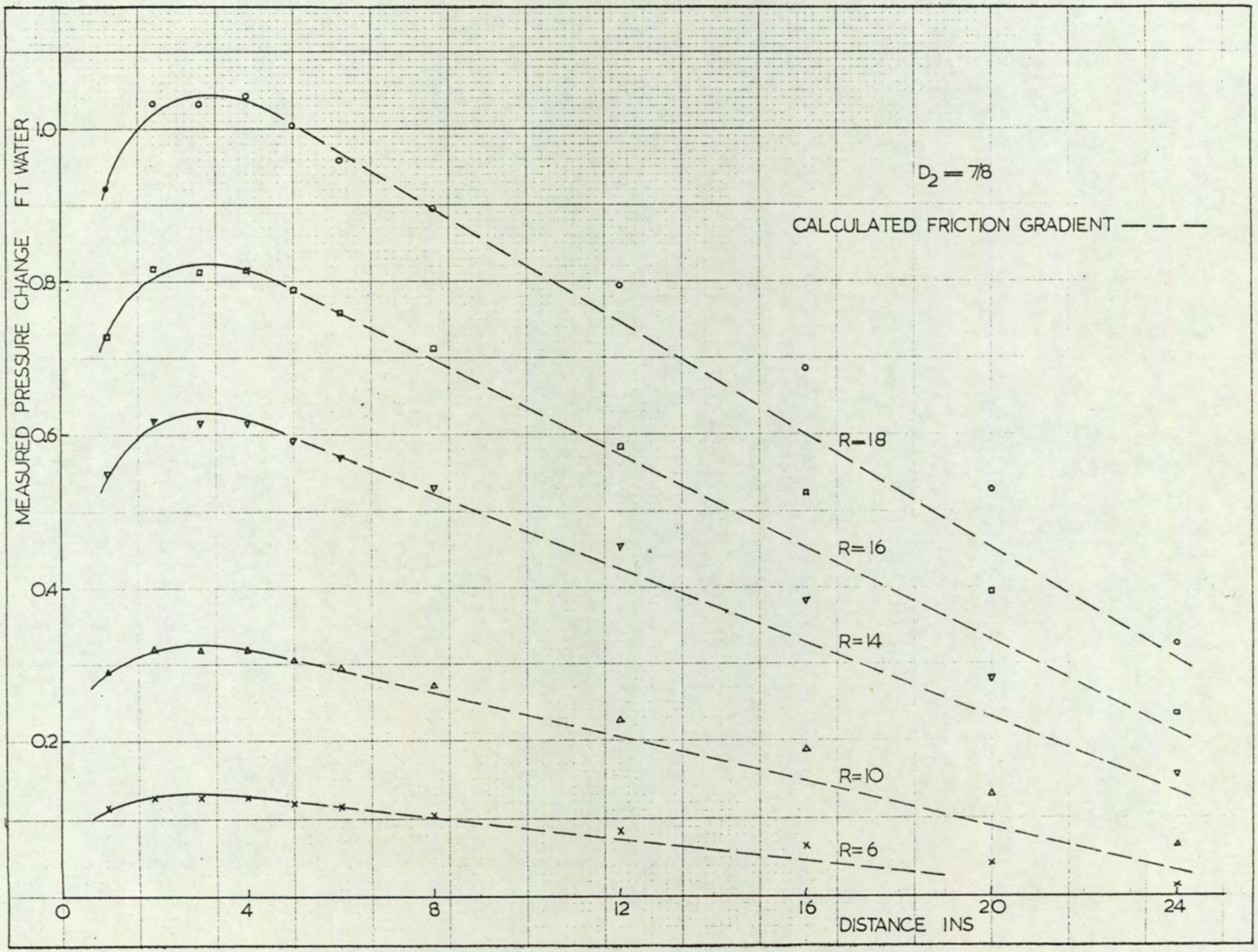
MEASURED PRESSURE CHANGE FT WATER
1.0
0.8
0.6
0.4
0.2
0
4
8
12
16
20
24
DISTANCE INS
D2 = 7/8
CALCULATED FRICTION GRADIENT — — —
R=18
R=16
R=14
R=10
R=6

Fig. 11

prepared of mean values at a particular station versus velocity (in terms of scale reading). Any consistently erroneous results at a given velocity would show a departure from the smooth curve. No serious discrepancies were in fact recorded. In those cases where different low velocities were employed such curves enabled experimental results to be interpolated at a rotameter setting of 4.5 cms. Figure (12) shows a typical set of curves for selected taps, when $D_2 = 2.085$ ins.

Mean values of the measured pressure change for a consistent set of upstream velocities at all expansion ratios are appended in Table (5).

5.2 Maximum Pressure Rise: Singly-corrected Data

Measured pressure changes recorded in Table (5) include a loss of static pressue due to wall friction in the short length of pipe between the upstream pressure tapping and the plane of enlargement. With regard to the question of wall friction in the jetting zone immediately downstream of the expansion, there is, as has been briefly mentioned elsewhere (section 3.3), an apparent discrepancy between theory and experiment. Improved insight into jet development and reattachment has been gained by resolving this question.

The theoretical equation for maximum pressure recovery is derived from a momentum balance between the plane of

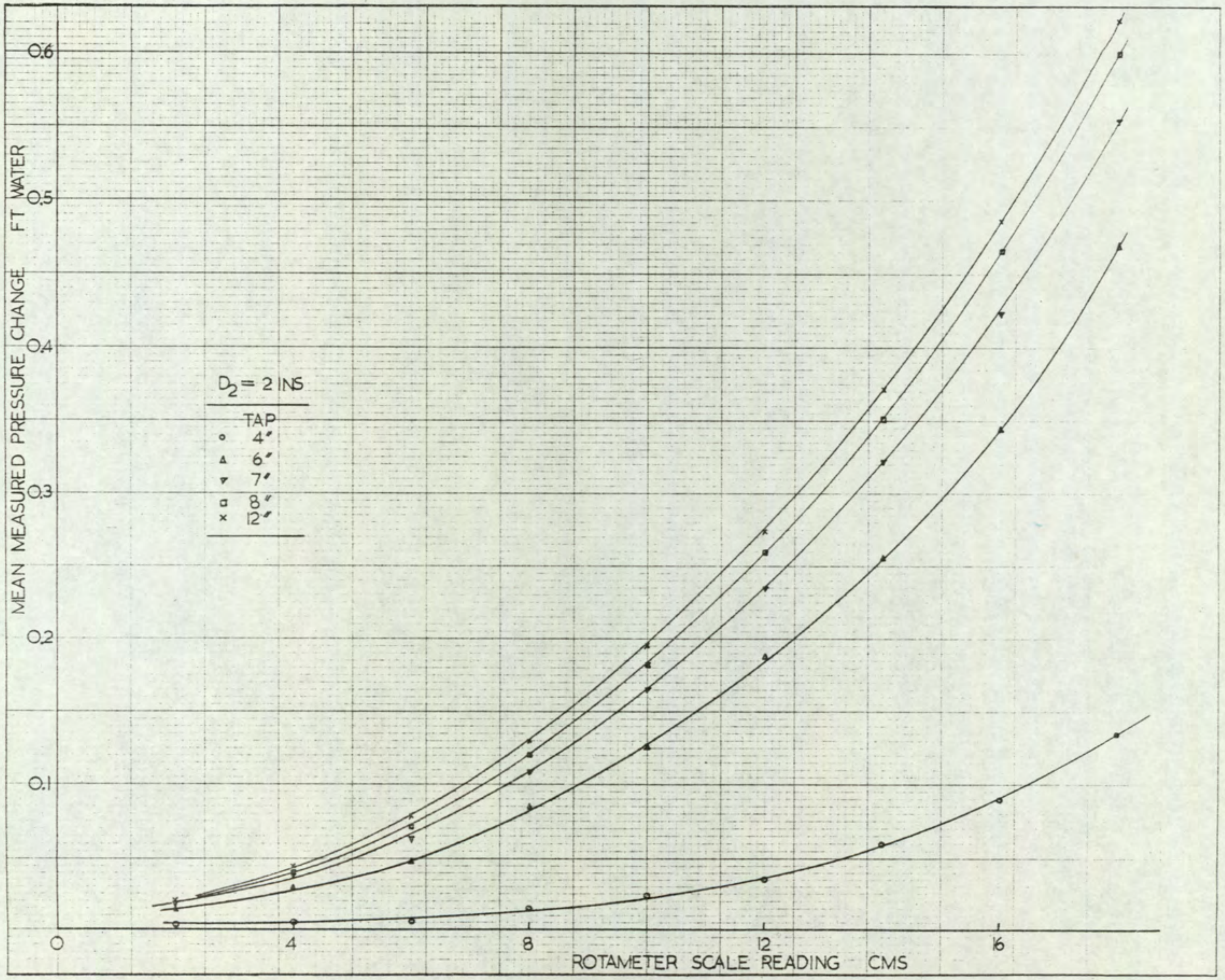
0.6
0.5
0.4
0.3
0.2
0.1
0
4
8
12
16
MEAN MEASURED PRESSURE CHANGE FT WATER
ROTAMETER SCALE READING CMS
D_2 = 2 INS
TAP
4″
6″
7″
8″
12″

fig. 12

enlargement and a section downstream of the zone of recirculatory flow (section 2 of fig. 2). By definition, the recovery of pressure head from velocity head is complete at section 2.

The experimental pressure rise conforming to the theoretical assumption of negligible wall friction between the plane of enlargement and section 2 may readily be obtained from the recorded data by adding to the measured peak pressure rise a correction for wall friction loss over the short length of pipe between the upstream piezometer opening and the plane of enlargement. Table (6) compares this value, $(\Delta h')$ max., with the predicted value according to simple theory, $(\Delta h)_s$, and the data are plotted in figure (13). For the sake of clarity values less than 0.1 ft. have been omitted in some cases. In figure (13) it is seen that $(\Delta h')$ max. tends towards $(\Delta h)_s$ with increasing expansion ratio, A_2/A_1, or more simply, with increasing downstream diameter, D_2. The dependence of $(\Delta h')$ max. on expansion ratio is not investigated further. Figure (13) suggests that discrepancies between $(\Delta h')$ max. and $(\Delta h)_s$ may be attributed to friction losses in the downstream section - such losses becoming less significant as D_2 increases for a fixed value of upstream diameter and velocity. Any error in the assumption of flat velocity profiles would, on the other hand, become more significant with increasing D_2,

TABLE 6. Maximum Pressure Rise - Singly-corrected Data

D_2/R	2	4.5	6	8	10	12	14	16	18
0.865 ins.									
Theory:	-	0.120	0.182	0.284	0.410	0.562	0.745	0.963	1.207
Experiment:		0.092	0.138	0.227	0.341	0.478	0.655	0.863	1.092
1.0 ins.									
Theory:	0.059	0.152	0.230	0.359	0.519	0.711	0.944	1.220	1.525
Experiment:	0.047	0.123	0.189	0.306	0.453	0.634	0.876	1.150	1.463
1.464 ins.									
Theory:	0.045	0.117	0.176	0.275	0.398	0.544	0.722	0.932	1.168
Experiment:	0.040	0.104	0.157	0.249	0.374	0.525	0.714	0.931	1.183
2.085 ins.									
Theory:	0.026	0.067	0.102	0.156	0.230	0.315	0.419	0.541	0.677
Experiment:	0.023	0.058	0.089	0.147	0.218	0.303	0.410	0.534	0.682
3.041 ins.									
Theory:	0.013	0.034	0.052	0.081	0.117	0.160	0.212	0.274	0.343
Experiment:	0.012	0.030	0.046	0.076	0.112	0.153	0.210	0.273	0.353
4.50 ins.									
Theory:	0.006	0.016	0.024	0.038	0.055	0.076	0.100	0.130	0.162
Experiment:	0.007	0.016	0.023	0.038	0.057	0.077	0.104	0.134	0.170

fig. 13

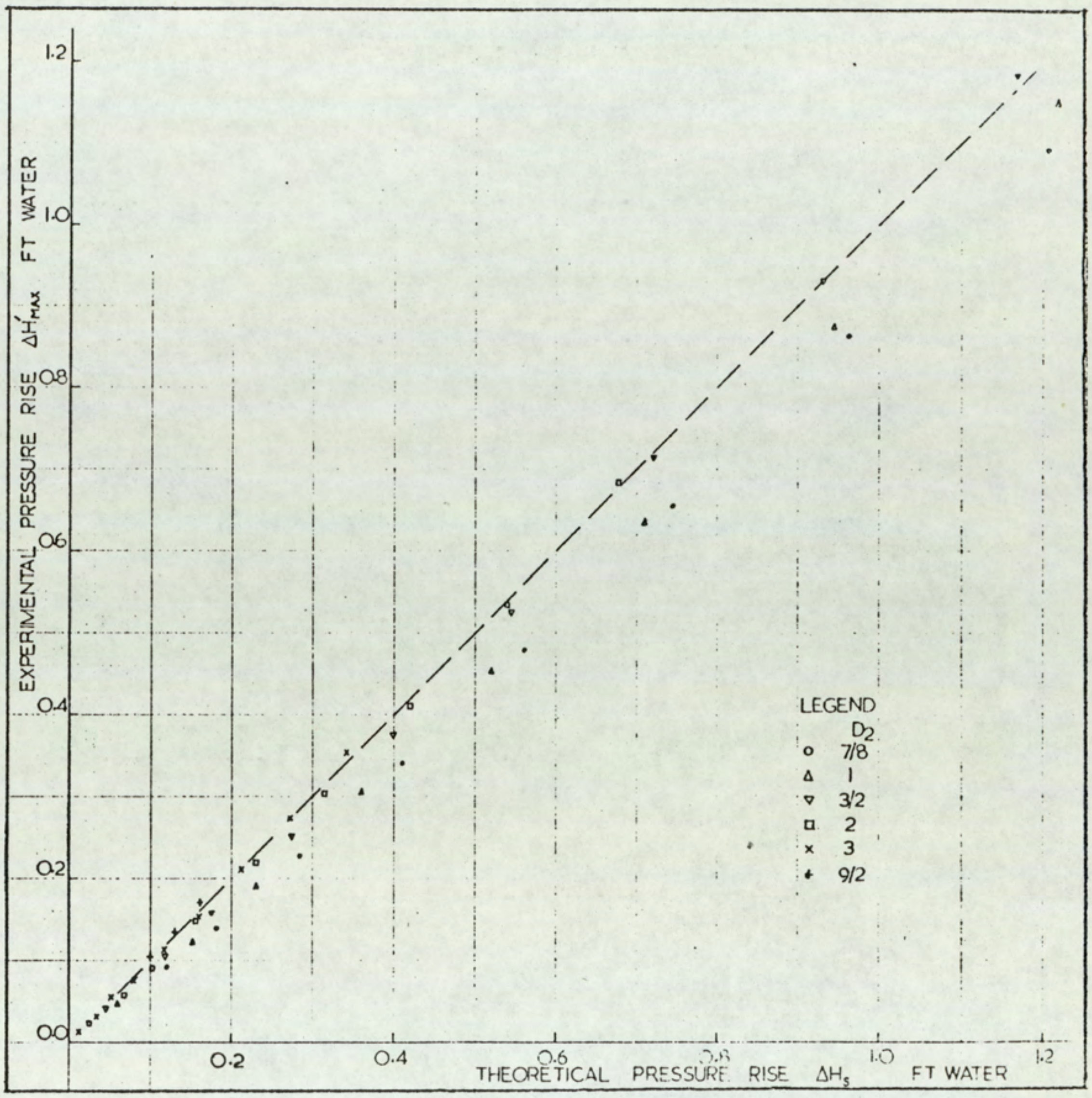

1.2
1.0
0.8
0.6
0.4
0.2
0.0
EXPERIMENTAL PRESSURE RISE $\Delta H'_{MAX}$ FT WATER
0.2
0.4
0.6
0.8
1.0
1.2
THEORETICAL PRESSURE RISE ΔH_s FT WATER
LEGEND
D_2
o 7/8
Δ 1
▽ 3/2
□ 2
x 3
+ 9/2

i.e. decreasing Re_2.

5.3 Maximum Pressure Rise: Doubly-corrected Data

This subsection is devoted to an examination of maximum experimental pressure rises evaluated in the usual fashion, which takes into account the loss of head in the downstream section due to wall friction.

When measured static pressure changes are corrected for friction loss between the respective pressure tappings upstream and downstream of the abrupt expansion the doubly-corrected pressure rise is found to increase until a constant maximum value is attained. The constancy of the maximum indicates good agreement between the experimentally determined hydraulic gradient and the calculated friction gradient and suggests that flow is essentially fully developed immediately downstream of the measured peak pressure rise. The application of friction loss corrections between the enlargement and the location of the measured peak rise according to a correlation for fully developed flow is evidently a considerable simplification. The efficiency of this simplification is not reflected by the doubly-corrected pressure rise curves: the same (doubly-corrected) peak pressure rise would be obtained by extrapolation of the hydraulic gradient back to the plane of enlargement. Figure (14) shows the general effect of downstream friction loss corrections at a low expansion ratio. The dashed lines on figure (14) correspond to measured mean values

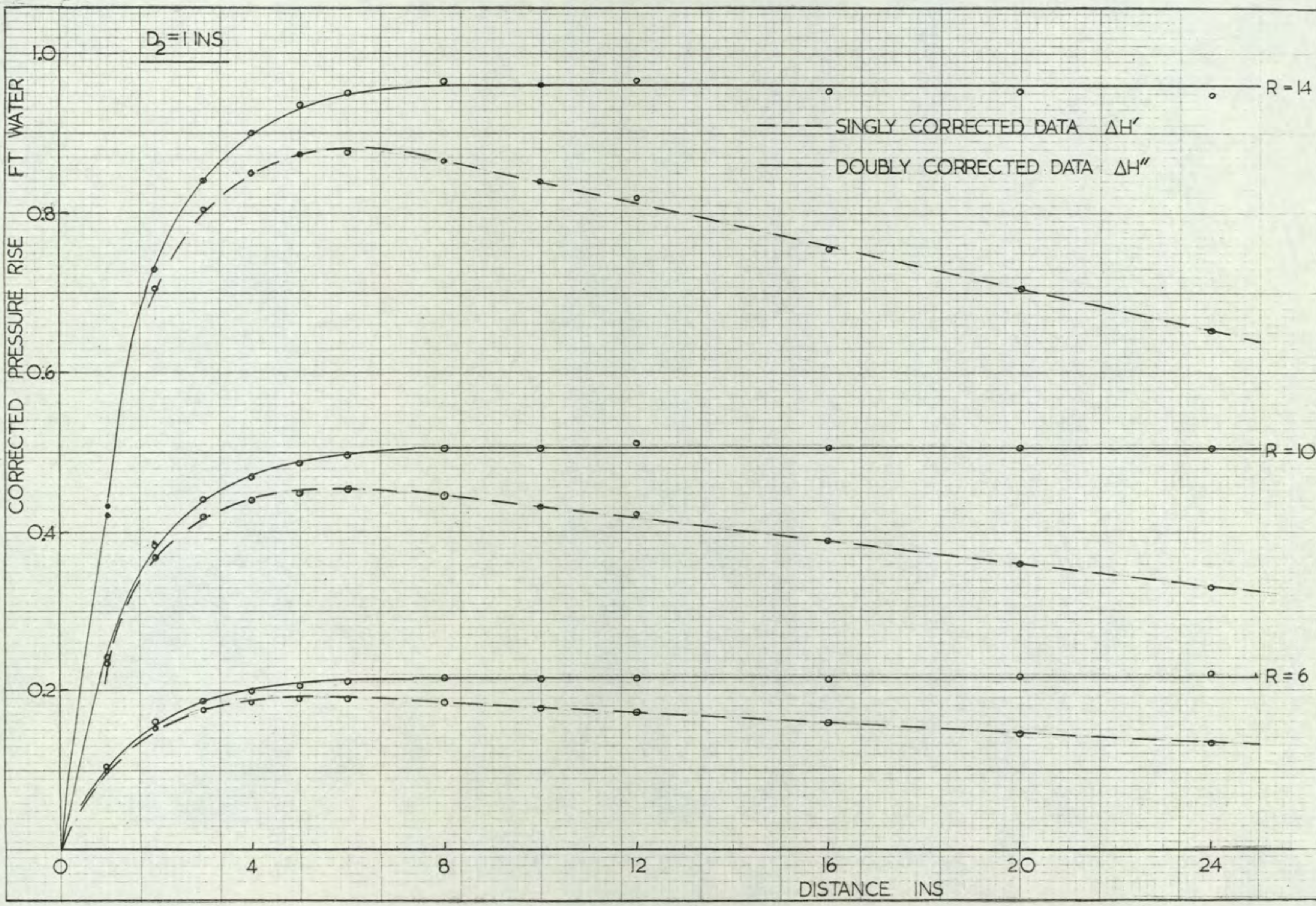
D2 = 1 INS
CORRECTED PRESSURE RISE FT WATER
1.0
0.8
0.6
0.4
0.2
0
4
8
12
16
20
24
DISTANCE INS
SINGLY CORRECTED DATA ΔH′
DOUBLY CORRECTED DATA ΔH″
R = 14
R = 10
R = 6

fig. 14

corrected only for upstream friction loss, i.e., $(\Delta h')max$.

The following definitions will be observed hereafter.

Measured pressure change - The mean pressure difference between the upstream tapping and any downstream tapping.

Singly-correct pressure change $(\Delta h')$ - The measured pressure change corrected for wall friction loss prior to the enlargement.

Doubly-corrected pressure change $(\Delta h'')$ - The measured pressure change corrected for friction loss both upstream and downstream of the enlargement.

Figures (15) to (20) show the doubly-corrected pressure changes for each expansion ratio as a function of distance, with upstream Reynolds number as a parameter. Data are tabulated in Table (7).

Interest is, for the moment, confined to the maximum values. Table (8) compares maximum values of the doubly-corrected pressure rise with the predicted rise according to simple theory. A graph of $(\Delta h'')$ max. versus $(\Delta h)_s$ confirms the usual observation that predicted values are accurate to within a few per cent (figure 21).

5.4 Correlation Between $(\Delta h)_s$ and $(\Delta h'')$ max.

The equation of the best straight line through the data of Table (8) was determined by a least mean squares

fig. 15

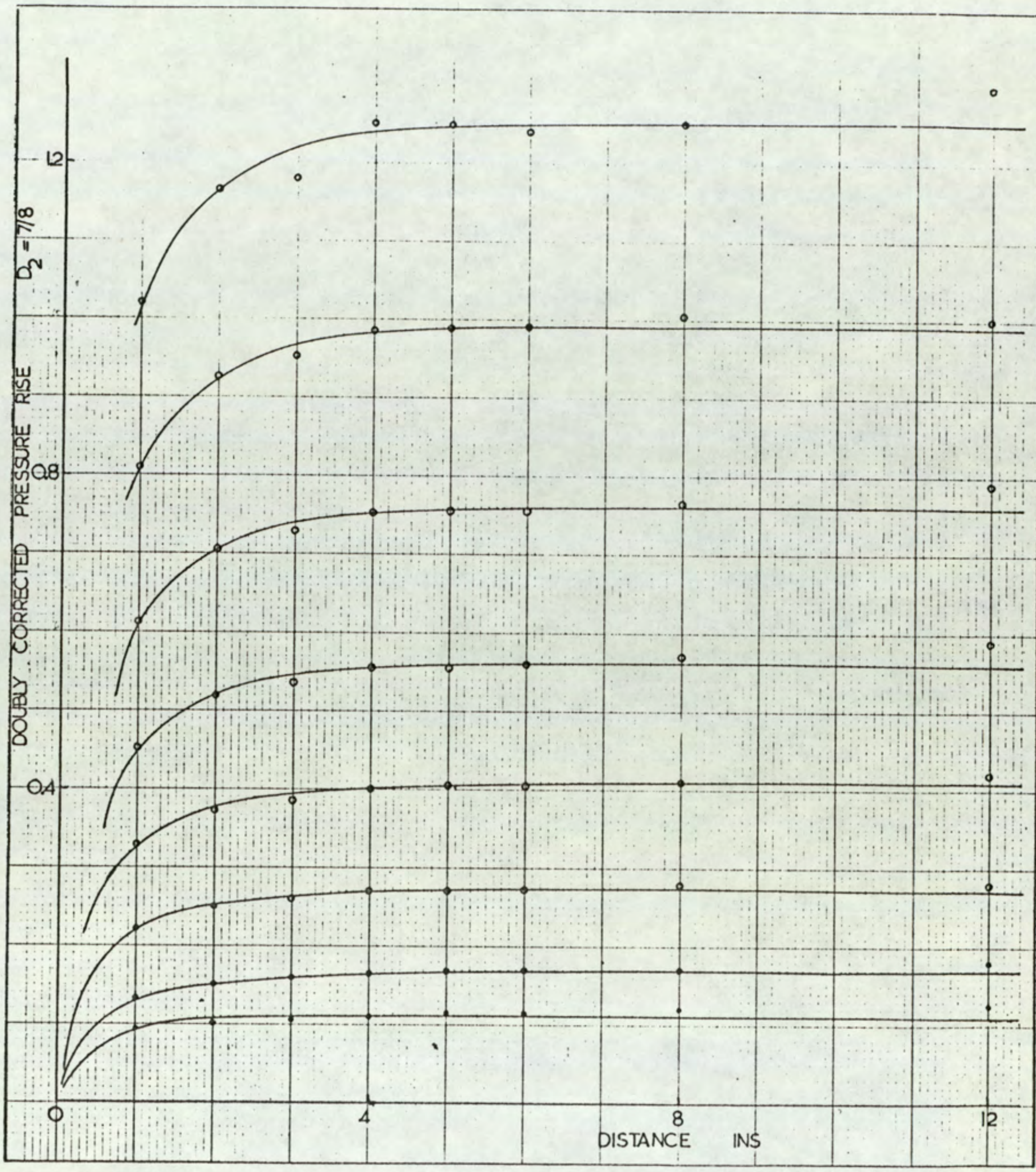
DOUBLY CORRECTED PRESSURE RISE
$D_2 = 7/8$
1.2
0.8
0.4
0
4
8
12
DISTANCE INS

fig. 16

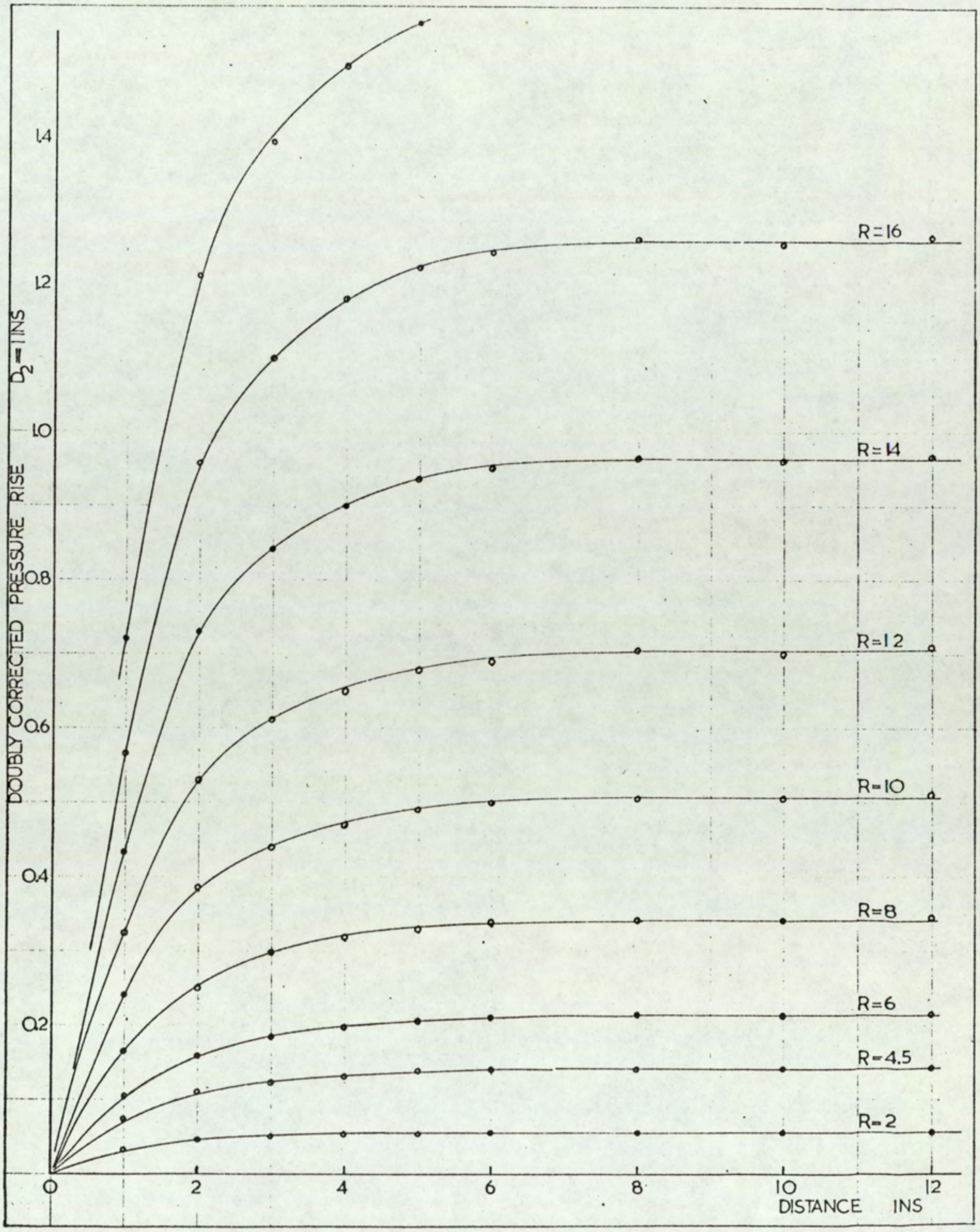

DOUBLY CORRECTED PRESSURE RISE D_2= I INS
1.4
1.2
1.0
0.8
0.6
0.4
0.2
0
2
4
6
8
10
12
DISTANCE INS
R=16
R=14
R=12
R=10
R=8
R=6
R=4.5
R=2

fig. 17

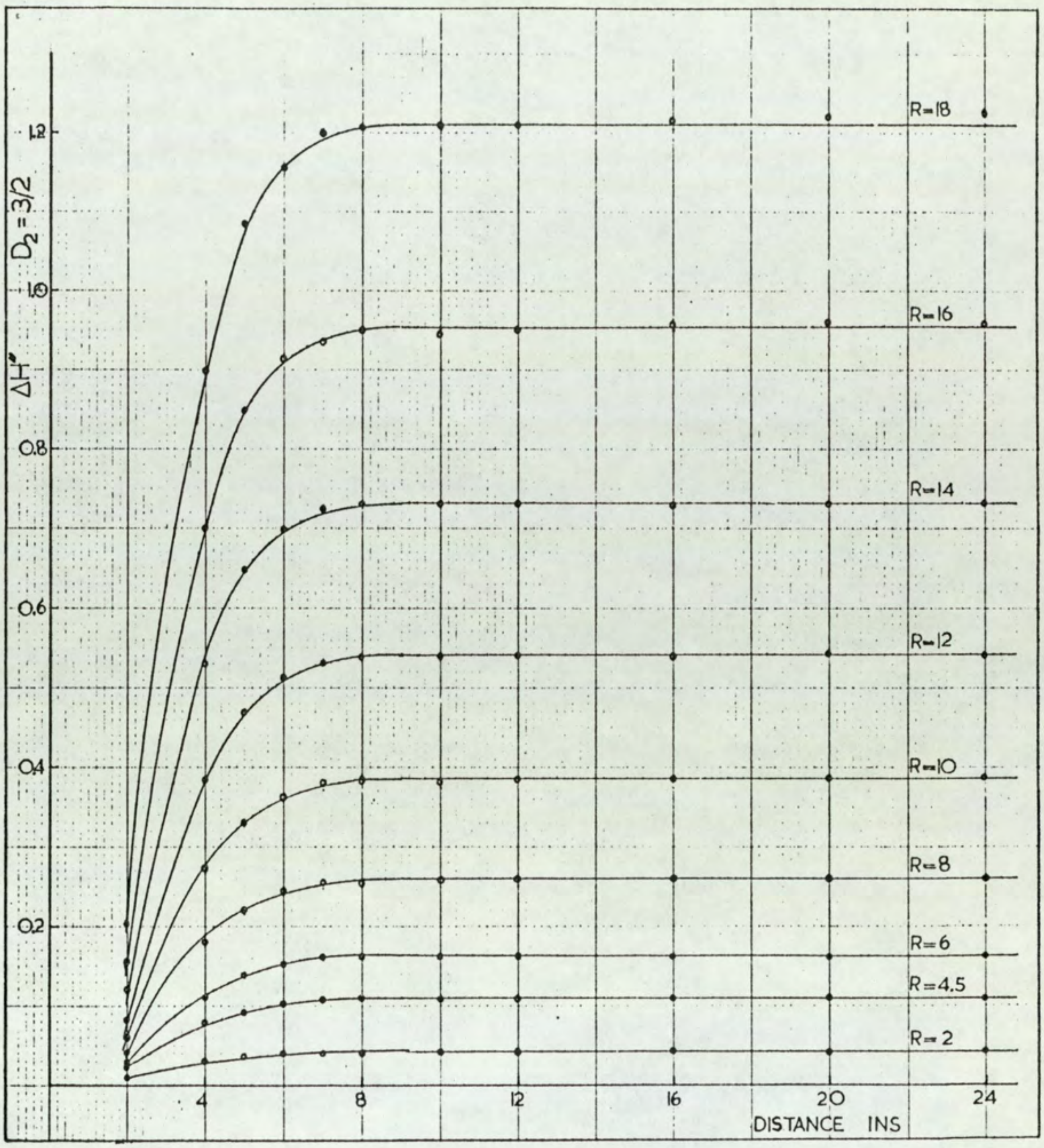

1.2
1.0
0.8
0.6
0.4
0.2
$\Delta H''$ $D_2 = 3/2$
R=18
R=16
R=14
R=12
R=10
R=8
R=6
R=4.5
R=2
4
8
12
16
20
24
DISTANCE INS

Fig. 18

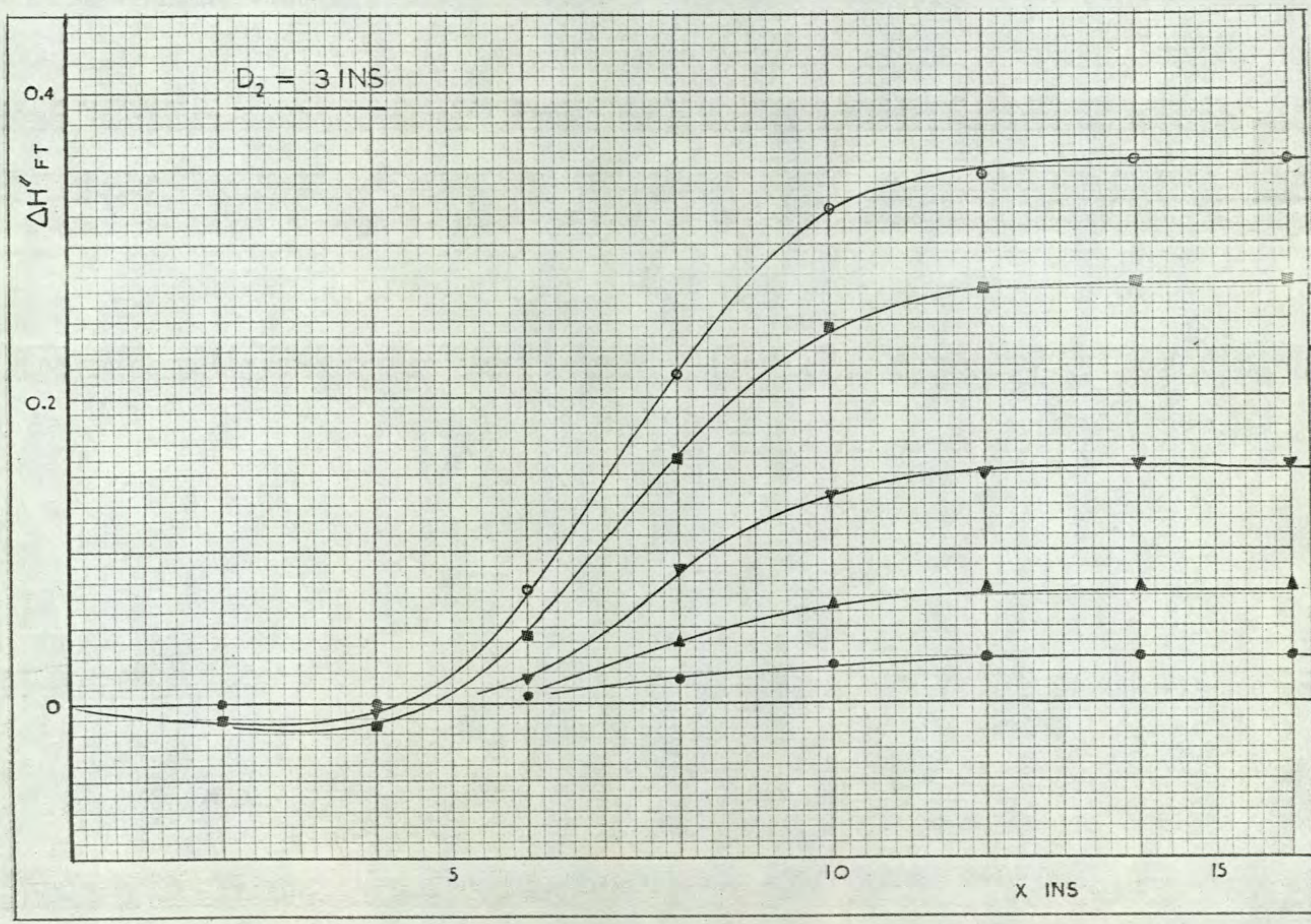

fig. 19

fig. 20

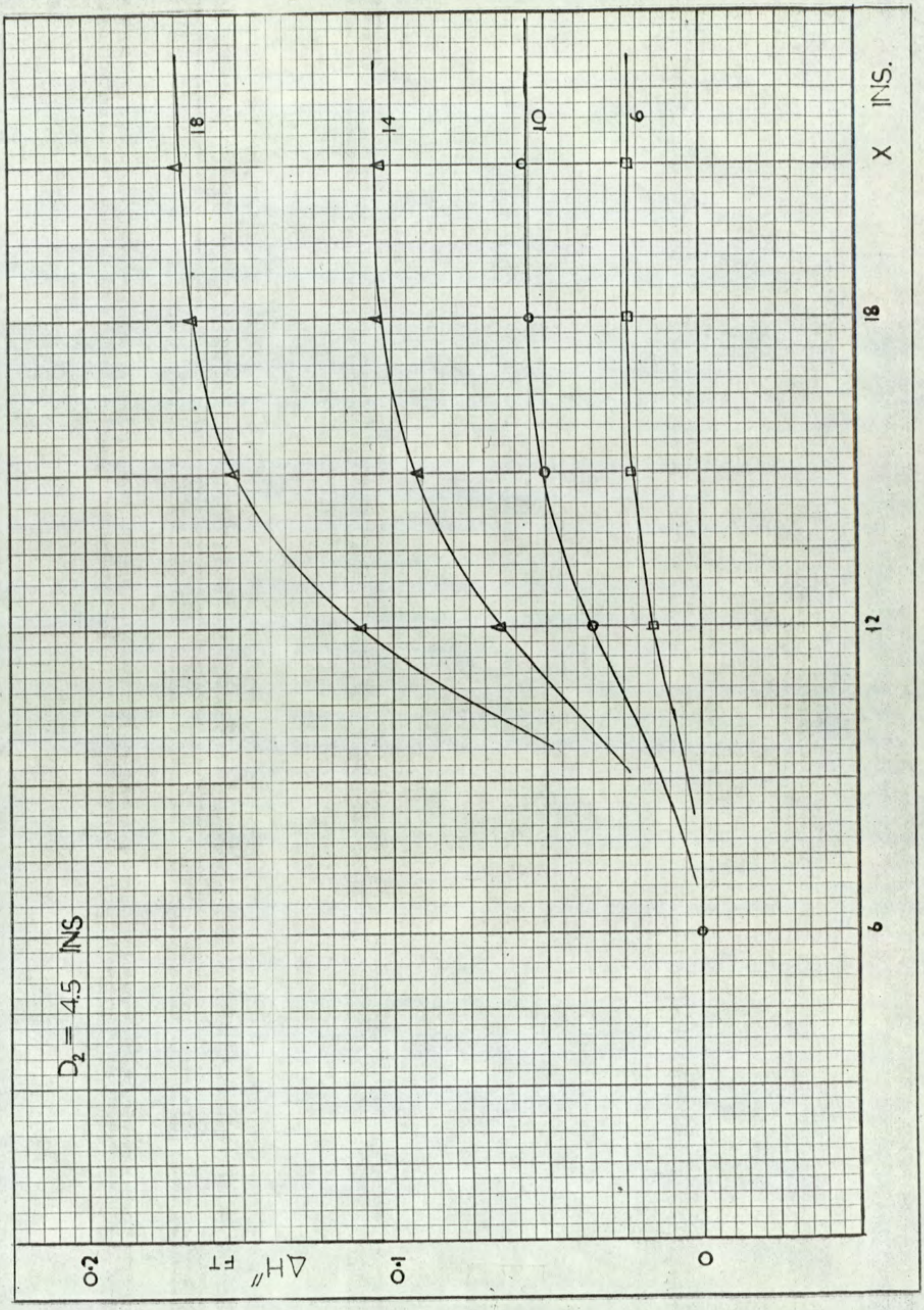

TABLE 8. Maximum Pressure Rise - Doubly-corrected Data

D_2/R	2	4.5	6	8	10	12	14	16	18
0.865 ins.									
Theory:		0.120	0.182	0.284	0.410	0.562	0.745	0.963	1.207
Experiment:		0.115	0.168	0.272	0.404	0.559	0.756	0.991	1.250
1.0 ins.									
Theory:	0.059	0.152	0.230	0.359	0.519	0.711	0.944	1.220	1.525
Experiment:	0.056	0.142	0.214	0.343	0.505	0.706	0.964	1.261	1.601
1.464 ins.									
T:	0.045	0.117	0.176	0.275	0.398	0.544	0.722	0.932	1.168
E:	0.041	0.107	0.162	0.256	0.384	0.538	0.730	0.958	1.207
2.085 ins.									
T:	0.026	0.067	0.102	0.156	0.230	0.315	0.419	0.541	0.677
E:	0.024	0.059	0.091	0.149	0.220	0.306	0.415	0.539	0.689
3.041 ins.									
T:	0.013	0.034	0.052	0.081	0.117	0.160	0.212	0.274	0.343
E:	0.012	0.030	0.046	0.076	0.113	0.154	0.213	0.275	0.355
4.50 ins.									
T:	0.006	0.016	0.024	0.038	0.055	0.076	0.100	0.130	0.162
E:	0.007	0.016	0.023	0.038	0.057	0.077	0.104	0.134	0.170

fig. 21

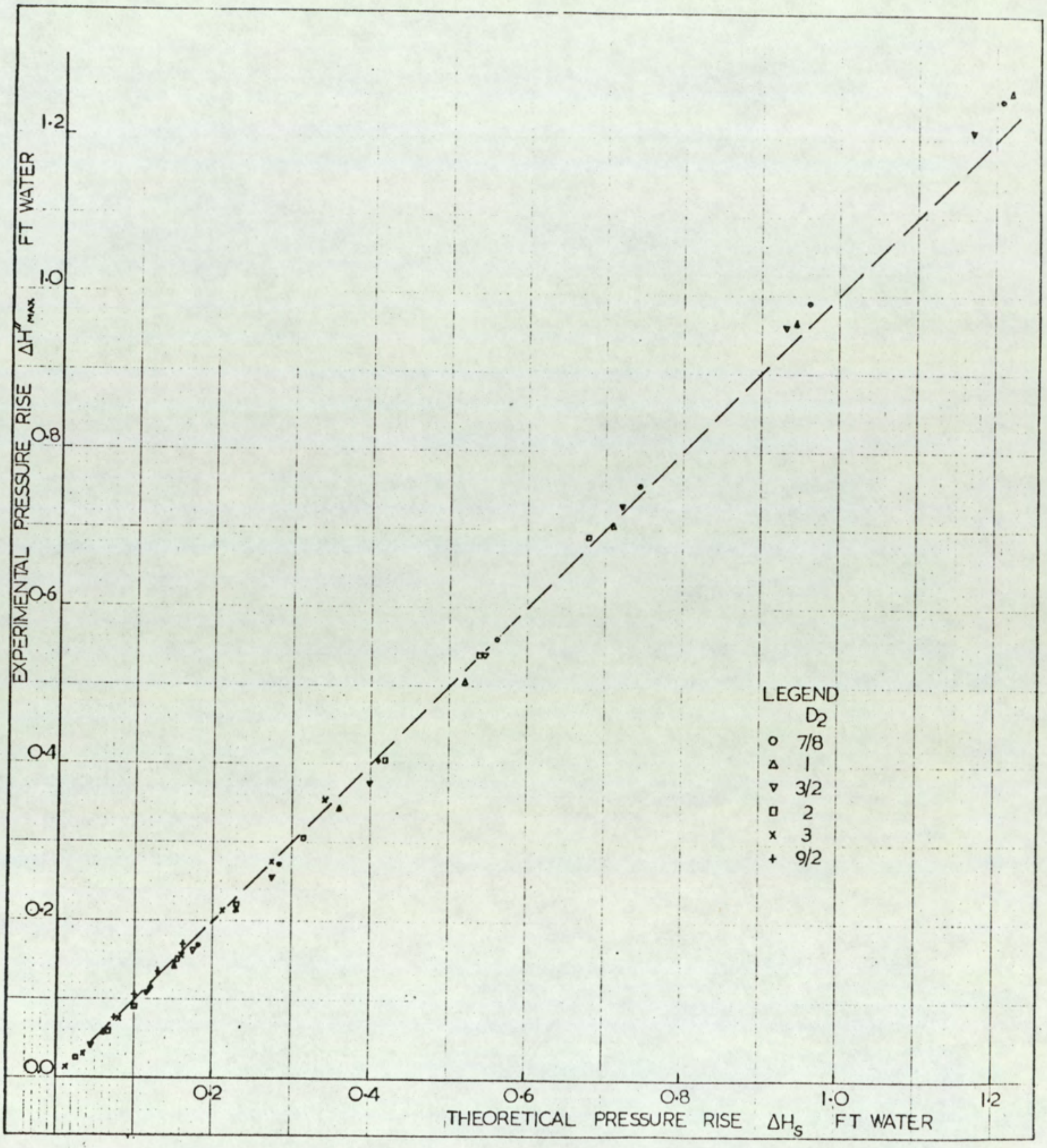

EXPERIMENTAL PRESSURE RISE $\Delta H''_{MAX}$ FT WATER
0.0
0.2
0.4
0.6
0.8
1.0
1.2
0.2
0.4
0.6
0.8
1.0
1.2
THEORETICAL PRESSURE RISE ΔH_S FT WATER
LEGEND
D_2
o 7/8
Δ 1
▽ 3/2
□ 2
x 3
+ 9/2

fit. The theory underlying this procedure is given in full in reference (50), and only a brief explanation of the steps in the calculation is given below.

The author's data consists of N pairs of observations of the maximum pressure rise: N values predicted by simple theory (the independent variable, x) and N experimental values (the dependent variable, y). The required line is known as the regression line of y on x. The statistical method is based on the assumption that y is distributed normally about an expected value η with variance σ^2 and that η is a simple linear function of x.

$$\eta = A + B(x - \bar{x})$$

The standard procedure is to choose as the estimated regression line,

$$Y = a + b(x - \bar{x})$$

that line which minimises the sum of the squares of the deviations of the observed from the estimated values of the dependent variable, i.e., the line which minimises the quantity

$$S = \sum_{i=1}^{N} \left[y_i - a - b(x_i - \bar{x}) \right]^2$$

The values of a and b which result in S having a minimum value are given by the expressions

$$a = \frac{\sum y_i}{N} = \bar{y}$$

$$b = \frac{\sum(x_i - \bar{x})(y_i - \bar{y})}{\sum(x_i - \bar{x})^2}$$

From the data given in Table (8) the following sums were calculated:

$$\sum x = 18.995 \qquad \sum y = 19.077 \qquad N = 53$$

$$\sum x^2 = 14.04097 \qquad \sum y^2 = 14.65859 \qquad \sum xy = 14.34179$$

Hence,

$$\sum(x_i - \bar{x})^2 = \sum x^2 - (\sum x)^2/N = 7.23323$$

$$\sum(y_i - \bar{y})^2 = \sum y^2 - (\sum y)^2/N = 7.79195$$

$$\sum(x_i - \bar{x})(y_i - \bar{y}) = \sum xy - \sum x \sum y/N = 7.50466$$

To estimate the regression line the following values are also required

$$\bar{y} = 0.35994, \qquad \bar{x} = 0.35840$$

$$b = 7.50466/7.23323 = 1.03753$$

Hence, the required relationship is,

$$Y = 1.0375(x - 0.3584) + 0.3599$$

Hence,

$$(\Delta h'')\text{max.} = 1.0375(\Delta h)_s - 0.0119$$

The values 1.0375 and - 0.0119 must not be regarded as absolute values since they merely represent an estimate of a random variable distributed in some fashion around the true value of the parameter. In order to establish whether the values obtained for the gradient and intercept are significant and not simply due to random errors, the scatter about the values 1.0375 and - 0.0119 was determined by establishing confidence limits for each parameter. The confidence interval is constructed in such a way that it has a known probability (e.g. 95% or 99%) of containing the true value of the gradient and intercept.

The variability of the constants a and b may be expressed by their variance, defined according to the equations:

$$V[a] = \sigma^2/N$$

$$V[b] = \sigma^2/\Sigma(x_i - \bar{x})^2$$

while for any given value of x

$$V[Y] = \sigma^2\left[\frac{1}{N} - \frac{(x - \bar{x})^2}{\Sigma(x_i - \bar{x})^2}\right]$$

The value of σ^2 can be estimated from the residual sum of the squares which is obtained by difference in the following table.

The sum of the squares due to regression,

$$\Sigma(Y - \bar{y}) = \left[\Sigma(x_i - \bar{x})(y_i - \bar{y})\right]^2/\Sigma(x_i - \bar{x})^2$$

$$= 7.23323/7.50466 = 7.78628$$

Source of variance	Sum of squares	Degrees of freedom	Mean Squares
Total	7.79195	53 - 1	0.14984
due to regression	7.78628	1	
Residual	0.00567	51	0.00011123

The estimated value of σ^2 = 0.00011123

Substituting for σ^2 gives the variance of b as

$$V[b] = 0.000013389$$

$$\text{and} \quad \sqrt{V[b]} = 0.003659$$

The ratio $(b - B)/\sqrt{V[b]}$ follows the t distribution with (N - 2) degrees of freedom. This fact can be used either to test a particular value of B or to construct a confidence interval for B. The upper 97.5 per cent point of the t distribution with 51 degrees of freedom was obtained by interpolation as 2.009. The 95% confidence interval for B is therefore:

$$1.0375 \pm (2.009)(0.003659).$$

Hence the confidence limits are 1.0301, 1.0449.

A confidence interval for the intercept may be constructed in similar fashion.

From the estimated regression line,

$$Y = 1.0375(x - \bar{x}) + 0.3599$$

$$\text{at} \quad x = o, \ [Y]_{x = o} = -0.0119$$

$$V[Y]_{x = o} = 0.0001112 \left[\frac{1}{53} + \frac{(0.3584)^2}{7.2332}\right]$$

$$= 4.0728 \times 10^{-6}$$

$$\text{Hence,} \quad \sqrt{V[Y]} = 2.0181 \times 10^{-3}$$

The 95% confidence limits for the intercept are therefore

$$- 0.0119 \pm (2.009)(0.002018)$$

i.e. $- 0.0079$ and $- 0.0159$

The confidence interval for the intercept shows conclusively that a straight line through the data on a graph of $(\Delta h)_s$ versus $(\Delta h'')$max. does not pass through the origin. Since the estimated regression line does not therefore satisfy the condition,

$$(\Delta h'')\text{max.} = 0 \text{ when } (\Delta h)_s = 0$$

i.e. when $V_1 = 0$ or $B = 1$

the assumption of a linear relationship cannot be strictly valid over the complete range of values. The curve which best fits the data must deflect away from the line defined by the equation,

$$(\Delta h'')\text{max.} = 1.0375\ (\Delta h)_s - 0.0119 \qquad \ldots(5.1)$$

at very low values of $(\Delta h)_s$.

Inspection of figure (21) reveals that the most significant discrepancies between theoretical and experimental values occur at the highest values of $(\Delta h)_s$; at low values of $(\Delta h)_s$ the experimental points lie close to the line defined by

$$(\Delta h'')\text{max.} = (\Delta h)_s$$

i.e. the 45° line shows dashed on figure (21).

The possibility that the negative intercept - 0.0119 could be the result of the excessive weighting of the positive deviations at high values of the predicted rise, $(\Delta h)_s$, was briefly examined. A straight line was fitted (by the method of least mean squares) to the data corresponding to values of corresponding to values of $(\Delta h)_s$ not exceeding 0.9. Details of the calculation are omitted since no significant improvement over the earlier calculation was obtained. The equation derived for this portion of the graph was,

$$(\Delta h'')_{max.} = 1.00637\,(\Delta h)_s - 0.00568 \qquad \ldots (5.2)$$

confidence limits for the intercept being,

- 0.00234 and - 0.00902.

5.5 Effect of Velocity Profile

The possibility of the discrepancies between theory and experiment being caused by the assumption of flat velocity profiles was examined.

For the range of Reynolds numbers employed in the experiments the value of the momentum correction factor varies between 1.02 and 1.03 (Appendix I).

Since $\alpha_1 \simeq \alpha_2$

we may write, in general,

$$(\Delta h)_M = \alpha_1 (\Delta h)_s \qquad \ldots$$

Thus, the modified theory predicts a consistent increase of 2 to 3 per cent over the simple theoretical values, which is not matched by the noted discrepancies between experimental values $(\Delta h'')$ max. and values predicted by the simple theory.

In a further attempt to account for the observed deviations values of α_2 were calculated from the experimental (maximum) pressure rise and the computed value of α_1 to determine whether such deviations could be attributed to differences between the velocity profile at section 2 (fig. 2) and the fully developed flow profile. Table (9) summarises computed values of α_2 at selected flowrates for low expansion ratios.

Table (9)

R	2	6	10	14	18	cms.
$Re_1 \times 10^{-3}$	15.8	31.2	47.0	63.4	80.5	
α_1	1.024	1.022	1.0205	1.0195	1.019	
α_2		1.061	1.035	1.021	1.014	$D_2 = 7/8"$
α_2	1.090	1.098	1.060	1.017	0.990	$D_2 = 1"$
α_2	1.40	1.306	1.172	1.042	0.983	$D_2 = 3/2"$

(R = ROTAMETER SCALE READING, CMS)

When $D_2 = 3/2$ ins. values of α_2 at extreme flowrates cease to have any real significance. The value 1.40 at the lowest flow exceeds the theoretical value $4/3$ corresponding to a parabolic profile, i.e. streamline flow, although the Reynolds number based on average downstream velocity is 8100. At the maximum flowrate the computed value of α_2 implies reverse flow, i.e. recirculation, although the measured pressure rise indicates full-bore flow at this section. This trend worsens with increasing expansion ratio.

5.6 Empirical Correlation

An empirical correlation was derived from the experimental results by expressing the maximum pressure rise, $(\Delta h'')$max., as a function of each of the two parameters expansion ratio and upstream velocity.

The graph of $(\Delta h'')$max. versus $(\Delta h)_s$, figure (21) suggests that discrepancies between simple theory and experiment depend upon velocity rather than expansion ratio. This is borne out by a plot, on logarithmic scales, of $(\Delta h'')$max. versus $B(1 - B)$ - i.e. the theoretical function - with velocity as a parameter. Figure (22) shows a series of parallel lines with a slope of unity.

Figure (23) shows $(\Delta h'')$max. plotted versus upstream velocity (log x log) for each expansion ratio. The exponent of v_1 is given by the gradient of each line and is shown in figure (22) as 2.10 in all cases. No significant deviations from the value 2.10 were detectable except in the case of the largest expansion ratio ($D_2 =$ 4.5 ins.), where the slope of the best straight line through the data was determined as 2.05. An exponent of 2.10 rather than 2.05 matters little, however, when $B = 0.027$ and since no systematic variation in slope

fig. 22a

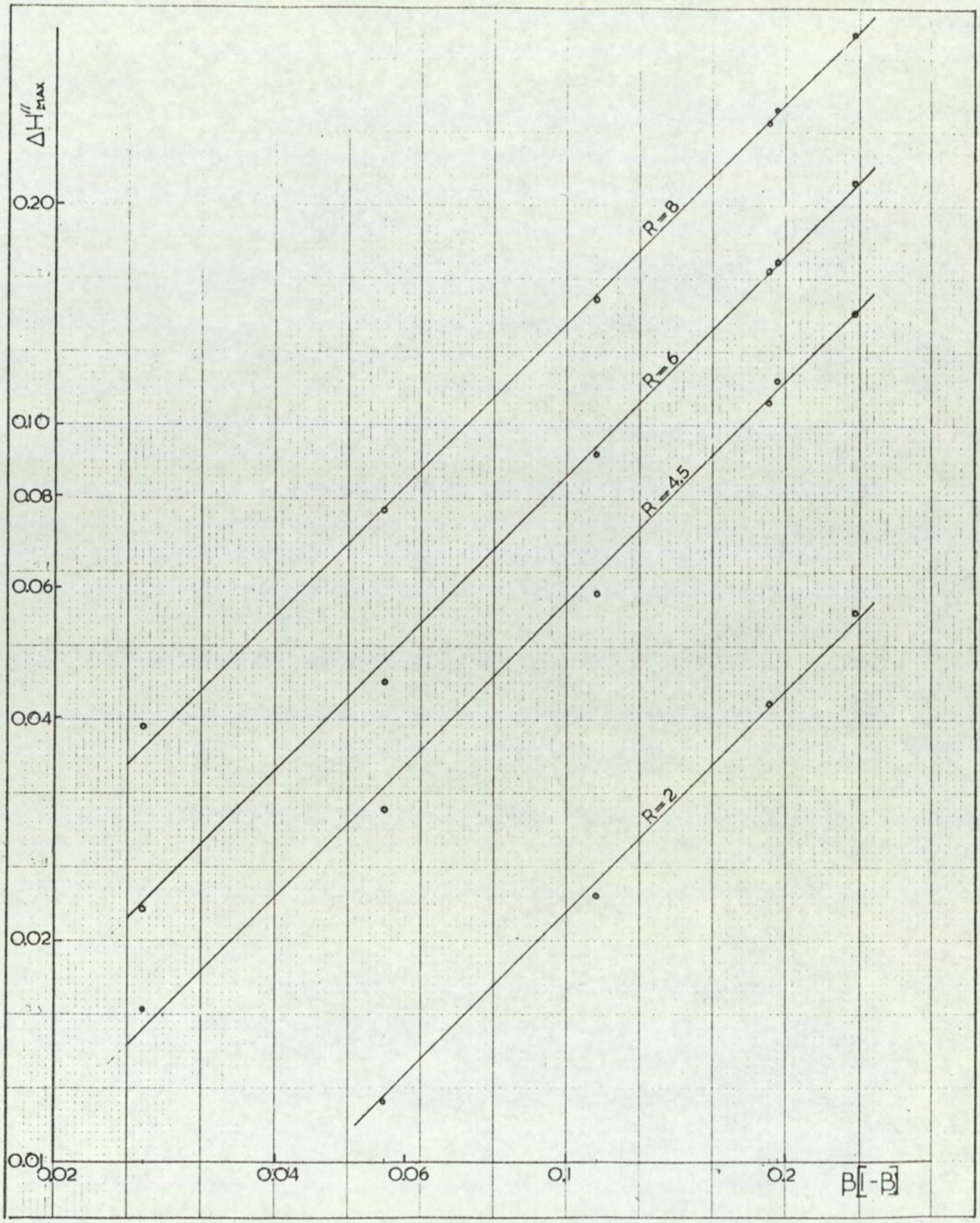

$\Delta H''_{max}$
0.20
0.10
0.08
0.06
0.04
0.02
0.01
0.02
0.04
0.06
0.1
0.2
$\beta[1-\beta]$
R=8
R=6
R=4.5
R=2

fig. 22b

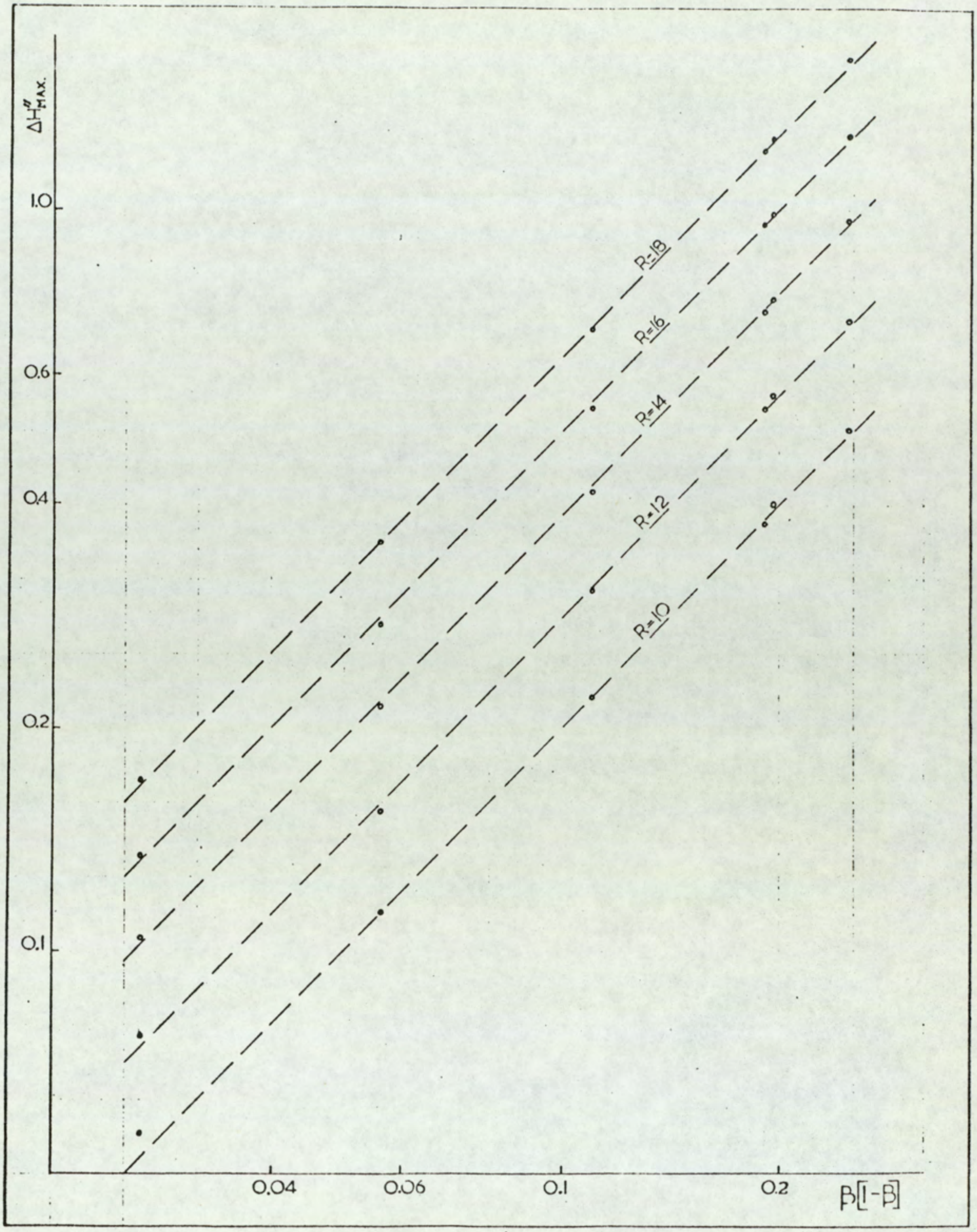
$\Delta H''_{MAX.}$
1.0
0.6
0.4
0.2
0.1
R=18
R=16
R=14
R=12
R=10
0.04
0.06
0.1
0.2
$\beta[1-\beta]$

fig. 23

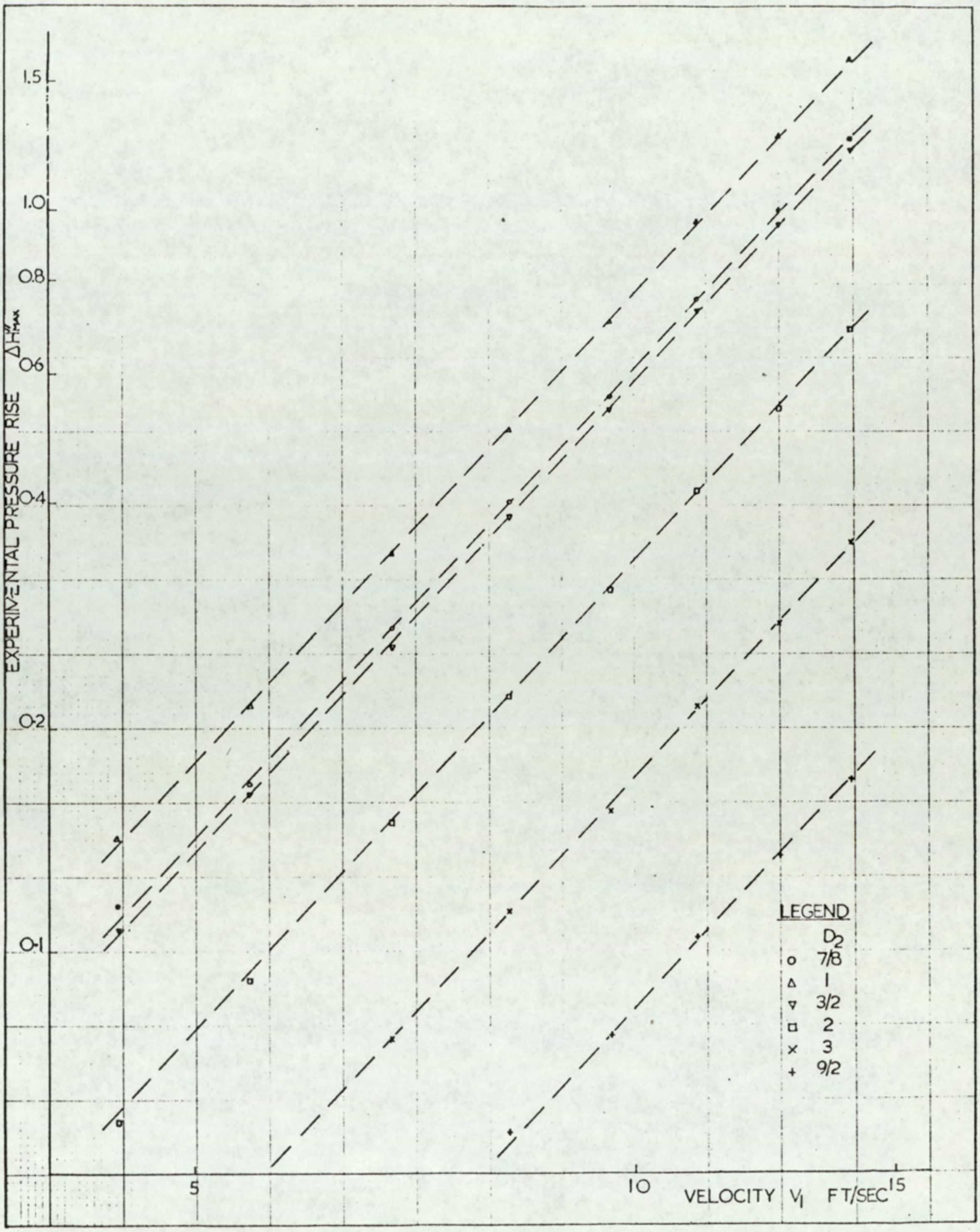

EXPERIMENTAL PRESSURE RISE $\Delta H''_{MAX}$
1.5
1.0
0.8
0.6
0.4
0.2
0.1
5
10
15
VELOCITY V_1 FT/SEC
LEGEND
D_2
o 7/8
Δ 1
∇ 3/2
□ 2
× 3
+ 9/2

with expansion ratio was discernible, the value 2.10 was assumed correct for all cases.

Thus, $(\Delta h'')max \propto v_1^{2.10}$

The intercept, c, with the ordinate for each expansion ratio was determined by substituting specimen values of log $(\Delta h'')$max. and log v_1 in the expression

$$\log (\Delta h'')max = 2.10 \log v_1 + c$$

rather than by extrapolation.

Thus $(\Delta h'')max = c(v_1)^{2.1}$

where c is an arbitrary coefficient which may be expressed

$$c = K(B - B^2)/g$$

A single value of K equal to 0.795 satisfactorily fitted the data for all values of B.

Hence, the final expression reads,

$$(\Delta h'')max = 0.795\, v_1^{2.1}(B - B^2)/g \qquad \ldots (5.3)$$

The empirical correlation may alternatively be expressed in the form,

$$(\Delta h'')max = K'v_1^{2}(B - B)^2/g$$

$$= K'(\Delta h)_s \qquad \ldots (5.4)$$

where K' is an arbitrary coefficient, independent of B, defined by

$$K' = 0.795v_1^{0.1} \qquad \ldots (5.5)$$

Values of K^1 for the range of velocities employed in the author's experiments are given overleaf.

Re_1	15,800	31,200	47,100	63,400	80,500
K'	0.880	0.942	0.981	1.011	1.035

Also, $K' = 1.00$ when $Re_1 = 57,000$

5.7 Head Losses

The results of investigations into the changes in pressure at abrupt expansions are normally presented in terms of head losses due to eddy turbulence. As was indicated earlier (section 3.2) the relative magnitudes of head loss and net rise vary with expansion ratio and discrepancies in the experimental rise may prove insignificant if results are expressed in the form of head losses. Theoretical and experimental head losses are compared in Table (10).

Experimental losses are evaluated as the difference between the theoretical pressure increase resulting from the conversion of kinetic energy into pressure energy and the maximum rise, $(\Delta h'')max$. In terms of the empirical correlation previously developed,

$$(H_L)_E = \frac{v_1^{\,2}}{2g}(1 - B^2) - 0.795\,\frac{v_1^{\,2.1}}{g}(B - B^2)$$

$$= \frac{v_1^{\,2}}{2g}\left[1 - B^2 - 2(0.795)v_1^{\,0.1}(B - B^2)\right]$$

cf $$(H_L)_S = \frac{v_1^{\,2}}{2g}\left[1 - B^2 - 2(B - B^2)\right]$$

For the range of velocities employed in the author's experiments $v_1^{0.1}$ varies between 1.1 and 1.3 and experimental losses may be expressed,

$$(H_L)_E = v_1^2(1 - K'B)^2/2g \qquad \ldots (5.6)$$

without serious loss of accuracy.

$$K' = 0.795\, v_1^{0.1}$$

and varies between 0.8745 and 1.0335 in the experiments.

A single example is given below to confirm this simplification.

Consider

$$v_1^{0.1} = 1.2$$

$$(H_L)_E = \frac{v_1^2}{2g}\left[1 - 2(0.954)B + 0.908B^2\right]$$

cf. $(1 - 0.954B)^2 = 1 - 2(0.954)B + 0.910B^2$

At large expansion ratios (B small) the value of K'B will differ but little from B. Although the effect of the factor K' will be more marked at low expansion ratios, the head loss will in such cases be very low. This is clearly shown (figure 24) on a plot of the data of table (10). The influence of K' (a function of velocity) is most pronounced when the downstream diameter is smallest.

fig. 24

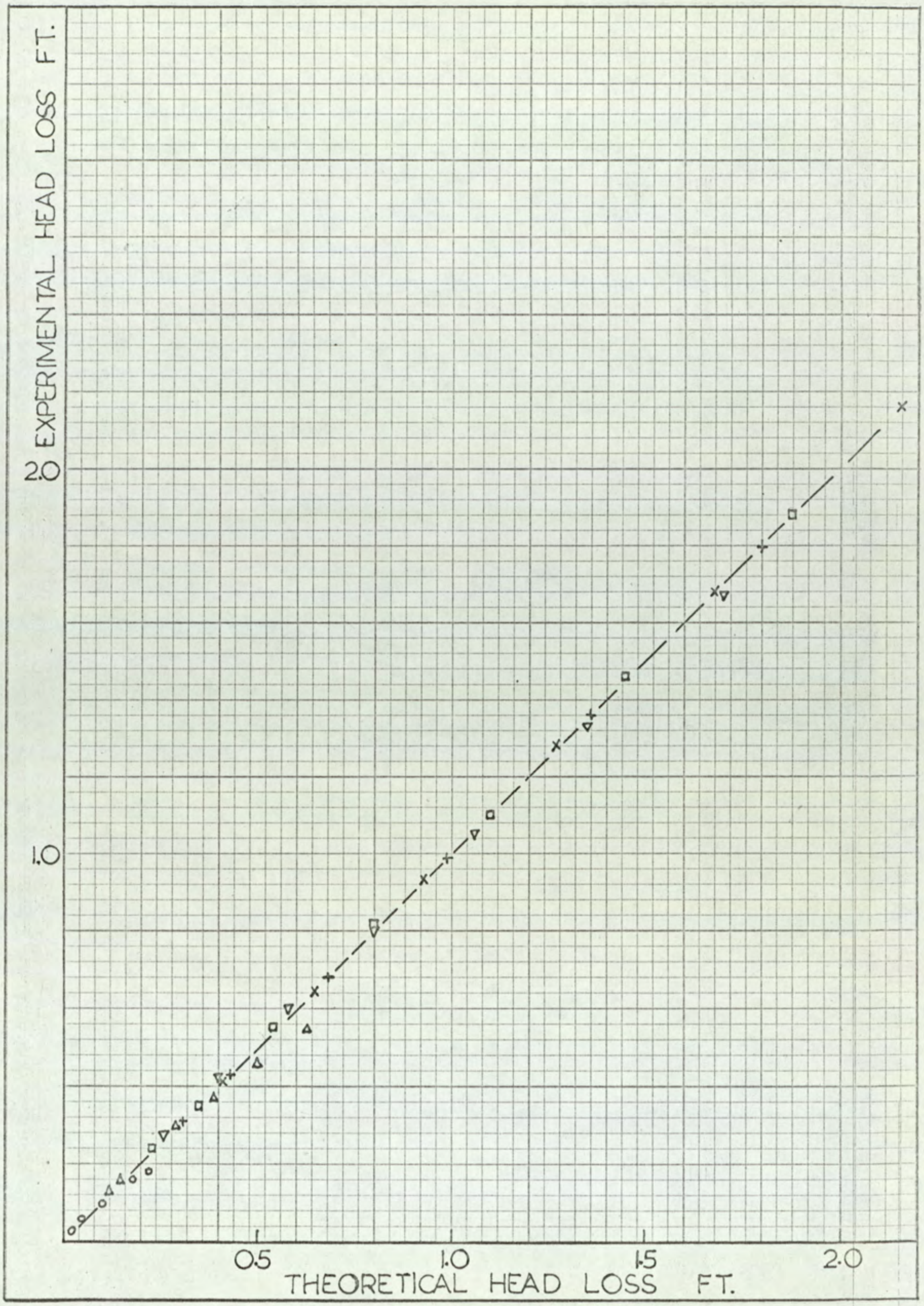
EXPERIMENTAL HEAD LOSS FT.
2.0
1.0
0.5
1.0
1.5
2.0
THEORETICAL HEAD LOSS FT.

5.8 Location of the Peak Pressure Rise

The downstream limit of the pressure recovery zone may be identified as the beginning of the constant maximum on graphs of the doubly-corrected pressure change versus distance. At this limit the velocity profile is essentially fully developed. The asymptotic nature of the curves makes precise definition of the limit very difficult, however, particularly at the highest expansion ratios where pressure differences are exceedingly low between successive pressure tappings. The exact point at which the phrase "essentially fully developed flow" may be interpreted as meaning that the boundary layer is fully established and velocity profiles are self-preserving is insufficiently well defined to allow duct entrance lengths to be specified other than as approximate values.

Attention may be focussed to greater advantage on the location of the observed peak pressure rise, i.e., the peak displayed by measured data and singly-corrected data. The physical significance of the observed peak is that it marks the stage at which the rate of pressure recovery due to dissipation of lateral gradients in the velocity field is equal to the rate of loss of head due to friction; the clear indication of full bore flow establishes a limit for the point of reattachment to the jet. The difficulty of defining the precise location of the peak is less acute than with doubly-corrected data

fig. 25

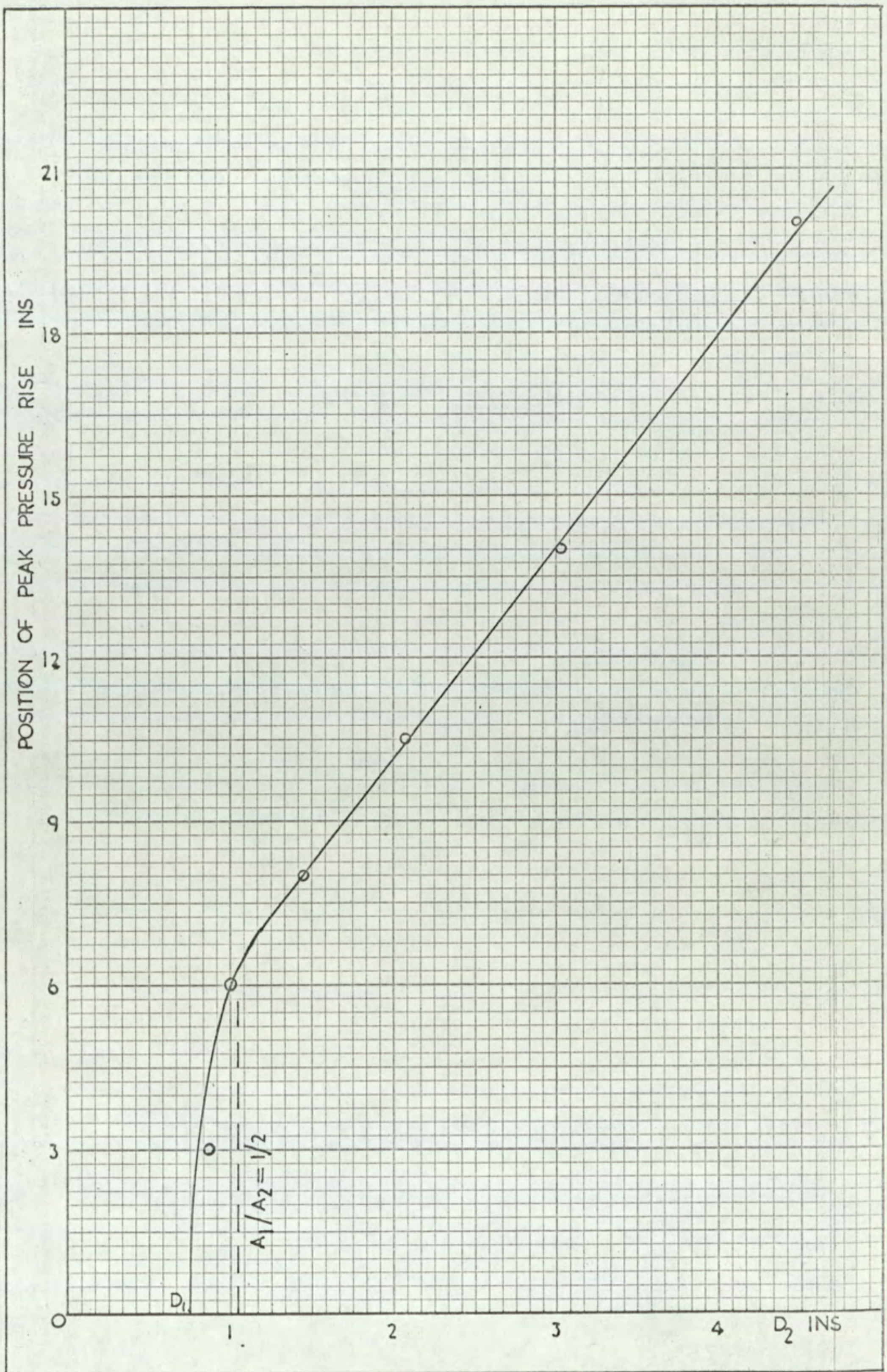

POSITION OF PEAK PRESSURE RISE INS
21
18
15
12
9
6
3
O
$A_1/A_2 = 1/2$
D_1
1
2
3
4
D_2 INS

but a degree of latitude is inevitable at the largest expansion ratios where pressure tappings were not more closely spaced than within $2D_2/3$ of one another. Over the range of velocities used, the position of the observed peak pressure rise is essentially independent of velocity for a particular expansion ratio. This is clearly shown when singly-corrected data are expressed as a fraction of the maximum value. Normalised data, based on singly-corrected results, are presented in table (11), and plotted in figure (30).

The position of the observed peak pressure rise was obtained by inspection of the mean, measured data of table (5) and graphs of the same. Although these graphs are not included, figure (30), of normalised, singly-corrected data, serves equally well. The peak is, unfortunately, ill-defined in the case where D_2 equals 7/8 ins. (See Figure 11). A plot of the peak position (distance L from the change of section) versus D_2 reveals a linear relationship for expansion ratios A_2/A_1 greater than 2/1. — see figure 25.

In order to obtain a general correlation for the position of the observed peak as a function of expansion ratio, the variables were plotted in dimensionless form.

Figure (26) suggests that the position of the observed peak expressed as $L/(D_2 - D_1)$ is a unique function of the diameter ratio D_1/D_2.

When $D_1 = D_2$, $L = 0$ (pipe flow)

and $L/(D_2 - D_1)$ becomes indeterminate.

fig. 26

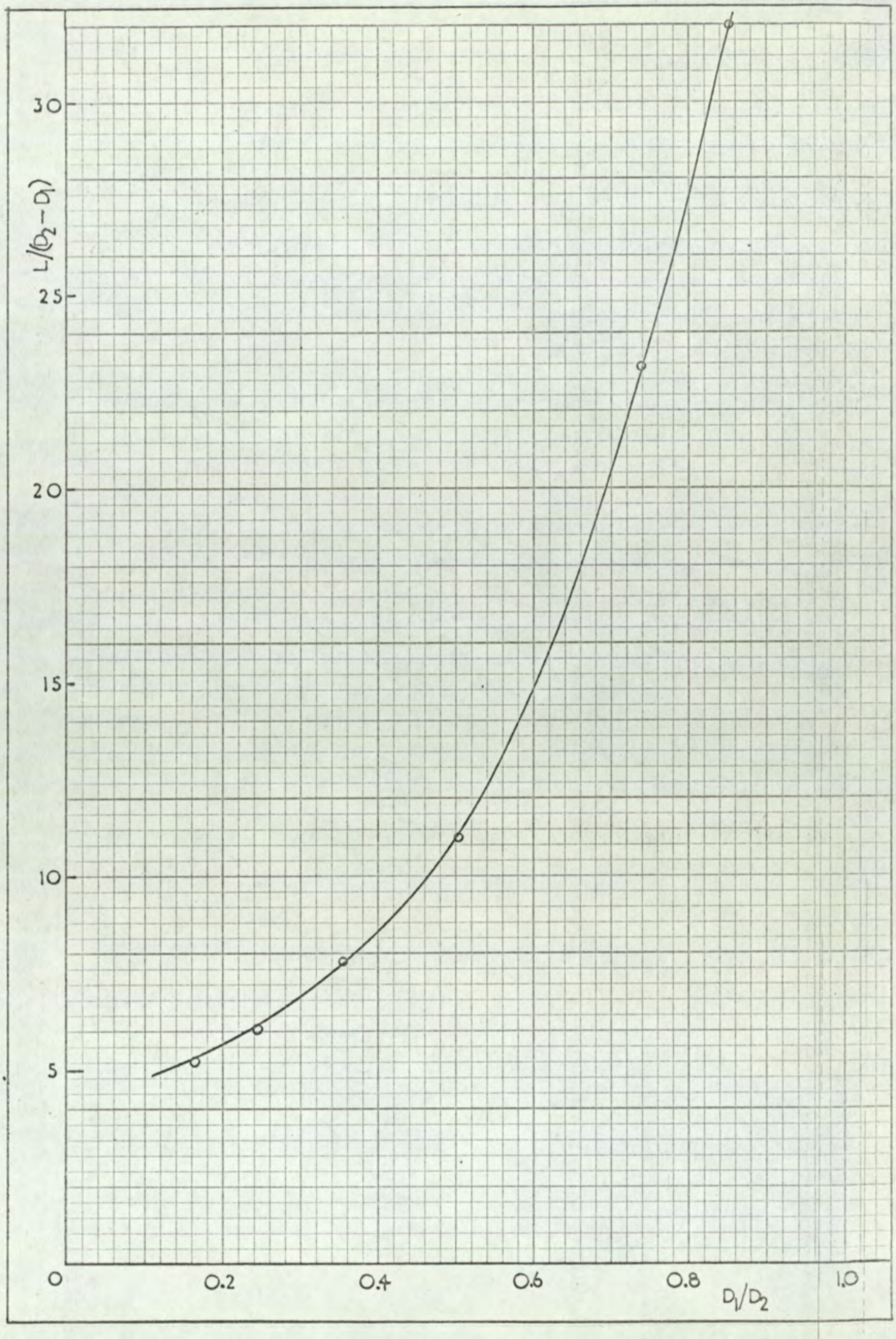

fig. 27

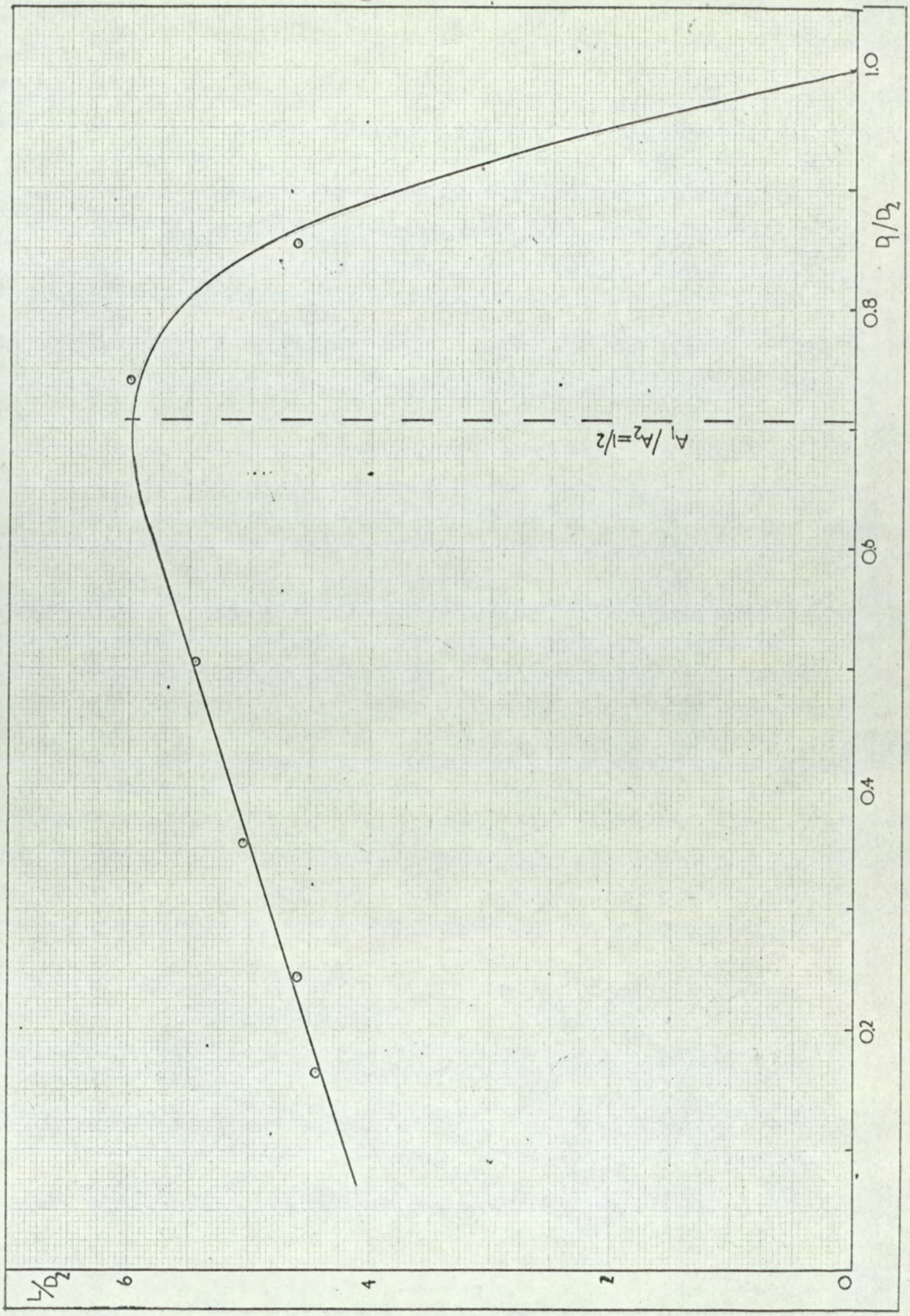

However, since L tends to zero less rapidly than $(D_2 - D_1)$, the curve approaches the ordinate at $D_1/D_2 = 1$ asymptotically. This point is confirmed by the results of Archer (see Fig. 49). Figure (26) indicates a value of L equal to 4 ins. when D_2 = 0.865 ins.

With the present experimental arrangement, a graph of L/D_2 versus D_1/D_2, figure (27), offers no advantage over figure (25), but in the general case does allow for changes in expansion ratio brought about by variation of the upstream diameter, D_1. Figure (27) shows that L/D_2 has a maximum value when A_1/A_2 approximately equals 1/2.

It is interesting to recall that the condition A_1/A_2 = 1/2 corresponds to a maximum in the value of the maximum pressure rise for a given upstream velocity.

If L/D_2 is plotted versus the Craya-Curtet parameter, C_t, a pair of straight lines is obtained which intersect at approximately $A_1/A_2 = 1/2$, (figure 28). The value of C_t is given by

$$C_t = (A_2/A_1 - 1/2)^{-\frac{1}{2}}$$

Figure (29) shows that $L/(D_2 + D_1)$ has an essentially constant value of 3.7 for expansion ratios A_1/A_2 less than 1/2.

5.9 <u>Universal Pressure Change Curve</u>

The primary purpose of measuring wall static pressures near to the plane of enlargement was to gain some insight into the rate of development of the jet. Before attempting to identify such features as the eye of the recirculation eddy or

fig. 28

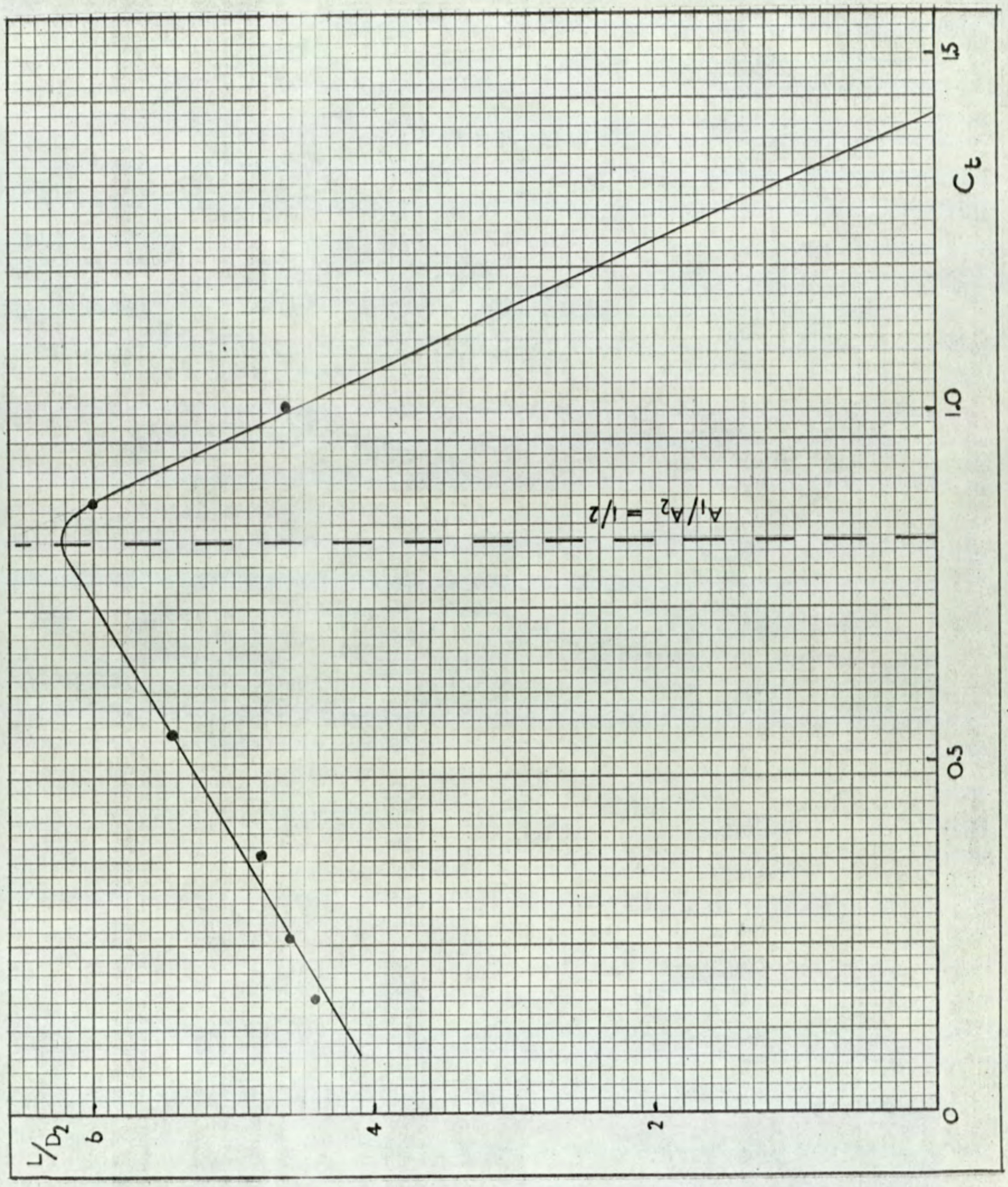

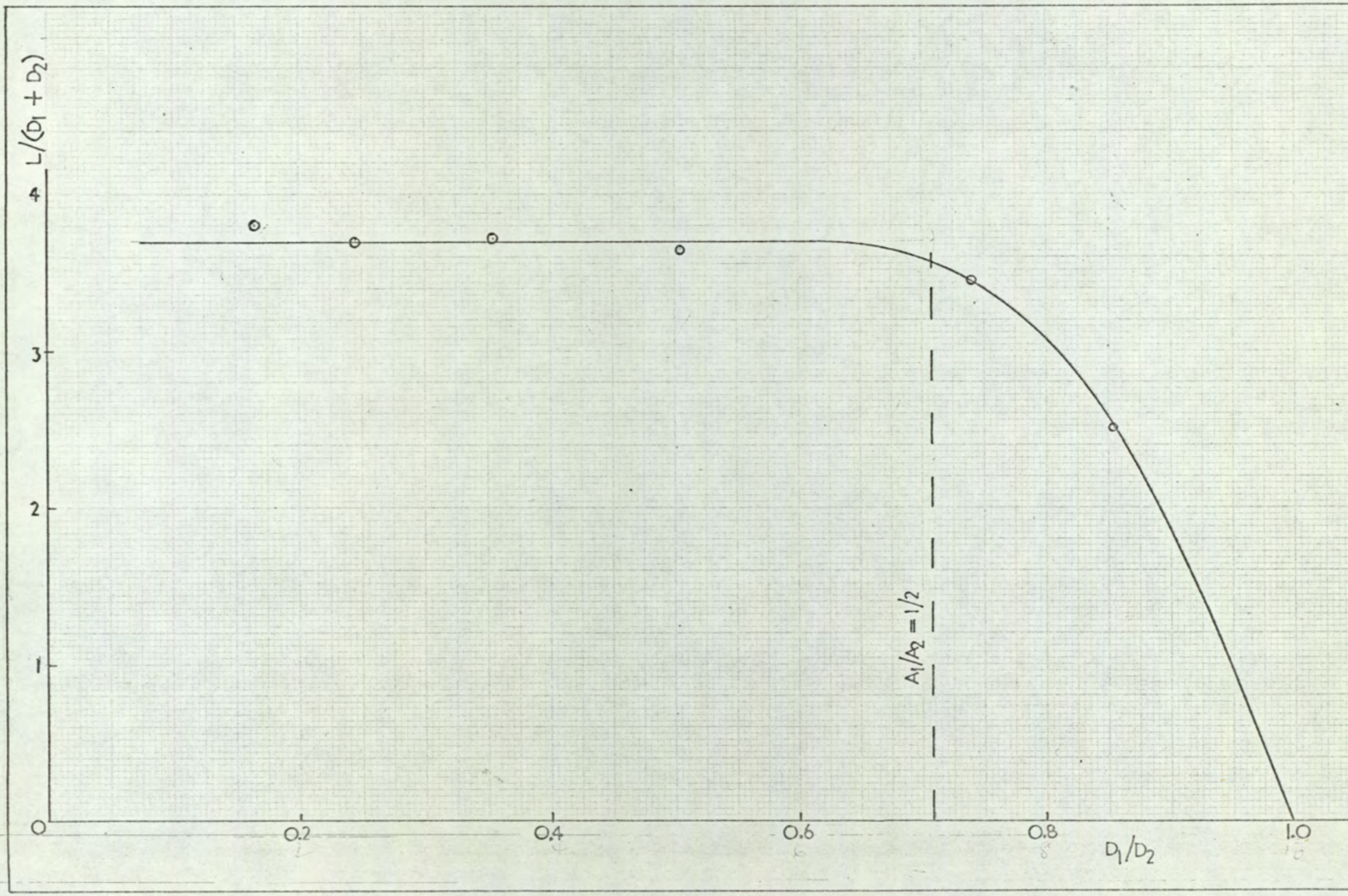

fig. 29

the point of reattachment of the jet, a means of expressing experimental results in a more compact form was sought: the possibility of developing a "universal" pressure rise curve was investigated using the singly-corrected pressure change data.

Mean static pressures at the wall in the region of the expanding jet were corrected for friction loss between the upstream pressure tapping and the plane of enlargement and expressed as a fraction of the peak value, (recorded in table 6). Table (11) presents these normalised values and shows that at a given position the value of the fraction is essentially constant. With increasing expansion ratio the random scatter becomes more pronounced as even a slight discrepancy may constitute a significant percentage of the peak rise. At the smallest expansions extraneous values of the normalised data may be detected by eye. For the larger expansion ratios calculation of the simple mean and mean deviation served to indicate which values to reject in recalculating a representative mean value. Figure (30) shows the family of curves at each expansion ratio reduced to single curves independent of velocity.

Figures (31) to (33) record attempts to reduce the individual curves for each expansion ratio to one universal

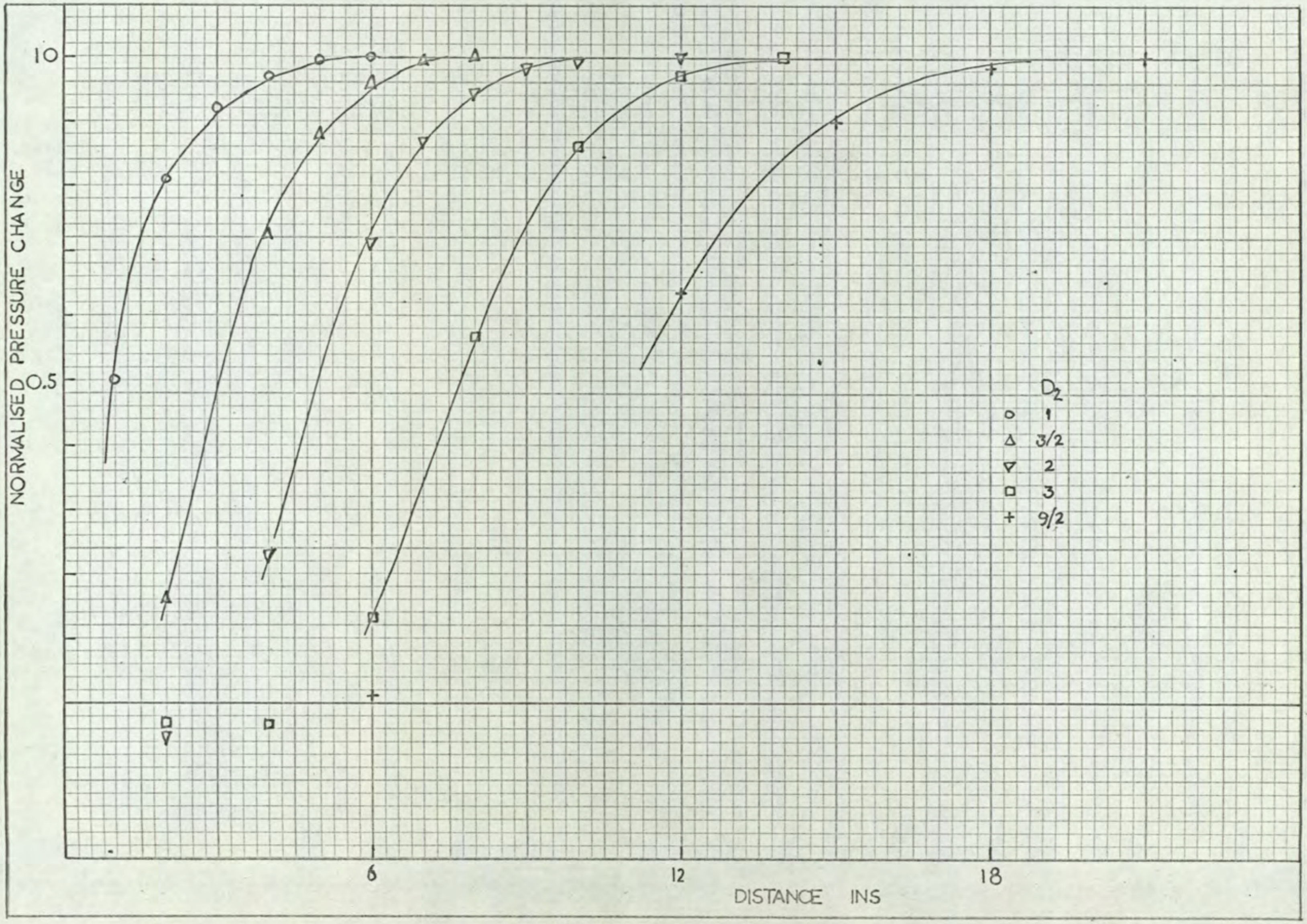

NORMALISED PRESSURE CHANGE
10
0.5
6
12
18
DISTANCE INS
D_2
1
3/2
2
3
9/2

fig. 30

fig 31

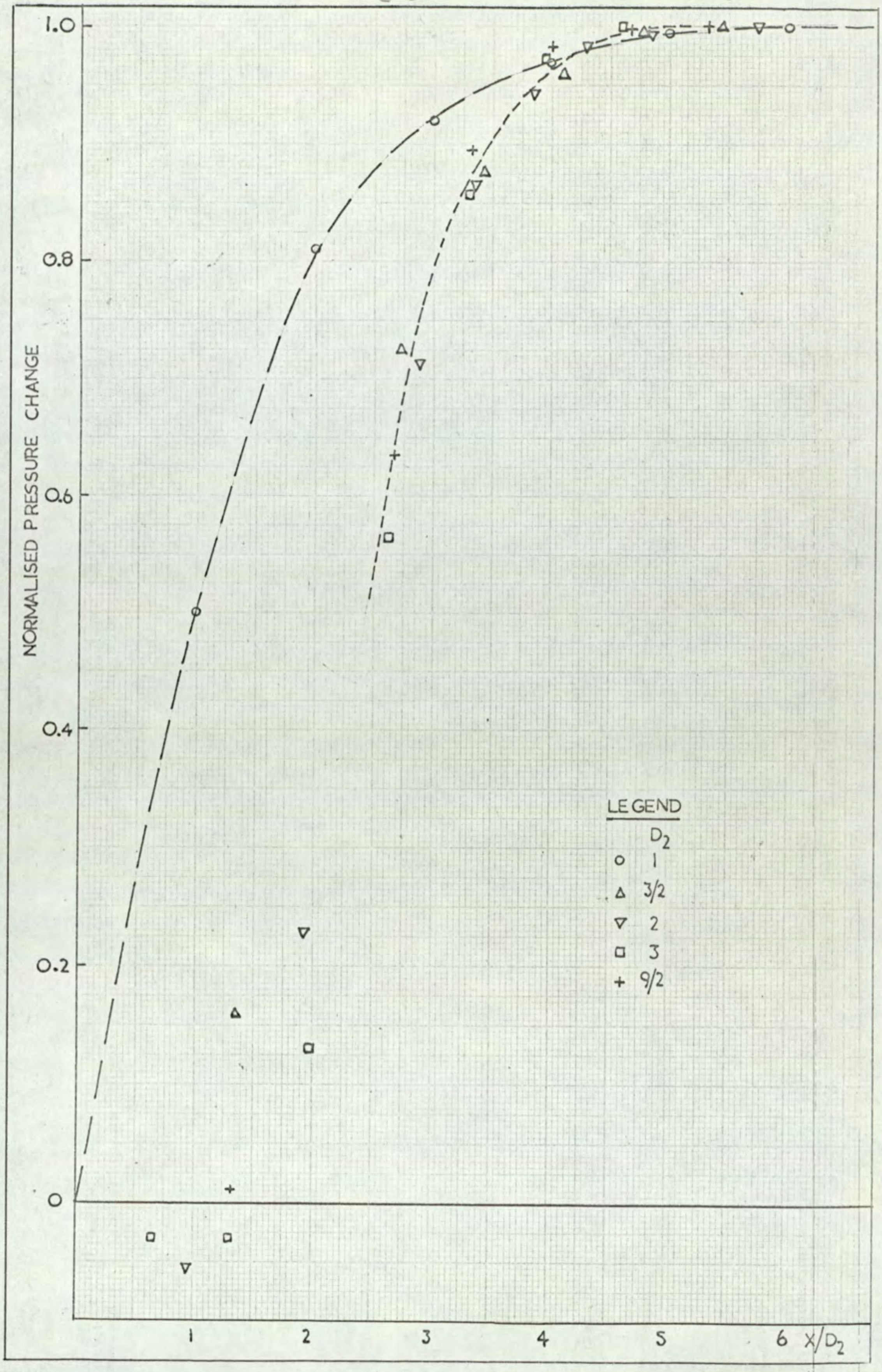
1.0
0.8
0.6
0.4
0.2
0
NORMALISED PRESSURE CHANGE
1
2
3
4
5
6
X/D2
LEGEND
D2
1
3/2
2
3
9/2

fig. 32

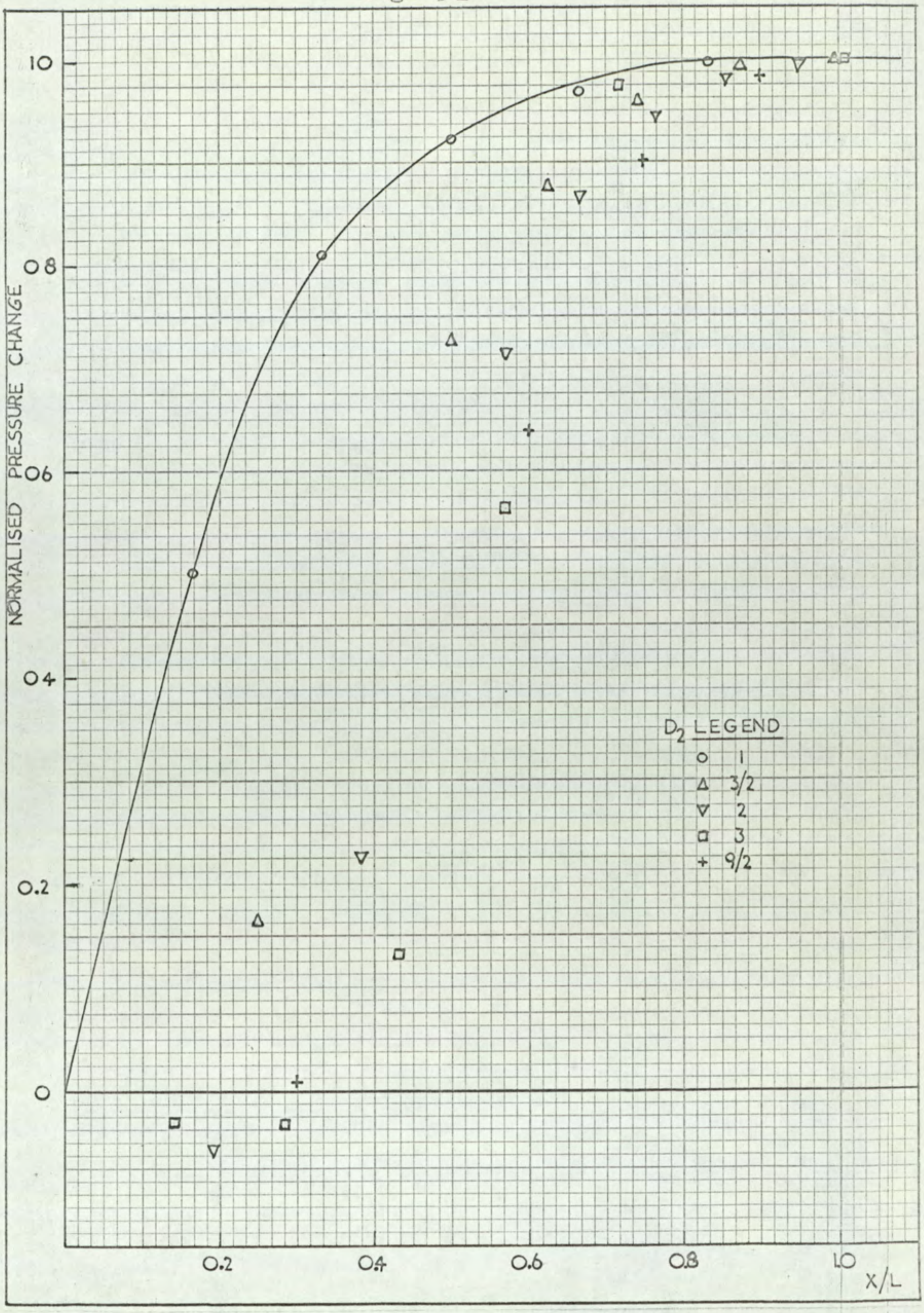
NORMALISED PRESSURE CHANGE
1.0
0.8
0.6
0.4
0.2
0
0.2
0.4
0.6
0.8
1.0
X/L
D2 LEGEND
o 1
Δ 3/2
∇ 2
□ 3
+ 9/2

fig. 33

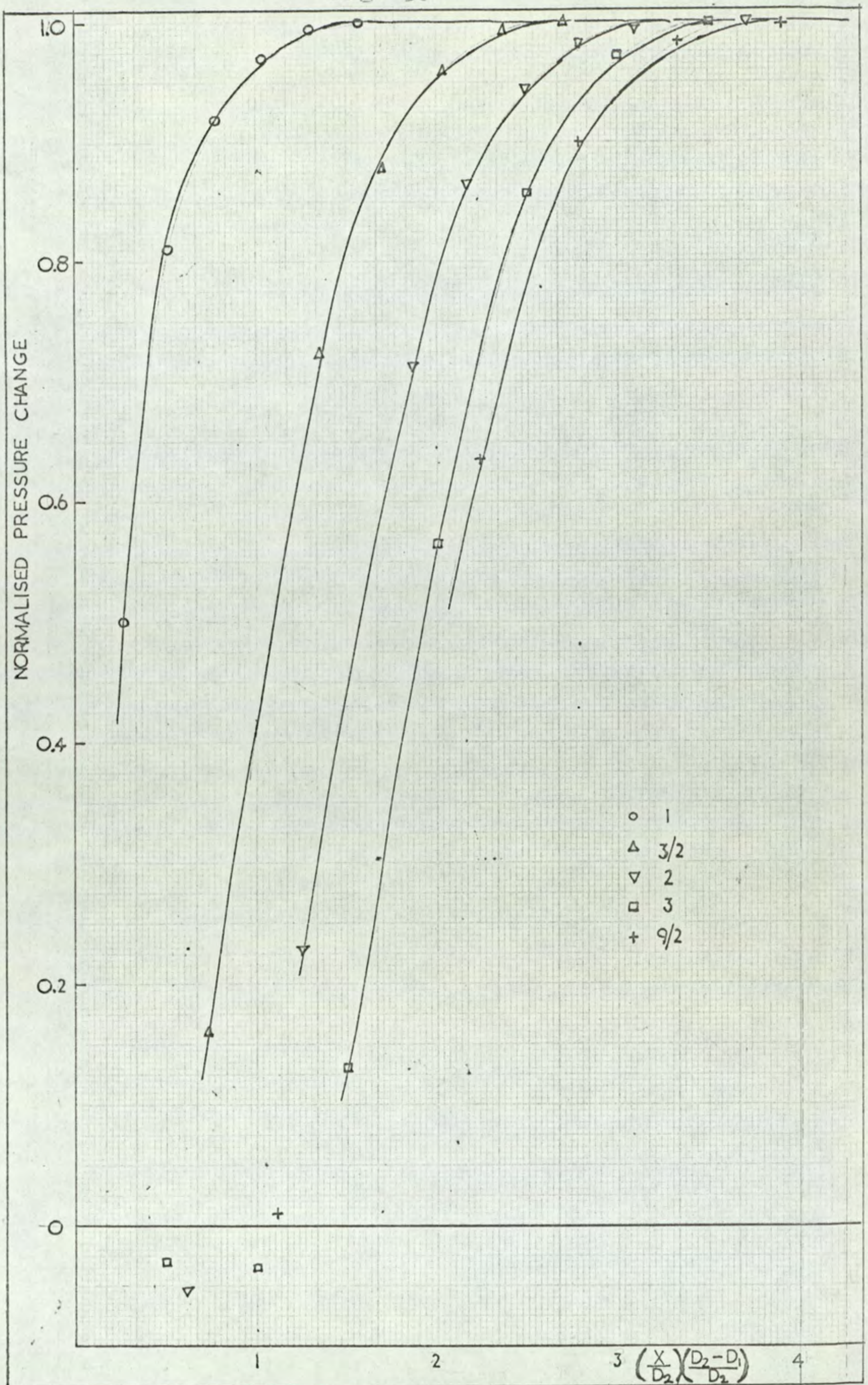

NORMALISED PRESSURE CHANGE
1.0
0.8
0.6
0.4
0.2
0
1
2
3
4
$\left(\frac{X}{D_2}\right)\left(\frac{D_2-D_1}{D_2}\right)$
○ 1
△ 3/2
▽ 2
□ 3
+ 9/2

curve by plotting the normalised pressure rise versus a dimensionless abscissa.

Even with the existing experimental arrangement whereby different expansion ratios where obtained by systematically varying the diameter of the downstream section, expressing distance in terms of pipe diameters fails to produce a unique curve for all expansion ratios, (Figure 31). For values of A_2/A_1 greater than 2/1, the upper sections of the curves approximate to a single curve. A virtually identical figure is obtained on plotting the normalised pressure rise versus xC_t/D_1 since

$$\text{when } D_1/D_2 = 1/2 \qquad C_t/D_1 = (8/7)^{\frac{1}{2}}/D_2 \text{ and}$$

$$\text{when } D_1/D_2 = 1/6 \qquad C_t/D_1 = (72/71)^{\frac{1}{2}}/D_2$$

Figure (32) shows the normalised pressure rise as a function of x/L. A similar set of curves is obtained on plotting distance as $x/(D_2 + D_1)$ in view of the noted relationship between L and $(D_2 + D_1)$.

Plotting $(x/D_2)\ (1 - D_1/D_2)$ as the abscissa reveals that the upper section of each curve is the same shape (figure 33). The dashed curve approximating to the data for the 1 inch downstream pipe has the equation

$$y \simeq 1 - e^{-0.31x}$$

6. Discussion of Results

6.1 Qualitative Conception of the Jetting Process.

In deriving theoretical expressions for the pressure changes at abrupt expansions it is assumed that the local loss of head due to eddy turbulence is consummated in a zone bounded by the plane of enlargement and a section downstream at which the velocity profile can be considered essentially flat or fully developed, and furthermore, that no other losses occur in this zone. The incompatibility of these assumptions with regard to the implied location of the downstream limit of this zone underlies the apparent discrepancy between theory and experiment on the matter of wall friction loss immediately downstream of the enlargement.

By definition, section 2 of figure 2 corresponds to maximum pressure recovery; the specification of an essentially fully-developed velocity profile precludes any further increase in static pressure due to dissipation of lateral gradients in the velocity field. Thus section 2 corresponds to the onset of fully developed flow. The assumption of negligible wall friction throughout the pressure recovery zone tacitly defines the downstream limit as the point of reattachment of the jet, since wall friction can scarcely be considered negligible after the onset of full-bore flow. In conjunction, these two assumptions lead to the conclusion that flow is essentially fully-developed at the end of the zone of recirculatory flow.

A more realistic picture of the jetting process allows a finite distance for the development of the established velocity profile after the onset offull bore flow. The existence of full bore flow upstream of the peak pressure rise is supported by the evident discrepancy between pressure rise data predicted by the simple theory and singly-corrected pressure rise measurements; the measure of agreement is much improved by adding a second correction for friction loss in the expanded section. (Compare figures 6 and 8).

The evident discrepancy between pressure rise data predicted by the simple theory and singly-corrected pressure rise measurements proves, if proof were needed, that such a hypothetical situation cannot exist. In addition, figure (14) shows that the onset of fully developed flow - indicated by the constant slope hydraulic gradient on a plot of the singly-corrected data - begins downstream of the observed peak pressure rise, contrary to the definition of section 2 of figure 2.

A more realistic conception of the jetting process allows a finite distance for the development of the established velocity profile after the onset of full bore flow; the pressure recovery zone is divided into two distinct regions, upstream and downstream of the point of reattachment of the jet. Within the region bounded by the plane of enlargement and the point of reattachment, section 2', the usual assumptions may be considered valid, i.e., eddy turbulence loss is completed and wall friction may be considered negligible. Between sections 2' and 2 flow becomes fully developed; there is a loss of static pressure due to wall friction within this region.

The force F in the direction of flow is thus comprised of the pressure force on the washer-shaped area in the plane of enlargement and the viscous force on the walls between 2' and 2. In the absence of detailed friction factor data for non-established flows the best correction for friction loss which can be made is obtained from empirical correlations for fully developed flow. Since the exact location of section 2' is unknown further approximation is necessary. The required friction correction is estimated as the loss occurring over the full length of pipe between the plane of enlargement and section 2.

The accuracy of these approximations is reflected in the measure of agreement between theoretical and experimental values of the maximum pressure rise. The author's results imply that frictional losses tend to be over-estimated at high velocities and underestimated at low velocities. Deviations arising from the approximations involved in estimating the friction loss appear to be more significant, under turbulent flow conditions, than deviations caused by the assumption of flat velocity profiles.

Under streamline flow conditions, however, the relative importance of the shear stress and velocity profile is reversed. In view of the extremely low frcition factors involved and the high values of the momentum and kinetic energy correction factors associated with parabolic velocity profiles (1.33 and 2.0, respectively), departures from simple theoretical predictions are almost wholly attributable to the assumption of flat profiles, as indicated by Kays (42).

7. <u>Recirculation Phenomena</u>

7.1. Published papers on confined fluid jets and recirculation phenomena were examined to aid interpretation of the pressure rise data, the parameters of interest being the location of the eye of the recirculation eddy and the point of reattachment of the jet. The possibility of incorporating the parameters of Curtet (26) or Hill (29) into a correlation of the author's data was investigated.

Curtet's expression

$$m = -3R_r^2/2 + R_r + kR_r^2/L_r^2 \qquad (2.3)$$

evaluated at the nozzle for zero secondary flow reduces to

$$m = A_2/A_1 - 1/2$$

since $R_r = 1.0$, $L_r = D_1/D_2$ and $k = 1.0$ for a flat velocity profile at the nozzle mouth. (For definition of the above terms, see section 2.1).

Hence,

$$C_t = (A_2/A_1 - 1/2)^{-\frac{1}{2}}$$

The Craya-Curtet parameter has been incorporated in figures (28) and (31).

The parameter developed by Hill (29) similarly reduced to a function of expansion ratio only, on substituting appropriate values into the simplified expression pertaining to conditions at the nozzle mouth section:

$$m_o/(M\rho)^{\frac{1}{2}} = (2)^{-\frac{1}{2}}(D_1/D_2)$$

Subsequent study suggested that this substitution was invalid, however, and that a finite secondary flow is an essential condition of the simplified expression.

7.2 Comparison with Theoretical Curves Presented by Hill (29)

Efforts to fit the author's experimental results to theoretical curves presented by Hill (29) were not successful. Difficulties with nomenclature prevent a definite conclusion on this point. Theoretical curves express the dimensionless term $(p - Po)/M$ as a function of x/D_2 for values of the parameter $(m_o)/(M\rho)^{\frac{1}{2}}$ ranging from zero to 0.8. Unfortunately, the term Po is not defined. The symbol P is defined as

$$P = p + \rho v^2$$

(but later, clearly a misprint, as the static pressure).

Interpreting Po as the total pressure at the nozzle mouth section, section 1 in the present nomenclature,

$$Po = p_1 + \rho v_1^2$$

where p_1 is the static pressure at the plane of enlargement.

Other terms are evaluated as follows:-

(a) $p - Po = \Delta h' \rho g - \rho v_1^2$

where p = wall static pressure at a point in the downstream duct,

and $\Delta h'$ = pressure difference between this point and the plane of enlargement,

i.e. $\Delta h'$ = singly-corrected pressure change.

(b) M = Twice the average sum of the momentum and pressure forces per unit area,

$$= 2(m_1 v_1 - m_2 v_2 + p_1 A_1 - p_2 A_2)/A_2$$

$$= 2p_1 (A_2 - A_1)/A_2$$

$$= 2p_1 (1 - B)$$

(c) $\frac{p - Po}{M} = \frac{(\Delta h')g - v_1^2}{2h_1 g(1 - B)}$

where h_1 = static pressure at the plane of enlargement (in feet of fluid).

(d) m_o = total mass flow per unit area through the duct

$$= \rho v_2$$

(e) $m_o/(M\rho)^{\frac{1}{2}} = (\rho v_2)/(2\ p_1(1 - B)\rho)^{\frac{1}{2}}$

$$= v_2/(2h_1 g(1 - B))^{\frac{1}{2}}$$

Static pressures at the plane of enlargement were determined by connecting the pressure tapping in the upstream section to a mercury manometer and reading the pressure, relative to atmospheric, at this point as the fluid velocity was increased through the range used in the earlier experiments. The addition of the appropriate correction for friction loss gave the required static pressure at the plane of enlargement.

Typical results are presented in table (12) for a single expansion ratio and selected velocities. Results are shown in relation to Hill's theoretical curves in figure (34).

7.3 Comparison with Theoretical Curves Presented by Curtet (26)

Sets of curves for the excess discharge and relative

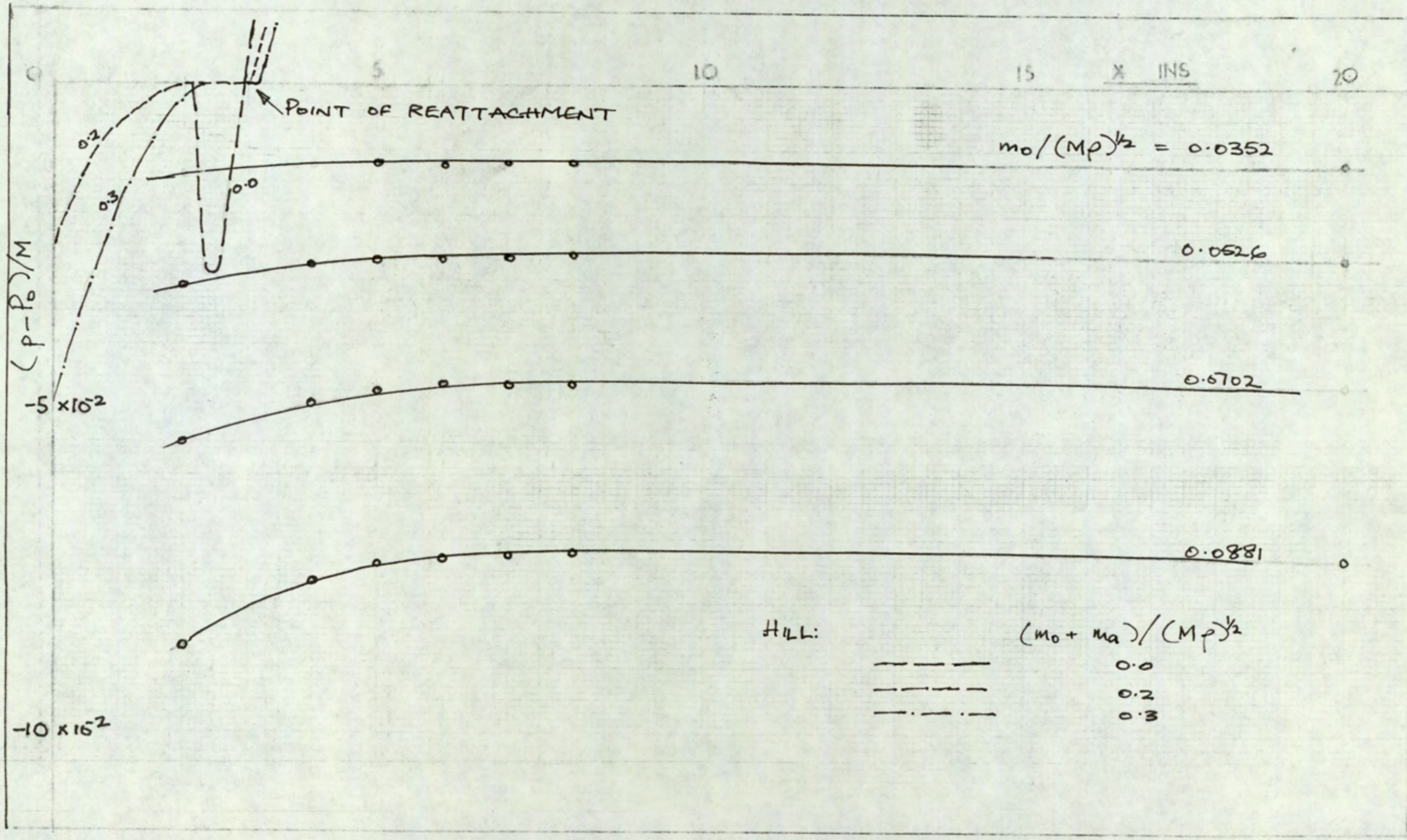

0
5
10
15
X INS
20
POINT OF REATTACHMENT
$m_0/(M\rho)^{1/2}$ = 0.0352
0.0526
0.0702
0.0881
0.2
0.3
0.0
$(p-p_0)/M$
-5×10^{-2}
-10×10^{-2}
HILL:
$(m_0 + m_a)/(M\rho)^{1/2}$
0.0
0.2
0.3

Fig. 34

effective jet width presented by Curtet (23) (26), as a function of a reduced abscissa, reveal that for large duct/nozzle ratios and a value of the similarity parameter, m, equal to 5, a confined fluid jet behaves as a free jet until it approaches the wall. For larger values of m confined jets spread more rapidly than free jets. Barchillon and Curtet (26) have checked the theoretical curves using an experimental system with a nozzle/duct area ratio of 180/1, and a range of m values obtained by varying the relative amount of the secondary stream; results were also obtained for zero secondary flow.

The largest area ratio used in the author's experiments was of the order of 36/1. Since this cannot be construed as large, the published curves proved of little assistance in determining the rate of jet development.

(a) Point of Reattachment of the Jet

Barchillon and Curtet have, however, indicated that the point of reattachment of the jet, is distinguishable from curves of the variation in static pressure measured at the duct wall. In the single instance in which the secondary flow was zero, the point of reattachment of the jet corresponded to the end of the essentially constant, positive gradient section of the pressure change curve.

Following this lead, the author has derived from figure (30) the approximate location of the point of reattachment: the change in gradient of the curve corresponded to a normalised pressure rise of 0.9. Jet lengths are quoted below for each downstream diameter.

Diameter D_2:	1.0	1.464	2.085	3.041	4.50 ins.
Jet Length:	2.8	5.2	7.4	10.7	15.0 ins.
Jet Length:	2.8	3.55	3.55	3.52	3.33 Duct Dia.

Except for the case where A_1/A_2 is greater than 1/2, the jet length expressed in duct diameters has an approximately constant value of 3.5.

Hubbard (25) in a general statement apparently relating to expansion ratios, D_1/D_2, between 0.0135 and 0.59 remarks that the jet is affected by the presence of the walls as soon as the zone of recirculation is reached, but after $x/D_2 = 3.5$ the jet completely fills the cross section and there is no further recirculation.

(b) Eye of the Recirculation Eddy

The results of photographic techniques, velocity measurements and static pressure measurements by Barchillon and Curtet (26) led to the identification of the eye of the recirculation eddy as the point at which the pressure gradient changes from positive to negative. This definition enabled the eye of the eddy to be located from the author's results. In figure (35) pressure gradients are shown as straight lines in the region of recirculatory flow owing to the paucity of the data. Superimposed on figure (35) are the values derived from results presented by Cohen de Lara et al (30) for the position of the eye. Striking agreement is evident between the author's findings and the published curve (30).

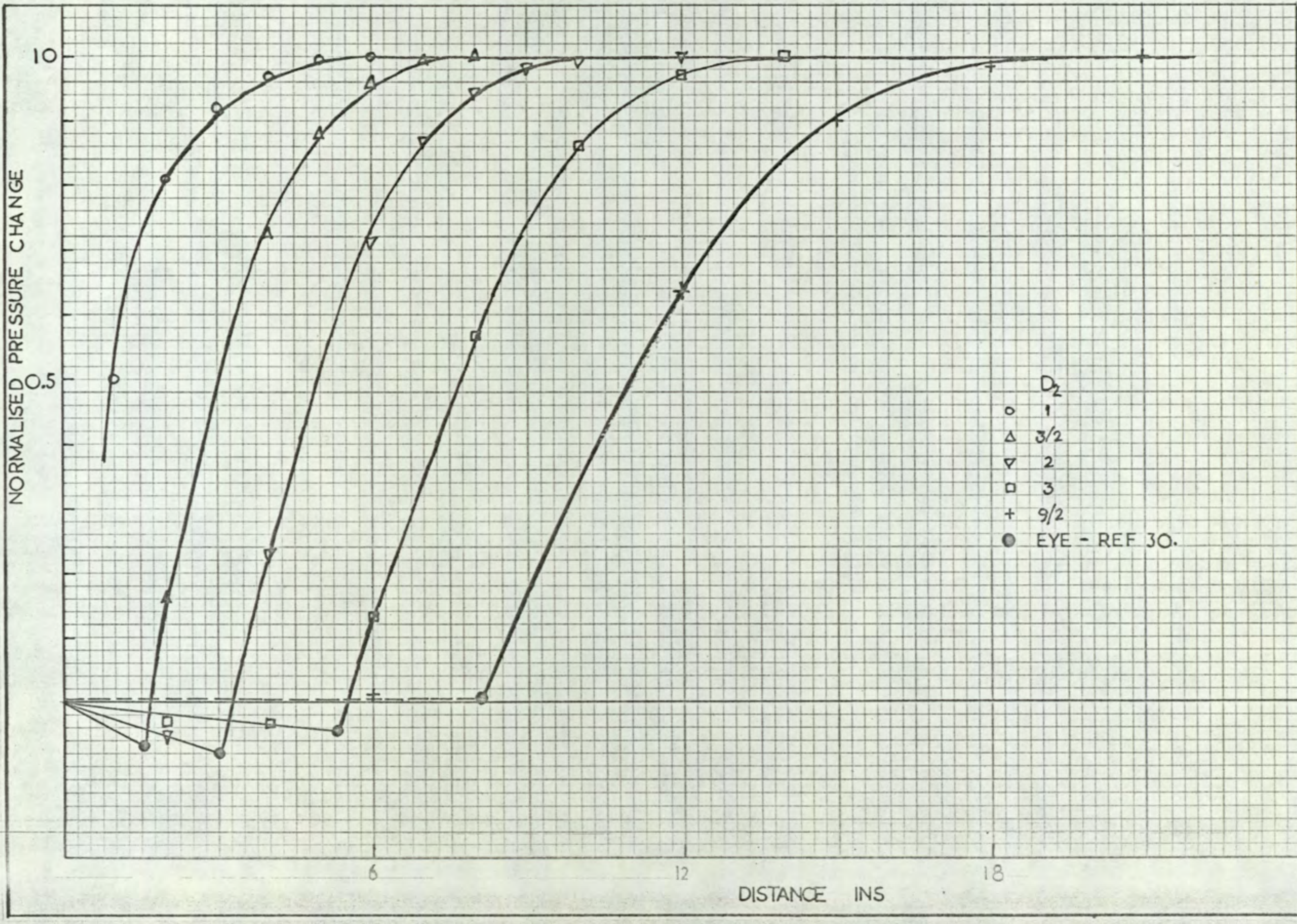

NORMALISED PRESSURE CHANGE
1.0
0.5
6
12
18
DISTANCE INS
D2
o 1
Δ 3/2
∇ 2
□ 3
+ 9/2
● EYE - REF 30.

fig. 35

SECTION B

8. Convective Heat Transfer in the Separation and Reattachment Regions of Confined Fluid Jets

8.1 Introduction

Heat transfer in pipes and ducts having been the subject of intensive study for many years, the heat transfer characteristics of jetting and wake flows in which separation occurs have latterly attracted increasing attention. Examples of practical situations involving separated flows are provided by abrupt changes of section, orifice plates, baffles and so forth. The present investigation is concerned with the variation of the heat transfer coefficient downstream of abrupt expansions.

The local heat transfer coefficient at any station is defined by

$$k_h = \frac{q}{Tw - Tb}$$

where, q = rate of heat transfer per unit area,

Tw = Inside wall temperature

Tb = Bulk temperature of flowing fluid,

(all quantities being local values).

In conducting experiments to measure variations in the local heat transfer coefficient, two approaches are possible, according to the direction of the heat transfer process. If heat is transferred from the test fluid to the pipe wall the section downstream of the abrupt expansion comprises a number of calorimeters in the form of a composite smooth-bore tube. This technique has been employed at the Gas Council's Midlands Research Station (confidential report (51)) using water cooled calorimeters. The alternative method is to transfer heat from the pipe to the flowing fluid. The use of an electrically heated, unbroken pipe length as the expanded section produces boundary conditions corresponding to constant heat flux, so that variations in the heat transfer coefficient appear as variations in the tube wall temperature (See section 8.2).

The evaluation of local heat transfer coefficients from the measurements made by either of these techniques requires some estimate of the local bulk temperature to be made. In previous studies a linear temperature gradient has been assumed for the fluid flowing through the expanded section. Whilst such an assumption is acceptable under full bore flow conditions, it cannot be presupposed to be valid in the recirculation zone immediately downstream of the plane of enlargement - the region of maximum interest. Heat transfer coefficients evaluated from an estimated bulk fluid temperature consequently incorporate an inherent degree of inaccuracy. Previous investigations have involved systems with duct/nozzle diameter ratios not exceeding 4:1. If the assumption is made that the recirculation zone is short so that full-bore flow is rapidly attained downstream of the change of section, the assumption of a linear temperature gradient between the plane of enlargement and the exit would not constitute a serious source of error.

Published results reveal the existence of a pronounced maximum in the value of the local transfer coefficient within a few duct diameters of the plane of enlargement. This has been variously interpreted as corresponding to the point of reattachment of the jet or the eye of the recirculation eddy (locations which themselves have been adequately defined in the past).

8.2 Alternative Technique for Determination of Heat Transfer Coefficients

The proposal to investigate larger expansion ratios demands a more rigorous experimental technique since the assumption of a linear fluid temperature gradient throughout the recirculation zone evidently becomes untenable and lack of detailed knowledge of the residence time and temperature distribution within the jetting zone precludes more accurate estimation of local bulk temperatures. The problem posed by the variation of the driving force in the jetting zone may be overcome by adopting a mass transfer technique, whereby transfer rates are measured as electrolysis currents. The large value of Faraday's constant results in appreciable readings even at low transfer rates. Thus, the use of small, well defined electrodes as the transferring surface allows local coefficients and even fluctuations in the instantaneous rate of transfer to be determined (52). Mass transfer coefficients may be calculated from the limiting current values obtained under diffusion controlled conditions, the driving force for the transfer process, then being the unvarying bulk concentration of the electrolyte. Heat transfer coefficients may readily be obtained from the mass transfer values by applying the Chilton-Colburn analogy. A brief account of the analogy between heat and mass transfer is given here (Section 9) preceding a detailed description of the theory and operation of the mass transfer technique.

8.3 Convective Heat Transfer - Literature Survey

The experimental work of Ede has been succinctly described in (53). The complete test section was electrically heated by passing direct current from end to end, the wall thickness of the upstream and downstream sections being such that the rate of generation of heat in each section was the same per unit length. With imposed boundary conditions of uniform heat flux, variations in the local heat transfer coefficient appeared as variations in the tube wall temperature. The rate of heating was obtained from current and potential difference measurement between tappings at various positions along the tube wall. 4 or 5 thermocouples stationed around the circumference of the tube at a particular distance downstream enabled the mean pipe wall temperature to be determined: this was essentially constant in a plane perpendicular to the axis. The necessary corrections were made for conduction of heat along the pipe wall due to the temperature gradient established in the jetting and reattachment region. Local bulk mean water temperatures were computed from the measured inlet temperature, water flowrate and measured heat input (allowing for external losses) up to the point in question.

Results were presented in the form of plots of the dimensionless group $NuPr^{-0.4}$ as a function of distance.

With fully turbulent flow conditions in both sections, all graphs were of the same basic shape. A pronounced peak was observed at a distance downstream (measured in pipe diameters) approximately equal to the diameter ratio (D_2/D_1). The ratio of the peak value to the measured value corresponding to fully developed flow conditions, was expressible in the form

$$\frac{(NuPr^{-0.4})\ max.}{(NuPr^{-0.4})\ f.d} = [1.53]^{*} \frac{(D_2)}{(D_1)}\ Re_2^{-0.22} \qquad [\text{REF } 53]$$

Values of D_2/D_1 used were 1.25, 2.0 and 3.33.

Although flow visualisation tests were performed no quantitative data were obtained. However, consideration of the hydrodynamics of the system led to the belief that the ability of the recirculation eddy in the annulus of the jet to communicate heat to the

* SHOULD READ [15·3]

swiftly flowing core is responsible for the peak values of the transfer coefficient near to the plane of enlargement.

The Reynolds number was decreased until flow in the downstream section switched from turbulent to laminar flow. Visualisation tests showed that laminar flow was very slow in developing. Graphs obtained in the heat transfer trials when the Reynolds number was reduced showed no significant difference from previous graphs until the onset of laminar flow in the upstream section. The position of the peak tended to drift downstream with falling Reynolds number and transfer coefficients in the immediate vicinity of the plane of enlargement were markedly lower than terminal values corresponding to fully developed flow conditions. (Coefficients were measured as far downstream as 40 duct diameters). Reducing the expansion ratio (B increased from 1/9 to 1/4) accentuated this effect. In the case where the diameter ratio, D_2/D_1, equalled 1.25 (i.e., B = 0.64) flow conditions became unstable with decreasing Reynolds number. Because of the small area change, Reynolds numbers upstream and downstream differed but little, so that the transition from turbulent to laminar flow occurred in both sections at approximately the same instant. Visualisation tests showed that the flow was liable to waver unpredictably between the laminar and turbulent regimes almost anywhere in the pipe for intermediate values of Reynolds number. When laminar flow conditions prevailed in both sections graphs of the transfer coefficient displayed no peak value and fully developed flow was attained within 10 duct diameters of the change of section.

Ede also examined the effect of using a heated upstream section; reports (54) and (55) describe experiments with and without the upstream section being heated. For these tests air was used as the fluid medium since lighter copper leads were required to reduce undesirable disturbances to the heat flow conditions at the expansion. A single expansion ratio was investigated ($D_2/D_1 = 2.0$). Measurements were corrected for longitudinal flow of heat along the pipe wall and results presented graphically to show the variation in the local value of the dimensionless group $Nu/Re^{0.8}Pr^{0.4}$ with distance.

When the upstream pipe was unheated the values of the group $Nu/Re^{0.8}Pr^{0.4}$ immediately downstream of the plane of enlargement were 16 to 22% higher than when the upstream section was heated. No explanation was offered for this difference.

A similar result was recorded with the pipes reversed to provide an abrupt convergence. In this case it was further noted that at Reynolds numbers (downstream) of the order of 20,000 and less, the deviation was sustained beyond 20 pipe diameters onwards. When the downstream (contraction) section only was heated, the limiting value corresponding to fully developed flow approximately agreed with the constant value given by the Dittus-Boelter equation:

$$Nu = 0.023(Re_2)^{0.8}(Pr)^{0.4}$$

When both sections were heated, values less than 0.023 were recorded. This point was not pursued further.

Krall and Sparrow (56) adopted the same experimental technique, heating only the downstream section of the test rig using an alternating current. Thermocouples were positioned at 32 axial stations along the pipe. No evidence of asymmetry in the temperature distribution pattern was detected. In the majority of tests the average bulk temperature in the test section was 140°F., corresponding to an average bulk Prandtl number of 3.0. The fully developed wall-to-bulk temperature difference ranged from 17 - 20°F. depending on the particular trial. The local heat transfer rate was determined directly from the current passed, external losses from the lagged test section being negligibly small and (maximum) estimated conduction rates along the pipe wall being only of the order of 2 or 3 per cent of the heat generated by the electric current. A linear temperature gradient between inlet and outlet values was assumed in estimating local bulk temperatures of the test fluid (water).

Abrupt expansions were produced by inserting a plastic orifice plate in a length of uniform bore tubing

(ID = 0.752 ins.). The ratios of the orifice bore to tube diameter were 2/3, 1/2, 1/3, 1/4 (i.e. $B < 1/2$). Fully turbulent flow conditions, both upstream and downstream of the expansion, prevailed throughout the experiments.

Results were presented graphically, the ratio of the local Nusselt number for each run to the corresponding fully developed value at the same Reynolds number, Prandtl number and wall-to-bulk temperature difference being shown as a function of distance.

Graphs were of the same general shape as those of Ede (for fully turbulent flows and B less than half) except in the case where the diameter ratio was 3/2: the peak of the curves was shown as a cusp. The relative magnitude of (Nu) max. to (Nu) fd was, in agreement with the findings of Ede, inversely related to Reynolds number and directly related to diameter ratio. A correlation of the overall results was given in the form

$$(Nu)_{max.} = 0.398\ Re_1^{2/3}$$

From the data of appendix II reference (57), (Nu) fd may be expressed

$$(Nu)_{fd} = 1.097\ (0.023)\ Re_2^{0.8} Pr^{0.4}$$

for Re_2 in the range $10^4 - 15 \times 10^4$

and $Pr = 3.0$

Hence, $$\frac{(Nu)_{max.}}{(Nu)_{fd}} = 10.16 \left(\frac{D_2}{D_1}\right)^{2/3} (Re_2)^{-0.14}$$

c.f. Ede's correlation:

$$\frac{(Nu)\ max.}{(Nu)\ fd} = 1.53 \frac{(D_2)}{(D_1)} Re_2^{-0.22}$$

Generally speaking, the position of the peak was found to move downstream with increasing expansion ratio:

$$x/D_2 \simeq 1.25 \text{ when } D_2/D_1 = 1.5$$

$$x/D_2 \simeq 2.25 \text{ when } D_2/D_1 = 4.0$$

At the largest expansion ratios slight drifting downstream was also detectable as Reynolds number was reduced.

The location of the peak is believed by the authors to coincide with the reattachment of the jet. The magnitude of the heat transfer coefficient in what is accordingly deduced to be the separated region suggests that this region is by no means a 'dead-water' region as it is sometimes designated (56). From comparison of the general shape of the curves the authors infer that the cusp obtained at B = 4/9 indicates well-defined reattachment while rounded peaks imply a gradual reattachment process, probably resulting from the action of more violent eddies. These conclusions are not in agreement with the interpretation offered by Ede (53).

Emerson (58) supports the theory that maximum transfer coefficients could be expected to be centred around the point of reattachment of the jet. Flow visualisation and heat transfer studies were carried outusing a single expansion ratio ($D_2/D_1 = 1.71$) and air as the test fluid. The pair of flanges forming the plane of enlargement was used as a common terminal for independent power supply to the two pipes. Heat fluxes produced a wall-to-air temperature difference of approximately 10°C. in the fully developed flow region. In order to reduce variations in heat, flux pipes were made of stainless steel sheeting, 0.002 ins. thick, reinforced with a thin covering of fibre glass. The conductance of the pipe wall (including fibre glass) was estimated as 8.7×10^{-4} watts/ °C/cm^2.

Reynolds numbers in the downstream section varied between 14,500 and 105,000. The velocity profile at the mouth of the nozzle was fully developed.

A graph of heat transfer coefficient versus distance revealed a rather flat maximum approximately $2\frac{2}{3}$ duct diameters from the change of section and a minimum between 0.8 and 1.25 step heights (step height being defined as $(D_2 - D_1)/2$). The ratio of the peak coefficient to fully developed value was approximately 2.5 irrespective of Reynolds number.

Flow visualisation trials were conducted to indicate the point of reattachment. A transparent test section constructed from a block of clear perspex bored to 3 ins$\frac{1}{2}$ diameter was connected by a flange to a long pipe $1\frac{3}{4}$ ins. internal diameter. Small spots of oil - approximately 1 mm. diameter - were placed in a line at regularly spaced intervals and the displacement of the spots with time was determined from a series of photographs.

The minimum heat transfer coefficient which was found to lie in the quasi stagnant "corner" of the expansion was attributed to small errors arising from conduction in the pipe wall.

Oil drop tests were interpreted as showing the reattachment point to be approximately 2 duct diameters from the change of section, i.e., slightly upstream of the position of the peak heat transfer coefficient.

Emerson suggests that a slight shifting of the peak heat transfer coefficient downstream from the point of reattachment could be caused by the existence of a temperature gradient transverse to the streamlines.

9. Analogy Between Mass and Heat Transfer

The rate of mass or heat transfer between a moving fluid and a boundary surface depends upon the molecular transport properties of the fluid and the dynamic characteristics of the flow. The eddies which occur in turbulent flow promote rapid mixing of the fluid and constitute a highly effective method for equalising concentration or temperature differences within the fluid stream. The effect is akin to molecular transport but occurs at a much faster rate than transport by individual molecules. In spite of the enormous difference in the scale of these phenomena it is possible to derive a useful analogy between the transport of heat, material and momentum by molecular and eddy processes. This analogy makes it possible to derive equations for the heat and mass transfer coefficients to fluids in pipes, using experimental data as fluid friction, and to calculate mass transfer coefficients from experimental data on heat transfer, and vice versa.

A general expression for heat or mass transfer to a turbulent fluid in any type of apparatus can be derived if it is assumed that the coefficient depends only on the average velocity of the fluid, v, a characteristic dimension of the apparatus, l, and the physical properties of the fluid. The relation for heat transfer is set down mathematically as

$$k_h = \text{fn}\ (v,\ l,\ \mu,\ c_p,\ k,\ \rho)$$

where fn denotes a general function

k_h = heat transfer coefficient

k = thermal conductivity

C_p = specific heat

μ = viscosity

ρ = density

The theory of dimensional analysis shows that these variables can be assembled in three dimensionless groups, one of which contains the heat transfer coefficient. For example,

$$\frac{k_h l}{k} = \text{fn}\left[\frac{vl\rho}{\mu}, \frac{\mu C_p}{k}\right]$$

$$\text{i.e.}\quad Nu = \text{fn}\,(Re, Pr)$$

where fn must be determined experimentally for any particular design of apparatus.

Making use of the relationship

$$St = Nu/(Re \times Pr)$$

the following alternative arrangement can be obtained,

$$St = \text{fn}'\,(Re, Pr)$$

Chilton and Colburn suggested the following equation for heat transfer,

$$j_H = St\, Pr^{\frac{2}{3}} = \tau/\rho v^2 = f/2$$

where j_H is a heat transfer factor, and

f is the Fanning friction factor.

The relation between the friction factor and Reynolds number for turbulent flow in a smooth straight pipe may be represented approximately by the equation

$$\frac{f}{2} = 0.023\, Re^{-0.2}$$

Hence, for heat transfer in smooth straight pipes under turbulent flow conditions

$$St = 0.023\ Re^{-0.2} Pr^{-\frac{2}{3}}$$

Similar equations may be derived for mass transfer between a turbulent fluid and a pipe wall, such as

$$\frac{k_m}{v} = fn\ (Re,\ Sc)$$

where k_m is a mass transfer coefficient (units of velocity) and Sc is the dimensionless group $\mu/\rho D$ in which D is the diffusivity. fn denotes some general function usually expressed by an approximate relation of the type

$$\frac{k_m}{v} = \text{constant}\ (Re)^n\ (Sc)^m$$

As suggested by Chilton and Colburn, the equation for mass transfer may be expressed in the form

$$j_D = \frac{k_m}{v} (Sc)^{\frac{2}{3}} = \frac{\tau}{\rho v^2}$$

where $\tau/\rho v^2$ is a friction factor dependent only on the Reynolds number.

The analogy between heat and mass transfer, which may be expressed as an equality between the j_H and j_D factors holds true within a close approximation for all types of mass transfer apparatus (59).

10. Fundamentals of Electrolysis

10.1 Limiting Currents and Mass Transfer Coefficients

The deposition of a metal during electrolysis involves three stages:

(a) The movement of ions from the bulk of the solution to the surface of the electrode,

(b) The electrochemical reaction, and

(c) Deposition on the surface of the electrode.

The Nernst hypothesis of a stagnant layer of electrolyte in contact with the electrode surface has been extensively used in describing the mechanism of the mass transfer process. From a hydrodynamic viewpoint this theory is no longer acceptable but the basic concept - the existence of a thin liquid layer, adjacent to the electrode, within which all the concentration change occurs - has been confirmed (61). Even when the electrolyte is vigorously stirred the concentration of the reacting ion decreases in the immediate vicinity of the cathode when a current is passed. Right at the cathode surface the velocity of the hydrodynamic flow is, of course, zero. Hence, mass transfer to the cathode is controlled by the rates of migration due to the potential field and diffusion due to the concentration gradient set up by the discharge of ions at the cathode.

The steady rate of discharge for a certain ionic species can be expressed as

$$N = D\left(\frac{dc}{dx}\right)_s + \frac{i\Gamma}{zF} \qquad \ldots (10.1)$$

where, N = total rate of transfer, gm ions/cm^2 sec.

D = diffusion coefficient cm^2/sec.

i = current density amps/cm^2

Γ = transference number of ionic species.

The terms on the right hand side of equation (10.1) represent the contributions of diffusion and migration, respectively.

Since $i = zFN$

$$\therefore \quad i = \frac{zFD\,(dc/dx)s}{(1-\Gamma)}$$

The transference number of the species participating in the electrode reaction may be made negligibly small - thus eliminating the effect of ionic migration - by adding an 'indifferent' electrolyte. The indifferent electrolyte does not react at the electrode, is present in relatively high concentration and has high conductivity in comparison with the ionic species being transferred.

Hence, $$\frac{i}{zF} = D\left(\frac{dc}{dx}\right)_s \qquad \ldots (10.2)$$

In an electrolysis cell in which the electrolyte is agitated by stirring or pumping the bulk concentration of the solution may be considered uniform. When a current is passed through the cell the concentration of the discharging ion at the solid/liquid interface changes from the average bulk concentration c_b to c_s, and a depleted zone called the diffusion layer is formed. If the diffusion layer were stationary as postulated by Nernst, the concentration profile would be linear. Interferometric measurements have shown that the concentration of the reacting species does in fact increase linearly with distance from the electrode over a considerable part of the diffusion layer (62). By assuming that this holds true for the whole of the diffusion layer, i.e., that the concentration gradient dc/dx remains constant, the diffusional term in the above expression may be integrated to give

$$\frac{i}{zF} = \frac{D}{\delta N}\left[c_b - c_s\right] \qquad \ldots (10.3)$$

where δN is the thickness of Nernst's hypothetical, stagnant diffusion layer.

Thus the rate of deposition is directly proportional to the concentration driving force and inversely proportional to the thickness of the diffusion layer.

The rate of transfer may, alternatively, be written

$$\frac{i}{zF} = k_m\ (c_b - c_s) \qquad \ldots (10.4)$$

where k_m = mass transfer coefficient, cm/sec.

If the current is increased by stepping up the applied voltage, the rate of discharge will steadily increase until it equals the rate of diffusion, while the surface concentration will gradually fall to zero. At the maximum rate of deposition, or "limiting current" the concentration driving force equals the bulk concentration, and the mass transfer coefficient can be calculated

$$i_L/zF = k_m c_b \qquad \ldots (10.5)$$

This condition will be shown on a plot of current versus voltage as a horizontal portion or plateau. Further increases in current can only be achieved if a consecutive electrode reaction is possible, for example, discharge of the hydrogen ions in solution.

10.2 Concentration Polarisation and Chemical Polarisation

When a metal is immersed in an electrolyte an equilibrium tends to be established, in which a steady difference of potential exists across the metal/solution interface. Although macroscopically a static situation exists, on a molecular scale, a constant exchange of ions or electrons takes place through the phase boundary. The constant transfer of charge in each direction corresponds to identical anodic and cathodic current densities. The magnitude of these mutually compensating current densities is called the exchange current density, i_o.

When an emf. is applied, the equilibrium at the metal/solution interface is destroyed and the potential of the electrode departs from its equilibrium value. The difference between the single electrode potential $E(i)$, for current density i, and the equilibrium value, $E(o)$, is termed the overpotential η. The value of η characterises the departure from equilibrium that exists in a cell through which a current is flowing. In electrochemistry this is commonly referred to as polarisation.

The effect of η is twofold; for the deposition of metal at a cathode, part of η increases the rate of deposition of metallic ions and the remainder diminishes the rate of dissolution of the metal surface. These respective effects are accomplished by increasing the free energy of activation for the dissolution process and decreasing the free energy of activation for the discharge process. In terms of the exchange current density, the current density corresponding to the net rate of deposition of metal at the cathode is given by

$$i_c = i_o \exp(\alpha' \eta F/RT) - i_o \exp(-(1-\alpha')\eta F/RT) \quad \ldots 10.6$$

where α' is the fraction of the overpotential assisting the overall direction of the reaction (63).

For the passage of a finite current through an electrolysis cell the applied potential difference must exceed the equilibrium difference by a finite amount. Part of this potential difference is necessary to overcome the internal resistance of the cell and is equal to the IR product. The corresponding electrical energy, I^2R, is dissipated as heat.

Two other sources of voltage difference are usually distinguished.

Concentration polarisation arises from concentration gradients within the electrolyte, caused, as we have seen, by a slow rate of transfer of ions from the bulk of the solution to the surface of the electrode. It is the change in electrode potential accompanying the change in metal ion concentration at the solution/electrode interface. For a change in concentration at the interface from the value at rest c_b to c_s the concentration polarisation is equal to the emf of a concentration cell with transference, in which the electrodes are in contact with solutions of concentration c_b and c_s respectively.

$$\eta_{conc} = RT.\ln(c_s/c_b)$$

assuming that transfer by migration of the metal ion is negligible and the ratio of ionic activity coefficients is unity (60).

Chemical polarisation occurs when the rate of electrolysis is affected by a slow process at the electrode surface. The overall reaction at the electrode is composed of a sequence of steps or partial reactions: the electrochemical reaction at the electrode including the discharge of ions: formation of final products from discharged ions, e.g., H_2 from hydrogen atoms; formation of new phase nuclei on the electrode surface, e.g., nuclei of crystalline deposits in the deposition of metallic ions; growth of the new phase, etc. Although Vetter (64) has examined in detail each of the various steps as possible sources of overvoltage, the general term "chemical polarisation" is commonly used irrespective of whichever step is the controlling factor. For deposition or solution at metal electrodes chemical polarisation is usually small. Much more noteworthy are the overvoltages required for the liberation of gaseous hydrogen and oxygen.

10.3 Concentration Polarisation at Dissolving Anodes

Quite different effects from those observed at the cathode are produced at anodes where, instead of the discharge of anions, dissolution of the anode itself occurs. In the electrolysis of copper sulphate solutions using copper anodes, for instance, increasing the applied voltage tends to increase the concentration of copper sulphate in the diffusion layer. The limit which the concentration in this layer can reach is determined by the solubility of the electrolyte. If the applied potential is increased to the stage where the rate of dissolution of the anode is such that a saturated solution of copper sulphate is formed in the immediate vicinity of the anode surface, any subsequent increase in voltage will lead to precipitation of copper sulphate crystals on the anode. Hence, instead of limiting currents which accompany cathodic processes, limiting concentration polarisation is reached (63).

10.4 Electrolysis of Acidified Copper Sulphate Solutions

A commonly used system which allows mass transfer rates to be determined by electrolysis consists of copper electrodes immersed in dilute copper sulphate solution with sulphuric acid as the indifferent electrolyte (65), (66), (67), (68). Normal working concentrations are 0.01 - 0.05 molar copper sulphate and 1.5 M H_2SO_4. Recalling the theory of single electrode potential, (69),

$$E = E^{o} - \frac{RT}{zF} \ln \frac{(\text{oxidised state})}{(\text{reduced state})}$$

where, Reduced state = oxidised state + ze z is the number of electrons (e) by which the oxidised and reduced states differ,

E is the oxidation potential of any reversible electrode, and

E^{o} is the corresponding standard oxidation potential.

The reduction potential of any electrode is equal to the oxidation potential for the same electrode with the sign reversed.

For the system $Cu/CuSO_4$ the feasible reactions are as follows

(a) At the cathode

(i) $Cu^{++} + 2e = Cu \qquad E^{o} = +\ 0.34$ volts

$$E_{Cu} = E^{o}_{Cu} + \frac{RT}{2F} \ln C_{Cu^{++}}$$

For 0.01 M $CuSO_4$ solution $C_{Cu^{++}} = 10^{-2}$ gm. ion/litre

Hence, $E_{Cu} = 0.28$ volts

(ii) $H^{+} + e = \frac{1}{2} H_2 \qquad E^{o}_{H} = 0.0$

$$E_{H} = \frac{RT}{F} \ln C_{H^{+}}$$

In a 1.5 M solution of H_2SO_4 the concentration of H^{+} ions is 3 gm.ion/litre

Hence, $E_{H} = 0.028$ volts

Since the deposition of copper requires a lesser expenditure of energy than the evolution of hydrogen, as the former process is spontaneous whereas the latter is not, copper is preferentially discharged at the cathode. In other words, cathodic processes occur in order of decreasing reduction potential.

Furthermore, a voltage in excess of the calculated value is required before any visible evolution of hydrogen occurs. The activation overpotential of hydrogen on a copper electrode is fairly high, the exact value, which will be negative in sign, depending on the current density and cell conditions.

(b) At the anode

(i) $Cu = Cu^{++} + 2e \qquad E^{o}_{Cu} = - 0.34$ volts

$$E_{Cu} = E^{o}_{Cu} - \frac{RT}{2F} \ln C_{Cu^{++}}$$

$$= - 0.28 \text{ volts}$$

(ii) $2OH^{-} = \frac{1}{2} O_2 + H_2O + 2e \qquad E^{o}_{OH} = - 0.401$

$$C_{OH^-} \times C_{H^+} = 10^{-14}$$

$$C_{OH^-} = 10^{-14}/3$$

$$E_{OH} = E^{o}_{OH} - \frac{RT}{F} \ln (3 \times 10^{14})$$

$$= - 0.401 - 0.853$$

$$= - 1.254$$

Since anodic processes occur in order of decreasing oxidation potential copper preferentially dissolves at the anode. In addition, the potential at which oxygen evolution commences is invariably greater (anodically) than the calculated reversible value, i.e., there is an overvoltage for oxygen evolution.

11. Experimental Study

11.1 Objectives

The direct objective of the second series of experiments was to determine variations in the local mass transfer coefficient downstream of abrupt expansions by means of the electrolytic technique. It was proposed to investigate the same range of expansion ratios as were used in the earlier experiments. Details of the flow pattern deduced from the previous experiments could then be used in interpreting the significance of the mass transfer distribution patterns obtained.

It was further proposed to determine heat transfer distribution patterns from the mass transfer results by means of the Chilton-Colburn analogy. Published papers on heat transfer were available for comparison with results derived for the smaller expansion ratios.

11.2 Electrolytic System

The ready availability of copper tubing of the required size range and the stability of acidified copper sulphate solutions were principal factors influencing the choice of system. The disadvantages of the most commonly used alternative for experiments of this nature were the prohibitive cost of nickel and the tendency of potassium ferrocyanide and ferricyanide to decompose slowly in daylight. Although chemical polarisation is known to be negligible in the case of the redox reaction, no difficulties have been recorded in using the copper/copper sulphate system (65), (66), (67), (68).

11.3 Design of Test Sections: Consideration and Development

The most commonly adopted experimental procedure when determining variations in the heat transfer coefficient downstream of abrupt enlargements has been seen to impose boundary conditions of constant heat flux. A notable advantage of the electrolysis technique is that the conditions existing in tunnel burners are more exactly reproduced.

In order to ensure correct modelling, it is essential to maintain consistent boundary conditions throughout experimental trials. Since heat transfer to the tunnel wall occurs from the change of section onwards, electrode-position in the model must also commence immediately downstream of the enlargement. The use of an isolated cathode section at various distances from the plane of enlargement does not provide the local average values of the transfer coefficient since the development of the diffusion boundary layer begins at the leading edge of the electrode in each instance.

A second experimental arrangement which springs to mind when the problem of determining mass transfer distribution patterns is considered consists of a series of cathode sections, insulated from one another and assembled in the form of a composite pipe section. From above, the insulating rings must be kept as short as possible to avoid disrupting the diffusion boundary layer, without leading to bridging of the insulation by deposited copper. The mechanical difficulties involved in producing such a leak-tight, uniform bore section are at once obvious but would, at first sight, appear to be offset by more economical operation - a multi-cathode section providing increased running time and hence more experimental data between cleaning periods. However, simultaneous operation of the separate cathode sections requires excessive instrumentation.

An alternative procedure using multi-cathode sections is to increase systematically the length of the working electrode by coupling up additional sections. There are, however, good reasons for rejecting this method. Cathode sections nearest the jet nozzle would become excessively coated with copper as a result of repeated use and short sections might, in consequence, suffer considerable changes in surface area. Ibl and Schaddegg (70) have shown that the roughness of the deposit which develops at the limiting current is a great potential source of error. Removal of freshly deposited copper between experimental trials by reversing the polarity of the electrodes would not necessarily remove all uncertainty as to the stateof the working surface. Furthermore the length of the plateau at limiting current densities would be substantially reduced by restricting voltages to values well below that at which the evolution of hydrogen begins. Such a precaution is necessary to avoid contamination of the cathode surface and the formation of pockets of gas which might lodge in the annulus of the expanding jet, obscuring the upper surface of the cathode and distorting flow patterns.

The extreme alternative to using multi-cathode sections is to employ single electrodes of different lengths one after another. The leading edge of the mass transfer section must in each case be located at the plane of enlargement. If average mass transfer coefficients are determined for cathode lengths, say, 1 in., 2 ins. and 3 ins., the local average coefficient for each inch may be found by difference. An obvious disadvantage of this mode of operation is the loss of running time due to cleaning and assembling the apparatus. This could, to some extent, be overcome if the plateaux were extremely well defined and allowed limiting current densities to be determined by a single measurement at a particular voltage, rather than by plotting the complete current versus voltage curve. Experimental results for a given cathode length at various flow rates could then be obtained by adjusting the voltage to the required value as the velocity was systematically increased. Unfortunately plateaux tend to become less well defined as limiting currents progressively increase (a consequence of increasing cathode length and/ or velocity) making it difficult to define a voltage setting which would provide a representative limiting current value. Hence strict accuracy can only be maintained by plotting the variation in current as a function of applied emf. for each cathode section at each fluid flowrate.

From values $(k_m)_1$ and $(k_m)_2$ determined for two cathode lengths L_1 and L_2 the local average coefficient for the increment $(L_2 - L_1)$ is given by

$$(k_m)_{loc}\ (L_2 - L_1) = (km)_2 L_2 - (km)_1\ L_1 \qquad \ldots (11.1)$$

A more serious disadvantage of this operating procedure is that a single erroneous limiting current measurement, at L_2 say, may considerably affect the local coefficient computed for the incremental distance $(L_2 - L_1)$ and also that for the following increment $(L_3 - L_2)$. The risk of inaccuracy in measuring limiting current values becomes increasingly severe as velocities and cathode lengths are increased, as mentioned briefly above.

A compromise between single or multiple cathode sections served to overcome the problem of ill-defined plateaux at long cathode lengths and high fluid flowrates. Two cathode sections, requiring two distinct circuits, are operated simultaneously, the true test piece being the downstream electrode of short, fixed length. By varying the length of the upstream one of the pair of cathodes the test section proper can be used to measure average transfer coefficients over a short distance at different positions in the downstream duct. If potential differences in each circuit are kept equal both cathode pieces approach limiting current conditions simultaneously. Since current values at the upstream cathode need not be recorded only one precision ammeter is required. Changes in limiting current values at the principal cathode will be a function of velocity and position only and hence may be determined with improved accuracy.

11.4 Circuitry

The basic electrical circuit is depicted in figure (36). When single cathode sections of various lengths were used in turn the anode of the cell comprised the upstream section plus the main portion of the downstream section. When two cathode sections were operated two anode sections were also required and the circuit shown in figure (36) was duplicated, using the upstream section, and that portion of the downstream section other than the test pieces, as distinct anodes.

Current was drawn from a 6 volt battery and limited to the required value by means of a variable resistor R_1 (maximum resistance 250 ohms) connected in series with the electrolysis cell. The potential difference across the cell could be increased by simply reducing the value of the resistance R_1. A greater current was thereby drawn from the battery and the volt drop across the cell thus increased by virtue of the increased current passed through it. Except at very low voltages the electrolysis cell does not behave as an ohmic resistor, i.e., V/I is not

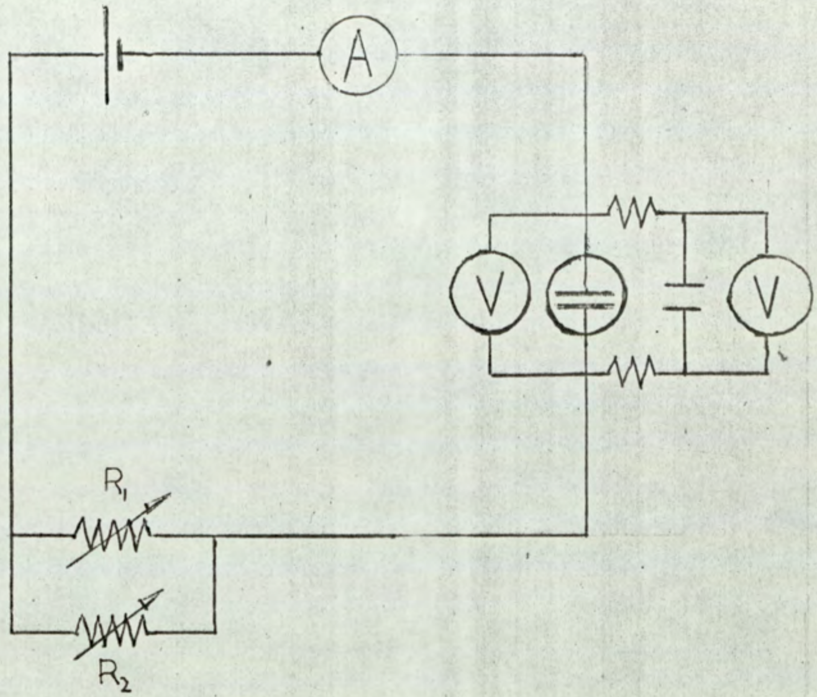

fig. 36

constant. With the approach of limiting current conditions, changes in R_1 bring about changes in the internal resistance of the cell such that the potential difference between the terminals increases without the current passing being increased. Since the applied emf. does not feature in the calculation for k_m, absolute values were not required and the use of a standard reference electrode was dispensed with. The potential of the cathode was measured relative to that of the anode which, by virtue of its large surface area, served as a convenient reference electrode. A second resistor R_2 (maximum value 150 ohms) was connected in parallel with R_1 to provide improved control over the rate of increase of applied potential. The resistor R_2 was initially set at zero resistance, and the potential difference across the cell increased steadily by varying R_1 only. Adjustment of R_2 enabled the applied voltage to be regulated with greater precision as limiting current conditions were approached. An electronic millivoltmeter was used to indicate instantaneous increases in the applied potential. The unsteady nature of the flow in the jetting zone produced considerable fluctuations in voltage which it was necessary to damp out in order to record the mean voltage corresponding to steady state current on a conventional voltmeter. The filter circuit comprising resistors R_3 (of the order of 10 KΩ) and a capacitor (approx. 10 μF) in series, was connected across the terminals of the cell, in parallel with the millivoltmeter (see figure 36). Currents were measured on an ammeter with a 12 ins. scale operated in conjunction with a set of shunts enabling full-scale deflection to be varied from 0.1 to 5.0 amps. In some instances, slight fluctuations in current were recorded. Fluctuating currents cannot be damped directly, the requisite procedure being to pass the current through a fixed resistance, thus converting it to a fluctuating voltage, and to damp out the fluctuations in voltage. This remedy was examined, but the relative accuracy of the additional voltmeter available offered no improvement over values read from the original ammeter.

11.5 Apparatus

The basic flow loop was essentially that employed in the investigation of static pressure variations at abrupt enlargements. Except for the copper tubing forming the abrupt expansion, the complete circuit was of an all-glass construction. An additional rotameter was incorporated, in parallel with the single rotameter from the earlier experiments, in order to measure lower flow-rates. The expansion ratio was varied, as before, by altering only the diameter of the downstream duct.

The upstream section was $\frac{3}{4}$ ins. I.D. copper tube, 6 ft. in length to ensure fully developed flow at the enlargement. The upstream section, with a welded-on flange, was made the anode of the electrolysis cell. A natural rubber gasket covered the face of the flange, insulating it from the cathode section immediately downstream of the plane of enlargement. A central hole was cut in the gasket (using a short length of $\frac{3}{4}$" I.D. copper tubing, sharpened in the manner of a cork borer) and the gasket glued on to the flange to avoid any distortion of the flow pattern. The cathode section, consisting of a length of the downstream tube, was located by means of a perspex guide plate and made a simple butt joint with the rubber gasket, so that the leading edge of the mass transfer section was at the plane of enlargement. The downstream end of the cathode section fitted into a polythene flange. A soft rubber gasket formed an effective seal between this flange and the flanged end of the main length of the downstream section. Small spigots on the face of the copper flange ensured that the cathode section was correctly aligned, giving a smooth boundary wall. The cathode test piece was held in position by tension bolts joining the main flanges on the upstream and downstream sections. Backing flanges prevented distortion of the copper flanges.

When two cathode sections were operated simultaneously a smooth joint was obtained by using a polythene ring with a 'T' shaped section (see figure 37) which also insulated the two cathode pieces from each other. Two distinct anodes were also required in these circumstances: the

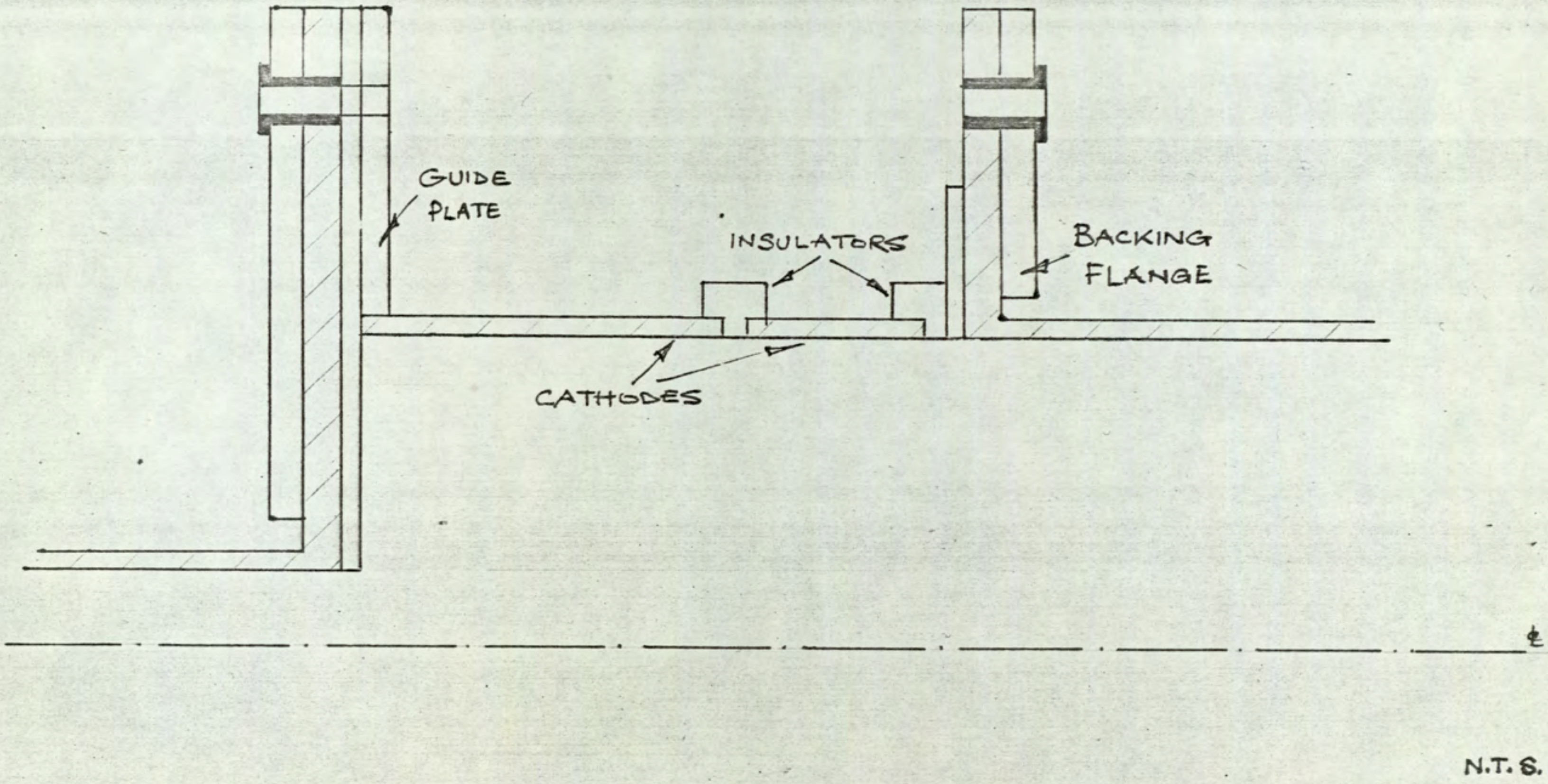

Fig. 37

upstream section and the main portion of the downstream section served as separate anodes. (At other times these were coupled together to form a single anode). Tension bolts between the flanged ends of the anode sections were insulated by lining bolt holes with perspex sleeves.

11.6 Chemical Analysis of the Electrolyte

(a) The acid strength of the solution was determined by diluting 10 ml. portions of the electrolyte with 25 mls. of distilled water and titrating with normal sodium carbonate solution using methyl red as indicator. Adding the carbonate solution from a burette ensured excess acid up to the end point and avoided precipitation of basic copper carbonate. The end point was marked by a change in colour from magenta to neutral grey. The addition of further sodium carbonate solution gave a yellow/green coloration and a precipitate of copper carbonate.

(b) Determination of copper (71)

(i) Using EDTA.

The standard procedure for determining copper ion concentrations using EDTA with Fast Sulphon Black as indicator failed to produce a sufficiently well defined end point probably due to the very low concentrations involved and the excessive quantity of ammonia necessary to neutralise the mineral acid present.

(ii) Using sodium thiosulphate solution.

25 ml. portions of the test solution were pipetted into an evaporating basin and the mineral acid present neutralised by adding sodium carbonate solution until a faint permanent precipitate remained. This was then removed by the addition of a drop or two of 1:1 acetic acid and the pH adjusted to 4 - 5.5. 5 mls. of 10% potassium iodide solution were added and the liberated iodine titrated with N/40 sodium thiosulphate solution. The contents of the basin were stirred continuously. When the brown colour of the solution turned to yellow, 2 mls. of starch solution and 5 mls. of 10% ammonium thiocyanate solution were added, giving an intense blue colouration. The titration was completed as rapidly as possible, continuous stirring and the use of an evaporating basin, continuous stirring and the use of an evaporating basin, rather than a conical flask, making the end point more readily detectable. At the end point a pale flesh colour was obtained. The titration was repeated using two further 25 ml portions of the electrolyte.

The reaction is:

$$2CuSO_4 + 4KI = Cu_2I_2 + I_2 + 2K_2SO_4$$

from which it follows that:

$$2CuSO_4 = I_2 = 2\ Na_2S_2O_3$$

$$\text{or } 1 \text{ ml } N\text{-}Na_2S_2O_3 = 0.06357 \text{ gms. Cu.}$$

The use of starch solution alone as indicator gives an ill-defined end point as the blue colour very slowly returns. It was imperative to use only freshly prepared starch as a permanent end point was not otherwise obtained despite the addition of the ammonium thiocyanate.

According to the standard procedure set out in (71) the addition of the ammonium thiocyanate should be delayed until, on the addition of further sodium-thiosulphate, the blue colour produced by the starch alone begins to fade. As it was found that the blue colour was dispersed almost immediately, and was extremely slow in reappearing, the starch and ammonium thiocyanate were added together.

Starch solution was prepared by making a paste with 1 gm of starch and a little cold water and pouring this into 100 mls. of boiling water. After boiling for 1 minute the solution was allowed to cool and 2 - 3 gms. of potassium iodide added.

The sodium thiosulphate solution required for the titration was prepared by weighing approximately

6.25 gms. of A.R. crystals and making up a litre of solution. 3 drops of chloroform were added to preserve the solution. Since sodium thiosulphate effloresces it is unsuitable as a primary standard and it was necessary to standardise analytical solutions before use by titration with copper sulphate solution of known concentration.

11.7 Physical properties of the electrolyte

Physical properties of aqueous copper sulphate/ sulphuric acid solutions have been determined by Eisenberg, Tobias and Wilke (72). Densities of copper sulphate solutions, 1.5 M in H_2SO_4 are given at temperatures, 15°, 20°, 25° and 30°C. for molarities of $CuSO_4$ ranging from zero to 0.8. Viscosities are also given for the same conditions. Diffusivities were determined at temperatures in the range $20^\circ - 25^\circ$C. in acid solutions approximately 1.5 M (73). Exact values of the diffusion coefficient may be determined from a graph of ionic strength versus $D\mu/T$, where D is the diffusion coefficient and T the temperature in degrees Kelvin. Such a plot gives a straight line. For $CuSO_4/H_2SO_4$ solutions the ionic strength, $\bar{I}$ is given by

$$\bar{I} = 4\text{conc}(CuSO_4) + 3\text{conc}(H_2SO_4)$$

with concentrations expressed as molarities (74). The copper sulphate concentration to be used in the present context is the average value for the diffusion zone. Assuming a linear concentration profile for the copper ion in the diffusion layer the average concentration under limiting current conditions is half the bulk concentration.

A least mean squares fit of the data of ref. (73) gives,

$$\frac{D\mu}{T'} \times 10^7 = 0.2375 + 0.00318\,\bar{I}$$

For copper sulphate solutions ranging from 0.005 to 0.015 molar sulphuric acid physical data are essentially constant:

$c_b = 0.005$; $\mu = 1.213$ cp; $\rho = 1.089$ gm/cc; $D = 0.619 \times 10^{-5}$ cm^2/sec.

$c_b = 0.015$; $\mu = 1.219$ cp; $\rho = 1.090$ gm/cc; $D = 0.615 \times 10^{-5}$ cm^2/sec.

11.8 Rotameter Calibration

The very slight variations in physical properties due to variations in the copper sulphate concentration of the electrolyte allowed the rotameters to be calibrated using an average value of density and viscosity:

$$\rho = 1.090 \text{ gms./cc.}$$

$$\mu = 1.216 \text{ cp.}$$

Calibration curves embodying these values are shown in figures (38) and (39) for rotameter models 35 and 65. The calibration procedure is exactly similar to that for the previous experiments.

fig. 38

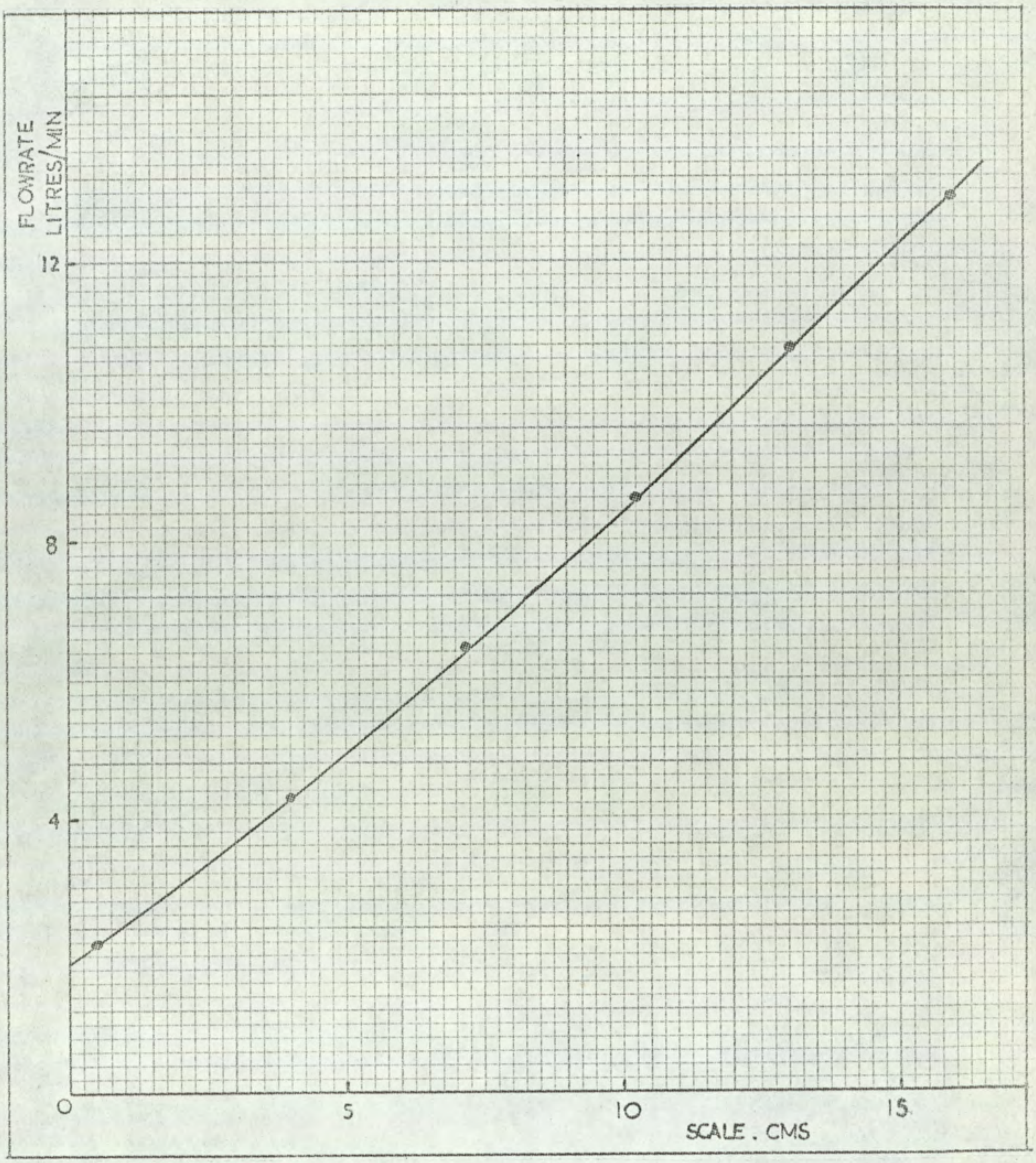

fig. 39

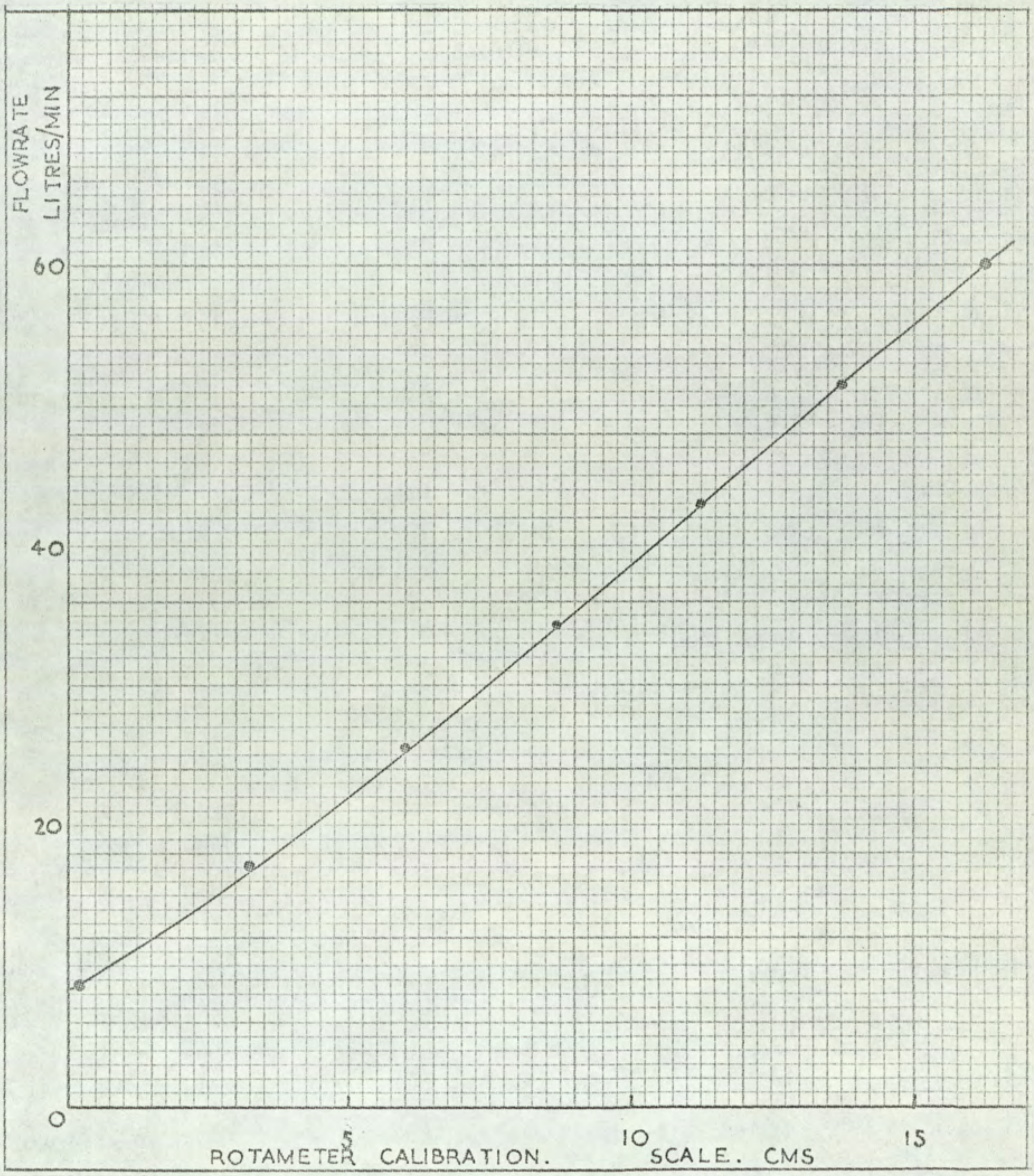
FLOWRATE
LITRES/MIN
60
40
20
0
5
10
15
ROTAMETER CALIBRATION.
SCALE. CMS

Calibration Data

Model 35

Scale reading (cms)	0.5	4.0	7.15	10.25	13.1	15.85	
Flowrate (litres/min.)	2.148	4.296	6.444	8.592	10.740	12.888	
Scale reading (cms.)	0.3	3.3	6.07	8.7	11.3	13.8	16.3
Flowrate (1/min.)	8.57	17.13	25.695	34.26	42.825	51.390	59.955

11.9 <u>Cathode Preparation</u>

Cathode sections were cleaned in the first instance by swabbing the surface with dilute nitric acid. When all traces of acid had been washed away the surface was cleaned with soft wire wool which was found to be more effective and less prone to scratch the electrode surface than emery cloth. The cathode was rewashed, degreased with acetone and finally rinsed with distilled water. After the initial cleaning process cathode sections were plated and cleaned several times before being used in test runs. In all cleaning operations to remove deposited copper the above procedure was followed without the nitric acid step.

11.10 <u>Pretreatment of Electrolyte</u>

Prior to each experimental trial the electrolyte was continuously pumped around the circuit to raise the temperature to 25°C. The cooling water rate was then adjusted to maintain this temperature. The electrolyte was deaerated by bubbling oxygen-free nitrogen through the solution in the reservoirs. The beck of each reservoir was covered with a polythene cap to maintain an atmosphere of nitrogen and avoid the entrainment of air. As the velocities employed produced little vortex formation the risk of entrainment was, in any event, slight.

11.11 Preliminary Investigations

Although the experimental technique for obtaining limiting current values is well established (68) (75), (76), preliminary trials were necessary to determine the most reliable cathode arrangements, suitable copper ion concentrations and so forth.

Details of the possible experimental arrangements for subdividing the test section into sufficiently short sections, capable of providing accurate values of the local mass transfer coefficient have already been presented (Section 11.3). Some of the points discussed in this earlier section were examined in the course of these exploratory trials, e.g., the question of renewing the cathode surface by reversing the polarity of the electrodes. Although the continual removal of the cathode for cleaning was extremely time consuming, comparison of the various schemes proposed in section 11.3 showed that the most reliable method of operation was to clean the cathode section immediately before use, according to the procedure set out in section 11.9 .

A disturbing discovery of the preliminary experiments was that the tube wall in the upstream section of the abrupt expansion developed a pronounced trumpet shape at the entrance to the downstream duct. As a consequence of the repeated draining of the complete copper section forming the abrupt enlargement (in order to remove the cathode for cleaning) and the subsequent refilling of this section, oxygen was continually being introduced into the system. The presence of dissolved oxygen renders copper soluble in dilute sulphuric acid and the rapidly expanding jet tended to wear down the sharp edge of the nozzle mouth. Results collected in the course of these initial experiments had, therefore, to be rejected and the upstream section replaced before formal experiments were begun. Thereafter, a close check was kept on the state of the nozzle mouth, the electrolyte was circulated slowly and oxygen-free nitrogen bubbled through it for not less than one hour each time the cathode was placed in position, and the copper ion concentration of the electrolyte was regularly determined.

Limiting current values are dependent upon the thickness of the diffusion layer which itself varies with the rate of flow or degree of agitation of the electrolyte. Since calculated Reynolds number for full bore flow upstream and downstream of the enlargement are a poor indication of the turbulence existing in the recirculation zone of the jet, a short series of experiments was necessary to establish the range of limiting current values which would be encountered using various concentrations of electrolyte. Published results on heat transfer served as a useful guide in this respect.

Irregular fluctuations in potential ($\pm$ 100 millivolts or more (64)) are a characteristic feature of limiting current conditions when the flow regime is turbulent. The unsteady nature of recirculating flow accentuated such fluctuations and in order to obtain experimental data for plotting complete polarisation curves a filter was required. Various combinations of resistors and capacitors were assembled in order to obtain the required damping effect without producing too slow a response to changes in voltage setting. Typical values of resistance and capacitance are quoted in section 11.4.

11.12 Experimental Procedure

With the freshly prepared cathode in position and the electrolyte circulating at the required velocity and temperature, a low current density was passed through the cell for a brief period (5-10 mins.) to establish a uniform, fresh deposit of copper on the cathode. The applied voltage was then increased to approximately 300 millivolts and thereafter increased systematically in steps of 30 - 50 millivolts. Some 2 minutes were allowed to elapse before the steady state value of the current corresponding to each voltage setting was recorded (77), (78). Voltages were increased until evolution of hydrogen occurred and a sharp increase in current was produced.

Fenech and Tobias (79) have shown that it is not necessary to start with zero potential difference; the initial voltage and the time required to reach limiting current conditions does not influence the observed value of the limiting current, except where excessive electrolysis times might lead to depletion of the bulk concentration. By keeping electrolysis times as short as possible, the risk of excessive copper deposits, which could invalidate results (70) (80), was reduced to a minimum. This was especially desirable when cathodes were several inches long as variations in mass transfer coefficient could conceivably lead to rather rough localised deposits.

Average mass transfer coefficients for the cathode length in question were calculated from the limiting current value obtained from the polarisation curve and a knowledge of the bulk concentration of the electrolyte, which was determined before and after each experimental run.

12. Experimental Results

12.1 Data

Table 13 presents measurements of total current, potential difference across the cell, and copper sulphate concentration for the following variables: expansion ratio, cathode length and position relative to the plane of enlargement and Reynolds number based on full bore flow in the downstream duct.

Also given in table 13 are the limiting current densities derived from the polarisation curves.

12.2 Polarisation Curves

A typical set of polarisation curves intended to show the effect of increasing velocity with a fixed cathode length is given in figure (41). Differences between the curves are not entirely attributable to the variation in flowrate as the electrolyte concentration is not exactly equal in all cases.

Figure (40) similarly shows the effect of increasing the cathode length with a fixed velocity. Again, the curves are not directly comparable because of variations in electrolyte concentration.

From an electrodynamic viewpoint the drop in potential across an electrolysis cell comprises the ohmic drop, concentration polarisation and chemical polarisation. The circuit can be regarded as a

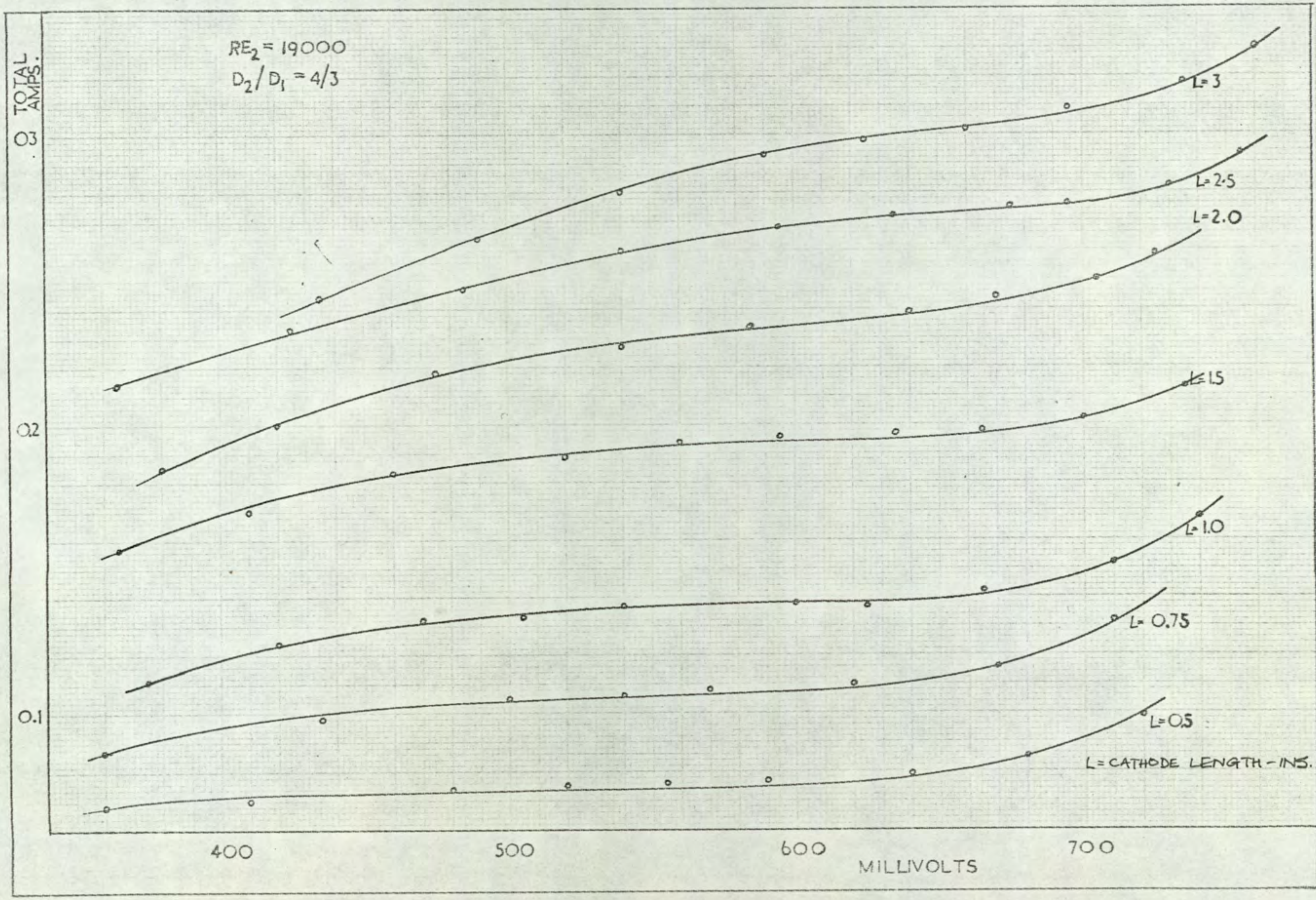

RE$_2$ = 19000
D$_2$/D$_1$ = 4/3
TOTAL AMPS.
0.3
0.2
0.1
400
500
600
700
MILLIVOLTS
L=3
L=2.5
L=2.0
L=1.5
L=1.0
L= 0.75
L=0.5
L=CATHODE LENGTH - INS.

Fig. 40

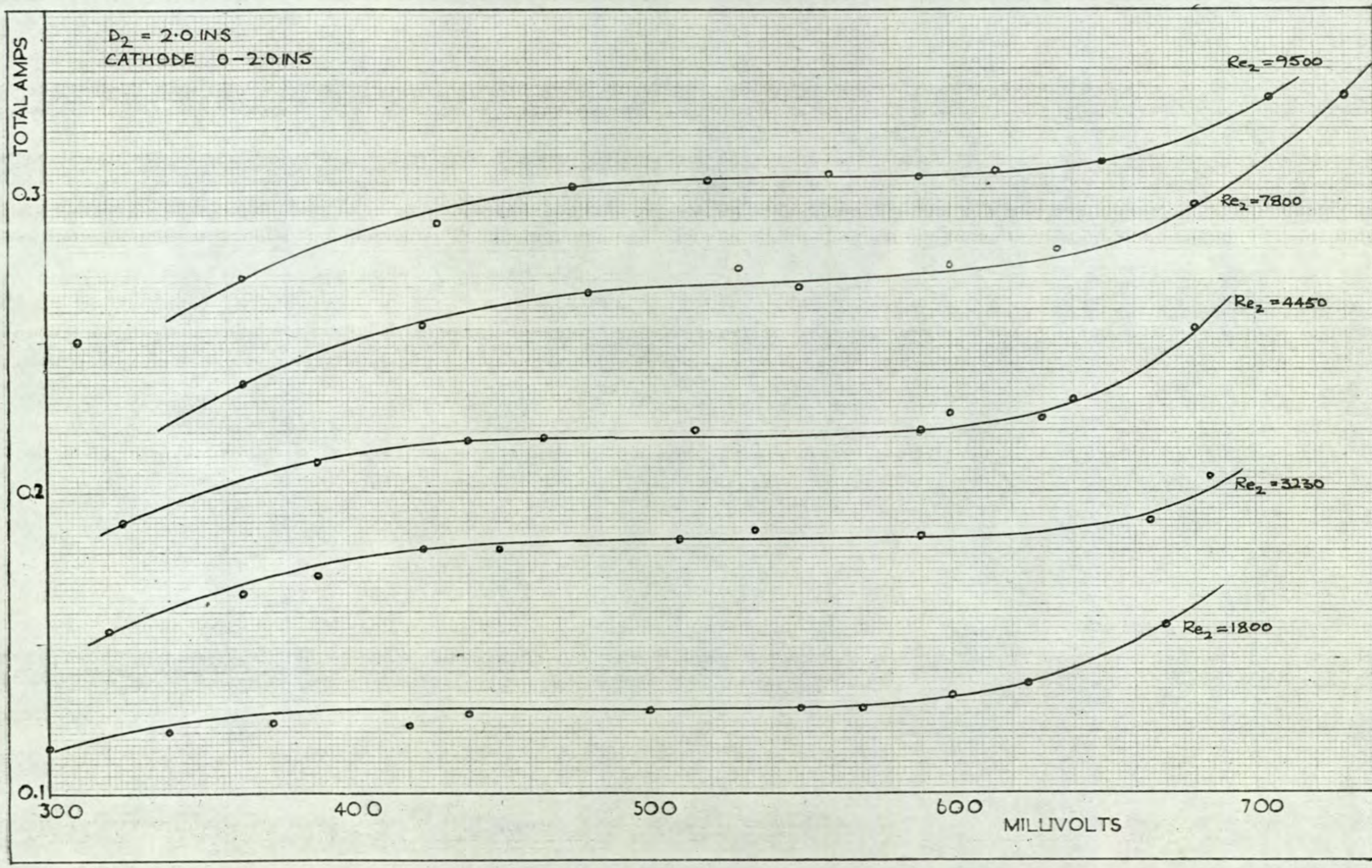

D_2 = 2·0 INS
CATHODE 0–2·0 INS
TOTAL AMPS
0.3
0.2
0.1
300
400
500
600
700
MILLIVOLTS
Re_2 = 9500
Re_2 = 7800
Re_2 = 4450
Re_2 = 3230
Re_2 = 1800

Fig. 41

combination of a linear element and two non-linear elements in series, the linear element corresponding to the solution of constant concentration, while the non-linear elements are equivalent to the diffusion layer of varying concentration and the zone of chemical reaction (61).

The influence of the individual element on the shape of polarisation curves is discussed in the following analysis of curves presented by the author.

(a) Ohmic Potential Drop

The resistance of any conductor varies directly as its length and inversely as its area,

i.e. Resistance = length/(k_s)(area) ...(12.1)

where k_s = specific conductance or conductivity (ohms^{-1} cm^{-1})

The potential change when a current, I amps, flows through the resistor is given by

$$(I)(\text{Res.}) = (I)(\text{length})/(k_s)(\text{area}) \qquad \ldots (12.2)$$

Hence the ohmic potential drop in a solution is a function of the current density, the geometric path of the current and the conductivity of the solution.

For the case of a cylindrical electrode rotating in a concentric cylindrical cell, Eisenberg, Tobias and Wilke (86), were able to evaluate the ohmic potential drop from the expression

$$(I)(\text{Res.}) = (I/2\pi k_s.\text{ht}).\ \ln(r_i/r_o) \qquad \ldots (12.3)$$

where, ht = height of cell,

r_i = radius of rotated inner electrode,

r_o = radius of outer electrode.

No equivalent expression was calculable in the author's case in view of the difficulty of accurately assessing the current path when electrodes are not directly opposed to each other.

It is clear that as far as the evaluation of mass transfer coefficients is concerned, the value of the ohmic potential drop (which is high in solutions of low concentration) is immaterial, since limiting current values are independent of potential difference under pure diffusion-controlled conditions.

Equations (12.2) and (12.3) show that the ohmic potential drop does not directly affect the flatness of the plateau developed under diffusion-controlled conditions: when the limiting value of current I is reached, the potential drop through the bulk of the solution will not vary with increasing applied potential. If, due to some other cause, the plateau is not exactly horizontal, i.e., the current density increases as the applied potential is stepped up, the ohmic drop will also increase. Even in such circumstances, the effect of increased ohmic potential drop is merely to reduce the magnitude of the applied increase in potential across the diffusion layer. Thus, the changes in the resistance of the electrolysis cell which occur at limiting current conditions are attributable to concentration and chemical polarisation.

(b) The thickness of the diffusion layer which develops at the electrode/solution interface is directly proportional to the degree of agitation or rate of stirring in an electrolysis cell. It follows therefore from the equation

$$i_L = zFDc_b/\delta_N$$

that increasing the Reynolds number will lead to higher limiting current values in a solution of constant concentration.

It is further found in the deposition of copper that increasing the turbulence delays the onset of diffusion-controlled conditions (see figure 41 and also polarisation curves published elsewhere (75) and (65)). Since the evolution of hydrogen occurs at an essentially constant voltage (i.e. the variation of overvoltage with current density (69) is very slight) the net effect of increasing the degree of agitation is to reduce the length of the plateau at the limiting current.

As the turbulence is increased polarisation curves develop a positive gradient rather than a flat plateau. The steepness of the curve is an indication of the relative importance of the electrode reaction rate in comparison with the rate of diffusion of copper ions to the cathode surface (81). The specification of limiting currents as the value at which hydrogen evolution is first observed (78) will be invalid if the overall reaction rate is not purely diffusion controlled and the concentration of copper ions at the cathode surface does not equal zero.

Shreir and Smith (82) have studied the variation of concentration polarisation and chemical polarisation with concentration and current density. For 0.25 molar copper sulphate solution in 0.5 molar sulphuric acid the chemical polarisation was expressed as

$$\eta_{ACTIVATION} = -0.090 + 0.071 \log i$$

The general form of this expression

$$\eta_{ACTIVATION} = a + b \log i$$

is obtained from equation 10.6; if the rate of the reverse electrode reaction is reduced to negligible proportions, the second term on the right hand side of equation 10.6 may be neglected.

Brown and Thirsk (83) have investigated the rate determining step in the electrode reaction during electrolysis of acidified copper sulphate solutions using a rotating disk electrode. Results were interpreted in terms of electrodeposition via a cuprous intermediate.

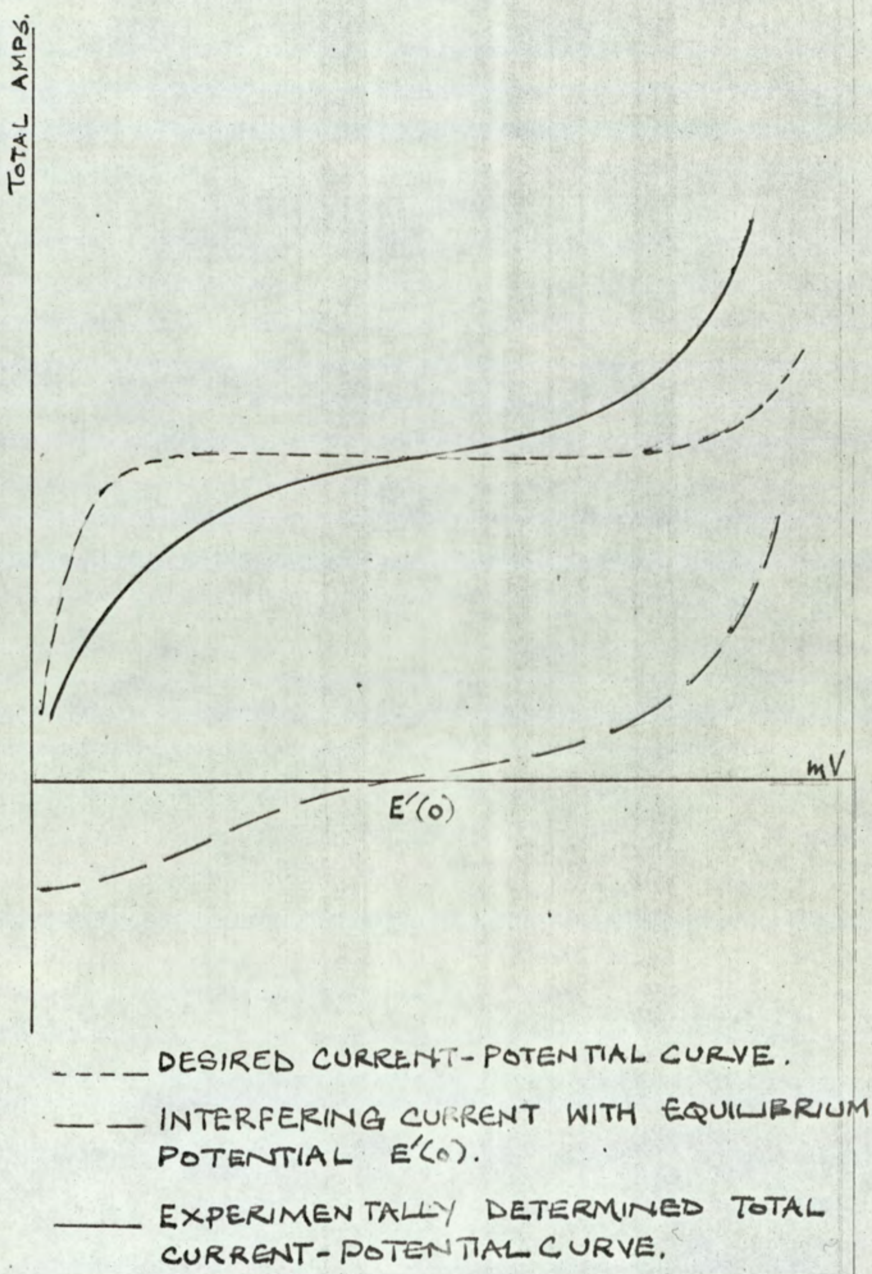
TOTAL AMPS.
mV
E′(0)
DESIRED CURRENT-POTENTIAL CURVE.
INTERFERING CURRENT WITH EQUILIBRIUM POTENTIAL E′(0).
EXPERIMENTALLY DETERMINED TOTAL CURRENT-POTENTIAL CURVE.

Figure (42) shows that experimental current-potential curves are produced by the summation of the current densities of two processes (64).

Although reduction of the bulk concentration helped to overcome the problem of non-flat plateaux due to the thin diffusion layers associated with highly turbulent conditions, it did not prove possible to work at increased flowrates except when cathode sections were short (of the order of 2 - 3 ins. maximum).

An effective solution to this problem was achieved by operating two circuits simultaneously, and using only a short length for the test section proper (as described in section 11.3).

(c) The definition of the plateau was further found to be directly dependent on the length of the cathode section. This was evidently due to variations in the values of local transfer coefficients which are to be expected in the light of published data on heat transfer coefficients in the recirculation and reattachment regions of confined fluid jets (53) (56) (58).

The overall reaction rate at different sections of the cathode is governed by different laws if the cathode surface is not uniformly accessible from a diffusional standpoint (64). Thus, the rate of deposition will not be diffusion-controlled if at any point the solution is not depleted, and the current-potential characteristic will accordingly differ at different sections. The experimental characteristic of the discharge total current on the electrode as a function of potential difference will therefore have a complex form. In particular, the horizontal plateau which expresses the limiting current will not be sharply defined.

Since the degree of variation in values of local transfer coefficients is directly related to the turbulence in the jetting zone the definition of the plateau was most affected at long cathode lengths and high flowrates.

12.3 Mass Transfer Coefficients

For a downstream diameter of 1.0 ins. limiting current values were determined for systematically increased lengths of cathode, each of which extended from the plane of enlargement. Average mass transfer coefficients based on the appropriate cathode length were determined from experimental measurements, according to equation 10.5

$$k_m = i_L / zFc_b \qquad \ldots (10.5)$$

Results are presented in table 14a. Local average coefficients per unit length were obtained from the tabulated values by difference:

$$(k_m)_{LOC}(L_2 - L_1) = (k_m)_2 L_2 - (k_m)_1 L_1 \quad \ldots (11.1)$$

Although average mass transfer coefficients for the separate cathodes show a general pattern of development, local average coefficients derived from these values are found to vary quite erratically. Results for $D_2 = 1.0$ ins. are given in table 15a.

For a downstream section 2.0 inches in diameter results were obtained in similar fashion for short cathode lengths. Tables 14b and 15b contain average mass transfer coefficients per unit cathode length and local average coefficients respectively.

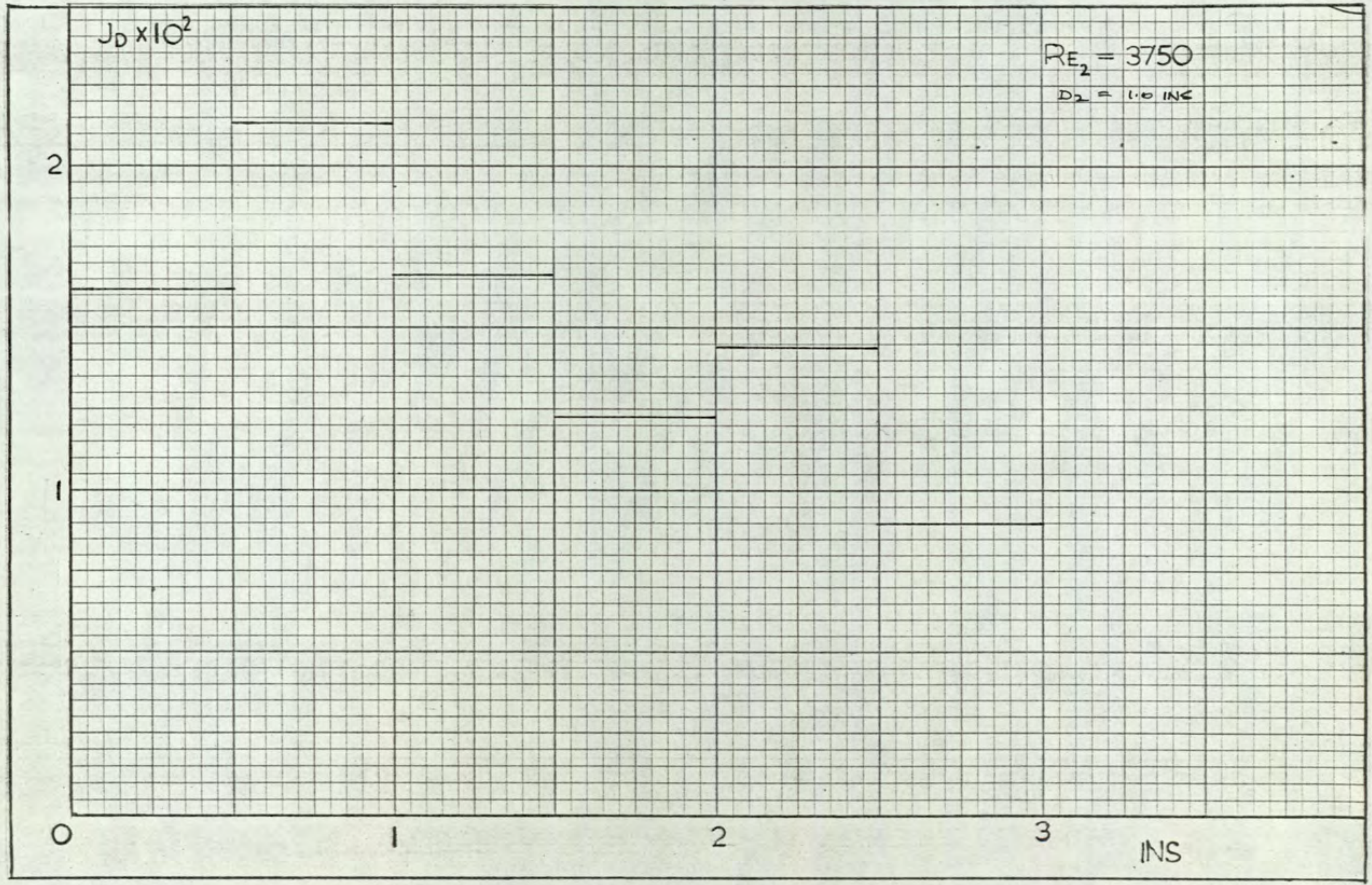

fig. 43a

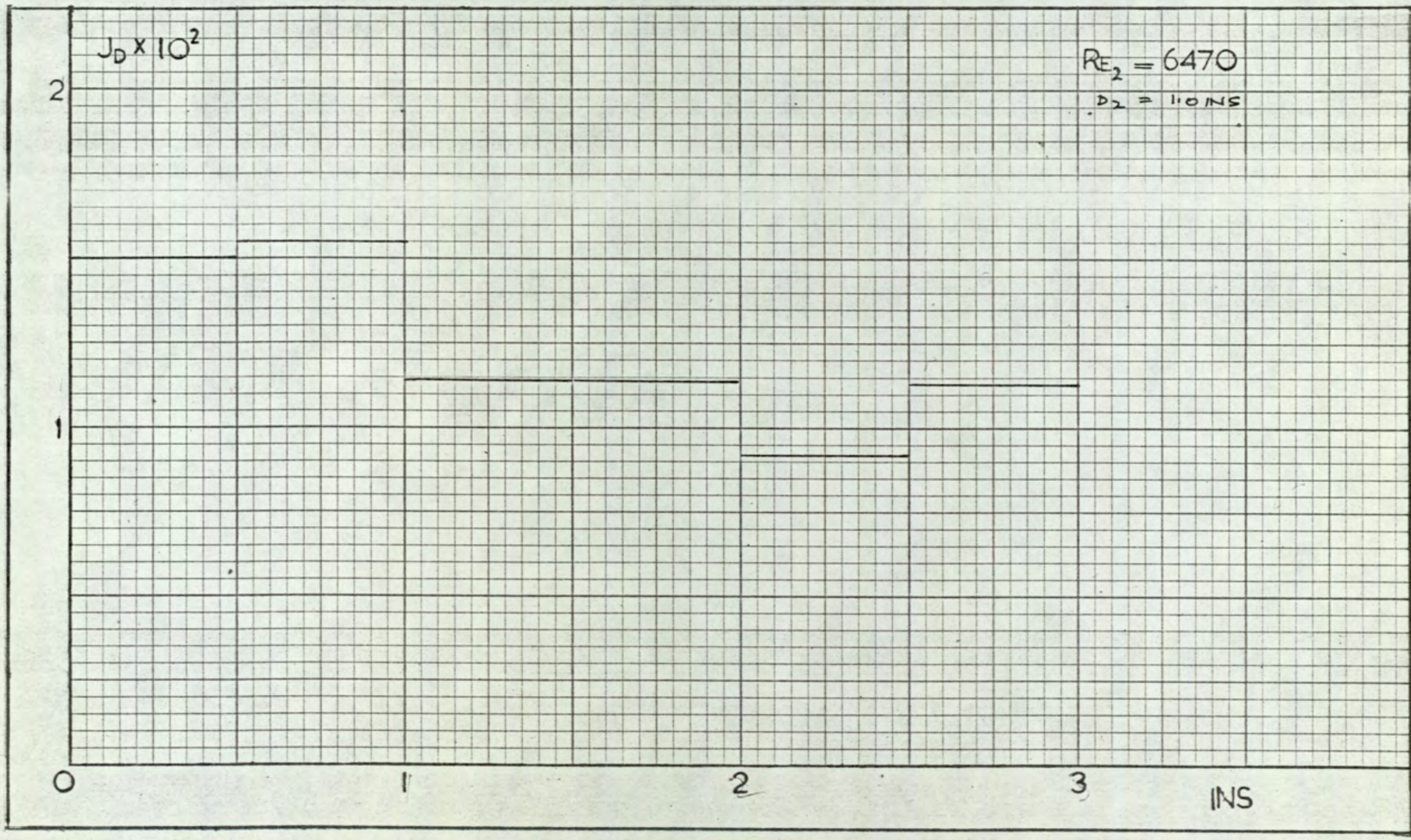

fig 43b

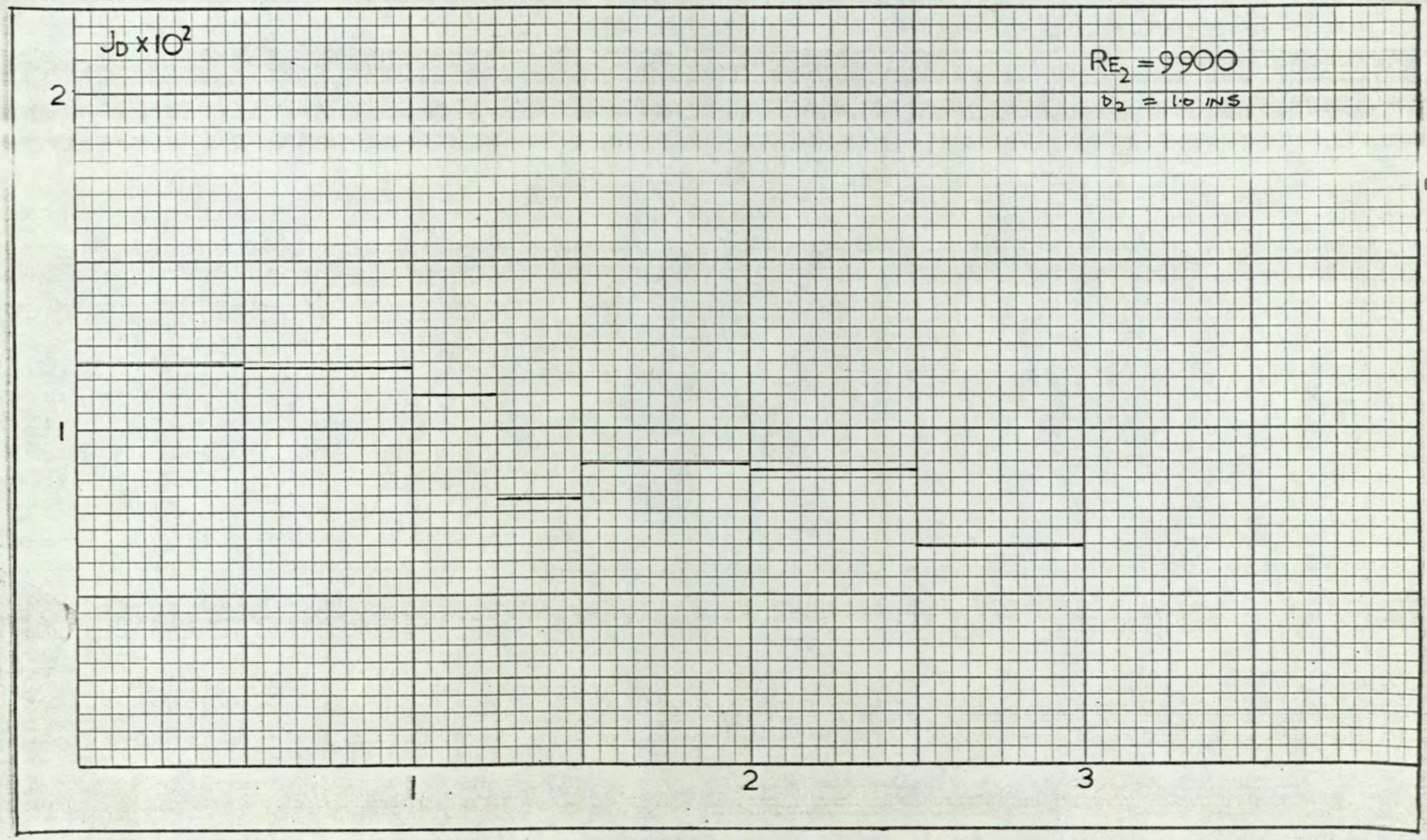

fig 43c

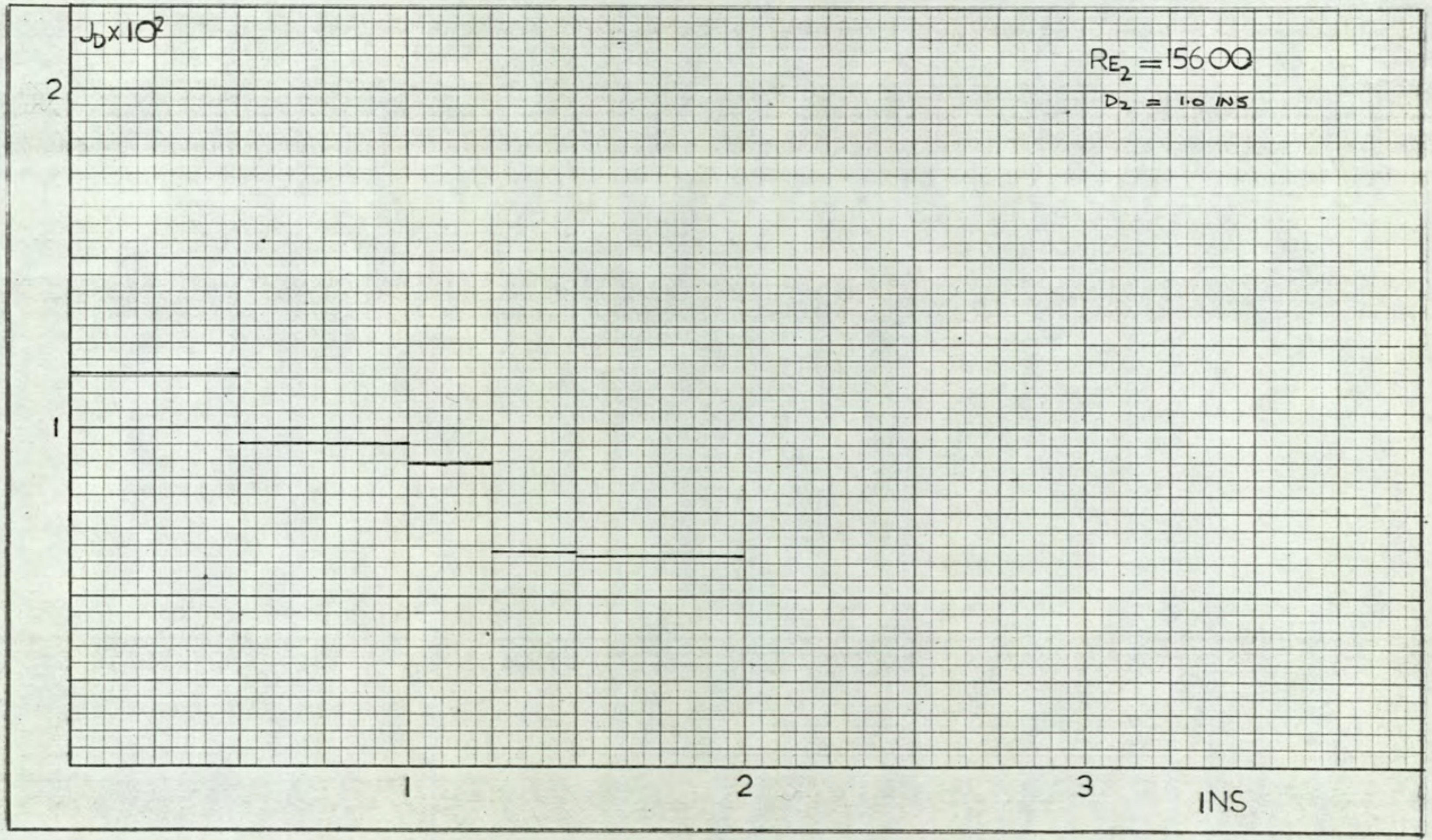

fig 43a

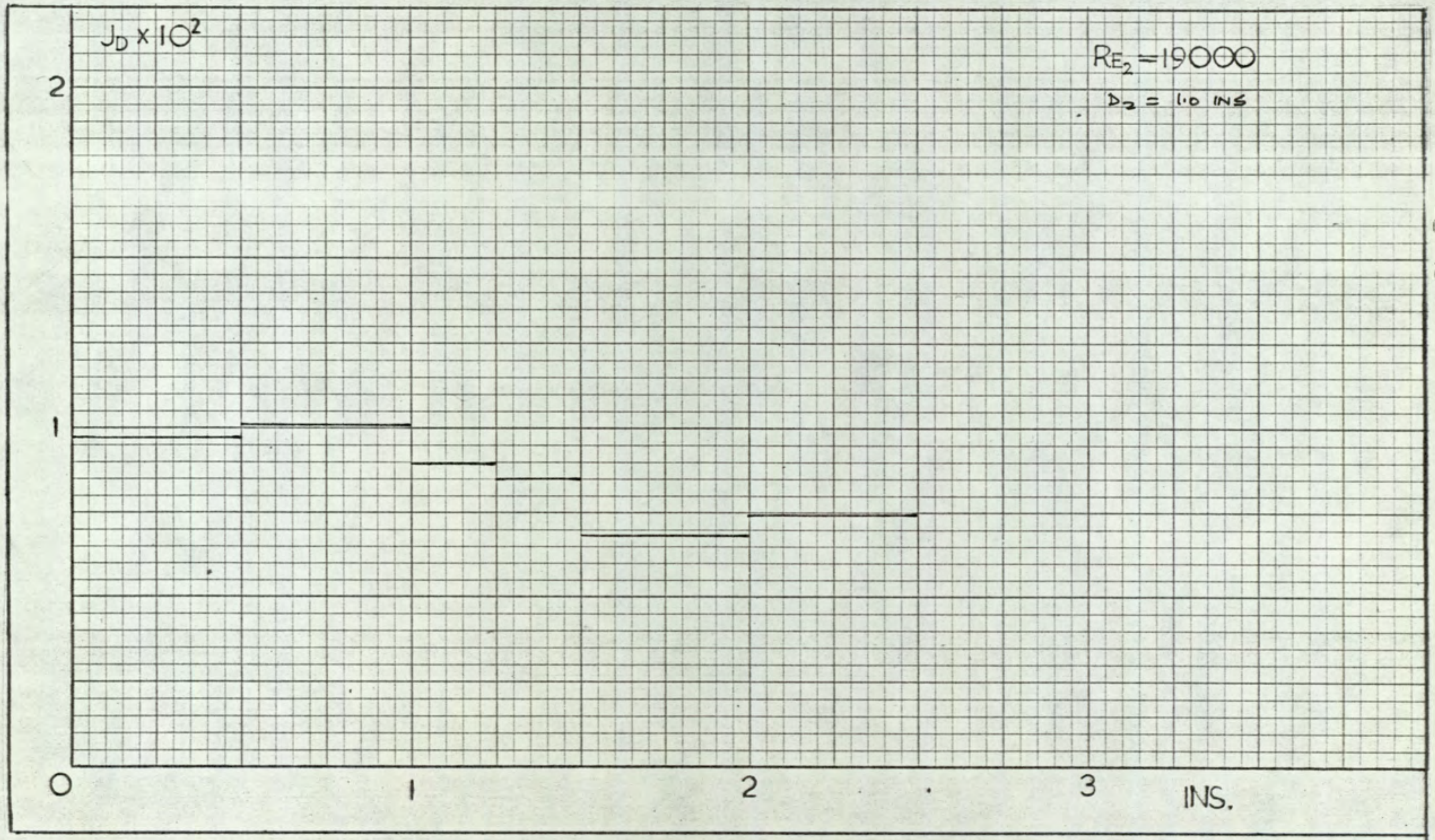

fig 43e

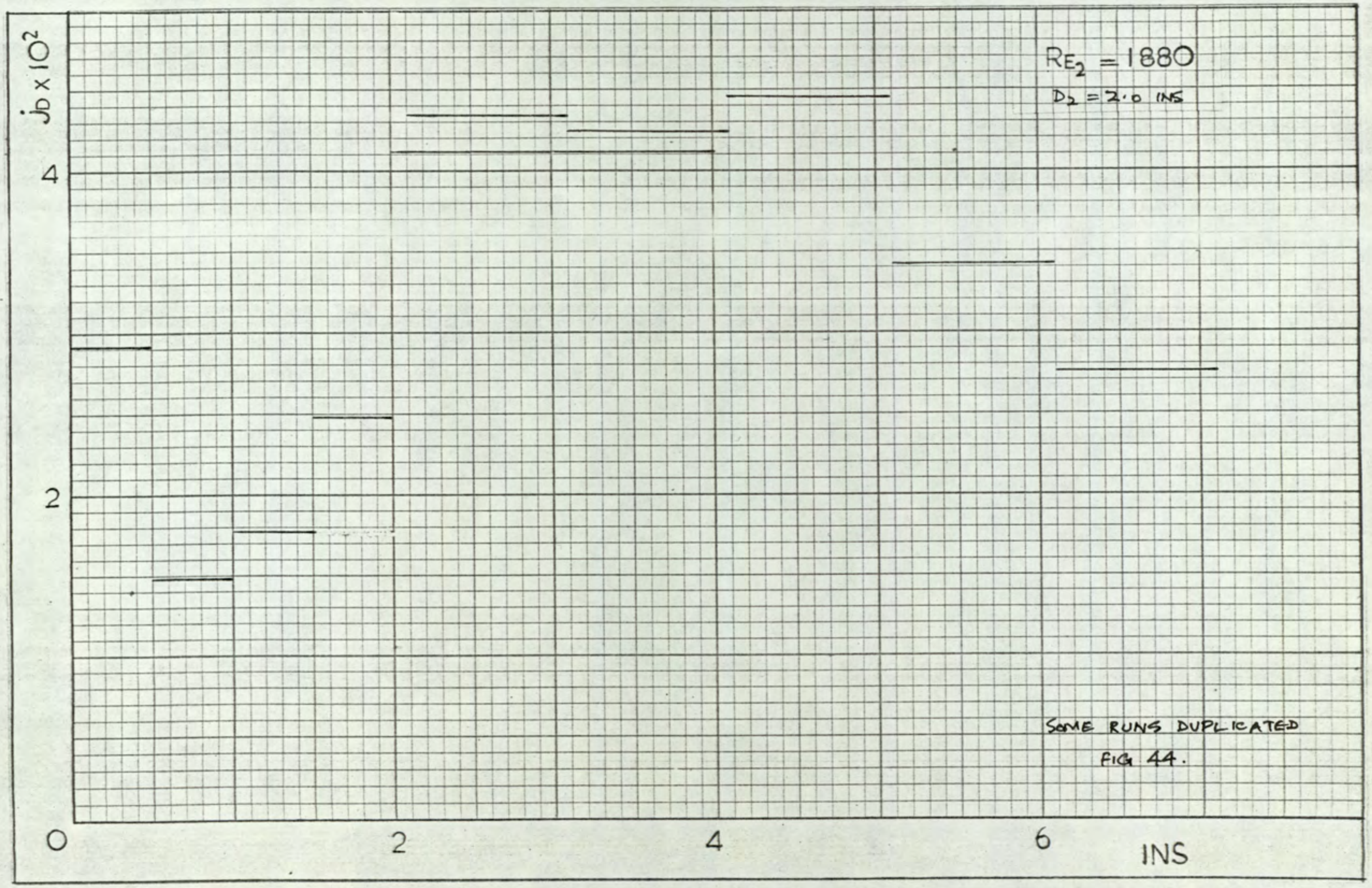
$j_D \times 10^2$
$Re_2 = 1880$
$D_2 = 2.0$ INS
SOME RUNS DUPLICATED
FIG 44.
0
2
4
6
INS

fig. 44a

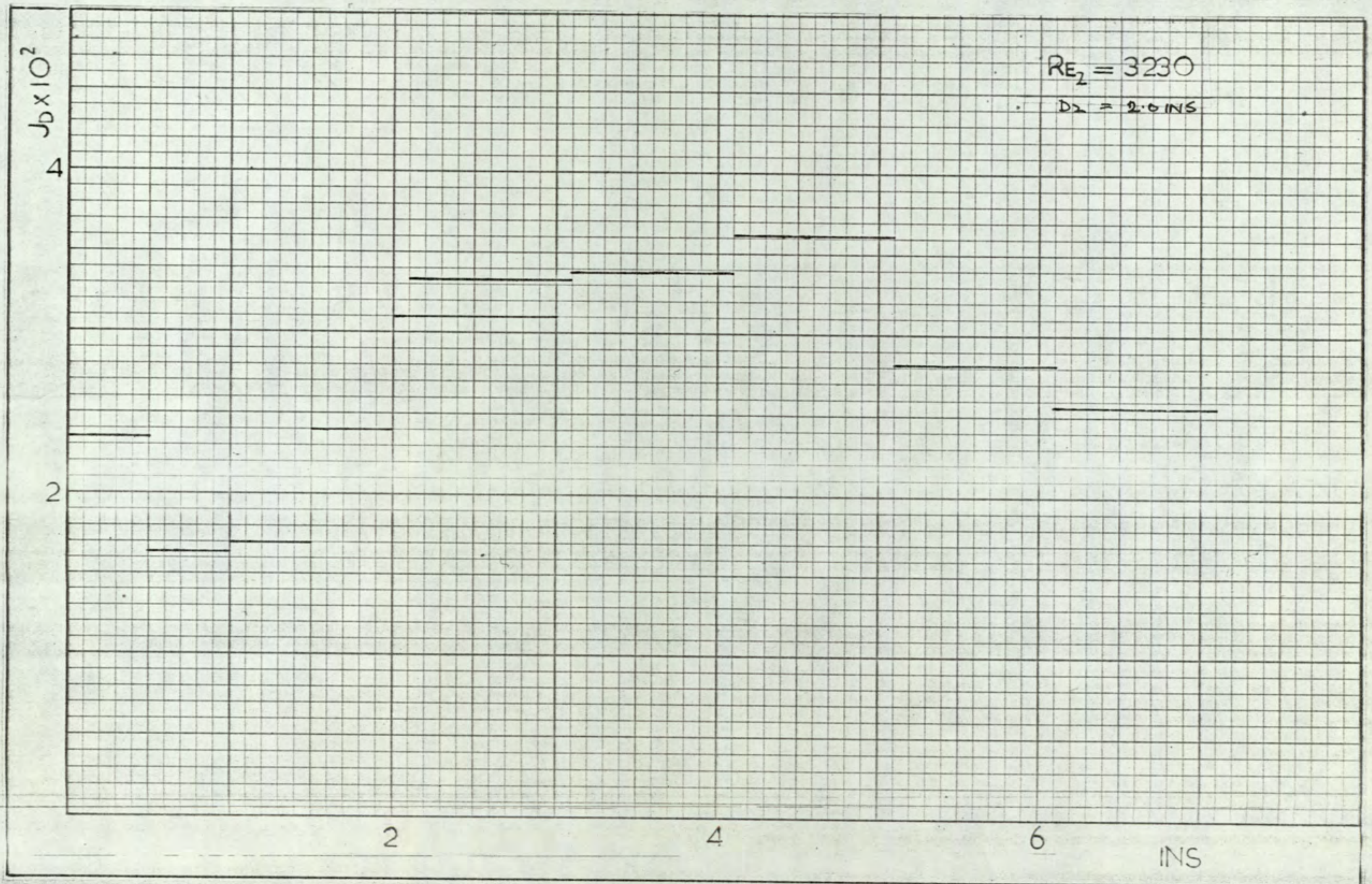

fig. 44b

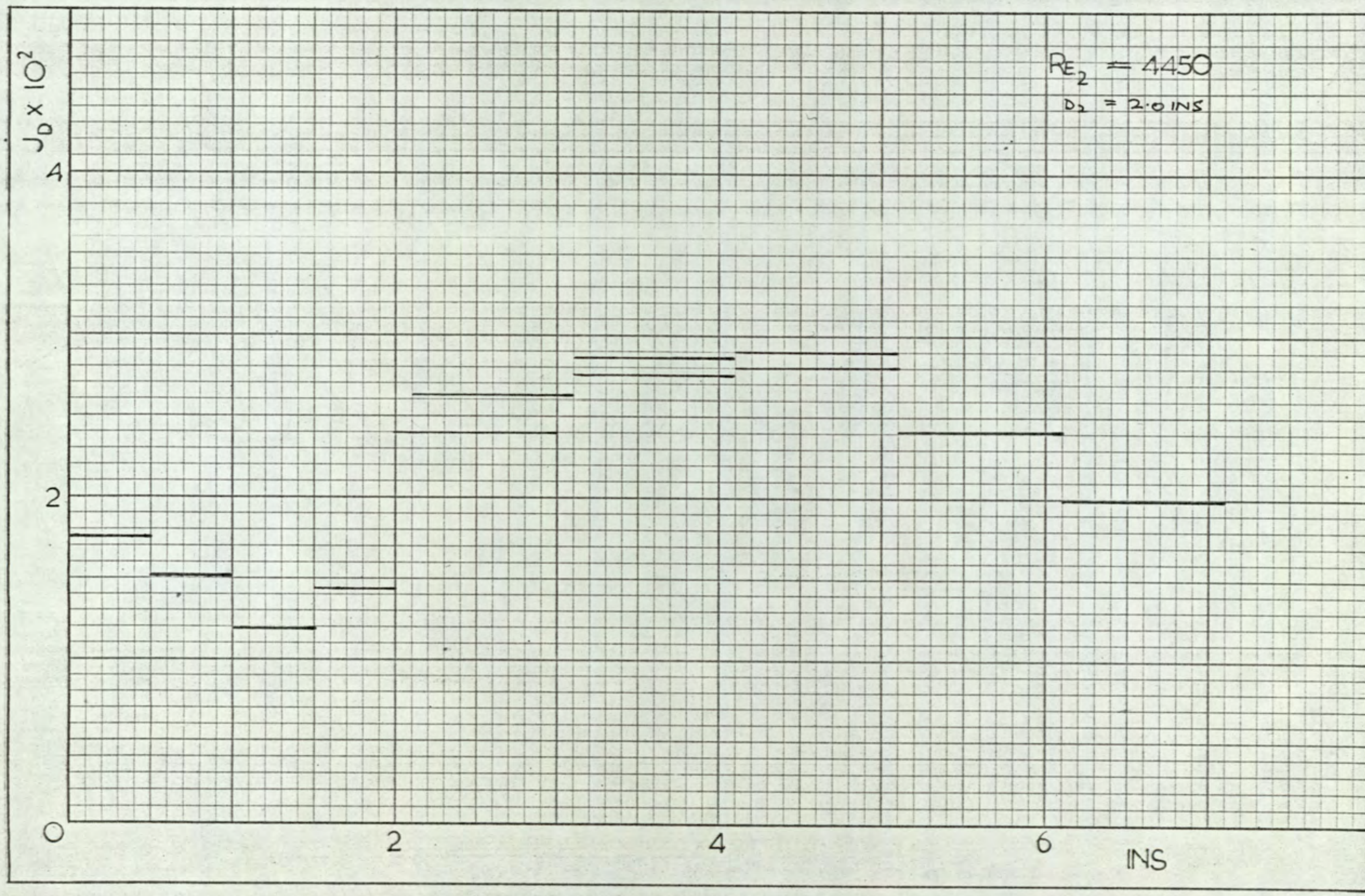

fig. 44c

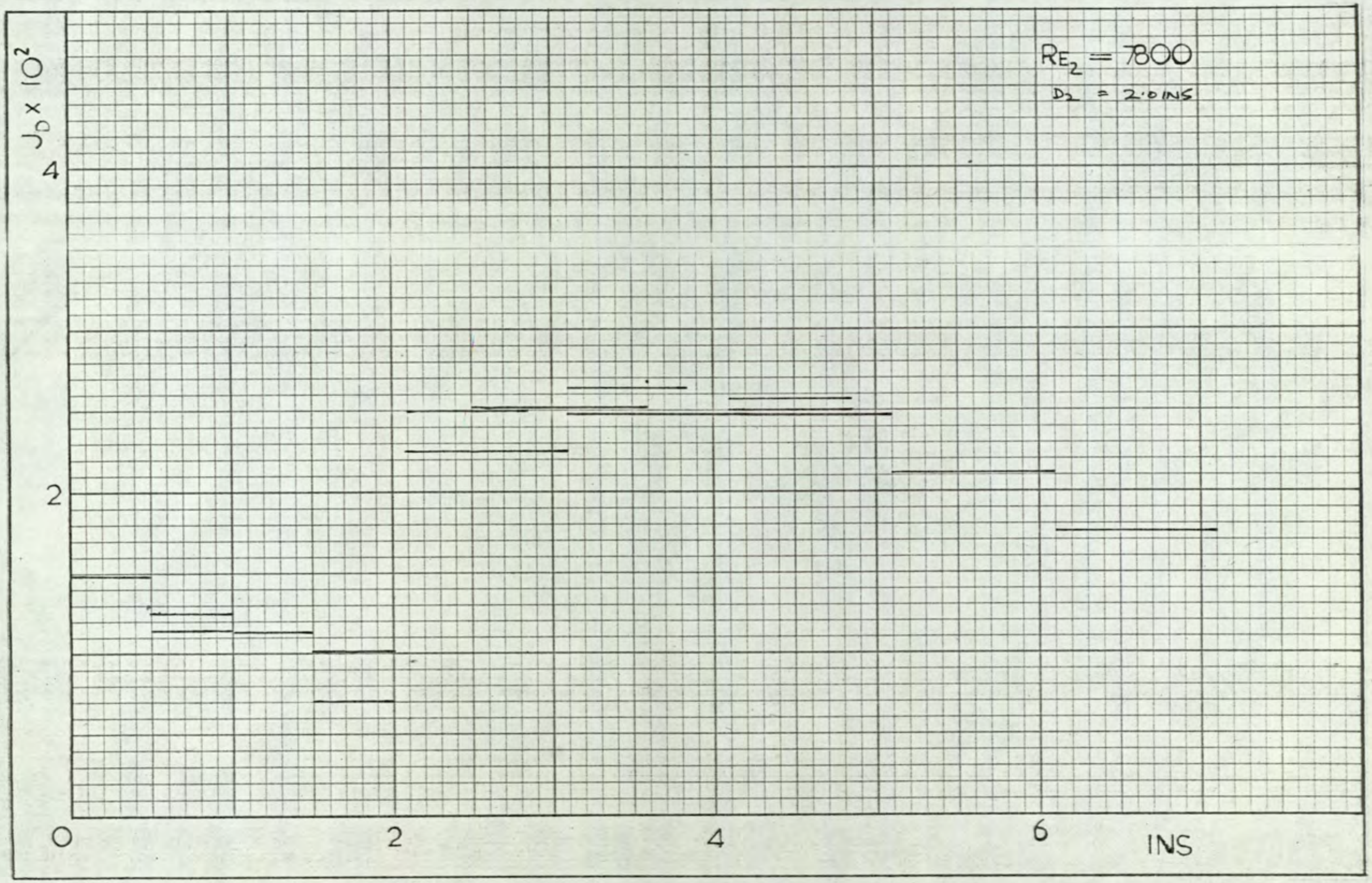

fig. 44d

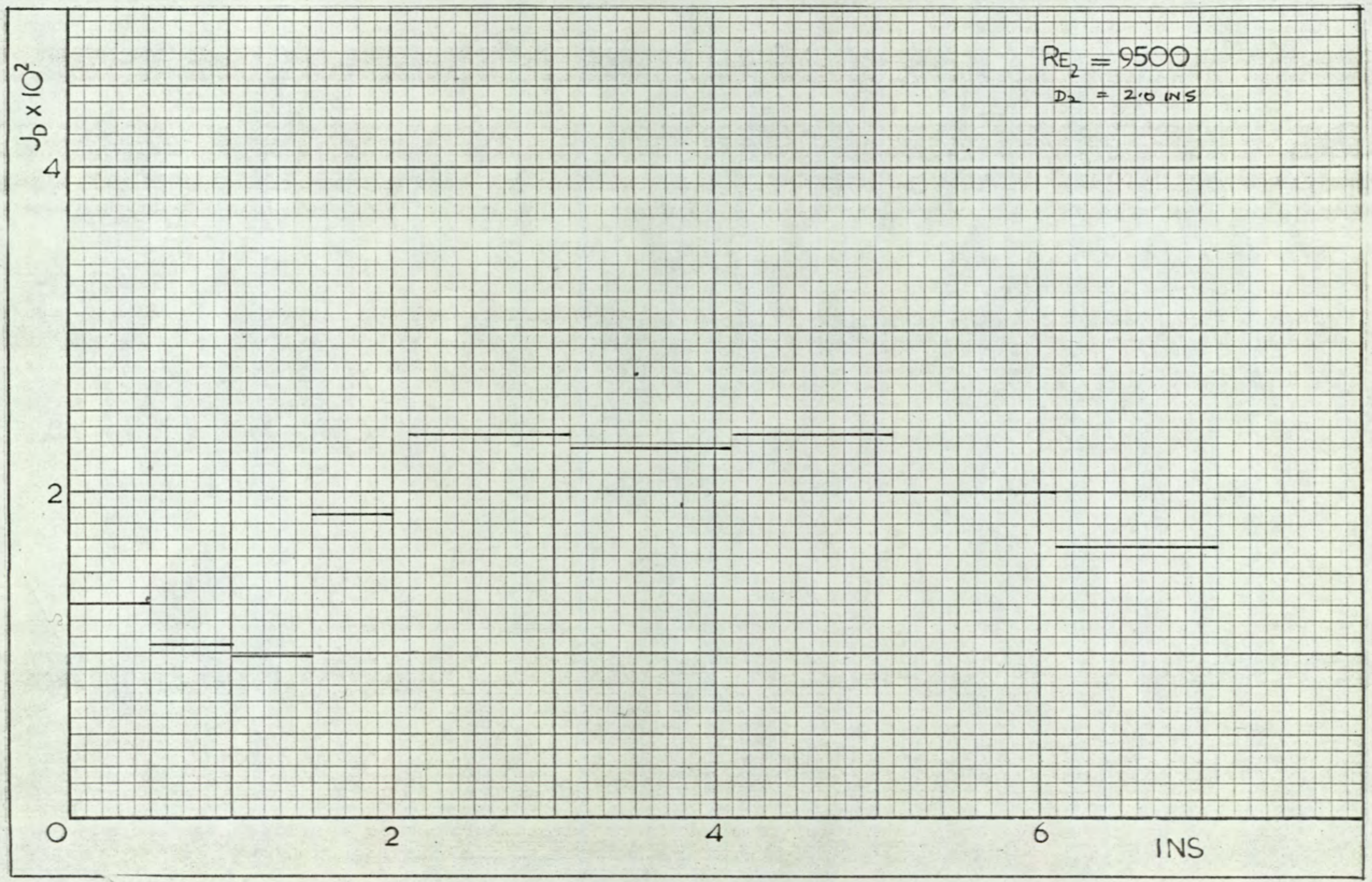

fig. 44e

In addition, table 15b contains the results of experiments involving two distinct electrolysis circuits. The use of a short separate cathode as the test section proper provided local average mass transfer coefficients directly.

12.4 Mass Transfer Factors j_D

Results are also presented graphically, figures 43 - 44, in the form of the dimensionless transfer factor j_D, to show the variation with distance from the plane of enlargement and the effect of Reynolds number

$$j_D = \left[k_m\right]_{Loc} v_2^{-1} Sc^{2/3}$$

where v_2 is the mean velocity based on full bore flow in the expanded section.

For copper sulphate concentrations of the order 0.005 - 0.015 molar, values of the Schmidt number vary from 1799 - 1818

Hence $Sc^{2/3} = 148.0 - 149.0$

Thus a constant mean value of 148.5 may be used throughout.

Figure 44 shows the improvement gained by the use of twin electrolysis circuits.

12.5 Heat Transfer Factors j_H

The analogy between heat and mass transfer may be expressed as an equality between the j_H and j_D factors. Hence, figures 43 - 44 also serve to show the variation of the heat transfer coefficient (as j_H) with distance.

Curves are similar in shape to published curves relating to heat transfer coefficients (53) (56) (58). A pronounced peak is evident in the immediate vicinity of the change of section. Thereafter, local coefficients decrease in value, tending asymptotically to the value corresponding to fully developed flow.

Curves for the larger of the two expansion ratios also display a well-defined minimum in the region between the plane of enlargement and the peak. A similar occurrence was observed by Emerson (58), Read (84) and Filletti and Kays (85).

12.6 Peak Values of the Transfer Factor

Under turbulent flow conditions (59)

$$j_H = 0.023\ Re^{-0.2} \quad \text{and}$$

$$j_D = k_m\ v^{-1} Sc^{2/3}$$

Equating the transfer factors, the theoretical fully developed value is given by

$$j_H = j_D = 0.023\ Re^{-0.2}$$

Figure (45) shows the peak value of the transfer factor (expressed as a fraction of the calculated

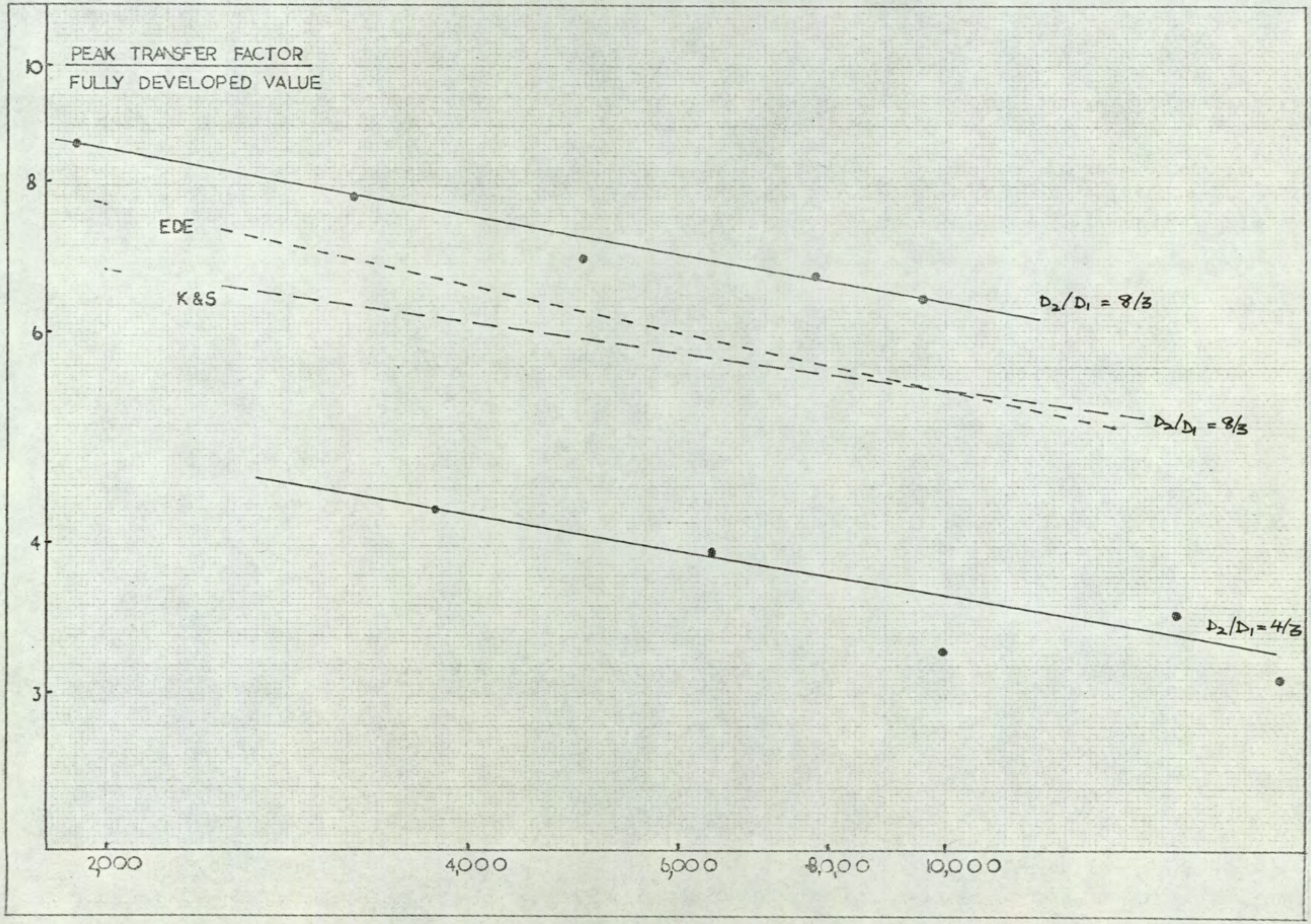

PEAK TRANSFER FACTOR
FULLY DEVELOPED VALUE
10
8
6
4
3
EDE
K&S
$D_2/D_1 = 8/3$
$D_2/D_1 = 8/3$
$D_2/D_1 = 4/3$
2,000
4,000
6,000
8,000
10,000

Fig. 45

fully developed value) as a function of Reynolds number, with expansion ratio as a parameter.

Results obtained when D_2/D_1 equals 8/3 may be correlated:

$$(j_H)max/(j_H)_{f.d.} = 15.25(D_2/D_1)^{0.8}(Re_2)^{-0.18}$$

For the smaller expansion ratio, $D_2/D_1 = 4/3$, the constant term is fractionally smaller at 15.0.

12.7 Location of Peak Transfer Factor

With D_2/D_1 equal to 4/3, the maximum value of the transfer coefficient occurred within 1 pipe diameter (D_2) of the plane of enlargement.

With D_2/D_1 equal to 8/3, the position of the peak relative to the plane of enlargement was more clearly defined; figure (44) shows the peak to lie in the region 1.75 - 2.0 pipe diameters from the change of section.

Thus the position of the peak is closer to the plane of expansion than was found by Ede (53). Since no systematic variation of peak position was indicated by the data of Krall and Sparrow, comparison with their results (56) is not possible.

Also included in figure (45) are the correlations of Ede (53) and Krall and Sparrow (56). Results obtained by the author are 26 - 16 per cent higher than predicted values according to the correlation of Krall and Sparrow (the deviation decreasing with increasing Reynolds number). Results are 11 - 16 per cent higher than values according to Ede's correlation, (p. 112).

Neither of these alternative correlations was obtained for experimental conditions exactly equivalent to the conditions obtaining in the author's experiments. In Ede's case (53) the whole of the test section, upstream and downstream of the abrupt expansion was heated (constant heat flux). If the same deviations were to be obtained with water as were obtained with air, when only the downstream section was heated (54, 55), Ede's correlation would lie much closer to the author's data. Although only the downstream section was heated in the investigations of Krall and Sparrow (56), the abrupt expansion was effected by means of an orifice plate.

The results obtained by Emerson (58) for a single expansion ratio, $D_2/D_1 = 1.71$, showed no dependence on Reynolds number.

SECTION C

13. Aerodynamics and Distribution of Transfer Coefficients

13.1 Comparison of Experimental Results

The purpose of this section is to compare the results of the two series of experiments in an effort to relate the noted variation in transfer factor with distance to the flow pattern deduced from the static pressure change investigations.

With D_2/D_1 equal to 1.35 the normalised pressure change curve is exponential in shape. Pressure tappings were not located less than 1 duct diameter (D_2) from the plane of enlargement; no change in the gradient of the pressure change curve capable of interpretation as the eye of the recirculation eddy was detected. The point of reattachment of the jet was deduced to be 2.8 inches from the change of section.

For an expansion ratio D_2/D_1 equal to 1.33 the peak transfer coefficient occurred within 1 pipe diameter (D_2) of the plane of enlargement. Peak values were 3 to 5 times as great as the calculated value for fully developed flow conditions. Transfer coefficients for the interval 2.5 - 3.0 ins. were not less than double the calculated fully developed value.

With an expansion ratio (D_2/D_1) equal to 2.82 the eye of the recirculation eddy was found to be 3.1 inches (1.49 duct diameters) from the plane of enlargement. For an expansion ratio of 2.67 the peak transfer coefficient occurred at 3.5 - 4.0 inches (i.e., 1.75 - 2.0 duct diameters). The point of reattachment derived from the normalised pressure change curve indicated a jet length of 7.4 ins., or 3.55 duct diameters.

On this evidence the peak transfer coefficient would appear to coincide with the eye of the recirculation eddy.

13.2 Discussion

The bulk of the published data on transfer coefficients suggest that the peak value corresponds to the point of reattachment of the jet.

Although Ede (53) was inclined to associate the peak transfer coefficient with the eye of the recirculation eddy, comparison of Ede's results with the predicted location of the eye of the eddy according to Cohen de Lara (30) reveals that for expansion ratios D_2/D_1 of 2.0 and 3.33, the eye of the eddy appears approximately midway between the plane of enlargement and the position of the peak transfer coefficient.

In addition, the results of Emerson's investigations showed the peak transfer coefficient to correspond to the point of reattachment of the jet as indicated by the displacement of oil spots on the duct wall. According to the curve of Cohen de Lara the eye of the recirculation eddy for the expansion ratio employed by Emerson is located 2.8 ins. from the change of section. Emerson's own investigations indicate maximum displacement towards the plane of enlargement at this point, confirming the location of the eye. The peak transfer coefficient and point of reattachment were determined by Emerson to be approximately 7.0 ins. from the plane of enlargement, i.e., somewhat nearer than Hubbard's note would suggest (3.5 x 3.0 ins, ie $3\cdot5 \times D_2$).

Additional evidence to suggest that the point of reattachment of the jet is marked by a maximum in the local heat transfer coefficient is furnished by the complementary experiments of Filletti and Kays (85) and Abbott and Kline (87), using rectangular ducts.

With boundary conditions of essentially constant wall temperature, however, Louise (51) recorded peak transfer coefficients in the region of maximum recirculatory flow. It is perhaps significant that boundary conditions in the author's experiments correspond to the same conditions. There is, however, no apparent reason why the choice of constant wall temperature rather than constant heat flux should produce such a marked disparity in results.

All results indicate that the eye of the recirculation eddy lies upstream of the peak transfer coefficient as found by most other researchers. The question may therefore be raised of the precision obtainable with a technique which requiresan estimate of the fluid temperature in the region of interest. The relationship, noted by the author, between the peak transfer coefficient and the eye of the eddy implies good transfer between the eddy and the swiftly flowing core. The indication of good mixing at this point is not conclusive proof of validity of the simplification made with regard to the variation of fluid temperature immediately downstream of the change of section; there is no evidence of a linear variation in fluid temperature throughout this zone. Since any error in the estimated bulk temperature would tend to have a cumulative effect at the point of reattachment, this could provide at least a partial explanation of the noted discrepancy.

The high value of the transfer coefficient adjacent to the plane of enlargement, giving rise to a minimum in the transfer coefficient distribution curve has previously tended to be dismissed. It seems likely that the effect is associated with the existence of subsidiary vortices upstream of the principal recirculation eddy (90). The existence of such vortices has been confirmed by the experimental investigations of Abbott and Kline (87) on step changes in area in rectangular ducts.

With the aid of the technique developed and a test section proper of, say, $\frac{1}{4}$ inch, it should prove possible to investigate the larger expansion ratios which the author was unable to cover due to the proportion of time devoted to the pressure rise studies and development of the experimental technique

TABLE 3.

Tube Diameter = 0.74 ins.

R	v	Re_1	$\phi \times 10^5$	h_f
2	2.82	16,100	349	0.059
4.5	4.40	25,200	313	0.128
6.0	5.46	31,200	298	0.179
8.0	6.83	39,100	282	0.266
10.0	8.21	47,100	269	0.365
12.0	9.61	55,000	258	0.482
14.0	11.07	63,400	250	0.615
16.0	12.58	72,000	242	0.771
18.0	14.07	80,500	235	0.944

Tube Diameter = 0.865 ins.

R	v	Re_2	$\phi \times 10^5$	h_f
4.5	3.22	21,500	325	0.061
6.0	4.00	26,700	310	0.084
8.0	5.00	33,400	290	0.126
10.0	6.01	40,200	280	0.174
12.0	7.04	47,000	270	0.228
14.0	8.10	54,200	260	0.294
16.0	9.20	61,600	250	0.367
18.0	10.30	68,900	244	0.444

LEGEND: R = rotameter setting (cms. of scale)
v = velocity (ft./sec.)
Re = Reynolds numbers
ϕ = friction factor
h_f = friction gradient (ft. fluid/ft.)

TABLE 3.

Tube Diameter = 1.0 ins.

R	v	Re_2	$\phi \times 10^5$	h_f
2	1.54	11,900	379	0.013
4.5	2.42	18,600	339	0.030
6	2.99	23,100	321	0.043
8	3.75	28,900	304	0.063
10	4.50	34,800	290	0.087
12	5.27	40,700	279	0.115
14	6.06	46,900	269	0.147
16	6.90	53,300	261	0.182
18	7.71	59,600	254	0.224

Tube Diameter = 1.464 ins.

R	v	Re_2	$\phi \times 10^5$	h_f
2	0.72	8,100	414	0.002
4.5	1.12	12,700	371	0.005
6	1.39	15,800	353	0.007
8	1.74	19,750	334	0.010
10	2.09	23,750	319	0.014
12	2.45	27,800	307	0.019
14	2.82	32,000	296	0.024
16	3.20	36,400	287	0.030
18	3.59	40,700	279	0.037

Tube Diameter = 2.085 ins.

R	v	Re_2	$\phi \times 10^5$	h_f
2	0.36	5,700	440	0.000
4.5	0.56	8,900	408	0.001
6	0.69	11,100	390	0.002
8	0.86	15,900	353	0.002
10	1.04	16,700	348	0.002
12	1.21	19,500	340	0.003
14	1.40	22,500	324	0.004
16	1.58	25,500	310	0.005
18	1.77	28,600	305	0.007

TABLE 3.

Tube Diameter = 3.041 ins.

R	v	Re_2	$\phi \times 10^5$	h_f
2	0.167	3,900	500	0.000
4.5	0.261	6,150	447	0.000
6	0.324	7,600	424	0.000
8	0.405	9,500	401	0.000
10	0.487	11,450	382	0.000
12	0.570	13,400	368	0.001
14	0.656	15,400	355	0.001
16	0.745	17,600	344	0.001
18	0.835	19,600	335	0.001

Tube Diameter = 4.50 ins.

R	v	Re_2
2	0.076	2,740
4.5	0.119	4,100
6	0.148	5,100
8	0.185	6,400
10	0.222	7,700
12	0.260	9,000
14	0.300	10,300
16	0.341	11,800
18	0.381	13,200

TABLE 4. Measured Pressure Change (Ft. of water)

Tube Diameter = 0.865 ins.

x/R	4.5(p)	6(p)	8(p)	10(p)	12(p)
1	0.080	0.115	0.195	0.290	0.402
2	0.083	0.126	0.213	0.320	0.447
3	0.083	0.126	0.212	0.318	0.446
4	0.082	0.126	0.210	0.319	0.446
5	0.079	0.121	0.201	0.304	0.429
6	0.076	0.115	0.194	0.294	0.415
8	0.070	0.103	0.178	0.272	0.386
12	0.055	0.086	0.147	0.230	0.340
16	0.044	0.067	0.119	0.188	0.278
20	0.025	0.042	0.081	0.132	0.204
24	0.005	0.013	0.035	0.064	0.106

x/R	4.5(p)	6(p)	8(p)	10(p)	12(p)
1	0.082	0.114	0.192	0.287	0.405
2	0.084	0.127	0.209	0.320	0.450
3	0.084	0.127	0.209	0.317	0.449
4	0.083	0.127	0.208	0.318	0.449
5	0.079	0.120	0.198	0.303	0.431
6	0.076	0.114	0.191	0.293	0.415
8	0.069	0.104	0.176	0.272	0.389
12	0.056	0.084	0.142	0.225	0.327
16	0.043	0.065	0.113	0.187	0.273
20	0.025	0.041	0.076	0.128	0.196
24	0.004	0.012	0.030	0.064	0.101

x/R	14(a)	16(a)	18(a)	14(a)	16(a)
1	0.548	0.725	0.922	0.551	0.732
2	0.617	0.814	1.033	0.620	0.820
3	0.614	0.810	1.033	0.617	0.817
4	0.614	0.810	1.043	0.617	0.820
5	0.592	0.786	1.004	0.594	0.789
6	0.571	0.760	0.964	0.571	0.759
8	0.531	0.712	0.896	0.531	0.712
12	0.454	0.584	0.794	0.458	0.610
16	0.382	0.525	0.686	0.385	0.525
20	0.279	0.395	0.528	0.282	0.397
24	0.151	0.233	0.325	0.157	0.235

Legend: x = distance (ins.)
R = rotameter setting, scale reading (cms)
p = paraffin, a = air, o = o-xylene

TABLE 4 Measured Pressure Change (Ft.)
(cont)

Tube Diameter = 1.0 ins.

x/R	2(o)	4.5(o)	6 (o)	8 (o)	6 (p)
1	0.025	0.064	0.092	0.144	0.084
2	0.037	0.096	0.144	0.233	0.139
3	0.040	0.109	0.165	0.266	0.163
4	0.041	0.113	0.173	0.281	0.172
5	0.042	0.117	0.178	0.289	0.177
6	0.042	0.116	0.178	0.290	0.178
8	0.040	0.113	0.174	0.286	0.174
10	0.037	0.108	0.167	0.274	0.166
12	0.036	0.104	0.162	0.267	0.161
16	0.032	0.094	0.147	0.242	0.144
20	0.028	0.086	0.135	0.225	0.132
24	0.022	0.077	0.125	0.204	0.120

x/R	2 (o)	4.5 (o)	6 (o)	8 (o)	8 (p)
1	0.030	0.062	0.092	0.143	0.139
2	0.041	0.095	0.144	0.231	0.230
3	0.042	0.108	0.163	0.264	0.263
4	0.044	0.113	0.172	0.280	0.278
5	0.045	0.116	0.177	0.287	0.285
6	0.045	0.114	0.177	0.288	0.287
8	0.044	0.112	0.174	0.285	0.281
10	0.042	0.107	0.166	0.273	0.270
12	0.040	0.104	0.161	0.266	0.261
16	0.035	0.094	0.146	0.243	0.239
20	0.032	0.085	0.135	0.225	0.220
24	0.028	0.076	0.120	0.203	0.198

x/R	2 (o)	10 (p)	12 (p)	10 (p)	12 (p)
1	0.030	0.209	0.286	0.212	0.282
2	0.040	0.345	0.483	0.348	0.478
3	0.043	0.395	0.555	0.397	0.552
4	0.045	0.416	0.586	0.418	0.580
5	0.045	0.427	0.604	0.426	0.599
6		0.428	0.606	0.431	0.601
8		0.423	0.601	0.424	0.598
10		0.409	0.578	0.408	0.574
12		0.400	0.566	0.400	0.560
16		0.366	0.525	0.365	0.513
20		0.336	0.492	0.339	0.480
24		0.306	0.451	0.309	0.438

TABLE 4.
(cont)

Measured Pressure Change

Tube Diameter = 1.0 ins.

x/R	14 (a)	16 (a)	18 (a)
1	0.384	0.505	0.645
2	0.666	0.883	1.119
3	0.768	1.107	1.273
4	0.810	1.076	1.362
5	0.833	1.102	1.368
6	0.837	1.106	1.404
8	0.825	1.096	1.391
10	0.796	1.056	1.342
12	0.778	1.037	1.306
16	0.715	0.956	1.207
20	0.666	0.897	1.127
24	0.614	0.827	1.053

x/R	14 (a)	16 (a)	18 (a)
1	0.384	0.499	0.640
2	0.669	0.876	1.109
3	0.764	1.004	1.280
4	0.814	1.066	1.358
5	0.837	1.096	1.401
6	0.838	1.099	1.404
8	0.830	1.086	1.391
10	0.804	1.050	1.348
12	0.781	1.029	1.322
16	0.719	0.945	1.217
20	0.669	0.889	1.145
24	0.614	0.820	1.061

TABLE 4. (cont)

Measured Pressure Change

Tube Diameter = 1.464 ins.

x/R	2 (o)	4.5 (o)	6 (o)	8 (o)	10 (o)
2	0.006	0.014	0.015	0.027	0.037
4	0.025	0.066	0.104	0.164	0.247
5	0.031	0.083	0.127	0.207	0.306
6	0.034	0.092	0.142	0.229	0.337
7	0.036	0.096	0.147	0.238	0.350
8	0.036	0.096	0.148	0.241	0.353
10	0.036	0.095	0.148	0.239	0.351
12	0.036	0.094	0.147	0.238	0.350
16	0.035	0.093	0.145	0.234	0.344
20	0.034	0.091	0.142	0.230	0.339
24	0.033	0.089	0.140	0.226	0.334

x/R	2 (o)	4.5 (o)	6 (o)	8 (o)	10 (o)
2	0.009	0.014	0.015	0.024	0.032
4	0.028	0.067	0.098	0.159	0.254
5	0.033	0.083	0.123	0.201	0.304
6	0.036	0.091	0.138	0.223	0.332
7	0.037	0.095	0.144	0.230	0.349
8	0.037	0.096	0.146	0.232	0.350
10	0.037	0.095	0.145	0.231	0.348
12	0.036	0.094	0.144	0.230	0.347
16	0.035	0.092	0.142	0.226	0.340
20	0.035	0.091	0.139	0.222	0.336
24	0.034	0.089	0.137	0.221	0.331

x/R	2 (o)	6 (o)	8 (o)	10 (o)
2	0.008	0.016	0.024	0.033
4	0.026	0.098	0.159	0.253
5	0.031	0.123	0.201	0.305
6	0.034	0.137	0.223	0.334
7	0.036	0.143	0.231	0.348
8	0.035	0.144	0.231	0.351
10	0.035	0.143	0.229	0.348
12	0.035	0.143	0.229	0.348
16	0.034	0.140	0.225	0.340
20		0.138	0.222	0.336
24		0.136	0.218	0.330

TABLE 4. Measured Pressure Change
(cont)

Tube Diameter = 1.464 ins.

x/R	8 (p)	10 (p)	12 (p)
2	0.020	0.034	0.049
4	0.158	0.240	0.344
5	0.197	0.302	0.425
6	0.221	0.334	0.466
7	0.231	0.347	0.483
8	0.232	0.348	0.487
10	0.231	0.346	0.485
12	0.231	0.345	0.484
16	0.226	0.339	0.478

x/R	12 (a)	14 (a)	6 (a)	18 (a)
2	0.049	0.079	0.102	0.134
4	0.347	0.485	0.643	0.830
5	0.400	0.597	0.747	1.007
6	0.475	0.649	0.850	1.073
7	0.493	0.672	0.875	1.121
8	0.494	0.672	0.885	1.122
10	0.489	0.669	0.877	1.117
12	0.490	0.667	0.877	1.115
16	0.482	0.659	0.867	1.103
20	0.475	0.649	0.857	1.097
24	0.469	0.643	0.846	1.085

x/R	12 (a)	14 (a)	16 (a)	18 (a)
2	0.049	0.075	0.102	0.141
4	0.359	0.482	0.639	0.823
5	0.434	0.600	0.786	1.010
6	0.477	0.469	0.856	1.085
7	0.497	0.674	0.885	1.114
8	0.503	0.679	0.894	1.126
10	0.501	0.674	0.884	1.121
12	0.500	0.672	0.884	1.126
16	0.493	0.660	0.872	1.112
20	0.489	0.656	0.863	1.102
24	0.479	0.646	0.850	1.092

TABLE 4. Measured Pressure Change
(cont)

Tube Diameter = 2.085 ins.

x/R	2 (o)	4 (o)	6 (o)	8 (o)	10 (o)
2	-0.006	-0.011	-0.019	-0.027	-0.038
4	+0.003	+0.005	+0.006	+0.010	+0.023
6	0.013	0.030	0.048	0.084	0.124
7	0.171	0.038	0.063	0.110	0.161
8	0.019	0.040	0.072	0.122	0.179
9	0.092	0.043	0.076	0.127	0.187
10	0.019	0.044	0.077	0.129	0.191
12	0.019	0.044	0.078	0.129	0.193
15	0.019	0.044	0.078	0.129	0.194
18	0.019	0.044	0.078	0.129	0.193
21	0.019	0.044	0.077	0.127	0.191
24	0.019	0.043	0.077	0.126	0.190
27	0.019	0.044	0.077	0.126	0.191

x/R	2 (o)	4 (o)	6 (o)	8 (o)	10 (o)
2	-0.004	-0.010	-0.019	-0.024	-0.035
4	+0.003	+0.005	+0.005	+0.015	+0.023
6	0.012	0.029	0.049	0.084	0.128
7	0.016	0.035	0.062	0.108	0.164
8	0.017	0.040	0.070	0.122	0.183
9	0.018	0.043	0.075	0.127	0.190
10	0.018	0.042	0.077	0.131	0.193
12	0.019	0.044	0.078	0.131	0.195
15	0.018	0.043	0.078	0.132	0.195
18	0.018	0.043	0.077	0.131	0.194
21	0.018	0.043	0.077	0.130	0.194
24	0.018	0.042	0.077	0.129	0.192
27	0.018	0.043	0.077	0.128	0.192

x/R	2 (o)	4 (o)	6 (o)	8 (o)	10 (o)
2	-0.001	-0.009	-0.016	-0.023	-0.031
4	0.005	-.007	0.006	0.015	0.027
6	0.016	0.031	0.048	0.083	0.135
7	0.019	0.038	0.064	0.108	0.169
8	0.020	0.042	0.073	0.120	0.188
9	0.021	0.043	0.076	0.127	0.193
10	0.021	0.043	0.078	0.129	0.195
12	0.021	0.044	0.079	0.130	0.197
15	0.021	0.045	0.079	0.130	0.196
18	0.021	0.044	0.079	0.130	0.195
21	0.021	0.044	0.078	0.129	0.194
24	0.020	0.044	0.077	0.128	0.193
27	0.020	0.043	0.077	0.128	0.193

TABLE 4. (Cont)

Measured Pressure Change

Tube Diameter = 2.085 ins.

x/R	12 (o)	14 (a)	16 (a)	18 (a)
2	-0.050	-0.046	-0.066	-0.066
4	0.034	0.062	0.089	
6	0.186	0.262	0.348	0.486
7	0.234	0.322	0.420	0.554
8	0.258	0.351	0.466	0.607
9	0.267	0.346	0.479	0.617
10	0.270	0.367	0.486	0.617
12	0.273	0.371	0.486	0.623
15	0.273	0.371	0.486	
18	0.273	0.362	0.486	
21	0.271	0.369	0.481	
24	0.271	0.367	0.479	
27	0.269	0.366	0.479	

x/R	12 (o)	14 (a)	16 (a)	18 (a)
2	-0.048	-0.062	-0.079	-0.095
4	0.038	0.056	0.085	0.135
6	0.189	0.256	0.344	0.453
7	0.238	0.322	0.423	0.551
8	0.260	0.351	0.466	0.600
9	0.272	0.364	0.479	0.607
10	0.273	0.367	0.492	0.614
12	0.276	0.371	0.490	0.617
15	0.275	0.371	0.494	0.620
18	0.275			
21	0.274	0.364	0.489	0.614
24	0.272			
27	0.271	0.364	0.479	0.612

x/R	12 (o)	14 (a)	16 (a)	18 (a)
2	-0.049	-0.059	-0.079	-0.085
4	0.035	0.059	0.089	0.135
6	0.188	0.253	0.344	0.472
7	0.233	0.325	0.427	0.558
8	0.261	0.354	0.466	0.600
9	0.268	0.367	0.466	0.617
10	0.270	0.374	0.479	0.617
12	0.273	0.374	0.486	0.623
15	0.272	0.374	0.486	0.623
18	0.272	0.374	0.484	0.628
21	0.270	0.367	0.481	0.620
24	0.269	0.367	0.479	0.617
27	0.269	0.367	0.478	0.612

TABLE 4. (cont)

Measured Pressure Change

Tube Diameter ; 3.041 ins.

x/R	2 (o)	4 (o)	6 (o)	8 (o)	10 (o)
2	-0.005	-0.005	-0.012	-0.018	-0.024
4	-0.005	-0.008	-0.012	-0.019	-0.025
6	-0.002	-0.004	-0.006	-0.008	-0.007
8	0.003	0.008	0.013	0.025	0.037
10	0.005	0.016	0.029	0.049	0.076
12	0.007	0.020	0.034	0.057	0.085
14	0.008	0.020	0.036	0.058	0.090
16	0.008	0.020	0.036	0.059	0.090
18	0.008	0.020	0.036	0.059	0.090
24	0.008	0.020	0.036	0.059	0.090

x/R	2 (o)	4 (o)	6 (o)	8 (o)	10 (o)
2	-0.002	-0.007	-0.011	-0.020	-0.027
4		-0.006	-0.012	-0.020	-0.027
6	0.000	-0.003	-0.007	-0.009	-0.008
8	0.005	0.008	0.012	0.023	0.041
10	0.008	0.016	0.026	0.046	0.072
12	0.010	0.020	0.033	0.054	0.083
14	0.010	0.021	0.034	0.056	0.086
16	0.010	0.021	0.034	0.056	0.086
18	0.010	0.022	0.034	0.056	

x/R	2 (o)	4 (o)	6 (o)	8 (o)	10 (o)
2	-0.002	-0.006	-0.013	-0.016	-0.025
4	-0.002	-0.006	-0.013	-0.016	
6	0.000	-0.002	-0.007		-01005
8	0.005	0.009	0.012	0.028	0.039
10	0.008	0.016	0.025	0.046	0.071
12	0.010	0.020	0.032	0.057	0.084
14	0.010	0.021	0.034	0.061	0.087
16	0.010	0.021	0.034	0.061	0.087
18	0.010	0.021	0.034	0.061	0.087

TABLE 4. Measured Pressure Change
(cont)

Tube Diameter = 3.041 ins.

x/R	2 (o)	4 (o)	6 (o)	8 (o)	10 (o)
2	-0.003	-0.008	-0.014	-0.018	-0.023
4	-0.003	-0.007	-0.015	-0.018	-0.023
6	-0.002	-0.003	-0.005	-0.005	-0.006
8	0.003	0.008	0.011	0.021	0.041
10	0.006	0.013	0.025	0.047	0.077
12	0.007	0.016	0.030	0.056	0.087
14	0.008	0.018	0.034	0.058	0.090
16	0.008	0.018	0.034	0.058	0.090
18	0.008	0.019	0.034	0.059	0.090

x/R	12 (o)	12 (o)	12 (o)	14 (o)	14 (o)
2	-0.037	-0.036	-0.035	-0.045	-0.049
4	-0.036	-0.036	-0.038	-0.044	-0.050
6					
8	0.056	0.066	0.057	0.082	0.080
10	0.105	0.109	0.099	0.145	0.142
12	0.118	0.117	0.119	0.163	0.163
14	0.123	0.121	0.122	0.170	0.167
16	0.124	0.121	0.122	0.170	0.167

TABLE 4. Measured Pressure Change

(cont)

Tube Diameter = 3.041 ins.

x/R	12 (a)	14 (a)	16 (a)	18 (a)
2	-0.036	-0.039	-0.059	-0.066
4	-0.043	-0.049	-0.062	-0.066
6	-0.013	-0.010	-0.003	0.030
8	0.052	0.080	0.108	0.154
10	0.102	0.138	0.194	0.262
12	0.118	0.167	0.220	0.282
14	0.121	0.171	0.226	0.299
16	0.125	0.171	0.226	0.299

x/R	12 (a)	14 (a)	16 (a)	18 (a)
2	-0.039	-0.046	-0.059	-0.072
4	-0.039	-0.049	-0.064	-0.071
6	-0.016	-0.007	-0.007	-0.013
8	0.056	0.072	0.112	0.154
10	0.105	0.144	0.197	0.259
12	0.121	0.164	0.217	0.282
14	0.125	0.167	0.223	0.289
16	0.125	0.169	0.225	0.295
18		0.172	0.226	0.299

x/R	12 (a)	14 (a)	16 (a)	18 (a)
2	-0.036	-0.049	-0.056	-0.066
4	-0.036	-0.049	-0.059	-0.072
6	-0.003	-0.013		0.016
8	0.064	0.079	0.118	0.180
10	0.102	0.143	0.197	0.262
12	0.121	0.164	0.221	0.285
14	0.125	0.171	0.226	0.295
16	0.125	0.171	0.226	0.295

TABLE 4. (cont) Measured Pressure Change

Tube Diameter = 4.50 ins.

x/R	3 (x)	5 (x)	8 (x)	10 (x)
6	-0.005	-0.008	-0.018	-0.023
12	0.003	0.003	0.004	0.012
15	0.004	0.008	0.018	0.027
18	0.004	0.008	0.021	0.032
21	0.004	0.008	0.021	0.034
24	0.004	0.009	0.022	0.034
27	0.005	0.009	0.022	0.034
30	0.005			

x/R	12 (x)	14 (x)	16 (x)	18 (x)
6	-0.032	-0.039	-0.051	-0.064
12	0.023	0.027	0.042	0.048
15	0.039	0.051	0.076	0.093
18	0.046	0.065	0.082	0.107
21	0.048	0.063	0.085	0.111
24	0.047	0.066	0.087	0.109
27	0.048	0.065	0.087	0.111
30	0.048	0.066	0.087	0.111

x/R	3 (x)	5 (x)	8 (x)	10 (x)
6	-0.003	-0.008	-0.014	-0.022
12	0.001	0.004	0.004	0.011
15	0.004	0.008	0.018	0.029
18	0.005	0.008	0.021	0.032
21	0.006	0.009	0.021	0.034
24	0.005	0.009	0.022	0.034
27	0.005	0.009	0.022	0.034

x/R	12 (x)	14 (x)	16 (x)	18 (x)
6	-0.031	-0.040	-0.049	-0.061
12	0.023	0.027	0.040	0.056
15	0.039	0.054	0.074	0.093
18	0.046	0.068	0.081	0.105
21	0.048	0.066	0.085	0.108
24	0.048	0.066	0.085	0.113
27	0.048	0.066	0.086	0.111
30	0.048	0.066	0.087	0.114
36		0.066	0.087	0.114
42		0.066	0.088	0.111

TABLE 5. Mean Measured Pressure Change

$D_2 = 0.865$ ins.

x/R	4.5	6.0	8.0	10.0
1	0.081	0.115	0.194	0.289
2	0.084	0.127	0.211	0.320
3	0.084	0.127	0.210	0.318
4	0.083	0.127	0.210	0.318
5	0.079	0.120	0.200	0.304
6	0.076	0.115	0.192	0.294
8	0.070	0.104	0.177	0.272
12	0.056	0.085	0.145	0.227
16	0.044	0.066	0.117	0.188
20	0.025	0.042	0.079	0.130
24	0.005	0.013	0.032	0.064

x/R	12	14	16	18
1	0.404	0.549	0.728	0.922
2	0.449	0.168	0.817	1.033
3	0.448	0.616	0.813	1.033
4	0.448	0.616	0.815	1.043
5	0.430	0.593	0.787	1.004
6	0.415	0.571	0.759	0.958
8	0.388	0.531	.712	0.896
12	0.333	0.456	0.597	0.794
16	0.276	0.383	0.525	0.686
20	0.200	0.281	0.396	0.528
24	0.104	0.154	0.234	0.325

X = DISTANCE , INS

R = ROTAMETER SCALE READING, CMS

Δh = FT OF WATER

TABLE 5. (cont)

Mean Measured Pressure Change

$D_2 = 1.0$ ins.

x/R	2.0	4.5	6.0	8.0	10.0
1	0.028	0.063	0.089	0.142	0.211
2	0.039	0.096	0.142	0.231	0.346
3	0.042	0.108	0.164	0.264	0.396
4	0.044	0.113	0.172	0.280	0.417
5	0.044	0.117	0.177	0.287	0.427
6	0.043	0.115	0.178	0.289	0.430
8	0.043	0.113	0.174	0.284	0.424
10	0.040	0.108	0.166	0.272	0.409
12	0.038	0.104	0.161	0.265	0.400
16	0.033	0.094	0.146	0.241	0.366
20	0.030	0.086	0.134	0.223	0.338
24	0.025	0.077	0.122	0.202	0.308

x/R	12	14	16	18
1	0.284	0.384	0.502	0.642
2	0.481	0.667	0.879	1.115
3	0.554	0.765	1.007	1.276
4	0.583	0.812	1.071	1.360
5	0.601	0.835	1.098	1.400
6	0.604	0.837	1.102	1.404
8	0.599	0.827	1.090	1.390
10	0.576	0.799	1.053	1.343
12	0.563	0.779	1.032	1.312
16	0.525	0.717	0.950	1.212
20	0.486	0.667	0.893	1.135
24	0.444	0.613	0.823	1.056

TABLE 5. Mean Measured Pressure Change
(cont)

$D_2 = 1.464$ ins.

x/R	2.0	4.5	6.0	8.0	10.0
2	0.008	0.014	0.015	0.024	0.034
4	0.026	0.067	0.098	0.159	0.248
5	0.031	0.083	0.124	0.201	0.304
6	0.034	0.092	0.139	0.223	0.334
7	0.036	0.096	0.145	0.232	0.348
8	0.036	0.096	0.146	0.232	0.351
10	0.036	0.095	0.145	0.232	0.348
12	0.036	0.095	0.145	0.232	0.348
16	0.035	0.093	0.142	0.228	0.341
20	0.035	0.091	0.140	0.225	0.337
24	0.034	0.089	0.138	0.221	0.331

x/R	12.0	14.0	16.0	18.0
2	0.049	0.077	0.102	0.138
4	0.349	0.483	0.641	0.827
5	0.430	0.599	0.786	1.009
6	0.473	0.649	0.853	1.079
7	0.491	0.673	0.880	1.118
8	0.495	0.675	0.890	1.124
10	0.492	0.671	0.881	1.119
12	0.491	0.669	0.881	1.115
16	0.484	0.660	0.869	1.108
20	0.482	0.653	0.860	1.100
24	0.474	0.645	0.850	1.092

TABLE 5. Mean Measured Pressure Change
(cont)

D_2 = 2.085 ins.

x/R	2	4.5	6.0	8.0	10
2	-0.005	-0.012	-0.018	-0.025	-0.035
4	0.003	0.005	0.005	0.015	0.023
6	0.014	0.034	0.048	0.084	0.126
7	0.017	0.042	0.063	0.108	0.165
8	0.019	0.046	0.071	0.121	0.182
9	0.019	0.049	0.076	0.127	0.190
10	0.019	0.049	0.077	0.129	0.193
12	0.020	0.050	0.078	0.130	0.195
15	0.019	0.050	0.078	0.130	0.195
18	0.019	0.050	0.078	0.129	0.194
21	0.018	0.050	0.078	0.129	0.193

x/R	12	14	16	18
2	-0.049	-0.060	-0.079	-0.090
4	0.035	0.059	0.089	0.134
6	0.188	0.256	0.344	0.470
7	0.234	0.322	0.423	0.554
8	0.259	0.351	0.466	0.600
9	0.268	0.364	0.479	0.617
10	0.270	0.367	0.485	0.617
12	0.273	0.371	0.486	0.623
15	0.273	0.371	0.486	0.623
18	0.273	0.371	0.485	0.623
21	0.273	0.367	0.481	0.620

TABLE 5. (cont)

Mean Measured Pressure Change

$D_2 = 3.041$ ins.

x/R	2.0	4.5	6.0	8.0	10.0
2	-0.004	-0.009	-0.013	-0.018	-0.025
4	-0.004	-0.009	-0.013	-0.018	-0.025
6	-0.002	-0.004	-0.006	-0.007	-0.007
8	0.003	0.007	0.012	0.023	0.039
10	0.006	0.016	0.026	0.048	0.074
12	0.007	0.022	0.033	0.057	0.086
14	0.008	0.022	0.035	0.059	0.089
16	0.008	0.022	0.035	0.059	0.089
18	0.008	0.022	0.035	0.059	0.089

x/R	12	14	16	18
2	-0.036	-0.046	-0.059	-0.066
4	-0.039	-0.049	-0.062	-0.069
6	-0.015	-0.010	-0.005	-0.005
8	0.057	0.079	0.111	0.154
10	0.104	0.141	0.197	0.262
12	0.119	0.161	0.220	0.283
14	0.123	0.171	0.225	0.294
16	0.124	0.169	0.226	0.294
18	0.121	0.172		

TABLE 5. Mean Measured Pressure Change
(cont)

D_2 = 4.50 ins.

x/R	2	4.5	6.0	8	10
6	-0.002	-0.007	-0.010	-0.016	-0.023
12	-1001	0.602	0.004	0.007	0.012
15	0.002	0.007	0.011	0.018	0.028
18	0.003	0.007	0.012	0.021	0.032
21	0.003	0.008	0.012	0.021	0.034
24	0.003	0.008	0.012	0.022	0.034
27	0.003	0.008	0.012	0.022	0.034

x/R	12	14	16	18
6	-0.031	-0.040	-0.050	-0.063
12	0.023	0.027	0.041	0.052
15	0.030	0.053	0.075	0.093
18	0.046	0.065	0.082	0.106
21	0.048	0.064	0.085	0.110
24	0.047	0.066	0.086	0.111
27	0.048	0.066	0.087	0.112

TABLE 6. Maximum Pressure Rise - Singly-corrected Data

D_2/R	2	4.5	6	8	10	12	14	16	18
0.865 ins.									
Theory		0.120	0.182	0.284	0.410	0.562	0.745	0.963	1.207
Experiment:		0.092	0.138	0.227	0.341	0.478	0.655	0.863	1.092
1.0 ins.									
Theory:	0.059	0.152	0.230	0.359	0.519	0.711	0.944	1.220	1.525
Experiment:	0.047	0.123	0.189	0.306	0.453	0.634	0.876	1.150	1.463
1.464 ins.									
Theory:	0.045	0.117	0.176	0.275	0.398	0.544	0.722	0.932	1.168
Experiment:	0.040	0.104	0.157	0.249	0.374	0.525	0.714	0.931	1.183
2.085 ins.									
Theory:	0.026	0.067	0.102	0.156	0.230	0.315	0.419	0.541	0.677
Experiment:	0.023	0.058	0.089	0.147	0.218	0.303	0.410	0.534	0.682
3.041 ins.									
Theory:	0.013	0.034	0.052	0.081	0.117	0.160	0.212	0.274	0.343
Experiment:	0.012	0.030	0.046	0.076	0.112	0.153	0.210	0.273	0.353
4.50 ins.									
Theory:	0.006	0.016	0.024	0.038	0.055	0.076	0.100	0.130	0.162
Experiment:	0.007	0.016	0.023	0.038	0.057	0.077	0.104	0.134	0.170

R = ROTAMETER SCALE READING, CMS.

$\Delta h'$ in FT. OF WATER.

TABLE 7. Doubly-corrected Pressure Change
(cont)

D_2 = 0.865 in.

x/R	4.5	6.0	8.0	10.0
1	0.094	0.133	0.222	0.327
2	0.102	0.152	0.249	0.372
3	0.107	0.159	0.259	0.385
4	0.111	0.166	0.269	0.399
5	0.114	0.167	0.270	0.406
6	0.115	0.168	0.272	0.404
8	0.119	0.171	0.278	0.411
12	0.125	0.180	0.288	0.421
16	0.134	0.189	0.302	0.443
20	0.135	0.193	0.306	0.443
24	0.133	0.194	0.301	0.438

x/R	12	14	16	18
1	0.453	0.613	0.807	1.018
2	0.517	0.706	0.926	1.166
3	0.535	0.728	0.953	1.203
4	0.554	0.753	0.985	1.250
5	0.555	0.755	0.988	1.248
6	0.559	0.756	0.991	1.239
8	0.570	0.766	1.004	1.251
12	0.588	0.787	1.000	1.297
16	0.610	0.814	1.061	1.337
20	0.610	0.810	1.055	1.327
24	0.592	0.781	1.016	1.272

X = DISTANCE, INS.
R = ROTAMETER SCALE READING, CMS
$\Delta h''$ in FT. of WATER.

TABLE 7. Doubly-corrected Pressure Change

(CONT)

D_2 = 1.0 ins.

x/R	2	4.5	6	8	10
1	0.033	0.074	0.004	0.164	0.241
2	0.045	0.109	0.160	0.259	0.384
3	0.049	0.124	0.186	0.297	0.441
4	0.052	0.131	0.198	0.318	0.469
5	0.053	0.138	0.206	0.330	0.487
6	0.055	0.139	0.211	0.338	0.497
8	0.056	0.142	0.214	0.343	0.505
10	0.054	0.142	0.213	0.342	0.505
12	0.055	0.143	0.215	0.346	0.511
16	0.054	0.144	0.213	0.343	0.505
20	0.055	0.146	0.217	0.346	0.507

x/R	12	14	16	18
1	0.324	0.433	0.565	0.720
2	0.530	0.730	0.957	1.212
3	0.613	0.841	1.100	1.392
4	0.652	0.900	1.180	1.495
5	0.680	0.936	1.222	1.554
6	0.692	0.950	1.242	1.577
8	0.706	0.964	1.261	1.601
10	0.702	0.961	1.255	1.592
12	0.709	0.966	1.264	1.599
16	0.708	0.952	1.244	1.575
20	0.708	0.952	1.249	1.574
24	0.706	0.948	1.239	1.571

TABLE 7. Doubly-corrected Pressure Change
(CONT)

D_2 = 1.464 ins.

x/R	2.0	4.5	6.0	8.0	10.0
2	0.012	0.023	0.027	0.041	0.059
4	0.031	0.077	0.111	0.179	0.276
5	0.036	0.093	0.138	0.222	0.333
6	0.039	0.102	0.153	0.245	0.364
7	0.041	0.107	0.160	0.255	0.379
8	0.041	0.107	0.162	0.256	0.384
10	0.042	0.107	0.162	0.258	0.383
12	0.042	0.107	0.163	0.259	0.385
16	0.042	0.108	0.163	0.259	0.384
20	0.043	0.109	0.163	0.260	0.384
24	0.043	0.107	0.163	0.258	0.382

x/R	12	14	16	18
2	0.082	0.120	0.155	0.203
4	0.385	0.530	0.699	0.898
5	0.468	0.648	0.847	1.083
6	0.513	0.700	0.916	1.156
7	0.532	0.726	0.935	1.198
8	0.538	0.730	0.958	1.207
10	0.538	0.730	0.954	1.208
12	0.540	0.732	0.959	1.211
16	0.540	0.731	0.957	1.216
20	0.544	0.732	0.958	1.220
24	0.542	0.732	0.958	1.224

TABLE 7. (CONT) Doubly-corrected Pressure Change

D_2 = 2.085 ins.

x/R	2.0	4.5	6.0	8.0
2	-0.001	-0.004	-0.007	-0.008
4	0.007	0.013	0.016	0.033
6	0.018	0.042	0.060	0.102
7	0.021	0.050	0.075	0.126
8	0.023	0.055	0.083	0.139
9	0.023	0.058	0.088	0.145
10	0.023	0.058	0.089	0.147
12	0.024	0.059	0.091	0.149
15	0.023	0.059	0.091	0.149
18	0.023	0.059	0.091	0.149
21	0.022	0.060	0.091	0.149

x/R	10	12	14	16	18
2	-0.012	-0.018	-0.021	-0.030	-0.035
4	0.046	0.066	0.099	0.137	0.196
6	0.151	0.220	0.297	0.396	0.521
7	0.189	0.266	0.364	0.475	0.613
8	0.207	0.291	0.393	0.518	0.664
9	0.215	0.300	0.406	0.531	0.681
10	0.218	0.303	0.410	0.537	0.682
12	0.220	0.306	0.415	0.539	0.689
15	0.221	0.308	0.416	0.540	0.688
18	0.221	0.308	0.415	0.541	0.687
21	0.221	0.309	0.414	0.538	0.686

TABLE 7. Doubly-corrected Pressure Change
(CONT)

$D_2 = 3.041$ ins.

x/R	2.0	4.5	6	8.0
2	0.000	-0.001	-0.002	-0.001
4	0.000	-0.001	-0.002	-0.001
6	0.002	0.004	0.005	0.010
8	0.007	0.015	0.023	0.040
10	0.010	0.024	0.037	0.065
12	0.011	0.030	0.044	0.074
14	0.012	0.030	0.046	0.076
16	0.012	0.030	0.045	0.077
18	0.012	0.030	0.046	0.077

x/R	10	12	14	16	18
2	-0.002	-0.006	-0.007	-0.011	-0.007
4	-0.002	-0.007	-0.007	-0.014	-0.010
6	0.016	0.016	0.029	0.043	0.075
8	0.062	0.087	0.118	0.160	0.214
10	0.097	0.134	0.184	0.246	0.322
12	0.109	0.150	0.205	0.269	0.344
14	0.113	0.154	0.213	0.275	0.355
16	0.113	0.154	0.213	0.274	0.355
18	0.113	0.154	0.213	0.274	0.356

TABLE 7. Doubly-corrected Pressure Change

(CONT)

$D_2 = 4.50$ ins.

x/R	2.0	4.5	6.0	8.0	10.0
6	0.002	0.001	0.001	0.001	0.000
12	0.005	0.010	0.015	0.024	0.035
15	0.006	0.015	0.022	0.035	0.051
18	0.007	0.015	0.023	0.038	0.055
21	0.007	0.016	0.023	0.038	0.057
24	0.007	0.016	0.023	0.039	0.057
27	0.007	0.016	0.023	0.039	0.056

x/R	12	14	16	18
6	-0.001	-0.001	-0.002	-0.004
12	0.053	0.066	0.089	0.111
15	0.069	0.092	0.123	0.152
18	0.076	0.104	0.130	0.165
21	0.078	0.103	0.133	0.169
24	0.077	0.105	0.134	0.170
27	0.078	0.105	0.135	0.171

TABLE 8. Maximum Pressure Rise - Doubly-corrected Data (FT. of WATER).

D_2/R	2	4.5	6	8	10	12	14	16	18
0.865 ins.									
Theory:		0.120	0.182	0.284	0.410	0.562	0.745	0.963	1.207
Experiment:		0.115	0.168	0.272	0.404	0.559	0.756	0.991	1.250
1.0 ins.									
Theory:	0.059	0.152	0.230	0.359	0.519	0.711	0.944	1.220	1.525
Experiment:	0.056	0.142	0.214	0.343	0.505	0.706	0.964	1.261	1.601
1.464 ins.									
T:	0.045	0.117	0.176	0.275	0.398	0.544	0.722	0.932	1.168
E:	0.041	0.107	0.162	0.256	0.384	0.538	0.730	0.958	1.207
2.085 ins.									
T:	0.026	0.067	0.102	0.156	0.230	0.315	0.419	0.541	0.677
E:	0.024	0.059	0.091	0.149	0.220	0.306	0.415	0.539	0.689
3.041 ins.									
T:	0.013	0.034	0.052	0.081	0.117	0.160	0.212	0.274	0.343
E:	0.012	0.030	0.046	0.076	0.113	0.154	0.213	0.275	0.355
4.50 ins.									
T:	0.006	0.016	0.024	0.038	0.055	0.076	0.100	0.130	0.162
E:	0.007	0.016	0.023	0.038	0.057	0.077	0.104	0.134	0.170

TABLE 10. Head Losses (FT. OF WATER).

D_2/R	2	4.5	6	8	10	12	14	16	18
0.865 ins.									
Theory:		0.022	0.033	0.052	0.075	0.103	0.136	0.176	0.220
Experiment:		0.027	0.047	0.064	0.081	0.106	0.125	0.148	0.177
1.0 ins.									
T:	0.024	0.063	0.095	0.148	0.214	0.293	0.388	0.503	0.628
E:	0.027	0.063	0.111	0.164	0.228	0.298	0.368	0.462	0.552
1.464 ins.									
T:	0.066	0.171	0.257	0.401	0.581	0.796	1.058	1.353	1.707
E:	0.070	0.181	0.271	0.420	0.595	0.802	1.050	1.327	1.668
2.085 ins.									
T:	0.090	0.233	0.354	0.541	0.799	1.103	1.453	1.879	2.351
E:	0.092	0.241	0.365	0.548	0.809	1.094	1.457	1.881	2.339
3.041 ins.									
T:	0.103	0.270	0.413	0.644	0.930	1.270	1.684	2.176	2.725
E:	0.104	0.274	0.419	0.649	0.934	1.276	1.683	2.175	2.713
4.50 ins.									
T:	0.108	0.287	0.431	0.682	0.987	1.364	1.796	2.334	2.908
E:	0.107	0.287	0.432	0.682	0.985	1.363	1.792	2.330	2.900

TABLE 11. Normalised Pressure Change Data (based on singly corrected values)

$D_2 = 1.0$ ins.

R/x	1	2	3	4	5	6
2.0	0.666	0.896	0.959	1.000	1.000	0.980
4.5	0.568	0.832	0.929	0.960	1.000	0.984
6.0	0.529	0.810	0.926	0.969	0.995	1.000
8.0	0.520	0.817	0.919	0.970	0.994	1.000
10	0.516	0.815	0.925	0.971	0.994	1.000
12	0.495	0.806	0.921	0.967	0.996	1.000
14	0.482	0.806	0.918	0.971	0.997	1.000
16	0.478	0.806	0.917	0.974	0.995	1.000
18	0.479	0.804	0.913	0.971	0.997	1.000
Av.	0.500	0.809	0.921	0.970	0.996	1.000

$D_2 = 1.464$ ins.

R/x	2	4	5	6	7	8
2.0	0.300	0.750	0.875	0.950	1.000	1.000
4.5	0.212	0.721	0.875	0.962	1.000	1.000
6.0	0.166	0.695	0.860	0.955	0.994	1.000
8.0	0.165	0.706	0.875	0.964	1.000	1.000
10	0.153	0.725	0.875	0.955	0.992	1.000
12	0.151	0.722	0.876	0.959	0.989	1.000
14	0.163	0.732	0.894	0.964	0.996	1.000
16	0.160	0.735	0.890	0.961	0.990	1.000
18	0.166	0.794	0.902	0.961	0.993	1.000
Av.	0.161	0.724	0.877	0.959	0.995	1.000

X = DISTANCE, INS.

R = ROTAMETER SCALE READING, CMS.

TABLE 11. Normalised Pressure Change Data
(cont)

D_2 = 2.085 ins.

R/x	2	4	6	7	8	9	10	12
2	-0.043	0.304	0.782	0.913	1.000	1.000	1.000	1.000
4.5	-0.069	0.224	0.724	0.862	0.931	0.983	0.983	1.000
6.0	-0.079	0.180	0.663	0.831	0.921	0.978	0.989	1.000
8.0	-0.054	0.218	0.687	0.850	0.939	0.980	0.994	1.000
10	-0.055	0.211	0.684	0.862	0.940	0.978	0.991	1.000
12	-0.063	0.214	0.720	0.871	0.954	0.984	0.990	1.000
14	-0.051	0.239	0.720	0.880	0.951	0.982	0.990	1.000
16	-0.058	0.256	0.734	0.881	0.963	0.987	0.998	1.000
18	-0.046	0.287	0.787	0.913	0.980	0.991	0.991	1.000
Av.	-0.055	0.227	0.712	0.866	0.943	0.983	0.992	1.000

D_2 = 3.041 ins.

R/x	2	4	6	8	10	12	14
2.0	0.000	0.000	0.167	0.584	0.834	0.917	1.000
4.5	-0.033	-0.033	0.133	0.500	0.800	1.000	1.000
6.0	-0.044	-0.043	0.111	0.511	0.800	0.978	1.000
8.0	-0.014	-0.013	0.131	0.526	0.855	0.974	1.000
10	-0.018	-0.018	0.143	0.554	0.866	0.974	1.000
12	-0.039	-0.059	0.098	0.569	0.876	0.974	1.000
14	-0.033	-0.043	0.138	0.562	0.857	0.953	1.000
16	-0.041	-0.051	0.157	0.583	0.898	0.982	1.000
18	-0.020	-0.028	0.125	0.604	0.910	0.970	1.000
Av.	-0.030	-0.036	0.130	0.564	0.858	0.972	1.000

TABLE 11. Normalised Pressure Change Data
(cont)

$D_2 = 4.50$ ins.

R/x	6	12	15	18	21
2.0	-	0.715		1.000	1.000
4.5	0.063	0.625	0.938	0.938	1.000
6.0	0.043	0.652	0.956	1.000	1.000
8.0	0.026	0.615	0.897	0.975	0.975
10	0.000	0.614	0.719	0.965	1.000
12	-0.013	0.689	0.780	0.986	1.010
14	-0.010	0.635	0.885	1.000	0.990
16	-0.015	0.740	0.918	0.970	0.993
18	-0.023	0.653	0.895	0.970	0.995
Av.	+0.009	0.636	0.899	0.983	0.997

Table 12

R(cms)	6	10	14	18
V_1 ft/sec	5.46	8.21	11.07	14.07
h_1 ft	32.5	32.9	33.6	34.4
$mo/(Mp)^{\frac{1}{2}}$	0.0352	0.0526	0.0702	0.0881

$\Delta h'$ (Singly corrected pressure difference)

R/x	2	4	5	6	7	8	20
6	0.026	0.109	0.135	0.150	0.156	0.157	0.150
10	0.057	0.271	0.327	0.357	0.371	0.374	0.360
14	0.116	0.522	0.638	0.688	0.712	0.714	0.692
18	0.197	0.886	1.068	1.138	1.177	1.183	1.159

(p - Po)/M

R/x	2	4	5	6	7	8	20
6	-0.0138	-0.0126	-0.0122	-0.0120	-0.0119	-0.0119	-0.0120
10	-0.0310	-0.0277	-0.0269	-0.0264	-0.0262	-0.0262	-0.0264
14	-0.0549	-0.0488	-0.0471	-0.0461	-0.0460	-0.0460	-0.0462
18	-0.0866	-0.0765	-0.0739	-0.0730	-0.0724	-0.0722	-0.0730

X - DISTANCE INS
R = ROTAMETER SCALE READING CMS.
$m_o/(Mp)^{1/2}$, $(p - P_o)/M$ PARAMETERS OF HILL.

TABLE 13 (a) Current - Voltage Measurements

$D_2/D_1 = 1.33$

LEGEND:
- I = Total current (milliamps)
- V = Potential difference across cell (millivolts)
- c_b = Molarity of copper sulphate solution
- i_L = Limiting current density (milliamps/cm^2)
- Re_2 = Reynolds number in downstream duct (based on full bore flow)

Cathode 0 - 0.5 ins. Re_2 = 3750 c_b = 0.00827

I	26	27	28	28	27	30	32	39
V	310	370	420	470	490	560	630	670

i_L = 2.77

Cathode 0 - 0.5 ins. Re_2 = 3750 c_b = 0.00720

I	20	23	25	26	27	27	29	37
V	295	345	410	480	520	555	615	675

i_L = 2.67

Cathode 0 - 0.5 ins. Re_2 = 6470 c_b = 0.00720

I	33	37	43	43	45	46	48	52
V	270	320	390	450	510	560	605	660

i_L = 4.56

Cathode 0 - 0.5 ins. Re_2 = 6470 c_b = 0.00720

I	32	35	38	37	39	39	41	46
V	275	360	410	480	510	565	610	660

Cathode 0 - 0.5 ins. $Re_2 = 9900$ $c_b = 0.00746$

I	41	45	46	48	48	50	50	54	65
V	330	390	425	490	515	570	610	645	705

$i_L = 4.85$

Cathode 0 - 0.5 ins. $Re_2 = 15600$ $c_b = 0.0070$

I	62	66	67	68	70	72	78	90
V	390	440	480	535	580	635	680	715

$i_L = 6.84$

Cathode 0 - 0.5 ins. $Re_2 = 19000$ $c_b = 0.00664$

I	68	70	74	75	76	77	79	85	99
V	360	410	480	520	555	590	640	680	720

$i_L = 7.62$

Cathode 0 - 0.75 ins. $Re_2 = 6470$ $c_b = 0.06720$

I	53	57	60	61	62	65	73
V	310	560	435	490	550	595	670

$i_L = 4.03$

Cathode 0 - 0.75 ins. $Re_2 = 9900$ $c_b = 0.00746$

I	64	69	72	72	76	75	80	88
V	340	400	445	500	545	590	630	675

$i_L = 5.01$

Cathode 0 - 0.75 ins. $Re_2 = 15600$ $c_b = 0.00692$

I	80	89	95	98	102	102	105	111	123
V	340	395	440	480	530	570	620	665	700

Cathode 0 - 0.75 ins. Re_2 = 19000 c_b = 0.00658

I	87	98	105	106	108	110	116	132
V	360	435	500	540	570	620	670	710

i_L = 7.13

Cathode 0 - 1.0 ins. Re_2 = 3750 c_b = 0.00773

I	55	58	59	60	61	62	62	69
V	335	390	430	480	525	575	610	675

i_L = 3.02

Cathode 0 - 1.0 ins. Re_2 = 6470 c_b = 0.00775

I	65	74	78	81	84	87	88	89	95
V	295	350	395	430	470	525	575	600	670

i_L = 4.36

Cathode 0 - 1.0 ins. Re_2 = 9900 M = 0.0072

I	80	87	90	93	96	97	100	103	115
V	350	400	434	480	515	560	600	660	715

i_L = 4.85

Cathode 0 - 1.0 ins. Re_2 = 15600 c_b = 0.00684

I	110	119	123	126	128	129	132	136	145
V	400	465	500	535	590	635	660	695	725

i_L = 6.34

Cathode 0 - 1.0 ins. Re_2 = 19000 c_b = 0.00653

I	111	124	132	133	137	138	137	142	152	168
V	375	420	470	505	520	600	625	665	710	740

i_L = 6.84

Cathode 0 - 1.0 ins. Re_2 = 19000 c_b = 0.00604

I	101	114	122	126	127	130	138	145
V	370	430	500	545	590	630	690	710

i_L = 6.34

Cathode 0 - 1.25 ins. Re_2 = 9900 c_b = 0.00805

I	85	95	98	106	107	108	110	117	129
V	325	380	430	500	540	570	615	675	710

i_L = 4.28

Cathode 0 - 1.25 ins. Re_2 = 15600 c_b = 0.00849

I	110	130	139	146	152	156	158	164	176
V	350	400	440	480	525	580	630	685	725

i_L = 6.22

Cathode 0 - 1.25 ins. Re_2 = 19000 c_b = 0.00685

I	142	158	165	173	178	181	190
V	385	455	495	535	590	650	705

i_L = 7.05

Cathode 0 - 1.25 ins. Re_2 = 15600 c_b = 0.00609

I	126	142	150	154	160	163	165	170	179
V	360	415	460	490	555	605	645	685	720

i_L = 6.44

Cathode 0 - 1.5 ins. Re_2 = 3750 c_b = 0.00774

I	77	80	83	84	87	88	89	90	94	105
V	320	365	400	435	475	530	570	600	640	685

i_L = 3.40

Cathode 0 - 1.5 ins. Re_2 = 6470 c_b = 0.00770

I	99	107	112	117	117	119	122	125	130
V	315	370	420	450	485	525	580	650	690

i_L = 3.96

Cathode 0 - 1.5 ins. Re_2 = 9900 c_b = 0.00652

I	98	109	114	119	120	122	124	126	133	145
V	330	380	430	470	510	540	580	625	680	720

i_L = 4.09

Cathode 0 - 1.5 ins. Re_2 = 15600 c_b = 0.00684

I	127	143	152	162	172	175	178	179	187	198
V	330	390	425	470	525	560	605	635	690	730

i_L = 5.87

Cathode 0 - 1.5 ins. $Re_2 = 19000$ $c_b = 0.00616$

I	157	170	183	189	194	196	197	198	202	213
V	360	410	460	520	560	595	635	665	700	735

$i_L = 6.50$

Cathode 0 - 1.5 ins. $Re_2 = 19000$ $c_b = 0.00610$

I	140	151	170	177	182	187	192	194	196	205
V	360	400	460	485	520	550	605	640	680	715

$i_L = 6.36$

Cathode 0 - 2.0 ins. $Re_2 = 6470$ $c_b = 0.00785$

I	118	137	147	148	153	155	157	159	165
V	320	380	435	475	520	565	600	625	670

$i_L = 3.86$

Cathode 0 - 2.0 ins. $Re_2 = 3750$ $c_b = 0.00756$

I	97	100	104	105	106	108	112	124
V	300	355	410	470	515	570	625	670

$i_L = 2.65$

Cathode 0 - 2.0 ins. $Re_2 = 9900$ $c_b = 0.00650$

I	114	135	141	149	155	157	162	166	171	187
V	315	380	415	460	495	530	580	640	675	720

$i_L = 4.01$

Cathode 0 - 2.0 ins. Re_2 = 9900 c_b = 0.00590

I	115	128	135	139	140	143	145	152	165
V	320	385	465	500	535	590	620	665	700

i_L = 3.52

Cathode 0 - 2.0 ins. Re_2 = 15600 c_b = 0.00696

I	153	178	191	208	216	219	222	228	235	254
V	340	380	430	510	565	600	640	685	710	750

i_L = 5.45

Cathode 0 - 2.0 ins. Re_2 = 19000 c_b = 0.00615

I	184	200	213	226	235	242	246	252	270
V	360	410	450	505	545	580	625	675	740

i_L = 6.09

Cathode 0 - 2.0 ins. Re_2 = 19000 c_b = 0.00582

I	175	194	209	220	226	230	234	240	256
V	360	420	490	555	590	640	675	700	730

i_L = 5.65

Cathode 0 - 2.0 ins. Re_2 = 19000 M = 0.00615

I	185	200	218	227	234	239	244	250	259
V	380	420	475	540	585	640	670	705	725

i_L = 5.89

Cathode 0 - 2.5 ins. $Re_2 = 19000$ M = 0.00582

I	214	233	247	260	268	272	275	276	282	293
V	365	425	485	540	595	635	675	695	730	755

$i_L = 5.47$

Cathode 0 - 2.5 ins. $Re_2 = 3750$ $c_b = 0.00687$

I	101	109	111	113	116	118	120	125	140
V	330	375	420	460	495	550	600	660	705

$i_L = 2.35$

Cathode 0 - 2.5 ins. $Re_2 = 6470$ $c_b = 0.00714$

I	134	144	146	152	157	162	165	165	174
V	325	375	400	430	455	510	560	620	680

$i_L = 3.26$

Cathode 0 - 2.5 ins. $Re_2 = 6470$ $c_b = 0.00714$

I	118	137	147	156	160	164	166	170	172	182
V	320	365	405	465	490	540	605	660	690	725

$i_L = 3.26$

Cathode 0 - 2.5 ins. $Re_2 = 9900$ $c_b = 0.00598$

I	124	149	157	164	168	171	174	177	181	194
V	320	380	435	470	510	540	580	630	675	725

$i_L = 3.46$

Cathode 0 - 2.5 ins. $Re_2 = 15600$ $c_b = 0.00657$

I	198	217	231	245	252	266	277	292
V	330	405	450	510	540	610	670	105

$i_L =$

Cathode 0 - 3.0 ins. $Re_2 = 3750$ $c_b = 0.00676$

I	114	122	123	126	129	130	134	146
V	330	390	420	470	525	580	630	685

$i_L = 2.14$

Cathode 0 - 3.0 ins. $Re_2 = 6470$ $c_b = 0.00722$

I	134	162	180	192	196	197	200	200	204	213
V	300	390	480	530	565	590	625	650	670	710

$i_L = 3.27$

Cathode 0 - 3.0 ins. $Re_2 = 3750$ $c_b = 0.00597$

I	90	103	110	112	114	117	130
V	310	385	460	525	590	640	695

$i_L = 1.88$

Cathode 0 - 3.0 ins. $Re_2 = 6470$ $c_b = 0.00592$

I	118	123	141	147	153	159	165	191
V	330	365	440	490	550	635	680	710

$i_L = 2.59$

Cathode 0 - 3.0 ins. $Re_2 = 9900$ $c_b = 0.00610$

I	149	168	174	186	190	195	196	198	202	210
V	310	380	420	475	515	550	600	630	650	690

$i_L = 3.24$

Cathode 0 - 3.0 ins. $Re_2 = 9900$ $c_b = 0.00602$

I	130	153	175	185	194	198	205	225
V	330	385	450	520	575	640	690	750

$i_L = 3.26$

Cathode 0 - 3.0 ins. $Re_2 = 15600$ $c_b = 0.00576$

I	160	187	215	230	247	259	265	275	296
V	350	405	465	505	560	605	650	725	785

$i_L =$

Cathode 0 - 3.0 ins. $Re_2 = 19000$ $c_b = 0.00590$

I	171	200	225	249	259	282	302	308	316	331
V	320	375	430	480	500	565	645	685	735	780

$i_L =$

Cathode 0 - 3.0 ins. $Re_2 = 19000$ $c_b = 0.00571$

I	218	244	264	280	293	298	302	309	318	333
V	375	435	490	540	590	625	660	695	735	760

$i_L = 5.04$

Cathode 0 - 4.0 ins. $Re_2 = 3750$ $c_b = 0.00632$

I	145	152	157	164	165	169	170	172	180	195
V	385	415	445	500	550	605	640	685	740	780

$i_L = 2.08$

Cathode 0 - 4.0 ins. $Re_2 = 6470$ $c_b = 0.00622$

I	180	202	216	223	228	230	230	233	239	258
V	360	425	490	530	570	600	630	670	740	800

$i_L = 2.85$

Cathode 0 - 4.0 ins. $Re_2 = 9900$ $c_b = 0.00576$

I	196	223	237	246	255	259	262	264	270	283
V	380	435	490	520	570	620	665	705	765	805

$i_L = 3.24$

Cathode 0 - 4.0 ins. $Re_2 = 15600$ $c_b =$

I	265	289	314	342	362	377	385	393
V	370	420	475	550	610	680	750	810

$i_L =$

Cathode 0 - 5.0 ins. $Re_2 = 3750$ $c_b = 0.00570$

I	146	152	155	158	160	160	161	164	173	196
V	370	435	490	525	565	605	650	685	725	780

$i_L = 1.58$

Cathode 0-5.0 ins. $Re_2 = 6470$ $c_b = 0.0055$

I	156	174	192	194	206	210	215	220	229	246
V	320	365	430	460	530	580	630	710	760	800

$i_L = 2.13$

Cathode 0 - 5.0 ins. $Re_2 = 3750$ $c_b = 0.00735$

I	178	190	199	204	208	209	212	219	233
V	380	435	485	520	570	615	705	750	790

$i_L = 2.08$

Cathode 0 - 5.0 ins. $Re_2 = 6470$ $c_b = 0.00710$

I	226	244	254	264	275	283	290	298	314
V	415	460	490	525	575	630	695	765	820

$i_L = 2.87$

Cathode 0 - 5.0 ins. $Re_2 = 9900$ $c_b = 0.0069$

I	252	280	298	322	335	346	361	370	382
V	400	445	480	530	575	615	690	745	800

$i_L =$

Cathode 0 - 5.0 ins. $Re_2 = 9900$ $c_b = 0.00556$

I	190	210	246	263	276	280	285	293	305
V	350	385	485	550	625	655	700	770	815

$i_L =$

TABLE 13(b) Current - Voltage Measurements

$D_2/D_1 = 2.67$

LEGEND:
- I = Total current (milliamps)
- V = Potential difference across cell (millivolts)
- c_b = Molarity of copper sulphate solution
- i_L = Limiting current density (milliamps/cm^2)
- Re_2 = Reynolds number in downstream duct (based on full bore flow).

Cathode 0 - 0.5 ins. $Re_2 = 3230$ $c_b = 0.0097$

I	36	39	41	42	43	43	43	45
V	285	315	380	425	475	510	555	600

$i_L = 2.12$

Cathode 0 - 0.5 ins. $Re_2 = 4450$ $c_b = 0.00955$

I	39	45	46	47	49	47	51	52	54
V	270	360	405	450	510	530	560	590	640

$i_L = 2.37$

Cathode 0 - 0.5 ins. $Re_2 = 7800$ $c_b = 0.0092$

I	46	53	55	56	57	58	59	62	66
V	285	340	370	425	470	530	590	630	685

$i_L = 2.82$

Cathode 0 - 0.5 ins. $Re_2 = 9500$ $c_b = 0.0098$

I	50	58	68	72	73	74	75	76
V	260	300	380	420	470	550	605	640

$i_L = 3.65$

Cathode 0 - 0.5 ins. $Re_2 = 1880$ $c_b = 0.01045$

I	27	30	31	32	33	31	32	35
V	300	380	435	475	500	560	605	660

$i_L = 1.68$

Cathode 0 - 0.5 ins. $Re_2 = 3230$ $c_b = 0.01045$

I	42	42	44	42	45	45	46	50
V	310	370	415	470	500	540	585	650

$i_L = 2.22$

Cathode 0 - 1.0 ins. $Re_2 = 1880$ $c_b = 0.01285$

I	55	59	60	62	61	62	64	74
V	300	355	410	465	535	590	630	670

$i_L = 1.51$

Cathode 0 - 1.0 ins. $Re_2 = 3230$ $c_b = 0.01285$

I	88	91	93	94	93	95	102
V	340	400	470	530	600	650	680

$i_L = 2.32$

Cathode 0 - 1.0 ins. $Re_2 = 4450$ $c_b = 0.0105$

I	87	92	98	98	99	101	115
V	270	305	400	455	500	575	670

$i_L = 2.44$

Cathode 0 - 1.0 ins. $Re_2 = 4450$ $c_b = 0.0109$

I	94	98	100	101	103	98	114
V	300	370	435	505	570	600	645

$i_L = 2.50$

Cathode 0 - 1.0 ins. $Re_2 = 7800$ $c_b = 0.01265$

I	128	142	147	145	152	149	152	169
V	330	385	440	510	545	580	620	710

$i_L = 3.68$

Cathode 0 - 1.0 ins. $Re_2 = 7800$ $c_b = 0.0109$

I	112	130	133	134	135	139	152
V	290	385	440	495	550	610	660

$i_L = 3.33$

Cathode 0 - 1.0 ins. $Re_2 = 9500$ $c_b = 0.0109$

I	138	150	157	163	163	171	168	174	188
V	325	370	420	500	560	600	620	660	700

$i_L = 4.08$

Cathode 0 - 1.5 ins. $Re_2 = 1880$ $c_b = 0.00715$

I	44	47	48	49	48	47	55	81
V	285	360	405	450	520	590	650	691

$i_L = 0.79$

Cathode 0 - 1.5 ins. $Re_2 = 3230$ $c_b = 0.00705$

I	63	67	68	71	71	74	75	75	82
V	305	330	390	440	485	505	550	580	630

$i_L = 1.22$

Cathode 0 - 1.5 ins. $Re_2 = 4450$ $c_b = 0.00695$

I	70	80	85	85	89	90	91	98	110
V	295	340	400	450	510	570	610	640	675

$i_L = 1.465$

Cathode 0 - 1.5 ins. $Re_2 = 7800$ $c_b = 0.00685$

I	90	106	112	115	116	118	120	126	136	150
V	310	370	400	460	520	560	575	605	640	665

$i_L = 1.91$

Cathode 0 - 1.5 ins. $Re_2 = 9500$ $c_b = 0.00730$

I	108	118	129	133	136	135	138	143
V	310	340	400	470	510	555	580	630

$i_L = 2.24$

Cathode 0 - 1.5 ins. $Re_2 = 9500$ $c_b = 0.00814$

I	105	131	141	146	146	148	152	154
V	285	340	410	480	530	560	600	630

$i_L = 2.42$

Cathode: 0 - 2.0 ins. $Re_2 = 1800$ $c_b = 0.0107$

I	115	120	123	122	126	127	128	128	132	136	155
V	300	340	375	420	440	500	550	570	600	625	670

$i_L = 1.58$

Cathode: 0 - 2.0 ins. $Re_2 = 3230$ $c_b = 0.0106$

I	154	166	172	181	181	184	187	185	190	205
V	320	365	390	425	450	510	535	590	665	685

$i_L = 2.31$

Cathode: 0 - 2.0 ins. $Re_2 = 4450$ $c_b = 0.0104$

I	176	194	199	204	207	209	220	218	240
V	325	370	420	460	490	540	610	640	690

$i_L = 2.58$

Cathode: 0 - 2.0 ins. $Re_2 = 4450$ $c_b = 0.0111$

I	190	210	217	218	220	220	226	224	230	254
V	325	390	440	465	515	590	600	630	640	680

$i_L = 2.75$

Cathode: 0 - 2.0 ins. $Re_2 = 7800$ $c_b = 0.0103$

I	198	236	255	266	274	268	275	280	295	331
V	285	365	425	480	530	550	600	635	680	730

$i_L = 3.40$

Cathode: 0 - 2.0 ins. Re_2 = 9500 c_b = 0.0102

I	250	271	289	301	303	305	304	306	309	330
V	310	365	430	475	520	560	590	615	650	705

i_L = 3.77

Cathode: 0 - 3.0 ins. Re_2 = 9500 c_b = 0.00701

I	255	293	303	316	328	333	334	340	349
V	340	420	450	500	555	600	635	680	710

i_L =

Cathode: 0 - 3.0 ins. Re_2 = 1880 c_b = 0.00759

I	135	141	146	147	146	151	144	151	150	154	157
V	310	340	390	450	490	540	565	590	630	650	670

i_L = 1.22

Cathode: 0 - 3.0 ins. Re_2 = 3230 c_b = 0.00747

I	173	186	195	193	195	195	196	205	202	219
V	300	340	400	440	500	535	570	625	650	690

i_L = 1.61

Cathode: 0 - 3.0 ins. Re_2 = 4450 c_b = 0.00732

I	197	218	218	225	231	232	239	250
V	310	370	395	440	520	590	650	680

i_L = 1.89

Cathode: 0 - 3.0 ins. $Re_2 = 7800$ $c_b = 0.00716$

I	215	243	265	281	286	294	298	300	307	311
V	315	365	430	475	520	550	620	665	685	720

$i_L =$

Cathode: 0 - 4.0 ins. $Re_2 = 1880$ $c_b = 0.00851$

I	177	214	225	231	232	232	231	232	245
V	285	390	450	510	535	570	610	645	685

$i_L = 1.425$

Cathode: 0 - 2.0 ins. $Re_2 = 1880$ $c_b = 0.0089$

I	72	78	79	81	82	83	83	88	95
V	270	330	390	435	480	520	565	630	650

$i_L = 1.023$

Cathode: 0 - 2.0 ins. $Re_2 = 3230$ $c_b = 0.00873$

I	113	122	124	126	129	131	129	128	135
V	285	360	410	440	490	520	550	600	645

$i_L = 1.59$

Cathode: 0 - 2.0 ins. $Re_2 = 7800$ $c_b = 0.0081$

I	150	165	186	191	196	195	200	206
V	305	350	400	460	500	550	610	650

$i_L = 2.43$

Cathode 0 - 2.0 ins. $Re_2 = 4450$ $c_b = 0.0091$

I	123	138	145	154	153	153	154	159
V	290	350	390	420	475	535	580	645

$i_L = 1.90$

Cathode 0 - 2.0 ins. $Re_2 = 9500$ $c_b = 0.0079$

I	170	190	200	211	221	224	224	228	245
V	325	365	420	475	525	560	610	640	730

$i_L = 2.76$

Cathode 2.10 - 2.85 ins. $Re_2 = 7800$ $c_b = 0.0089$

I	122	134	143	149	150	146	151	154	160
V	330	390	460	510	530	560	580	600	650

$i_L = 5.0$

Cathode 2.10 - 2.85 ins. $Re_2 = 4450$ $c_b = 0.0089$

I	95	100	102	107	107	110	114
V	335	380	420	510	555	600	640

$i_L = 3.60$

Cathode 2.10 - 3.10 ins. $Re_2 = 1880$ $c_b = 0.0102$

I	79	89	94	96	97	97	98
V	300	340	400	445	490	530	600

$i_L = 2.37$

Cathode 2.10 - 3.10 ins. $Re_2 = 3230$ $c_b = 0.0100$

I	109	119	121	123	121	123	125	130
V	320	400	455	500	535	585	635	675

$i_L = 3.32$

Cathode 2.10 - 3.10 ins. $Re_2 = 4450$ $c_b = 0.00636$

I	86	92	98	100	102	104	105	110
V	310	355	415	455	495	525	590	630

$i_L = 2.54$

Cathode 2.10 - 3.10 ins. $Re_2 = 7800$ $c_b = 0.0062$

I	112	122	130	135	139	141	145	157
V	300	360	420	455	515	565	620	665

$i_L = 3.46$

Cathode 2.10 - 3.10 ins. $Re_2 = 9500$ $c_b = 0.0062$

I	119	136	144	148	155	159	161	171
V	310	370	415	435	480	540	590	640

$i_L = 3.92$

Cathode 3.10 - 3.85 ins. $Re_2 = 7800$ $c_b = 0.00677$

I	69	83	108	120	125	129	144
V	290	360	415	490	520	580	660

$i_L = 4.20$

Cathode 3.10 - 4.10 ins. $Re_2 = 1880$ $c_b = 0.0088$

I	68	76	81	80	81	83	86	92
V	290	310	395	440	505	560	605	640

$i_L = 2.025$

Cathode 3.10 - 4.10 ins. $Re_2 = 3230$ $c_b = 0.0089$

I	96	105	107	109	109	113	115	120
V	320	365	415	470	510	560	600	650

$i_L = 2.72$

Cathode 3.10 - 4.10 ins. $Re_2 = 4450$ $c_b = 0.0108$

I	132	146	150	154	159	156	162	161	168
V	300	360	405	430	485	510	550	600	650

$i_L = 3.95$

Cathode 3.10 - 4.10 ins. $Re_2 = 7800$ $c_b = 0.0104$

I	161	185	200	206	210	211	214	239
V	315	375	445	490	525	580	625	715

$i_L = 5.21$

Cathode 3.10 - 4.10 ins. $Re_2 = 9500$ $c_b = 0.01065$

I	162	193	210	227	232	235	240	241	253
V	300	355	410	460	490	515	550	605	665

$i_L = 5.9$

Cathode 3.10 - 4.10 ins. $Re_2 = 4450$ $c_b = 0.0085$

I	102	117	126	131	137	138	140
V	335	400	445	510	555	580	630

$i_L = 3.38$

Cathode 3.10 - 4.60 ins. $Re_2 = 1880$ $c_b = 0.0117$

I	124	143	151	150	155	157	160	158	170
V	295	355	419	450	470	510	560	600	650

$i_L = 2.60$

Cathode 3.10 - 4.60 ins. Re_2 = 3230 c_b = 0.0116

I	167	181	198	204	207	209	214	213	219
V	290	315	380	425	470	510	565	600	645

i_L = 3.49

Cathode 3.10 - 4.60 ins. Re_2 = 4450 c_b = 0.014

I	192	209	218	231	239	239	243	250
V	310	355	390	445	500	555	590	630

i_L = 3.93

Cathode 3.10 - 4.60 ins. Re_2 = 3230 c_b = 0.0091

I	124	140	151	162	168	167	169	182	184
V	300	355	405	470	510	535	575	620	660

i_L = 2.78

Cathode 3.10 - 4.60 ins. Re_2 = 4450 c_b = 0.0090

I	133	160	170	176	187	193	197	200	207
V	300	365	400	425	475	535	575	615	670

i_L = 3.21

Cathode 3.10 - 4.60 ins. Re_2 = 7800 c_b = 0.0088

I	186	215	230	247	255	257	258	264
V	315	370	420	480	540	585	630	670

i_L = 4.21

Cathode 4.10 - 4.85 ins. $Re_2 = 4450$ $c_b = 0.0092$

I	95	102	107	110	111	111	116	122
V	315	380	440	490	515	565	630	665

$i_L = 3.71$

Cathode 4.10 - 4.85 ins. $Re_2 = 7800$ $c_b = 0.00923$

I	117	138	147	151	156	161	167
V	330	405	450	485	550	630	675

$i_L = 5.20$

Cathode 4.10 - 4.85 ins. $Re_2 = 7800$ $c_b = 0.00677$

I	83	100	107	112	115	120	123
V	310	390	420	480	520	565	625

$i_L = 3.94$

Cathode 4.10 - 4.85 ins. $Re_2 = 9500$ $c_b = 0.00677$

I	104	119	122	130	135	140	138	142	153
V	315	380	410	475	540	580	600	640	695

$i_L = 4.54$

Cathode 4.10 - 5.10 ins. $Re_2 = 1880$ $c_b = 0.00776$

I	68	71	74	75	73	75	76	79
V	305	350	405	445	470	520	580	620

$i_L = 1.85$

Cathode 4.10 - 5.10 ins. $Re_2 = 3230$ $c_b = 0.00776$

I	86	97	98	101	102	104	103	106	108
V	300	360	400	440	475	520	560	590	630

$i_L = 2.52$

Cathode 4.10 - 5.10 ins. $Re_2 = 4450$ $c_b = 0.00757$

I	114	120	121	125	125	126	129	130	143
V	325	370	400	460	515	550	590	630	670

$i_L = 3.09$

Cathode 4.10 - 5.10 ins. $Re_2 = 7800$ $c_b = 0.00747$

I	105	141	157	163	166	169	167	173
V	300	390	465	505	525	570	590	630

$i_L = 4.12$

Cathode 4.10 - 5.10 ins. $Re_2 = 9500$ $c_b = 0.0074$

I	134	156	168	177	186	190	191	194	196	216
V	300	350	400	440	480	515	555	580	630	700

$i_L = 4.74$

Cathode 5.10 - 6.10 ins. $Re_2 = 1880$ $c_b = 0.0073$

I	45	49	52	51	54	53	55	57
V	300	340	400	465	500	535	555	610

$i_L = 1.33$

Cathode 5.10 - 6.10 ins. $Re_2 = 3230$ $c_b = 0.0073$

I	70	75	75	74	77	79	81
V	310	400	460	505	550	570	620

$i_L = 1.88$

Cathode 5.10 - 6.10 ins. $Re_2 = 4450$ $c_b = 0.0073$

I	88	95	97	98	101	100	103	106
V	310	370	410	450	510	545	580	630

$i_L = 2.495$

Cathode 5.10 - 6.10 ins. $Re_2 = 7800$ $c_b = 0.0073$

I	118	127	135	134	137	141	142	144
V	335	380	440	480	520	575	605	640

$i_L = 3.43$

Cathode 5.10 - 6.10 ins. $Re_2 = 9500$ $c_b = 0.0073$

I	125	136	145	154	159	161	163	167
V	315	365	415	480	530	585	620	660

$i_L = 3.95$

Cathode 6.10 - 7.10 ins. $Re_2 = 1880$ $c_b = 0.0080$

I	47	50	51	51	52	53	55
V	300	370	415	460	505	560	600

$i_L = 1.31$

Cathode 6.10 - 7.10 ins. $Re_2 = 3230$ $c_b = 0.0080$

I	62	69	76	72	75	76	76	79
V	320	360	410	435	495	540	585	630

$i_L = 1.875$

Cathode 6.10 - 7.10 ins. $Re_2 = 4450$ $c_b = 0.00778$

I	78	84	85	87	90	91	91
V	330	400	445	500	540	590	625

$i_L = 2.2$

Cathode 6.10 - 7.10 ins. $Re_2 = 7800$ $c_b = 0.00783$

I	107	118	120	123	124	125	128	130
V	310	360	420	480	520	565	600	620

$i_L = 3.06$

Cathode 6.10 - 7.10 ins. $Re_2 = 7800$ $c_b = 0.00788$

I	120	136	138	142	144	148	158
V	320	400	450	505	550	610	645

$i_L = 3.53$

<u>TABLE 14</u>.

<u>14a</u>. D_2 = 1.0 ins. $k_m \times 10^3$

Length/Re_2	3750	6470	9900	15600	19000
0.5 ins.	1.79 1.91	2.75 2.85	3.49	5.35	5.49
0.75 ins.			3.48	5.27	5.55
1.0 ins.	2.02	2.90	3.48	4.88	5.45 5.49
1.25 ins.			3.43	4.73	5.45 5.48
1.5 ins.	1.96	2.66	3.24	4.44	5.45 5.39
2.0 ins.	1.81	2.54	3.19 3.08	4.04	5.05 4.95
2.5 ins.	1.77	2.38	2.98		4.85
3.0 ins.	1.64 1.63	2.34 2.26	2.74 2.81		
4.0 ins.	1.72	2.37 2.47	2.91		
5.0 ins.	1.46 1.43	2.05 2.00			

14b. D_2 = 2.0 ins. $k_m \times 10^3$

Length/Re_2	1880	3230	4450	7800	9500
0.5 ins.	0.79	1.10	1.29	1.58	1.85
	0.83	1.13		1.69	1.93
				1.73	
1.0 ins.	0.607	0.936	1.19	1.58	1.65
			1.21	1.51	
1.5 ins.	0.573	0.894	1.09	1.44	1.58
					1.54
2.0 ins.	0.765	0.95	1.29	1.71	1.91
	0.595	0.945	1.08	1.36	1.81
3.0 ins.	0.776	1.12	1.34	1.77	2.01
	0.830	1.07			
4.0 ins.	0.868	1.20			

TABLE 15

15a. D_2 = 1.0 ins. $(k_m)_{LOC} \times 10^3$

Length/Re_2	3750	6470	9900	15600	19000
0 - 0.5 ins.	1.79 1.91	2.75 2.85	3.49	5.35	5.49
0.5 - 0.75 ins.			3.46	5.11	5.67
0.5 - 1.0 ins.	2.25 2.13	3.05 2.95	3.47	4.41	
0.75 - 1.0 ins.			3.48	3.71	5.15 5.31
1.0 - 1.25 ins.			3.23	4.13	5.45/5.29 5.60/5.44
1.0 - 1.5 ins.	1.84	2.18	2.76	3.56	
1.25 - 1.5 ins.			2.29	2.89	5.45/5.30 5.09/5.84
1.5 - 2.0 ins.	1.36	2.18	3.04 2.60		3.85/4.03 3.45/3.57
2.0 - 2.5 ins.	1.62	1.74	2.14 2.58	2.84	4.05 4.45
2.5 - 3.0 ins.	0.99 0.94	2.14 1.66	1.54 1.96		
3.0 - 4.0 ins.	1.96 1.99	2.46 2.70	3.42 3.21		
4.0 - 5.0 ins.	1.96 2.01	0.77 0.57			
3.0 - 5.0 ins.	1.19 1.13	2.11 1.99			

15b. $D_2 = 2.0$ ins. $\left[k_m\right]_{loc} \times 10^3$

Length/Re_2	1880	3230	4450	7800	9500
0 - 0.5 ins.	0.81 av	1.11 av	1.29	1.71 av	1.85 1.93
0.5 - 1.0 ins.	0.41	0.77	1.11	1.45 1.31	1.45 1.37
1.0 - 1.5 ins.	0.49	0.80	0.87	1.16 1.30	1.38
1.5 - 2.0 ins.	1.341 0.661	1.13	1.05 1.89	1.12 2.52	2.96 2.46
2.0 - 3.0 ins.	1.138/ 0.798	1.63	1.86	2.59	2.21
	0.960/ 1.300	1.43	1.44	1.89	2.41
3.0 - 4.0 ins.	0.982/ 1.144				
2.1 - 3.1 ins.	1.21	1.57	2.07	2.59	3.29
3.1 - 4.1 ins.	1.18	1.59	2.03 2.10	2.86	3.19
4.1 - 5.1 ins.	1.24	1.71	2.05 2.12	2.86	3.31
5.1 - 6.1 ins.	0.95	1.33	1.77	2.44	2.80
6.1 - 7.1 ins.	0.85	1.21	1.46	2.03	2.32

NOMENCLATURE

A	=	Cross sectional area (sq.ft.)
A_1	=	Cross sectional area upstream of expansion (sq.ft.)
A_2	=	Cross sectional area downstream of expansion (sq.ft.)
B	=	Expansion ratio A_1/A_2
c	=	Concentration (gm. moles/litre)
c_b	=	Bulk concentration (gm. moles/litre)
c_s	=	Concentration at electrode surface (gm. moles/litre)
C_t	=	Craya-Curtet parameter.
D	=	Diffusion coefficient (cm^2/sec.)
D_1	=	Diameter of upstream section of abrupt expansion (ins.)
D_2	=	Diameter of downstream section of abrupt expansion (ins.)
E	=	Oxidation potential.
E^o	=	Standard oxidation potential.
f	=	Excess velocity profile (p.17)
F	=	Faraday's constant
F'	=	Water flowrate (litres/Min.)
h_1	=	Static head at abrupt expansion (ft. of water)
h_f	=	Friction gradient (ft. head of water/ft. length)

Δh^o = Observed static head difference (cms)

Δh = Measured static head difference (ft. of water)

$\Delta h'$ = Singly-corrected difference in static head (ft. of water)

$\Delta h''$ = Doubly-corrected difference in static head (ft. of water)

Δh_M = Theoretical maximum difference in static head (modified theory).

Δh_S = Theoretical maximum difference in static head (simple theory)

H_L = Loss of static head caused by eddy turbulence (ft. of water)

$(H_L)_E$ = Experimentally determined eddy turbulence loss (ft. of water)

$(H_L)_M$ = Theoretical eddy turbulence loss (modified theory)

$(H_L)_S$ = Theoretical eddy turbulence loss (simple theory)

$H_L{}^*$ = Theoretical eddy turbulence loss (partially modified theory).

i = Current density (milliamps/cm^2)

i_o = Exchange current density (milliamps/cm^2)

i_L = Limiting current density (milliamps/cm^2)

I = Total current (milliamps)

$\bar{I}$ = Ionic strength (gm. moles/litre)

j_D = Mass transfer factor.

j_H = Heat transfer factor.

k = Shape factor for excess velocity profile (p.17)

k = Coefficient = 0.795

k' = Coefficient = $0.795\ v_1{}^{0.1}$

k_h = Heat transfer coefficient.

k_m = Mass transfer coefficient.

K = Loss coefficient = $(1 - \beta)^2$

K^* = Loss coefficient = $1 - 2x_1 B + B^2(2x_2 - 1)$

l = Reference width related to spreading of jet (p.16)

L = Location of maximum static head relative to plane of enlargement, (ins.)

L_r = l/r_2

m = Similarity parameter of Craya and Curtet

m_a = Mass flowrate of ambient fluid.

m_L = Mass of fluid entrained over distance x_L

m_o = Mass flowrate of nozzle fluid.

m_r = Mass flowrate of recirculating material.

m_x = Mass of fluid entrained over distance x

m_1 = Mass flowrate in upstream section of abrupt expansion

m_2 = Mass flowrate in downstream section of abrupt expansion

M = 2 x average sum of momentum and pressure forces per unit area

N = Total rate of mass transfer (gm ions/cm^3 sec)

p = Static pressure at a point (lb./ft^2)

p_1 = Wall static pressure immediately upstream of abrupt expansion (lbs./$ft.^2$)

p_2 = Maximum static pressure downstream of abrupt expansion (lbs./$ft.^2$)

q = "Excess" volumetric flowrate (p.16)

q_r = Recirculation flowrate

Q = Total volumetric flowrate

r_1 = Radius of upstream section of abrupt expansion.

r_2 = Radius of downstream section of abrupt expansion.

R = Rotameter scale reading (cms.)

R_r = q/Q

T = Temperature (^{o}C.)

u = Point velocity

u_a = Velocity of ambient stream at a point

u_{max} = Maximum point velocity.

u_o = Velocity on jet axis

V = Potential difference

v_1 or V_1 = Mean tube velocity upstream of abrupt enlargement (ft./sec.)

v_2 or V_2 = Mean tube velocity downstream of abrupt enlargement (ft./sec.)

w = Excess velocity $= u - u_a$

w_o = Excess velocity on jet axis $= u_o - u_a$

x = Distance (ins.)

x_a = Distance required to entrain total mass of ambient fluid.

x_L = Distance at which a free jet would touch the wall if enclosed in a duct.

z = Valency

Z = Distance of eye of recirculation eddy from plane of enlargement (ins.)

α = momentum correction factor

α' = momentum correction factor (non Newtonian fluid)

γ = kinetic energy correction factor

γ' = kinetic energy correction factor (non Newtonian fluid)

Γ = transport number

δ_N = diffusion layer thickness

η = overpotential

θ = Thring-Newby parameter

λ = jet radius

μ = viscosity

ρ = density

τ = sheer stress

ϕ = friction factor

ψ = friction factor

APPENDIX I.

Momentum and Energy Correction Factors

(a) Streamline Flow

Momentum and kinetic energy correction factors for streamline flow conditions may readily be determined by integration of the well known parabolic velocity profile defined by

$$u = 2v(1 - (r/R)^2)$$

where, in accordance with nomenclature introduced previously,

u = point velocity at a radial distance r from the centreline of the pipe,

R = pipe radius,

v = average velocity over cross-sectional area (A) of pipe.

(i) Momentum correction factor (α)

This has previously been defined as

$$\alpha = \frac{1}{Av^2} \int_0^A u^2 dA$$

Substituting for u

$$\alpha = \frac{1}{\pi R^2 v^2} \int_0^R (2v(1 - r^2/R^2))^2 (2\pi r dr) = 4/3$$

(ii) Kinetic energy factor (γ)

$$\gamma = \frac{1}{Av^3} \int_0^A u^3 dA$$

whence,

$$\gamma = \frac{1}{\pi R^2 v^3} \int_0^R (2v(1 - r^2/R^2))^3 (2\pi r dr)$$

$$= 2$$

(b) Turbulent Flow

Velocity profiles under turbulent flow conditions vary with Reynolds number, becoming progressively flatter as the Reynolds number increases. Results are generally expressed in dimensionless form as graphs of u/u_m versus $(R - r)/R$, where u_m is the maximum value of the point velocity (at centreline). The profile may be represented by the empirical equation

$$u/u_m = (y/R)^{1/n}$$

where $y = (R - r)$

and n is an arbitrary constant determined by the value of the Reynolds number.

From this equation one may derive expressions for the average velocity and mean square velocity in terms of n and u_m and by combining these express α as a function of n. α may then be evaluated using data for n available in the literature.

(i) Mean velocity in terms of n and u_m

To avoid confusion, the mean velocity will be written $\langle v \rangle$ instead of simply v as formerly.

$$\langle v \rangle = \frac{Q}{A} = \frac{1}{A}\int_0^A u\,dA$$

$$= \frac{1}{\pi R^2}\int_0^R u_m (y/R)^{1/n}(2\,(R - y)dy)$$

$$= \frac{2u_m}{R^{(2n + 1)/n}}\int_0^R Ry^{1/n} - y^{(n + 1)/n}\;dy$$

Hence $$\frac{\langle v \rangle}{u_m} = \frac{2n^2}{(n + 1)(2u + 1)} \qquad \ldots \text{(A.1)}$$

as quoted elsewhere. (88)(89)

Hence $\dfrac{\langle v\rangle^2}{u_m^{\,2}} = \dfrac{4n^4}{(n+1)^2(2n+1)^2}$ ... (A.2)

where $\langle v\rangle^2$ is the square of the mean velocity.

(ii) The mean square velocity may be expressed

$$\langle v^2\rangle = \frac{1}{A}\int_0^A u^2\,dA$$

$$= \frac{1}{\pi R^2}\int_0^R u_m^{\,2}\,(y/R)^{2/n}(2\pi(R-y)\;dy)$$

$$= \frac{2u_m^{\,2}}{R(2n+2)/n}\int_0^R Ry^{2/n} - y^{(n+2)/n}\,dy$$

whence $\dfrac{\langle v^2\rangle}{u_m^{\,2}} = \dfrac{2n^2}{(n+2)(2n+2)}$ ... (A.3)

Combining equations (A2) and (A3)

$$\alpha = \frac{\langle v^2\rangle}{\langle v\rangle^2} = \frac{(n+1)(2n+1)^2}{4n^2(n+2)} \quad \text{... (A.4)}$$

Kinetic energy correction factors (γ)

An expression for γ may be derived in exactly similar fashion

writing $\langle v^3\rangle = \dfrac{1}{A}\displaystyle\int_0^A u^3\,dA$

and substituting for u gives

$$\langle v^3\rangle = \frac{1}{\pi R^2}\int_0^R (u_m)^3 (y/R)^{3/n}(2\pi(R-y)dy)$$

which leads to

$$\frac{\langle v^3\rangle}{u_m^{\,3}} = \frac{2n^2}{(n+3)(2n+3)} \quad \text{... (A.5)}$$

From equation (A1)

$$\frac{\langle v\rangle^3}{u_m^{\,3}} = \frac{8n^6}{(n+1)^3(2n+1)^3} \quad \text{... (A.6)}$$

$$\therefore \quad = \frac{\langle v^3\rangle}{\langle v\rangle^3} = \frac{(n+1)^3(2n+1)^3}{4n^4(n+3)(2n+3)} \quad \text{... (A.7)}$$

Because of their practical significance velocity profiles under turbulent flow conditions have been thoroughly investigated in the past. The results of several workers essentially produce a single straight line when values of $1/n$ are plotted against log Re. Over the Reynolds number range 4000 - 10^6 the equation of this line is given by Jakob (89) as

$$1/n = 0.2697 - 0.02715 \log Re$$

From this expression (extrapolated for Reynolds numbers as low as 2100) values of n were obtained for the author's experimental conditions.

Thus at any particular Reynolds number the value of n may be ascertained and the corresponding values of α and γ calculated from equations (A.4) and (A.7). Values obtained in this manner have been plotted versus log Reynolds number in figure (46).

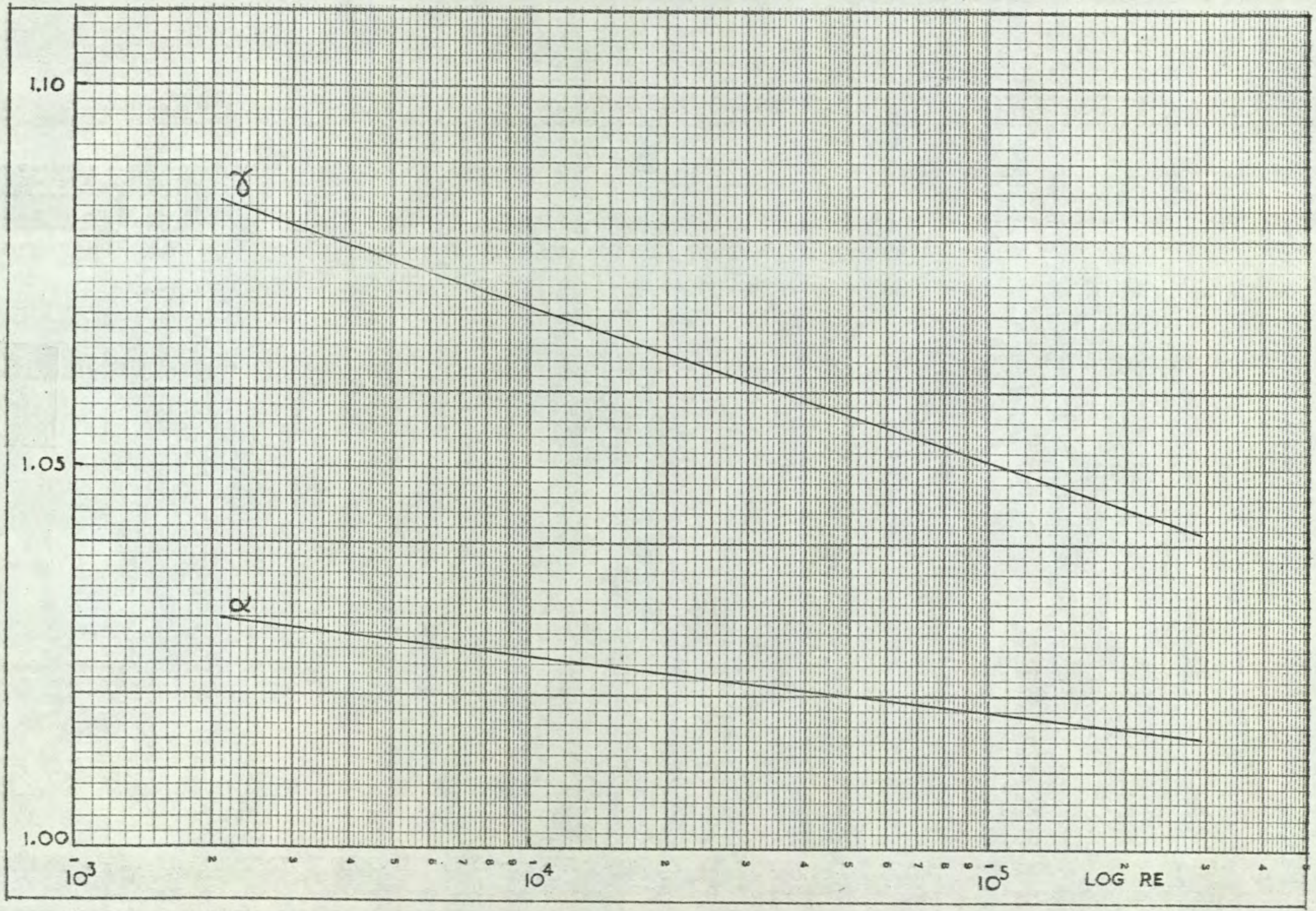

fig. 46

APPENDIX II.

Re-examination of Archer's Data

The work of Archer (40) on pressure changes at abrupt enlargements has been briefly reviewed in section (3.4). In the following section measurements published by Archer are re-examined in the light of the author's own findings. This analysis applies to only four of the five expansion ratios investigated by Archer since measurements in the remaining case appeared unreliable and were mainly devoted to a narrow range of upstream velocities (70 per cent of the reported measurements cover the range v_1 = 21.38 - 25.82 ft. per sec.).

(i) Maximum pressure rise

Friction factors for Archer's experimental conditions were computed from the empirical correlation:

$$\phi^{-\frac{1}{2}} = -2.5 \ln \frac{e/d}{3.7} + \frac{\phi^{-\frac{1}{2}}}{1.13Re}$$

using an initial value of $\phi^{-\frac{1}{2}}$ given by the expression:

$$\phi^{-\frac{1}{2}} = 3.2 - 2.5 \ln(e/d)$$

The standard value of absolute roughness for drawn tubing (e = 0.000005) was assumed for the brass sections employed by Archer (40).

Figure (47) shows specimen doubly-corrected pressure curves at a selected expansion ratio. Computed friction losses would appear to have been under-estimated. In spite of this, figure (48) shows that the experimental maximum

fig. 47

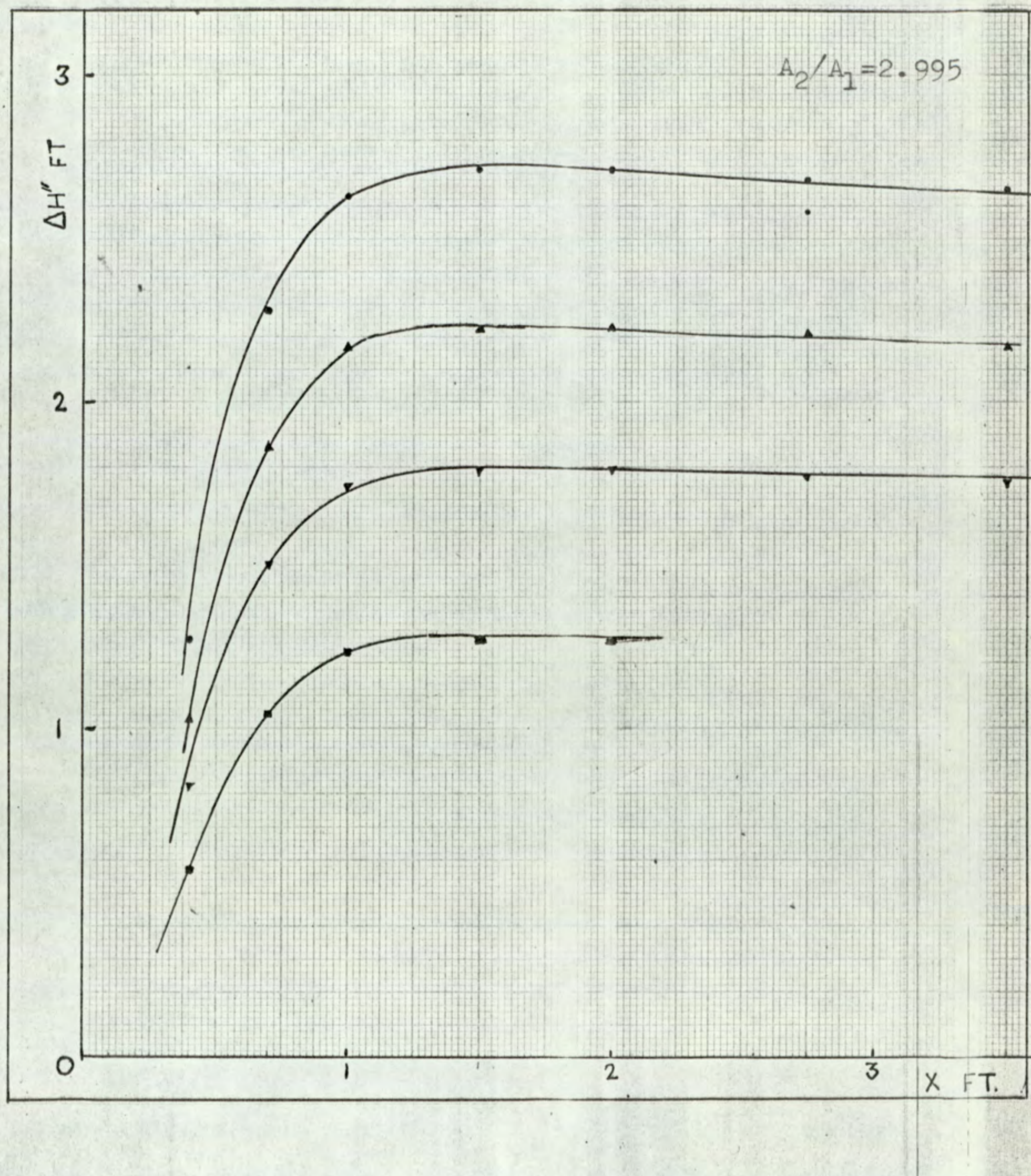

fig. 48

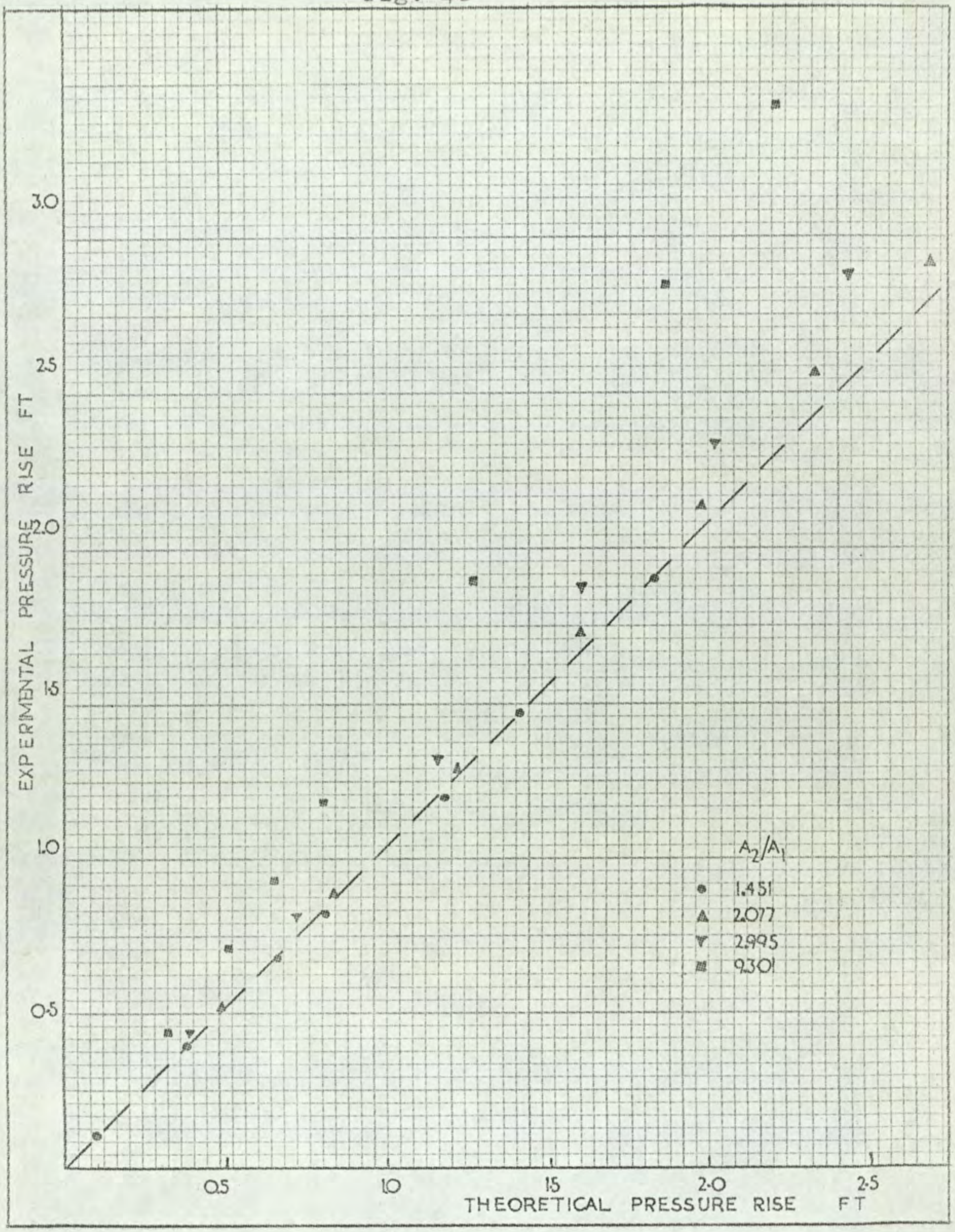

EXPERMENTAL PRESSURE RISE FT
THEORETICAL PRESSURE RISE FT
0.5
1.0
1.5
2.0
2.5
3.0
A2/A1
1.451
2.077
2.995
9.301

pressure rise deduced from such curves becomes progressively greater than the value predicted by the simple theory as the expansion ratio is increased. In the case of the largest expansion ratio ($D_2/D_1 = 3.05$) the maximum experimental pressure rise at the higher velocities exceeds the theoretical value by more than 40 per cent: the corresponding discrepancy between the experimentally determined head loss due to eddy turbulence and the value predicted by the Borda-Carnot equation is approximately 10 per cent.

In view of the large discrepancies between theoretical and experimental values of the maximum pressure rise it is evident that results derived from Archer's measurements will not fit the author's correlation,

$$(h'')\text{max.} = 0.795\, v_1^{2.1}(B - B^2)/2g.$$

(ii) Position of the observed peak rise

Archer's expression for the position of the observed maximum pressure rise reads:

$$L_A = 17.4(D_2 - D_1)^{0.4}$$

where L_A, D_2 and D_1 are expressed in inches.
Such an expression predicts a unique value for an infinite range of expansion ratios which are not dynamically similar.

Figures (49) and (50) show values derived from Archer's results in relation to the author's experimental curves. Agreement is quite good except at the larger expansion ratios (max. $D_2/D_1 = 3.05$) where measurements are somewhat suspect.

fig. 49

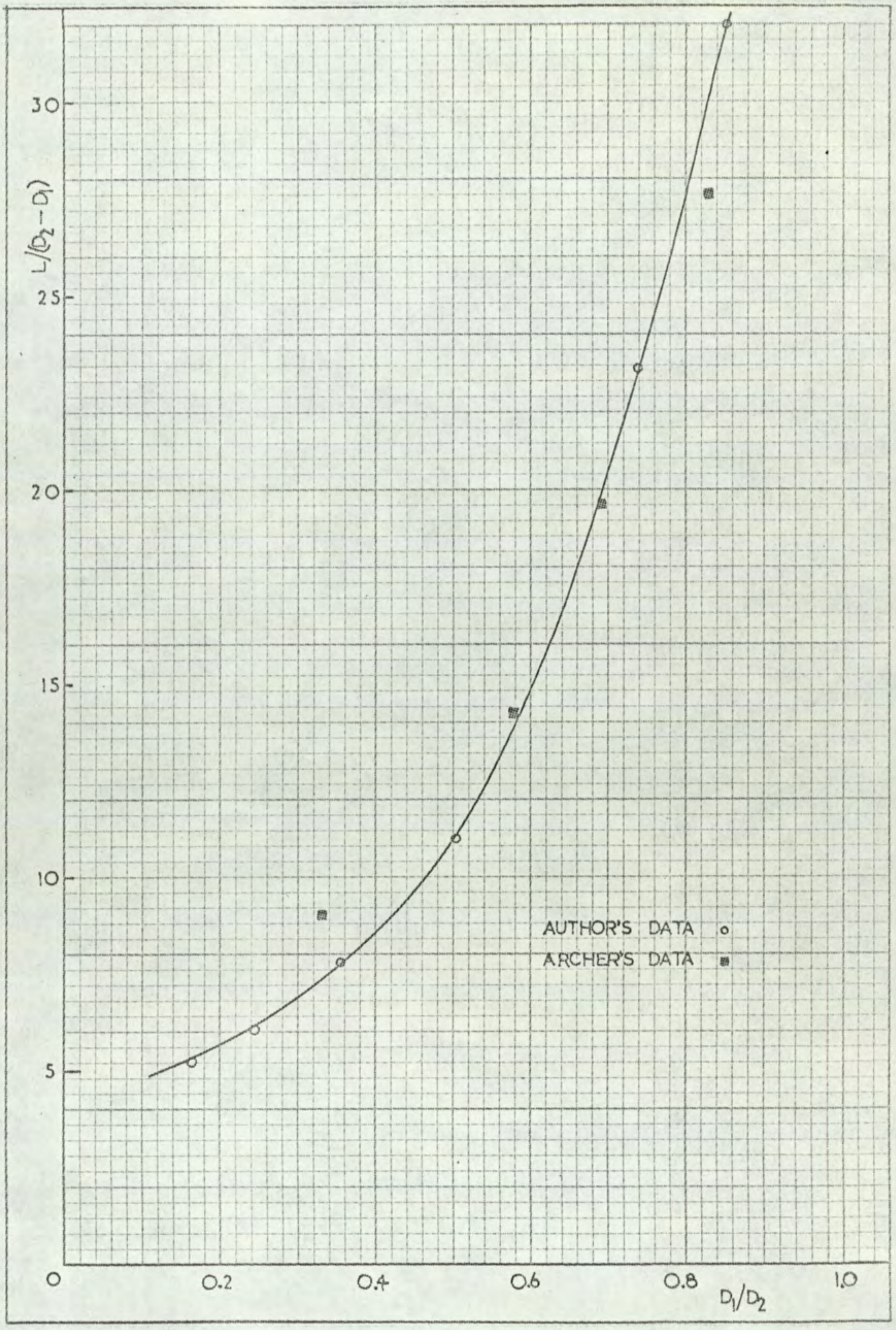

30
25
20
15
10
5
0
0.2
0.4
0.6
0.8
1.0
$L/(D_2 - D_1)$
D_1/D_2
AUTHOR'S DATA
ARCHER'S DATA

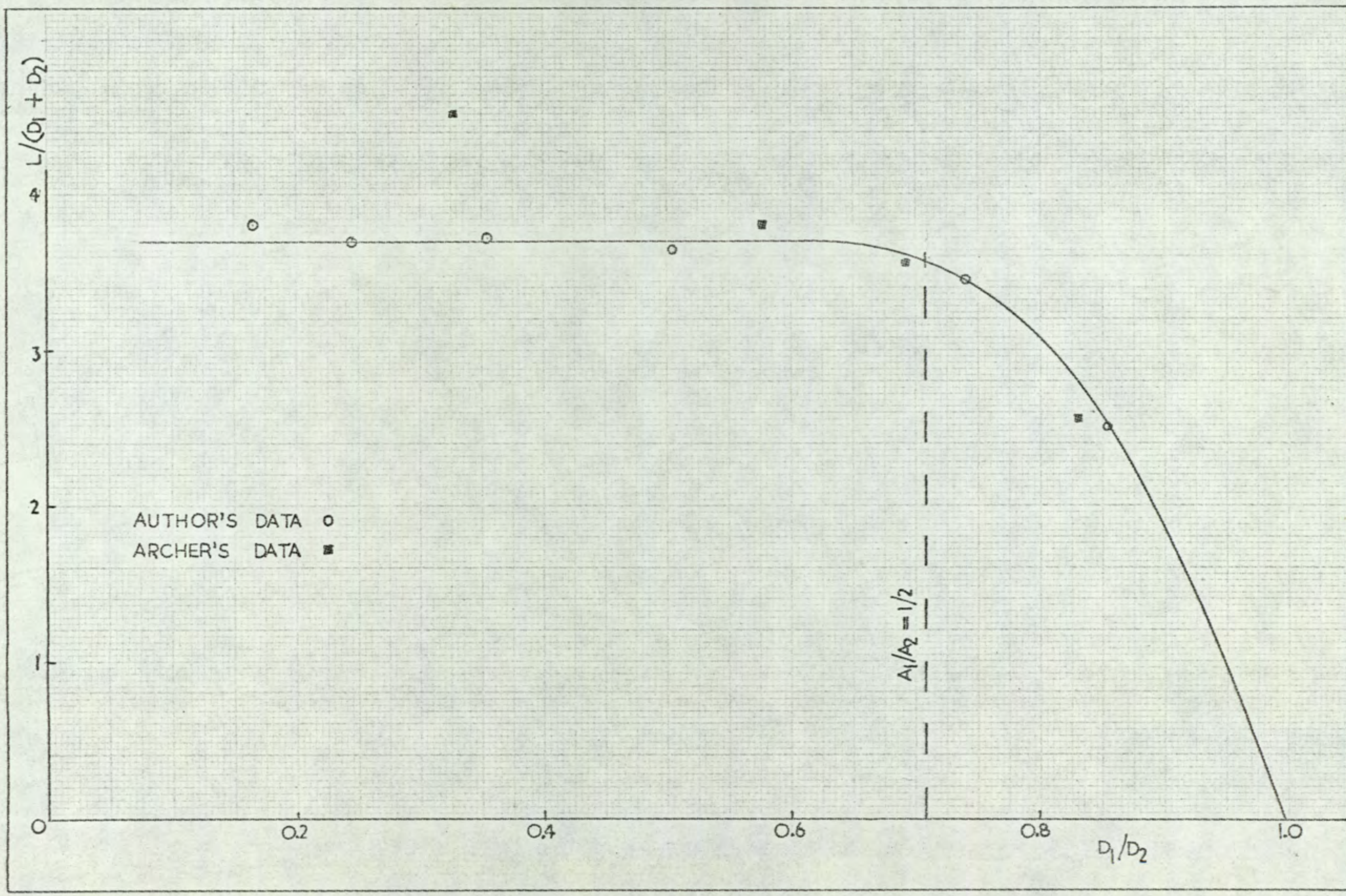
L/(D1 + D2)
4
3
2
1
0
0.2
0.4
0.6
0.8
1.0
D1/D2
AUTHOR'S DATA o
ARCHER'S DATA
A1/A2 = 1/2

fig. 50

(iii) Principal features of the recirculation zone.

Graphs of the normalised, singly-corrected data are presented in figure (51). Superimposed on this figure are the locations of the eye of the recirculation eddy as predicted by Cohen de Lara (30).

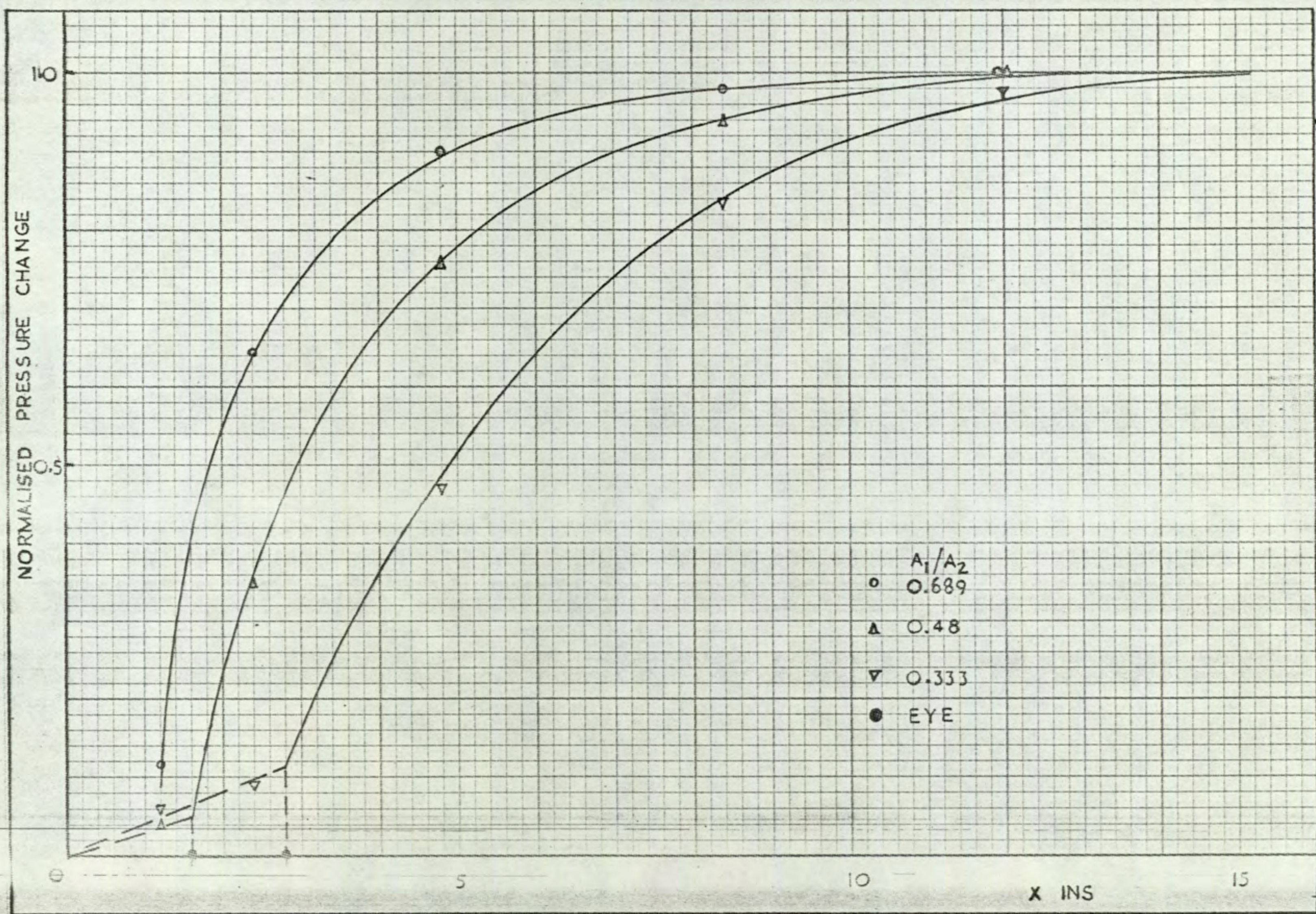
NORMALISED PRESSURE CHANGE
1.0
0.5
5
10
15
X INS
A_1/A_2
0.689
0.48
0.333
EYE

fig. 51

BIBLIOGRAPHY

Ref.

1 Lawrence, M.N. & Spittle, J. Forced-convection techniques for gas-fired rapid billet heating. Gas Council Research Communication GC108.

2 Francis, W.E., Moppett B.E., & Read G.P. Studies of flow patterns and convection in rapid heating furnaces using model techniques
J. Inst. Gas Engineers Vol. 7, 1967, p335

3 Francis, W.E. The design of air blast tunnel burners
Gas Council Research Communication GC48.

4 Hottel, H.C. & Cohen, E.S. Radiant heat exchange in a gas filled enclosure.
A.I.Ch.E.J Vol. 4, 1958, p3

5 Hottel, H.C. & Sarofim, A.F. The effect of gas flow patterns on radioactive transfer in cylindrical furnaces. Int. J. of heat and mass transfer. Vol. 8, 1965, pp1153 - 1169.

6 Chesters, J.H. The growth of an idea
Iron and Coal Trades Review Vol. 66, 1953, pp179 - 187

7 Chesters, J.H. The aerodynamic approach to furnace design
Trans. A.S.M.E. Vol. 81, 1959 p361.

8 Thring, M.W. Research on turbulent diffusion combustion
J. Inst. Fuel Vol. 34 1961 p494

9 Hedley & Jackson
J. Inst. Fuel Vol. 38 1965 p 290

10 Thring, M.W. The science of flames and furnaces.
Chapman & Hall 2nd edition London 1962.

11 Chiciier, N.A. & Beer, J.M.
Trans. A.S.M.E. Journal of basic engineering Vol. 86 1964 pp 788 - 796, 797 - 804.

12 Chedaille, J., Leuckel, W. & Chesters, A.K.
J. Inst. Fuel Vol. 39, 1966, p 506.

Ref.

13 Lefebvre, A.H., Ibrahim, A.R.A.F., & Benson, N.C.
Combustion and Flame Vol. 10 1966 p 231.

14 Kerr, N.M., & Fraser, D.
J. Inst. Fuel Vol. 38 1965 p 519

15 Efficient use of fuel Ministry of Power H.M.S.O.
London, 1958

16 Spalding, D.B. Seventh symposium (International) on combustion p 595 Butterworths 1959

17 Spalding, D.B. The spread of turbulent flames confined in ducts.
11th Symposium (International) on Combustion 1967 p 807

18 Francis, W.E. Studies of industrial high intensity gas combustors.
10th Symposium (International) on Combustion p 1219
The Combustion Institute 1965

19 Abramovich, G. Theory of turbulent jets
Trans. by Scripta Technica Cambridge (Mass) MIT Press 1963

20 Sunavala, P.D.
J. Sci. Indust. Res. Vol. 20B 1961 p 246

21 Thring, M.W. & Newby, M.P. Combustion length of enclosed turbulent jet flames
4th Symposium (International) on Combustion 1953 p 789
William & Wilkins, Baltimore.

22 Curtet, R. Sur l'ecoulement d'un jet entre parois
Publications Scientifiques et Techniques du Ministere de l'air Paris No. 359 1960

23 Curtet, R. Confined jets and recirculation phenomena with cold air
Combustion and Flame Vol. 2 1958 p 383

24 Craya, A., & Curtet, R.
C.R. Acad. Sci. Paris Vol. 241 (1955) p 621

25 Hubbard, E.H. Recirculation in cold models of furnaces.
J. Inst. Fuel Vol. 35 1962 p 160

Ref.

26 Barchilon, M., & Curtet, R.
Trans. A.S.M.E. Journal of basic eng. Vol. 86 1964 p 777

27 Becker, H.A., Hottel, H.C., & Williams, G.C.
9th Symposium (International) on Combustion 1963
Academic Press. pp 7 - 20.

28 Becker, H.A., Hottel, H.C., & Williams, G.C.
10th Symposium (International) on Combustion. The
Combustion Institute 1965 p 1253.

29 Hill, P.G. Turbulent jets in ducted streams
J. Fluid Mech. 1965 Vol. 22 pp 161 - 186

30 Cohen, De Lara, G., Poux, J., & Perrin, R. I.F.R.F. Doc.
No. Tb-F61/bc/3 Grenoble October, 1960.

31 Ricou, F.P., & Spalding, D.B.
8th Symposium (International) on Combustion 1961 p 21

32 Streeter, V.L. Handbook of fluid dynamics
McGraw Hill 1961

33 Daugherty, R.L., & Franzini, J.B.
Fluid mechanics with engineering applications
McGraw Hill 1965 p 224.

34 Nusselt, W.
Forschung auf dem Gebiete des Ingenieurwesens
Vol. 11 1940 pp 250 - 255.

35 Baer, H.
Dinglers Polytech. J. March 23 1907

36 Brightmore, A.W.
Proc. Inst. Civ. E. Vol. 169 1906-7 p 323

37 Gibson, A.H.
Proc. Roy. Soc. (A) Vol. 83 1910 p 366

38 Gibson, A.H.
Trans. Roy. Soc. Edin. Vol. 48 1911 p 97

39 Schütt, H.C.
Trans. Am. Soc. Mech. E. Hyd-51-10 p 83

40 Archer, W.H.
Trans. A. S. C. E. 1913 Vol. 76 pp 999 - 1026

Ref.

41 Rouse, H. Fluid mechanics for hydraulic engineers Dover Publications Inc. NY 1961 p 262.

42 Kays, W.M. Trans. A.S.M.E. 1950 pp 1067 - 1074

43 Mendler, O.J. Sudden Expansion losses in single and two phase flow. Ph.D. Thesis University of Pittsburg, PA

44 Bissiri, P.G. Thesis Dept. Mech. Eng. Stanford University Calif. 1949.

45 Astarita, G. & Nicodemo, L. I. & E.C. Fundamentals Vol. 5 1966 pp 237 - 242

46 Benedict, R.P., Carlucci, N.A., & Swetz, S.D. Trans. A.S.M.E. Vol. 88 1966 p 73.

47 Perry, R.H. Chemical Engineers Handbook 4th edition McGraw Hill, N.Y.

48 Timmermans, J. Physico-chemical constants of pure organic compounds. Trans. from French. G. Middleton, Elsevier, Amsterdam.

49 Akers, J.B. Ph.D. thesis University of Aston, in Birmingham, 1967

50 Brownlee, K.A. Statistical theory and methodology in science and engineering 2nd edition Wiley 1965

51 Louise, K.D. Circulation in furnaces Pt. 1 The Gas Council Midlands Research Station. Internal Report IR70 June, 1963

52 Shaw, P. Van, Reiss, L.P., & Hanratty, T.J. A.I.Ch.E.J. Vol. 9 1963 p 362

53 Ede, A.J., Morris, R., & Birch, E.S. N.E.L. Report No. 73 D.S.I.R. Dec. 1962

54 Ede, A.J. Effect of an abrupt disturbance of the flow on the local heat transfer coefficient in a pipe N.E.L. Report Heat 169, Aug. 1959

55 Ede, A.J. N.E.L. Report Heat 164 Jan. 1959.

Ref.
56 Krall, K.M., & Sparrow, E.M.
Trans. A.S.M.E. J. Heat. Trans. Vol. 88 1966 p 131

57 Malina, A.J., & Sparrow, E.M.
Chem. Eng. Sci. 1964 Vol. 19 p 953

58 Emerson, W.H. N.E.L. Report No. 256 November, 1966

59 Norman, W.S. Absorption, distillation and cooling towers.
Longmans 1961

60 Tobias, C.W., Eisenberg, M., & Wilke, C.R. Diffusion and convection in electrolysis - a theoretical review
J. Electrochem. Soc. Vol. 99 No. 12 1952 p 359c

61 Levich, V.G. Physico-chemical hydrodynamics
Englewood Cliffs (N.J) Prentice Hall 1962

62 Ibl, N. Advances in electrochemistry and electrochemical engineering Vol. 2
Interscience Publishers NY.

63 Potter, E.C. Electrochemistry
Cleaver-Hume Press London, 1956

64 Vetter, K.J. Electrochemical kinetics
Trans. by Scripta Technica Academic Press. 1967

65 Bazan, J.C. & Arvia A.J.
Electrochimica Acta Vol. 9 1964 pp 17 - 30; 667 - 684

66 Wragg A.A. & Ross T.K. Superposed free and forced convective mass transfer in an electrochemical flow system
Electrochimica Acta 1967 Vol. 12 pp 1421 - 1428

67 Böhm U., Ibl N., & Frei A.M. Zur kenntnis der naturlichen konvektion bei der elektrolyse in engen räumen
Electrochimica Acta 1966 V11 pp 421 - 434

68 Wilke C.R., Tobias C.W., & Eisenberg M. Free convection mass transfer at vertical plates
Chem. Eng. Progress. 1953 V49 pp 663 - 674

69 Glasstone S. Textbook of physical chemistry 2nd edition
Macmillan, London, 1956.

Ref.

70 Ibl, N. + Schaddegg. Surface roughness effects in the electrodeposition of copper in the limiting current range
J. Electrochem. Soc. V114 1967 p 54.

71 Vogel A.
Textbook of quantitative inorganic analysis
3rd edition 1961 Longmans

72 Eisenberg, M., Tobias, C.W., & Wilke, C.R. Selected physical properties of ternary electrolytes employed in ionic mass transfer
J. Electrochem. Soc. 1956 V103 p 413

73 Wilke, C.R., Eisenberg, M., & Tobias C.W. Correlation of limiting currents under free convection conditions.
J. Electrochem. Soc. 1953 V100 p 513.

74 Daniels F. + Alberty R.A.
Physical Chemistry 2nd edition
Chapman & Hall 1963

75 Ross T.K. & Wragg A.A. Electrochemical mass transfer studies in annuli
Electrochim. Acta 1965 V10 pp 1093 - 1105

76 Wagner C.J. Current distribution in galvanic cells involving natural convection
J. Electrochem. Soc. 1957 V104 p 129

77 Fouad M.G. & Ibl N.
Electrochim. Acta. 1969 V3 pp 233 - 243

78 Wranglen, G. & Nilsson O.
Electrochim. Acta. 1962 V7 pp 121 - 137

79 Fenech E.J. & Tobias C.W. Mass transfer by free convection at horizontal electrodes.
Electrochim. Acta. 1960 V2 p 311

80 Arvia A.J., Bazán J.C., & Carrozza J.S.W.
Electrochim Acta. 1966 V11 pp 881 - 889

Ref

81 Lin, C.S., Denton, E.B., & Putnam, G.L.
Diffusion controlled electrode reactions.
Ind. Eng. Chem. Vol. 43, 1951, p2136

82 Shreir, L.L., & Smith, J.W.
Cathode polarisation potential during electrodeposition. of copper.
J. Electrochem. Soc. Vol. 99, 1952 p64

83 Brown, O.R., & Thirsk, H.R.
Electrochimica Acta. Vol. 10, 1965, p383

84 Read, G.P. Model techniques applied to flow problems in furnaces.
The Gas Council.
Midlands Research Station. Internal Report I.R. 70, 1963

85 Filletti, E.G., & Kays, W.M.
Trans A.S.M.E. J. Heat Transfer Vol. 89, 1967, p163

86 Eisenberg, M., Tobias, C.W., & Wilke, C.R.
Ionic mass transfer and concentration polarisation at rotating electrodes.
J. Electrochem. Soc. Vol. 101, 1954, p306

87 Abbott, D.E., & Kline, S.J.
Trans. A.S.M.E. J. Basic Eng. Vol. 84, 1962, p317

88 Schlichting.
Boundary Layer Theory

89 Jakob
Heat Transfer Vol II JOHN WILEY 1959.

90 Davies, R.M.
The Gas Council. Midlands Research Station.
Internal Report No. 322, October 1967

- FIGURE 10 -

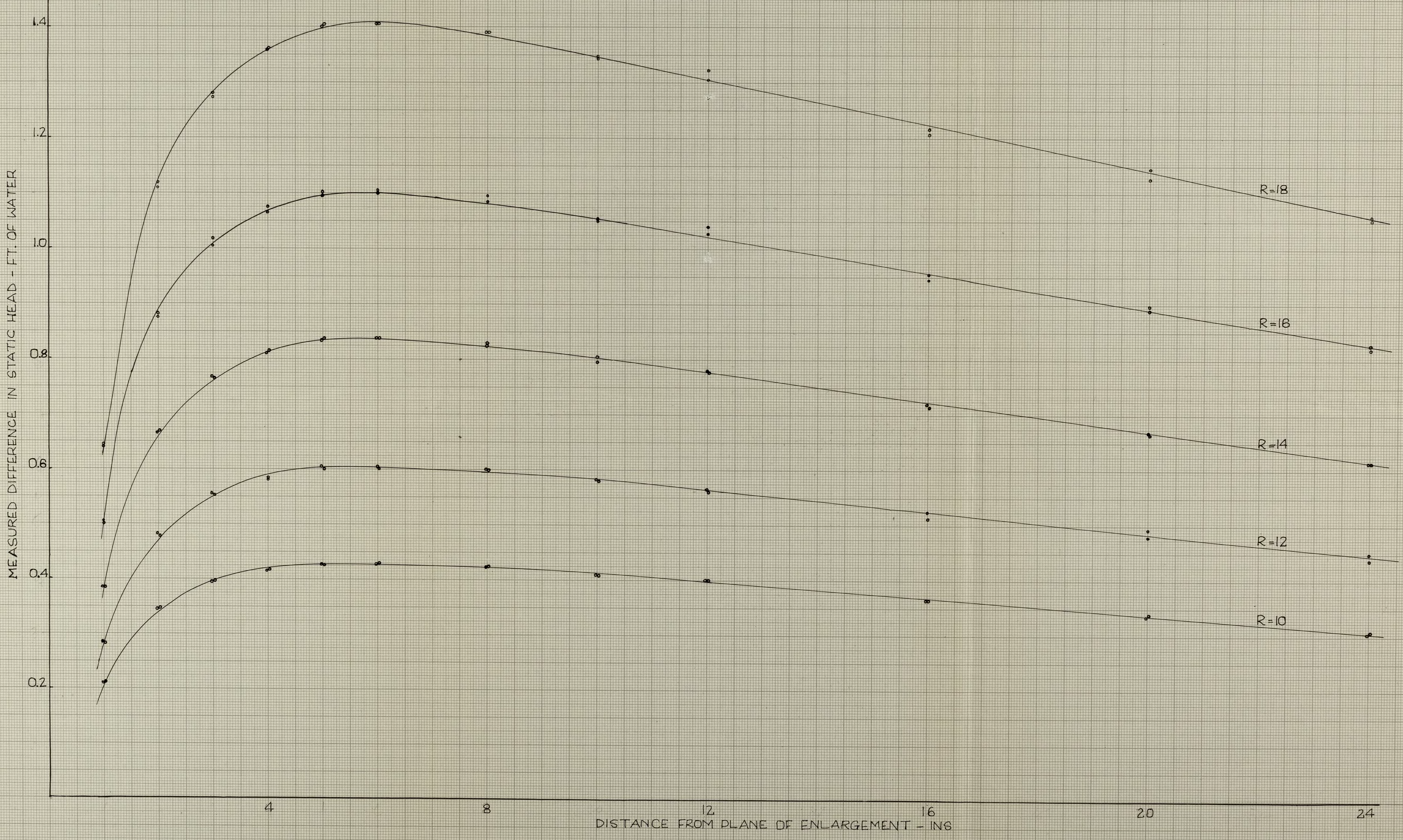

RESULTS OF DUPLICATED RUNS - DATA OF TABLE 4, D_2 = 1.0 INS, SELECTED VELOCITIES [R = ROTAMETER SCALE READING, CMS]